

Dissertation zur Erlangung des Doktorgrades der
Fakultät für Chemie und Pharmazie der Ludwig-
Maximilians-Universität München

**Cab45 – analysis of key features of
a multifunctional secretory
pathway component**

Birgit Renate Karin Blank

Aus
Burglengenfeld, Deutschland

2017

Erklärung

Diese Dissertation wurde im Sinne von § 7 der Promotionsordnung vom 28. November 2011 von Herrn Prof. Dr. Reinhard Fässler betreut.

Eidesstattliche Versicherung

Diese Dissertation wurde eigenständig und ohne unerlaubte Hilfe erarbeitet.

München, 7.10.2017

.....
(Birgit Blank)

Dissertation eingereicht am 12.10.2017

1. Gutachter: Prof. Dr. Reinhard Fässler
2. Gutachter: Prof. Dr. Jürgen Soll

Mündliche Prüfung am 5.12.2017

Table of contents

1	List of abbreviations	4
2	Summary	6
3	Introduction	7
3.1	THE SECRETORY PATHWAY – THE CELLULAR PROTEIN HIGHWAY	7
3.2	THE ENDOPLASMIC RETICULUM	8
3.2.1	<i>Protein translocation across the ER membrane</i>	<i>9</i>
3.2.2	<i>Protein modifications and processing after RER import</i>	<i>11</i>
3.2.3	<i>ER to Golgi transport</i>	<i>12</i>
3.3	THE ER-GOLGI INTERMEDIATE COMPARTMENT	14
3.4	THE GOLGI COMPLEX.....	14
3.4.1	<i>Golgi structure</i>	<i>14</i>
3.4.2	<i>Golgi functions and intra Golgi transport.....</i>	<i>16</i>
3.4.3	<i>PTMs in the Golgi.....</i>	<i>17</i>
3.4.3.1	Glycosylation in the Golgi	17
3.4.3.2	Phosphorylation of secretory pathway proteins	18
3.4.3.2.1	Fam20C and the Fjx family of secretory pathway kinases.....	19
3.4.3.2.2	Tyr phosphorylation by extracellular tyrosine-protein kinase PKDCC.....	20
3.4.4	<i>Calcium in the secretory pathway</i>	<i>21</i>
3.4.4.1	Calcium pumps.....	22
3.4.4.2	Calcium release channels of the Golgi	24
3.4.4.3	Calcium binding proteins in Golgi	25
3.5	THE TGN – THE SORTING HUB.....	27
3.5.1	<i>Sorting by lipids</i>	<i>27</i>
3.5.2	<i>Sorting of TM proteins.....</i>	<i>28</i>
3.5.3	<i>Sorting of soluble proteins.....</i>	<i>30</i>
3.5.3.1	Sorting into secretory storage granules.....	30
3.5.3.2	Sorting by receptors.....	32
3.5.3.3	Sorting by the Cofilin1/SPCA1/Cab45 machinery	33
3.5.3.4	Cab45 – the missing link	35
4	Aims of this thesis	- 38 -
5	Material and Methods.....	- 39 -
5.1	MOLECULAR BIOLOGICAL METHODS	- 39 -
5.1.1	<i>Polymerase Chain Reaction (PCR) for standard cloning</i>	<i>- 39 -</i>
5.1.2	<i>Annealing of sgRNAs and insertion into pX backbone vectors</i>	<i>- 39 -</i>
5.1.3	<i>Agarose gel analysis and DNA purification.....</i>	<i>- 40 -</i>
5.1.4	<i>Restriction digest.....</i>	<i>- 40 -</i>
5.1.5	<i>Ligation.....</i>	<i>- 40 -</i>
5.1.6	<i>Transformation of ligated DNA into E.coli cells.....</i>	<i>- 40 -</i>
5.1.7	<i>Single clone isolation, DNA preparation and sequencing</i>	<i>- 41 -</i>
5.1.8	<i>Mutagenesis for introduction of single point mutations</i>	<i>- 41 -</i>
5.1.9	<i>Generation of chemically competent E.coli cells</i>	<i>- 41 -</i>
5.1.10	<i>Plasmids</i>	<i>- 41 -</i>
5.1.11	<i>Primers and restriction enzymes</i>	<i>- 43 -</i>
5.2	CELL CULTURE METHODS	- 44 -
5.2.1	<i>General culture conditions.....</i>	<i>- 44 -</i>
5.2.2	<i>Freezing and thawing of cells</i>	<i>- 44 -</i>
5.2.3	<i>Plasmid transfection of cells.....</i>	<i>- 44 -</i>

5.2.4	<i>Fluorescence activated cell sorting (FACS) of HeLa cells</i>	- 45 -
5.2.5	<i>Single clone isolation</i>	- 45 -
5.2.6	<i>Generation of stable cell line</i>	- 45 -
5.2.7	<i>Generation of CRISPR/Cas9 KO cell lines</i>	- 45 -
5.2.8	<i>Generation of CRISPR/Cas9 MIN-tagged cell line</i>	- 47 -
5.3	BIOCHEMICAL METHODS	- 47 -
5.3.1	<i>Sample preparation for SDS Page analysis and western blotting</i>	- 47 -
5.3.2	<i>Western blot analysis</i>	- 48 -
5.3.3	<i>Protein expression and purification</i>	- 48 -
5.3.4	<i>Protein fluorescence labeling</i>	- 49 -
5.3.5	<i>NativePage analysis</i>	- 49 -
5.3.6	<i>In vitro IPs with recombinant full-length proteins</i>	- 50 -
5.3.7	<i>In vitro IPs with peptides</i>	- 50 -
5.4	CELL BIOLOGICAL METHOD.....	- 51 -
5.4.1	<i>Sample preparation for analysis of overexpressed Cab45 in HeLa cells</i>	- 51 -
5.4.2	<i>Cargo secretion assays</i>	- 52 -
5.4.3	<i>Proliferation assays</i>	- 52 -
5.5	PHYSICAL METHODS AND BIOINFORMATICS METHODS	- 52 -
5.5.1	<i>Isolation of Golgi membranes for NativePage analysis and mass spectrometry</i>	- 52 -
5.5.2	<i>Mass spectrometry for phosphoproteomic analysis</i>	- 53 -
5.5.3	<i>Mass spectrometric screen for comparison of secretomes</i>	- 54 -
5.5.4	<i>Peptide identification</i>	- 55 -
5.5.5	<i>Structural model of Cab45</i>	- 56 -
5.5.6	<i>Circular dichroism spectroscopy (CD)</i>	- 56 -
5.6	MICROSCOPY METHODS	- 56 -
5.6.1	<i>Immunofluorescence (IF) analysis</i>	- 56 -
5.6.2	<i>Quantifications of vesicular structures in calcium-binding deficient mutants</i>	- 57 -
5.6.3	<i>Retention using selective hooks (RUSH)</i>	- 57 -
5.6.4	<i>Oligomerization assays</i>	- 58 -
5.6.5	<i>Fluorescence recovery after photobleaching (FRAP)</i>	- 58 -
5.6.6	<i>Three-dimensional structured illumination (3D-SIM) microscopy</i>	- 59 -
5.7	BUFFERS.....	- 60 -
6	Results	- 61 -
6.1	CAB45 WAS PURIFIED FROM SF9 CELLS IN HIGH AMOUNTS	- 61 -
6.2	SUCCESSFUL GENERATION OF TWO CRISPR/CAS9 CELL LINES	- 62 -
6.2.1	<i>CRISPR/Cas9 KO targeting by two different sgRNAs was highly efficient</i>	- 64 -
6.2.2	<i>CRISPR/Cas9 KO cell lines show no change in Golgi morphology</i>	- 65 -
6.2.3	<i>CRISPR/Cas9 KO could also be verified on genomic level</i>	- 66 -
6.2.4	<i>Modified cell lines proliferate normally</i>	- 68 -
6.2.5	<i>CRISPR/Cas9 KO cell lines mimic siRNA KD phenotype in secretion assays</i>	- 69 -
6.2.6	<i>MIN-tag was successfully integrated into SDF4 locus</i>	- 70 -
6.3	CAB45 OLIGOMERIZES IN A CALCIUM-DEPENDENT MANNER	- 71 -
6.3.1	<i>Cab45 exhibits high molecular weight fraction in NativePage analysis</i>	- 72 -
6.3.2	<i>Recombinant Cab45 forms oligomers in vitro</i>	- 73 -
6.3.3	<i>Calcium binding induces conformational change of Cab45</i>	- 74 -
6.3.4	<i>Only four EF hand motifs are required for calcium binding and oligomerization</i> ...	- 76 -
6.3.5	<i>Only EFh2 undergoes conformational change in the presence of calcium</i>	- 82 -
6.3.6	<i>All EFh mutants mimic the phenotype of the 6EQ mutants in cells</i>	- 84 -
6.3.7	<i>Predicted oligomerization-prone mutant can still oligomerize</i>	- 85 -
6.3.8	<i>N- and C-terminal fragments of Cab45 oligomerize independently</i>	- 87 -
6.4	OLIGOMERIC CAB45 DIRECTLY INTERACTS WITH CARGO VIA TYROSINE RESIDUES	- 88 -
6.4.1	<i>The Cab45-cargo interaction is direct</i>	- 89 -

6.4.2	<i>Cab45 oligomerizes together with cargo</i>	- 90 -
6.4.3	<i>Formed Cab45-cargo oligomers are highly stable in vitro</i>	- 91 -
6.4.4	<i>Cab45 colocalizes with SPCA1 and LyzC in super-resolution microscopy</i>	- 92 -
6.4.5	<i>Tyrosine residues are crucial for the Cab45-cargo interaction</i>	- 93 -
6.4.6	<i>Mutation of cargo binding site and KO show same delay in export dynamics</i>	- 96 -
6.5	CAB45 IS PHOSPHORYLATED BY FAM20C.....	- 98 -
7	Discussion	- 102 -
7.1	THE CRISPR/Cas9 SYSTEM - BOON AND BANE.....	- 103 -
7.2	CAB45 OLIGOMERIZES IN A CALCIUM-DEPENDENT MANNER UNDER PHYSIOLOGICAL CONDITIONS.....	- 105 -
7.2.1	<i>But is this oligomeric phenotype of Cab45 physiological relevant?</i>	- 106 -
7.2.2	<i>The remaining problem of the Cab45 oligomerization domain</i>	- 107 -
7.2.3	<i>Oligomerization might be a potential retention mechanism for Cab45</i>	- 107 -
7.3	CAB45 RELEASES CARGO UPON PHOSPHORYLATION	- 108 -
8	Outlook and open questions	- 111 -
9	Supplementary Figure and Tables	- 113 -
10	References	- 115 -
	Acknowledgements	- 147 -

1 List of abbreviations

SHORT NAME	FULL NAME		
AA	Amino acids	MGP	Matrix Gla protein
ADP	Adenosine diphosphate	MIN	Multifunctional integrase tag
AP	Adaptor protein	MMP	Matrix metallo proteinase
APS	Ammonium persulfate	NAADP	Nicotinic acid adenine dinucleotide phosphate
ASN	Asparagine	NC	Non-compact zone
ATF6	Activating transcription factor 6	NE	Nuclear envelope
ATP	Adenosine triphosphate	NHEJ	Non-homologous end joining
BSA	Bovine serum albumin	NUCB	Nucleobindin
BP	Base pairs	OMIM	Online Mendelian inheritance in man
CADPR	Cyclic adenosine dinucleotide phosphate ribose	O.N.	Over night
CAB45	Calcium-binding protein of 45 kDa	OST	Oligosaccharyl transferase
CAS9	CRISPR associated protein	PAM	Protospacer adjacent motif
CATHD	CathepsinD	PBS	Phosphate-buffered saline
CD	Circular dichroism	PERK	PKR (dsRNA-dependent protein kinase)-like ER kinase
CDG	Congenital disorders of glycolylation	PI4P	Phosphatidylinositol-4-phosphate
CFL1	Cofilin 1	PIP₂	Phosphatidylinositol-4,5-bisphosphate
CGN	Cis Golgi Network	PKDCC	Protein kinase domain containing, cytoplasmic
COMP	Cartilage oligomeric matrix protein	PKL	Protein kinase like
COPII	Coat protein complex II	PLC	Phospholipase C
CRISPR	Clustered regularly interspaced short palindromic repeat	PM	Plasma membrane
		PMCA	Plasma membrane calcium ATPase
CRRNA	CRISPR RNA	PTM	Posttranslational modification
CALU	Calumenin	RCN	Reticulocalbin
CS	Chondroitin sulfate	RER	Rough endoplasmic reticulum
COX	Cyclooxygenase	RNA	Ribonucleic acid
DAG	Diacylglycerol	RT	Room temperature
DMEM	Dulbecco's modified eagle medium	RUSH	Retention using selective hooks
DNA	Deoxyribonucleic acid	RYR	Ryanodine receptor
DIA1	Deleted in Autism-1	SDF4	Stromal derived factor 4
EFH	EF hand	SER	Smooth endoplasmic reticulum
EPSINR	Epsin-related	SERCA	Sarcoplasmic/endoplasmic reticulum ATPase
ER	Endoplasmic reticulum	SER/PRO	Serine/Proline
ERAD	Endoplasmic reticulum associated degradation	SER/THR	Serine/Threonine
ERC-55	ER calcium binding protein of 55 kDa	SSG	Secretory storage granule
ERES	Endoplasmic reticulum exit sites	SGRNA	Single guide RNA
ERGIC	ER-Golgi intermediate compartment	SIBLING	Small integrin-binding ligand N-linked glycoprotein
FAM	Family with sequence similarity	SN	Supernatant
FBS	Fetal bovine serum	V-SNARE	Vesicle soluble N-ethylmaleimide-sensitive factor attachment receptors
FGF23	Fibroblast growth factor 23	T-SNARE	Target soluble N-ethylmaleimide-sensitive factor attachment receptors
FJ	Four-jointed	SN	Supernatant
FJX1	Four-jointed box protein 1	V-SNARE	Vesicle soluble N-ethylmaleimide-sensitive factor attachment receptors
FT	Flow through	SN	Supernatant
GAP	GTPase activating protein	V-SNARE	Vesicle soluble N-ethylmaleimide-sensitive factor attachment receptors
GEF	Nucleotide exchange factor	T-SNARE	Target soluble N-ethylmaleimide-sensitive factor attachment receptors
GGA	Golgi-localized, γ -ear-containing, Arf-binding protein	SN	Supernatant
		V-SNARE	Vesicle soluble N-ethylmaleimide-sensitive factor attachment receptors
GLC	Glucose	T-SNARE	Target soluble N-ethylmaleimide-sensitive factor attachment receptors
GLCNAC	N-acetylglucosamine	SN	Supernatant
GPI-AP	Glycosylphosphatidylinositol anchored protein	V-SNARE	Vesicle soluble N-ethylmaleimide-sensitive factor attachment receptors
GRASP	Golgi reassembly stacking proteins	T-SNARE	Target soluble N-ethylmaleimide-sensitive factor attachment receptors
GS	Golgi stack	SN	Supernatant
GTP	Guanosine triphosphate	V-SNARE	Vesicle soluble N-ethylmaleimide-sensitive factor attachment receptors
HHD	Haily-Haily disease	T-SNARE	Target soluble N-ethylmaleimide-sensitive factor attachment receptors
HDR	Homology directed repair	SN	Supernatant
HS	Heparin sulfate	V-SNARE	Vesicle soluble N-ethylmaleimide-sensitive factor attachment receptors
IP₃	Inositol-1,4,5-triphosphate	T-SNARE	Target soluble N-ethylmaleimide-sensitive factor attachment receptors
IP₃R	Inositol-3-phosphate receptor	SN	Supernatant
IRE1	Inositol-requiring enzyme 1	V-SNARE	Vesicle soluble N-ethylmaleimide-sensitive factor attachment receptors
KD	Knockdown	T-SNARE	Target soluble N-ethylmaleimide-sensitive factor attachment receptors
KDA	Kilo dalton	SN	Supernatant
KDEL	Lysine-aspartic acid – glutamic acid - leucine	V-SNARE	Vesicle soluble N-ethylmaleimide-sensitive factor attachment receptors
KO	Knockout	T-SNARE	Target soluble N-ethylmaleimide-sensitive factor attachment receptors
LIMP2	Lysosomal integral membrane protein type 2	SN	Supernatant
LYZC	Lysozyme C	V-SNARE	Vesicle soluble N-ethylmaleimide-sensitive factor attachment receptors
MAN	Mannose	T-SNARE	Target soluble N-ethylmaleimide-sensitive factor attachment receptors
MAN6P	Mannose-6-phosphate	SN	Supernatant
MCS	Membrane contact site	V-SNARE	Vesicle soluble N-ethylmaleimide-sensitive factor attachment receptors

2 Summary

Effective intracellular protein trafficking and secretion is one of the crucial aspects of cell viability and cell-cell communication. Thus, nature evolved highly elaborated and finely tuned machineries to transport and sort proteins and membranes to their correct destinations. For this purpose, the trans-most part of the Golgi apparatus, the trans Golgi Network (TGN), functions as central sorting hub for the cell. Although for example the sorting and transport of transmembrane proteins is already well described, a mechanism for the sorting of soluble secretory cargo for secretion remained elusive for a long time.

In recent years, publications of our group could demonstrate that a sorting machinery consisting of three central components is required for the directional sorting of a subset of soluble, secretory cargo molecules: the actin-binding protein Cofilin 1 (CFL1), the TGN-resident calcium pump Secretory Pathway Calcium ATPase 1 (SPCA1) and the Calcium-binding Protein of 45 kDa (Cab45). Cell biological and biochemical assays revealed that dephosphorylated CFL1 interacts with a cytosolic loop of SPCA1 and recruits F-actin to TGN membranes. This interaction activates SPCA1 and stimulates calcium influx into the TGN lumen. The corresponding luminal increase in calcium concentrations enables the Golgi-resident Cab45 to sort and pack cargo molecules into transport carriers, however, the detailed mechanism underlying this process remained obscure. Therefore, this work was focused on structural and functional aspects of the Cab45 protein to gain detailed insights into the processes necessary for cargo secretion.

In the framework of this thesis, I was able to demonstrate that Cab45 reversibly assembles into oligomers, probably due to conformational changes in the presence of calcium *in vitro* and in isolated Golgi fractions. These Cab45 oligomers specifically bind secretory proteins directly, such as COMP and LyzC, in a calcium-dependent manner. Furthermore, tyrosine phosphorylation of cargo was demonstrated to abolish Cab45-cargo interaction and might serve as release mechanism under physiological conditions. Finally, also several Fam20C-dependent phosphorylation sites in Cab45 with so far unknown function were identified in this study.

Taken together, this thesis shed light on several aspects of the CFL1/SPCA1/Cab45 sorting machinery, including Cab45 Golgi retention, cargo interaction and posttranslational modifications and paved the way to a better understanding of secretion processes involved in a multitude of vital aspects of cellular function and life.

3 Introduction

3.1 The secretory pathway – the cellular protein highway

At the beginning of evolution first cellular structures consisted of only one membrane enclosed space. However, the development of more diverse and complicated organisms required the formation of compartments with different properties, concerning e.g. pH, salt concentrations or lipid compositions. One severe problem that arose out of this process was the translocation of proteins – the molecular machineries – across membranes and also between these membrane compartments called organelles. Nature overcame this difficulty by establishing a protein transport system – the secretory pathway ¹ (Figure 1). In highly developed cells the secretory pathway harbors and transports around one third of all cellular proteins ².

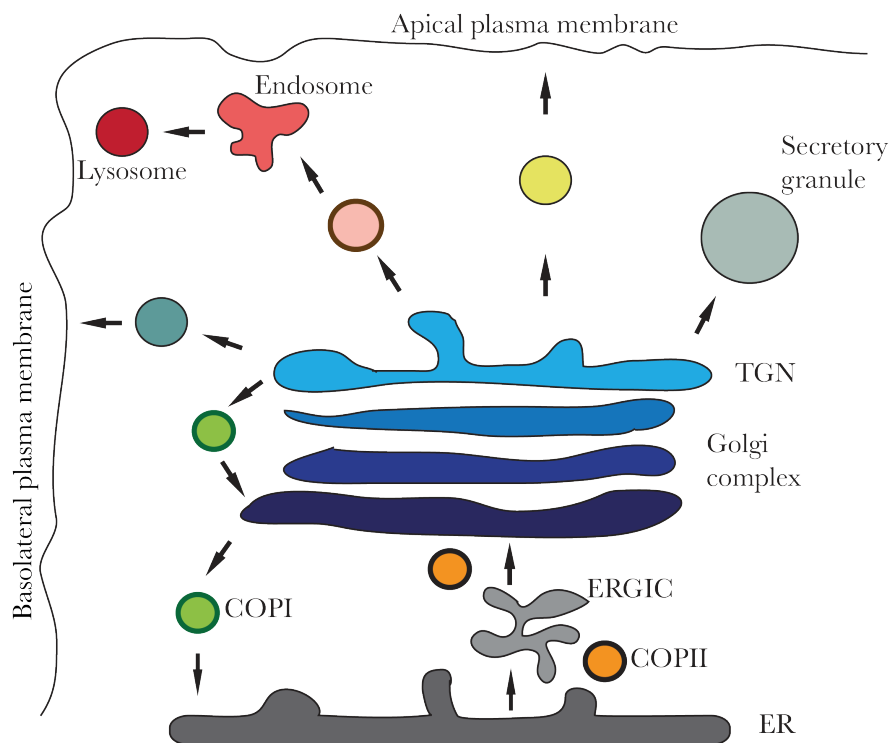


Figure 1: Schematic depiction of the secretory pathway. After cotranslational insertion into the endoplasmic reticulum (ER) lumen (grey), correctly folded proteins are transported in COPII coated vesicles (orange) across the ER-Golgi intermediate compartment (ERGIC, light grey) to the Golgi complex (blue). After traversing the different Golgi cisternae, proteins are sorted at the trans Golgi Network (TGN, light blue) by highly sophisticated mechanisms into a broad variety of transport carriers. These vesicles deliver the proteins to defined subcellular destinations including the apical and basolateral membrane (yellow and dark turquoise), endosomes (red), secretory granules (light turquoise), earlier Golgi cisternae (blue) or the ER (grey).

It ensures not only that all organelles contain their crucial set of proteins to fulfill their function, but also that the cell can communicate with its environment by uptake or release of proteins.

As this thesis is focused on the mechanisms of protein sorting at the Golgi apparatus, the introduction will describe the major organelles involved in this process, starting with the site of protein synthesis, the endoplasmic reticulum (ER) ³.

3.2 The endoplasmic reticulum

The endoplasmic reticulum (ER) is present in all eukaryotic cells. It is a membranous system which often comprises nearly 50 % of the whole cellular membranes and encloses around 10 % of the cell volume ⁴. This enclosed space – the ER lumen - provides a continuous sphere spanning the mammalian cell from the nuclear envelope (NE) to the plasma membrane (PM) ⁵ (Figure 2).

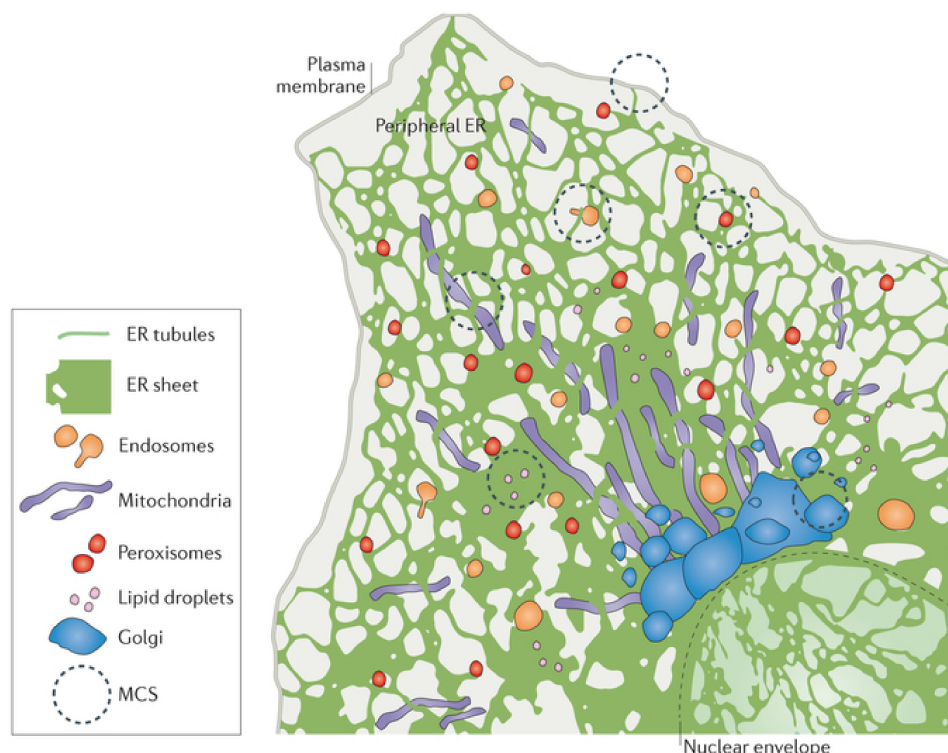


Figure 2: Schematic depiction of the endoplasmic reticulum and other endomembrane systems. In mammalian cells the ER spans the whole cell in a complex network of ER tubules and sheets (green). In addition, this network is highly intertwined with other endomembrane compartments like endosomes (orange), mitochondria (purple), peroxisomes (red), lipid droplets (rose) as well as the Golgi apparatus (blue) in the perinuclear region (nuclear envelope depicted by dashed line). With all those organelles, the ER forms membrane contact sites (MCS, dashed circles) for enhanced vesicle-independent exchange between the different compartments. Figure was adjusted from Phillips and Voeltz, 2016 ⁶.

The major structural elements of the ER are tubes of around 60 nm in diameter and sheets, which often appear in stacks and are connected by twisted membranes with helical edges ^{7,8}. This complete meshwork is highly dynamic and constantly subject to rearrangements like tubule branching, branchpoint sliding, tubule retraction, ring closure or tubule-tubule membrane fusion ^{9,10}. In mammals, many of these processes happen in close collaboration with the microtubule cytoskeleton ¹¹⁻¹³.

As one of the major secretory pathway compartments the ER is responsible for a multitude of different functions including protein synthesis, protein folding and quality control, protein modification and lipid biogenesis ¹⁴⁻¹⁸. To fulfil all these tasks, the ER subdivides into functional domains like the smooth ER (SER), the rough ER (RER), the transitional ER (TER), the nuclear envelop (NE) and membrane contact site (MCS) ¹⁹⁻²².

RER is defined by a high density of ribosomes on the surface ²³. As a consequence, RER consists mainly of sheet structures, because they offer enough space to accommodate large polysomes on their cytosolic surface ²¹. In contrast, the highly bend membranes of the tubules are often part of the SER, as ribosomes only rarely attached here. Cell lines producing high amounts of secretory or transmembrane proteins (like pancreatic or B cells) therefore prefer formation of RER or sheets ^{24,25}. Thus, the RER is the origin of basically all secreted proteins. Their first two steps towards the PM are signal particle recognition and translocation across the ER membrane – two highly sophisticated and regulated processes, which will be shortly summarized in the following.

3.2.1 Protein translocation across the ER membrane

In general, there are two different ways of protein translocation across the ER membrane. The first possibility is the cotranslational import of the polypeptide chain into the ER, the second is a posttranslational transport mechanism ^{26,27}. Which of these systems is preferred is dependent on the position of the so-called signal peptide (SP) inside the nascent polypeptide chain. The SP is a stretch of 16-30 amino acids with a hydrophobic core region of 6-12 amino acids flanked by positively charged residues ^{28,29}. In case the SP is located at the N-terminal end of the sequence, proteins are imported cotranslationally, while a SP at the C-terminus triggers posttranslational ER import ^{30,31}.

The N-terminal SP is recognized immediately after emerging the 60S subunit of the ribosome by the signal recognition particle (SRP), which binds to the hydrophobic core by several methionine residues in its p54 subunit ^{28,32,33} (Figure 3). This interaction arrests

protein translation, to provide the time necessary for the translocation of the ribosome-RNA-SRP complex to the ER surface²⁸.

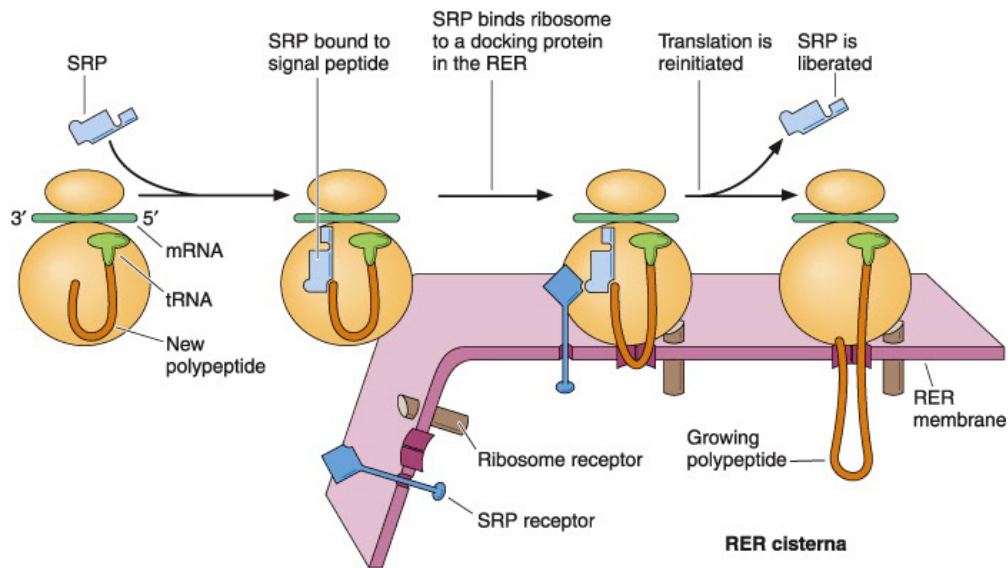


Figure 3: Cotranslational import is regulated by a complex machinery. In proteins destined for the secretory pathway the signal peptide (SP) is recognized by the signal recognition particle (SRP) when the new polypeptide chain (orange) emerges from the ribosome (yellow). While protein translation is arrested the whole ribosome/SRP complex is translocated to the rough ER membrane (RER, pink), where the SRP interacts with its receptor (SRP receptor, dark blue). Subsequently, translation is reassumed and the polypeptide is translocated across the membrane into the RER cisterna. Figure was obtained from dehistology.blogspot.de/2011/06/ribosomes.html 16.05.2017 21.40 p.m.

Here, the SRP interacts with the alpha subunit of the transmembrane signal recognition particle receptor (SR) and transports the ribosome-RNA-SRP complex to a huge pore complex called the translocon³⁴⁻³⁶. The central part of the translocon consists of the heterotrimeric protein complex Sec61p^{37,38} forming a gated channel in which 30 amino acids of the hydrophobic SP are directly inserted. Subsequently, SRP and SP dissociate from the complex in a GTP-dependent manner and translation of the protein directly through the translocon into the lumen of the ER is resumed³⁹. Inside the ER lumen, a cohort of enzymes including chaperones, isomerases and sugar modifying enzymes are responsible for proper folding and processing of the secretory pathway proteins.

For proteins with C-terminal signal sequence translation occurs entirely in the cytosol^{27,40}. The SP peptide emerging at the end of translation from the ribosome is bound by the TMS recognition/insertion complex 40 (TRC40) to prevent aggregation of the hydrophobic stretches and to keep the protein in an unfolded state for subsequent protein translocation^{27,41}. In a similar manner as for the cotranslational import, the Sec61p translocon machinery mediates the import and further processing of the proteins.

Recently, a high-content screen in *S.cerevisiae* revealed an additional pathway in parallel to the SRP and the TRC40 (GET pathway in yeast). The group of Maya Schuldiner showed that the three SRP-independent targeting proteins (SND proteins) act in a jointed pathway and preferentially target proteins with signal peptides located in the middle of the nascent polypeptide sequences for ER translocation⁴². Therefore, the SND pathway acts in synergy to the SRP and the TRC40/GET to facilitate ER targeting of proteins bearing signal motifs in all possible positions. If the human homolog of SND2 fulfills a similar task remains to be elucidated.

3.2.2 Protein modifications and processing after RER import

During the translocation process via the Sec61p channel the cell already starts to modify the polypeptide on the luminal side of the ER membrane (Figure 4). First, the SP is cleaved by the transmembrane signal peptidase, which associates tightly with the import pore complex^{43,44}. Hence, the SP is not part of the mature secretory pathway proteins. Secondly, many of the imported proteins gain a $\text{Glc}_3\text{Man}_9\text{GlcNAc}_2$ sugar modification *en bloc* at an Asn-X-Ser/Thr motif, which was previously assembled on a dolichol anchor at the ER membrane^{45,46}. This carbohydrate backbone subsequently enables the cell to track the folding state of the nascent polypeptide, because after removal of two glucose residues by glucosidase I, two chaperones of the lectin family namely calnexin and calreticulin are able to recognize and bind unfolded proteins and support their folding process^{16,47-49}. The chaperones do not only support the folding itself, but are also able to recruit additional enzymes like disulfide isomerases and peptidyl prolyl cis-trans isomerases to catalyze rate limiting steps along the way to a native protein conformation^{50,51}.

Throughout this folding process, nascent proteins are constitutively subject of glucose removal and addition by glucosidase II or UDP-glucose glycoprotein glycosyltransferase (UGGT), respectively^{52,53}. Removal of the glucose leads to dissociation of the chaperones and access to specialized export platforms for further transport to later secretory pathway compartments. However, proteins still exposing hydrophobic regions retrieve the glucose modification as indicator for a new cycle of protein chaperoning as well as ER retention⁵⁴. In case proteins are unable to fold after a certain period or accumulate in the ER lumen, the unfolded protein response (UPR) is initiated by the three transmembrane sensors PKR (dsRNA-dependent protein kinase)-like ER kinase (PERK), inositol-requiring enzyme 1 (IRE1) and activating transcription factor 6 (ATF6)⁵⁵⁻⁵⁷. The UPR upregulates proteins involved in chaperoning and ER associated degradation (ERAD) and reduces global

protein synthesis to prevent massive aggregates in the cell. During ERAD, unfolded ER proteins are translocated back into the cytosol via hydroxymethyl glutaryl-coenzyme A reductase degradation protein 1 (Hrd1), where oligosaccharide modifications are removed and U3 ligases add ubiquitin modifications, which mark the unfolded proteins for proteasome-mediated degradation in the cytosol⁵⁸⁻⁶⁰.

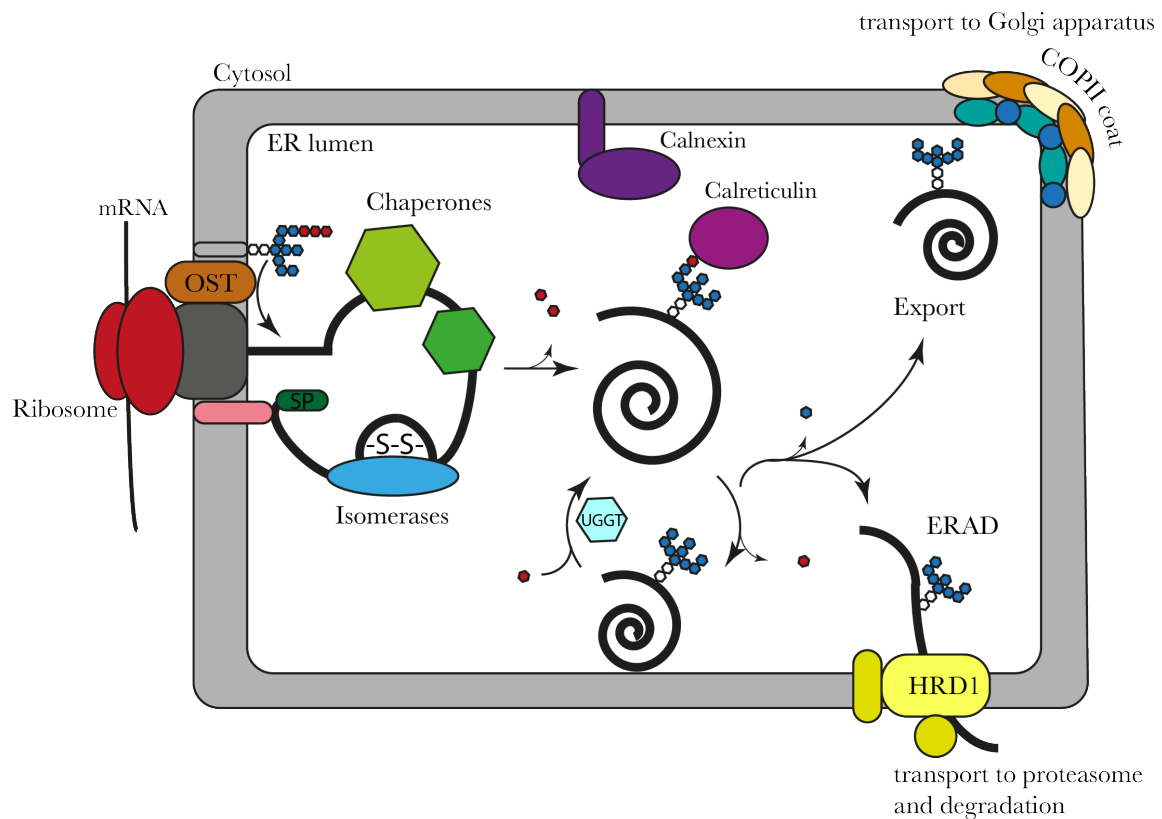


Figure 4: Schematic depiction of ER-dependent protein modifications. During protein translation by the ribosome (red), the growing polypeptide chain (black line) is translocated across the ER membrane (grey box). In the ER lumen, the oligosaccharyl transferase (OST, orange) transfers a sugar modification (white, blue and red hexagons) *en bloc* from a membrane-incorporated dolichol anchor onto the polypeptide chain. In addition, the signal peptide (SP, dark green) is cleaved off by the signal peptide peptidase (light red). In the following chaperones (green) and isomerases (blue) help the protein to fold properly. After removal of two glucoses (red hexagons) by glucosidases the two chaperones calnexin (purple) and calreticulin (pink) of the lectin family control the folding state of the protein by interacting with the remaining glucose. To achieve its native conformation the proteins runs through several cycles of trimming of this glucose modification and re-addition by UDP-glucose glycoprotein glycosyltransferase (UGGT, light blue). When the protein is either correctly assembled or needs to be degraded, one mannose residue (blue hexagon) is removed by mannosidases and the protein is either exported in COPII coated vesicles or is translocated by the ERAD machinery (yellow) into the cytosol for degradation in the proteasome. Figure was adjusted from McCaffrey et al., 2016⁵⁵.

3.2.3 ER to Golgi transport

Proteins which finally achieved their proper native conformation are exported from the ER at stable ER exit sites (ERES) in COPII coated vesicles^{61,62} (Figure 5). ERES are part of the TER (section 3.2) and several hundreds of them are found per mammalian cell⁶³. The

Introduction

first step in ERES formation is the activation of the small GTPase Sar1 by its transmembrane GTP activating protein (GAP) Sec12⁶⁴⁻⁶⁶. Upon activation Sar1 exhibits an amphipathic helix, which is inserted in the outer leaflet of the ER membrane to anchor the protein⁶⁷. In the next step Sar1 recruits the heterodimer Sec23/Sec24 by direct interaction with Sec23 to the ER membrane, which forms the first layer of the COPII coat. Sec24 exhibits multiple cargo binding sites and recognizes a multitude of different cargo receptors and accumulates them inside the forming vesicle at ERES for efficient export to the Golgi⁶⁸⁻⁷¹.

The three main ER cargo receptor families (ERGIC-53, p24 and Erv proteins) known to date contain Sec24 and COPI recognition sites within their cytoplasmic domains⁷². This feature enables the receptors to cycle back and forth between the ER and post-ER compartments like the ERGIC or the cis Golgi (section 3.3 and 3.4.1) and release their attached cargo in the acceptor compartment, probably due to changes in environmental conditions like pH or calcium concentrations⁷³. While for example the lectin ERGIC53 recognizes carbohydrate modifications and protein sequences of soluble proteins, Erv proteins interact with type II membrane proteins and connect them to the COPII coat for efficient transport^{74,75}. However, exact recognition signals and mechanisms need to be further investigated for all types of ER sorting receptors.

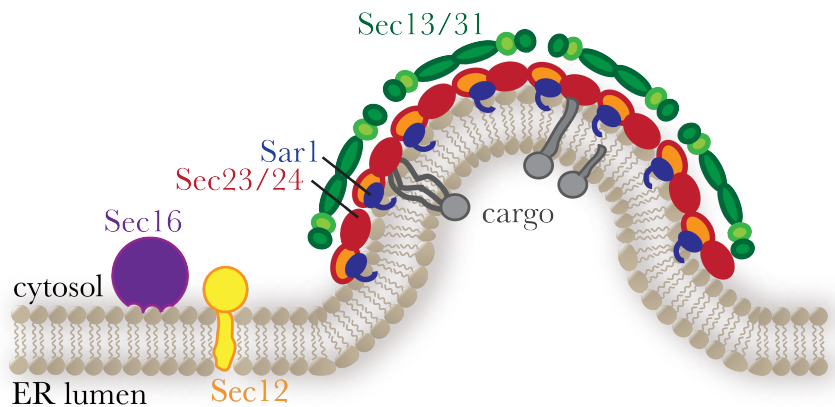


Figure 5: Schematic depiction of COPII vesicle formation at ER exit sites (ERES). Cargo proteins (grey) which reached their native conformation in the ER lumen are exported at ERES in COPII coated vesicles for transport to the Golgi apparatus. Therefore, the small GTPase Sar1 (dark blue) is activated by Sec12 (yellow/orange) and stabilized by Sec16 (purple). This activation recruits first the inner Sec23/24 (red) layer, which binds transmembrane cargos or their specific receptors and accumulates them inside the forming vesicles. Subsequently, the outer coat consisting of Sec13/31 (green) is recruited, which induces membrane curvature for pinching of the COPII vesicle. Figure was adjusted from Gillon et al., 2012⁷⁹.

When the cargos are attached via the receptors to the inner coat components, Sec23/Sec24 bind the heterotetrameric Sec13/Sec31 complex of the outer COPII coat,

which induces membrane curvature necessary to bud the vesicle from the ER membrane. After vesicle release the newly formed vesicle soon uncoats due to GTP hydrolysis by Sar1 to uncover its soluble N-ethylmaleimide-sensitive factor attachment receptors (SNAREs)⁷⁶. These vesicle SNAREs (v-SNAREs) interact with target SNAREs (t-SNAREs) and mediate the fusion of the vesicle with the correct acceptor compartment – in this case the ER-Golgi intermediate compartment^{77,78}.

3.3 The ER-Golgi intermediate compartment

The ER-Golgi intermediate compartment (ERGIC) is located between the ER and the Golgi apparatus and considered as the first anterograde/retrograde sorting station of the secretory pathway of mammalian cells (Figure 1). It consists of independent tubulovesicular membrane clusters distinct from ER or Golgi which are positive for the transmembrane lectin cargo receptor ERGIC-53 and for COPI coat proteins⁸⁰⁻⁸⁵.

The ERGIC is necessary to distinguish proteins destined for anterograde traffic to the Golgi from proteins for ER return^{86,87}. This differentiation is achieved by cargo receptors cycling between the three compartments, like the KDEL receptor, which mediates ER retention of ER-resident proteins⁸⁸. In contrast, proteins of the late secretory pathway pass the ERGIC and arrive at the central protein sorting station – the Golgi complex⁸⁹.

3.4 The Golgi complex

The Golgi complex or Golgi apparatus is one of the most prominent organelles in a mammalian cell and with a size ranging between 0.7 to 1.1 μm big enough for analysis by light microscopy⁹⁰⁻⁹². As a consequence, the Italian physician Camillo Golgi, the eponym of the Golgi apparatus, was the first to discover and describe the structure in nerve cells already at the end of the 19th century^{93,94}. But although fundamental advances in the area of electron and light microscopy contributed immensely to our understanding, many questions about Golgi organization, function and vesicular transport processes remain unanswered to this point⁹⁵⁻¹⁰¹.

3.4.1 Golgi structure

The Golgi complex is a membranous organelle present in all eukaryotic cells, including animals, plants, fungi and yeast. In mammalian cells the observed conglomerate of large

Introduction

vacuoles, small granules and lamellae is arranged in several flat cisternae that form tightly packed stacks ¹⁰⁰ (Figure 6). Dozens of these stacks accumulate in the supra- or juxtannuclear region and are interconnected by homo- or heterotypic membrane bridges. These can either form between two cisternae within one stack or also connect cisternae of adjacent Golgi stacks ¹⁰²⁻¹⁰⁸. This interconnected network is called Golgi ribbon ^{102,109}. Within the stacks, single cisternae are not equal, but can be classified according to their protein and lipid content. Thereby, the most commonly used system for classification is based on the position of the cisternae inside the stack and divides the tubules and membrane sacks into cis Golgi Network (CGN), cis Golgi, medial Golgi, trans Golgi and trans Golgi Network (TGN) ^{110,111}. Furthermore, it was suggested to categorize the different cisternae according to their vesicular import and export systems, which reflects more adequately the connection to their individual function ¹¹².

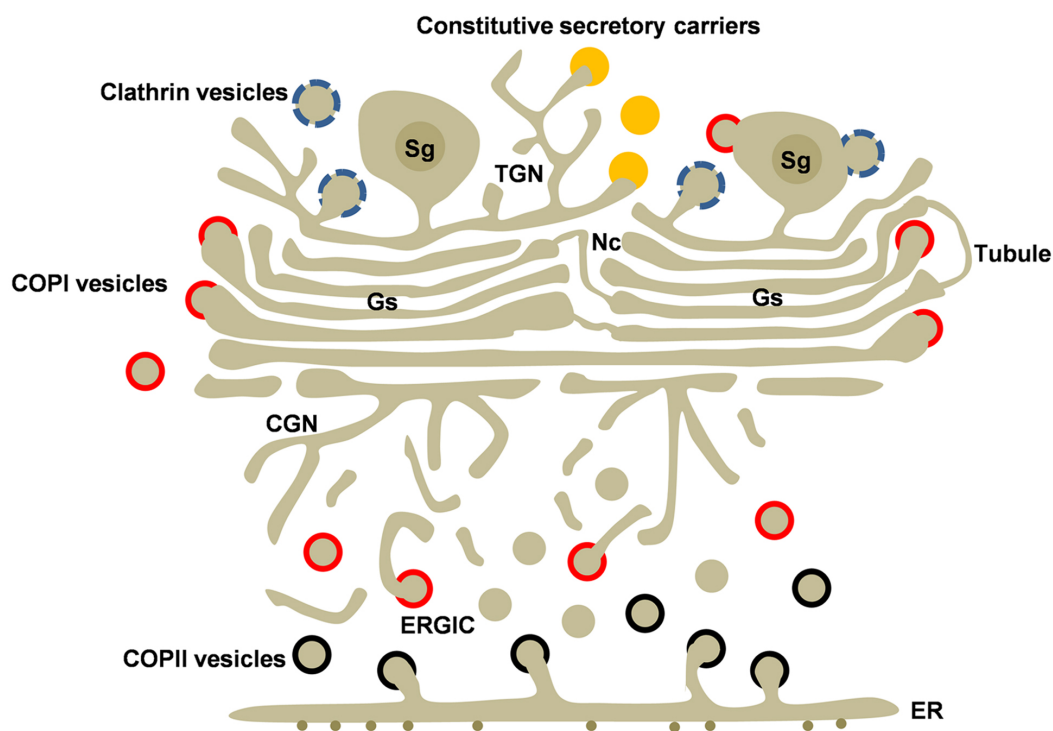


Figure 6: Schematic depiction of the highly dynamic Golgi structure. Proteins of the secretory pathway travel from the endoplasmic reticulum (ER) in COPII coated vesicles (black rimmed circles) via the ER-Golgi intermediate compartment (ERGIC) to the cis Golgi Network (CGN). Then they traverse the Golgi cisternae (light brown) before the arrive at the trans Golgi Network (TGN), where they are sorted in different transport carriers like clathrin vesicles (blue rimmed circles), constitutive secretory vesicles (yellow circles), secretory granules (Sg) or COPI vesicles (red rimmed circles). Inside the Golgi cisternae, proteins gain different modifications and sorting signals. To manage this crucial task and to guarantee fast and efficient transport the Golgi cisternae are tightly compressed into a Golgi stack (Gs). In addition, cells harbor more than one stack in the perinuclear region, which are laterally connected by homotypic or heterotypic membrane bridges in the non-compact zone (Nc). Figure was adjusted from Martinez-Alonso et al., 2013 ¹¹³.

Maintaining either the position of the Golgi within the cell as well as its stacked morphology the Golgi is dependent on a multitude of interactions with its protein environment. These interactions are mediated in large part by a protein network surrounding the Golgi like tentacles called the Golgi matrix^{114,115}. The major component of this Golgi matrix are proteins of the Golgin family¹¹⁶. Golgins contain several cytosolic coiled-coil domains and are anchored in the Golgi membrane either by transmembrane domains or by interaction with small GTPases like Arl1 or Arf1 via GRIP and GRAP domains, respectively. The long and flexible domains extend into the cytosol and support processes like vesicle capture and fusion by interaction with the small Rab GTPases as well as interaction with cytoskeleton dependent motor proteins¹¹⁷⁻¹²⁰. In addition, Golgins collaborate with GRASP proteins to establish the Golgi ribbon and the stacked morphology of the Golgi. GRASP65 and GRASP55 are both peripheral membrane proteins that are attached to the cytosolic Golgi membranes via an N-myristoylation anchor¹²¹⁻¹²³. The conserved N-terminal GRASP domains form trans-oligomers, which serve as proteinaceous bridges between adjacent cisternae and link them together. During mitosis, the C-terminal Ser/Pro-rich domains of GRASPs are phosphorylated by mitotic kinases which induces dissociation of the oligomers and unstacking of the Golgi¹²⁴⁻¹²⁶. Based on this multitude of interactions a tremendous amount of possible modifications renders the Golgi a highly dynamic compartment, which can rapidly adjust to environmental changes and cellular requirements.

3.4.2 Golgi functions and intra Golgi transport

The stacked shape of the Golgi is ideally adjusted to fulfil the main functions – protein and lipid transport, protein sorting, protein and lipid modifications and production of complex carbohydrates. Although the stacked morphology slows protein transport, the small gaps between the stacks minimize transport distances and energy consumption and enable the cell to coordinate consecutive posttranslational modifications (PTMs) by a cohort of enzymes, which localizes exclusively to certain cisternae, each offering certain conditions for optimal enzymatic reactions¹²⁷. However, this morphology also poses the problem of constant protein transport across the cisternal membranes. Although a couple of possible scenarios are discussed in literature, leading scientists of the field agreed in 2009 that the cisternal progression/maturation model is able to accommodate most of the recent findings and results¹²⁸⁻¹³¹. This idea of Golgi protein trafficking suggests that new cis Golgi cisternae arise by homotypic fusion of ER-derived COPII vesicles. These cis Golgi

cisternae gradually mature into medial and trans cisternae and finally disintegrate into different kinds of transport carriers at the TGN. During this process COPI coated vesicles are responsible to maintain the asymmetric distribution of Golgi-resident proteins by retrograde transport to younger cisternae.

Based on this, proteins enter the Golgi at the cis cisterna, pass the medial Golgi and finally arrive at the trans Golgi cisternae, whose trans-most cisterna is connected to the tubular network of the TGN. Here, they get packed into diverse carriers for transport to their final subcellular destination or for secretion. This stepwise transport offers also the possibility to add posttranslational modifications to proteins on their way through the stack. But which modifications are necessary for secretory pathway proteins and how are they connected to the transport mechanisms?

3.4.3 PTMs in the Golgi

Several kinds of PTMs were described in connection with the Golgi. They can either occur at the cytoplasmic side of the Golgi membrane or inside the lumen and can either directly influence trafficking by modifying cargo proteins or indirectly by changing Golgi function and morphology. Therefore, it seems not surprising that mutations in corresponding genes were connected to a variety of different diseases in human patients ¹³². Although this was also true for PTMs like acetylation ^{133,134}, sulfation ^{135,136}, methylation ¹³⁷, palmitoylation ¹³⁸ and proteolytic cleavage ¹³⁹ the next two sections are focused on glycosylation and phosphorylation, as both PTMs are directly connected to this work.

3.4.3.1 Glycosylation in the Golgi

Approximately 80 % of all secreted or membrane proteins receive covalently linked carbohydrate chains on their travel through the secretory pathway ¹⁴⁰. Hence, glycosylation is one of the most frequent and most important PTM in mammalian cells. The most significant modification in this context is N-linked glycosylation as this process is involved in the regulation of crucial cellular mechanisms like ER quality control, the UPR, ERAD, migration and adhesion as well as transport and sorting.

As already described above, secretory pathway proteins receive a preassembled carbohydrate modification during entry into the ER lumen (section 3.2.2 and Figure 4). This is used in the following to ensure proper folding of the proteins. When the native state is achieved ER mannosidase I removes one mannose residue (“trimming”), which functions as a signal for ER-Golgi export (Figure 4). In the Golgi, the different cisternae house Golgi

mannosidases and transferases in a specific succession. These cycles of trimming and processing provide a multitude of possibilities how the sugar backbones can be arranged and, as a consequence, also many opportunities to fine-tune cellular processes like protein-protein interactions or protein stabilization and turnover ^{140,141}. Taken together sugar modification influence immensely overall Golgi function and trafficking and are critical players in the maturation of secretory pathway proteins.

3.4.3.2 Phosphorylation of secretory pathway proteins

Phosphorylation is the key mediator of cellular signal transduction. Furthermore, it extends the functionality of proteins inside and outside the cell. Therefore, phosphate modifications on substrates can influence multiple crucial processes like metabolism, transcription, cell cycle progression, cytoskeletal rearrangement, cell movement, apoptosis and differentiation ¹⁴²⁻¹⁴⁶. In order to master all these challenging tasks, 1.7 % of human genes encode the human “kinome”, which corresponds to more than 500 kinases ¹⁴⁷. Although the first hints concerning protein phosphorylation were already detected by Hammersten at the end of the 19th century in the secreted milk casein protein, kinases localizing to the secretory pathway remained elusive for more than 100 years ¹⁴⁸. Finally, the *D.melanogaster* protein Four-jointed (Fj) was shown to exhibit kinase activity on the extracellular cadherin domains of the Dachshous protein ¹⁴⁹. Nonetheless, the number of secretory pathway kinases remains small to date and is subject to ongoing research.

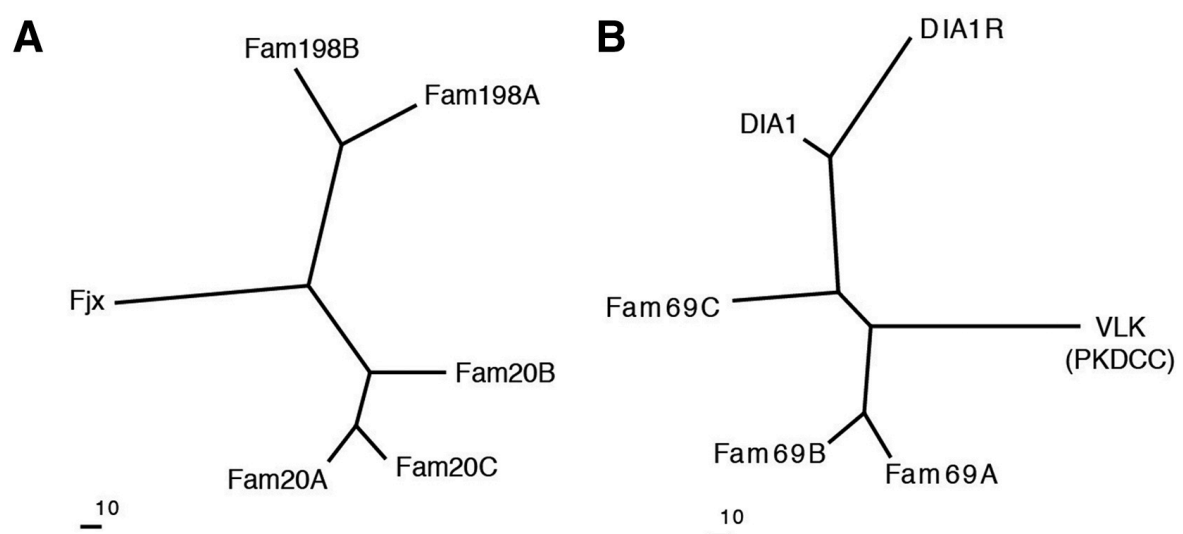


Figure 7: Phylogenetic trees for secretory pathway kinases. Phylogenetic trees show relationships of Fam20C (A) and TPK-PKDCC/VLK (B) to their respective family members. Trees were built with MOLPHY using distances (-J option) calculated from an alignment of representative human proteins. (Fjx, four-jointed box 1; DIA1, Deleted in Autism 1; DIA1R, DIA1-related). Figure originates from Tagliabracci et al., 2015 ¹⁵⁰.

3.4.3.2.1 Fam20C and the Fjx family of secretory pathway kinases

The human homologue of Four-Jointed Box protein 1 (Fjx1) was the first member of the Fjx1 family of protein kinases (Figure 7A). The six members of this family Fjx1, Family with sequence similarity 20 A (Fam20A), Fam20B, Fam20C and Family with sequence similarity 198 (Fam198A) and Fam198B belong to the 40 atypical human kinases, because they contain a protein kinase like (PKL) fold instead of the canonical motif in the eukaryotic protein kinase catalytic domain^{147,151}. All of them localize to the secretory pathway, though only Fjx1 and Fam198B contain a transmembrane domain with their catalytic domains facing the Golgi lumen^{149,152}. The other members are considered as soluble proteins, as no transmembrane domains are known¹⁵².

Member C of the Fam20 kinases was identified in 2012 as the physiological casein kinase¹⁵². Fam20C is ubiquitously expressed, although especially high in mineralized tissues^{153,154}. In addition to the conserved structural features mentioned above, Fam20C contains predicted disulfide bonds and three N-glycosylated asparagine residues. These sugar modifications were shown to be crucial for protein folding and stability and as a consequence also for kinase activity^{150,152}. Besides a remarkable resistance to the broad-spectrum kinase inhibitor staurosporine and a preference for manganese as divalent cation, Fam20C exhibits autophosphorylation *in vitro*, which seems not to be essential for kinase activity and secretion^{149,150,152}.

Although initially especially proteins involved in biomineralization were designated as Fam20C targets, recent mass spectrometry based screens in combination with GO Term analysis identified more than 100 proteins, which are involved in wound healing, lipid homeostasis, endopeptidase inhibitor activity, cell adhesion and cell migration¹⁵⁰. These targets were mainly phosphorylated at a serine residue inside an S-X-E/pS or an S-X-Q-X-X-D-E-E motif^{150,152,155}. This and other studies prove that Fam20C generates a majority of the secreted phosphoproteome¹⁵⁶⁻¹⁵⁸, including targets like the fibroblast growth factor 23 (FGF23), small integrin-binding ligand N-linked glycoprotein (SIBLING) proteins and osteopontin^{149,150,152,159,160}.

Mutations of Fam20C in humans cause a severe autosomal recessive osteosclerotic bone dysplasia known as Raine syndrome¹⁶¹. The crystal structure of *C.elegans* Fam20C indicates that these Raine syndrome associated mutations cause impaired substrate binding¹⁶². Finally, recent reports about Fam20A regulating secretion and kinase activity of Fam20C linked the kinase also to amelogenesis imperfecta, a disease causing improper enamel formation in teeth¹⁶³⁻¹⁶⁵.

3.4.3.2.2 Tyr phosphorylation by extracellular tyrosine-protein kinase PKDCC

Extracellular tyrosine-protein kinase PKDCC (in the following TPK-PKDCC) is the human homolog of mouse vertebrate lonesome kinase (Vlk). The first description of Vlk by Kinoshita and colleagues in 2009 opened the long-expected research field for secreted tyrosine kinases of the secretory pathway ¹⁶⁶ (Figure 7B). TPK-PKDCC is highly conserved in vertebrates, however, no invertebrate homologs were detected so far ¹⁶⁷. It is distantly related to the poorly characterized Family with sequence similarity 69 A to C (Fam69), Deleted in Autism-1 (DIA1) and DIA1-related, but not to Fam20 proteins, which indicates that the two families of secretory kinases developed independently of each other and not from a primordial secreted kinase ^{168,169}.

As indicated above, TPK-PKDCC is a soluble tyrosine kinase, which localizes to the Golgi as well as the ECM and was shown to phosphorylate several resident or secreted proteins throughout the secretory pathway in an ATP-consuming manner ^{169,170}. It contains a characteristic N-terminal SP for ER import, but the canonical DFG HRD motif in the catalytic C-terminal domain is replaced against other functional residues ¹⁵¹. Furthermore, TPK-PKDCC exhibits several glycosylation sites and an autophosphorylated tyrosine residue, however, modification of this residue seems not to be involved in kinase activity or secretion ¹⁶⁹. In contrast, indeed necessary for its activity is the presence of calcium and magnesium as divalent cations, because manganese only poorly supports the kinase activity of TPK-PKDCC ¹⁶⁹. But although several targets of TPK-PKDCC are known, including matrix metallo proteinases (MMPs), no consensus pattern for target phosphorylation could be determined to date ¹⁶⁸.

TPK-PKDCC/Vlk activity was linked to several pathobiological processes. For example, experiments conducted in mice revealed the involvement of the kinase in tissue morphogenesis and organogenesis ^{166,171}. In addition, Vlk null mice showed defects in long bone and lung formation ¹⁷². In trabecular meshwork cells secreted proteins phosphorylated by VLK controlled cell shape, actin stress fibers and focal adhesion formation¹⁷⁰. Interestingly, overexpression of the wild type kinase or a kinase dead mutant caused delayed transport of a viral protein in NIH3T3 cells from Golgi to PM, although the detailed mechanism remained elusive ¹⁶⁶. Nonetheless, this last observation already indicates that phosphorylation is closely linked to protein sorting and secretion. However, which other factors are important for efficient Golgi function and, as a consequence, organized protein sorting and transport?

3.4.4 Calcium in the secretory pathway

The divalent cation calcium governs all aspects of cellular life. Therefore, cells put high effort in controlling calcium influx and efflux processes by a cohort of pumps, channels, transporters and buffering proteins. So far, one of the most important aspects of secretory pathway function was neglected in this introduction, as the secretory pathway components, especially the ER, are the major regulators of intracellular calcium signaling ¹⁷³.

In general, cells try to uphold a steep gradient between extracellular calcium (in mM area) and a very low cytosolic calcium concentration 50 – 100 nM ^{174,175} (Figure 8). This characteristic enables the cell to signal extracellular stimuli to the cell interior by small changes of cytosolic calcium levels. The calcium necessary for this change is released from internal stores, mainly the secretory pathway, but also other organelles like peroxisomes and mitochondria ¹⁷⁶. This system requires active, energy-consuming transport of calcium ions out of the cytosol into the lumina of the secretory calcium compartments and the organelles when no calcium signal is required.

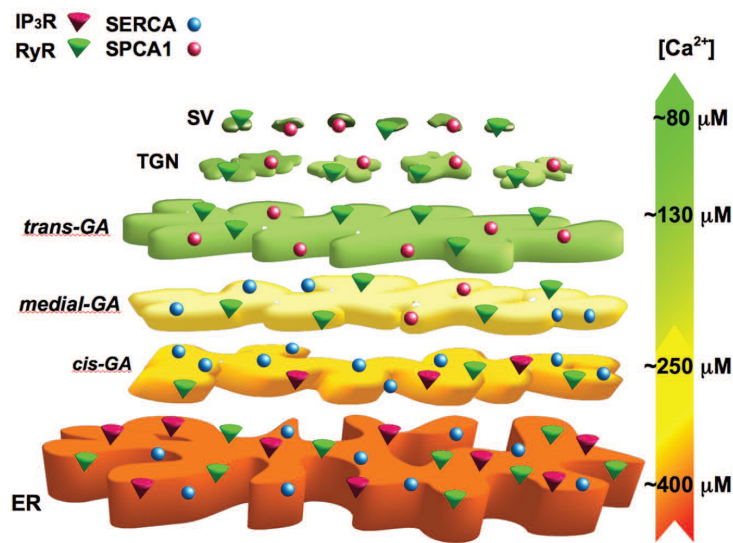


Figure 8: Calcium gradient and homeostasis at the Golgi apparatus (GA) is maintained by several players. Calcium concentrations inside the secretory pathway decline gradually from around 400 μM in the ER to around 80 μM in vesicles (SV). These concentrations are regulated by the two calcium pumps SERCA (blue circles) and SPCA1 (red circles) and by the release channels IP₃ receptor (IP₃R; red cylinders) and Ryanodine receptor (RyR, green cylinders). The figure depicts the assumed distribution of channels and pumps along the secretory pathway. Figure originates from Pizzo et al., 2010 ¹⁷⁷.

But not only the differences in concentrations between the inside and the outside of the cell are vital for calcium homeostasis, but also a gradient across the secretory pathway itself ¹⁷⁸. According to fluorescence-based calcium sensors, the ER houses calcium concentrations of about 400 μM , while concentrations gradually decrease across the Golgi from 250 μM in cis Golgi, to around 130 μM in trans Golgi and 80 μM in secretory vesicles ¹⁷⁹⁻¹⁸². However, absolute numbers vary according to cell line and technique used in the studies. Although, for a long time only the ER was considered as the main calcium release organelle, also the Golgi apparatus contains all elements, namely calcium pumps,

transporters and binding proteins (see below), to act as a *bona fide* calcium store and gains more and more importance in intracellular calcium signaling¹⁸³⁻¹⁸⁶.

3.4.4.1 Calcium pumps

A well-studied aspect of calcium transport is the active pumping of the cation across the membranes. Three mammalian calcium pumps of the P-type ATPases are described to guarantee calcium homeostasis of the cytosol: (1) the Sarcoplasmic/endoplasmic reticulum ATPase (SERCA), (2) the Secretory Pathway Calcium ATPase (SPCA) and (3) Plasma Membrane Calcium ATPase (PMCA). As indicated by their names, all pumps are integrated into certain membranes and pump calcium in an ATP-consuming manner into the lumen of the ER, the Golgi or into the extracellular space, respectively. However, the localization of SPCA and SERCA partly overlaps in the Golgi, i.e. SERCA also contributes to calcium influx at the cis Golgi cisternae, while SPCA is more accumulated in the medial and trans Golgi membranes¹⁸⁴⁻¹⁸⁶. The contributions of both ATPases on total calcium influx varies in different cell lines.

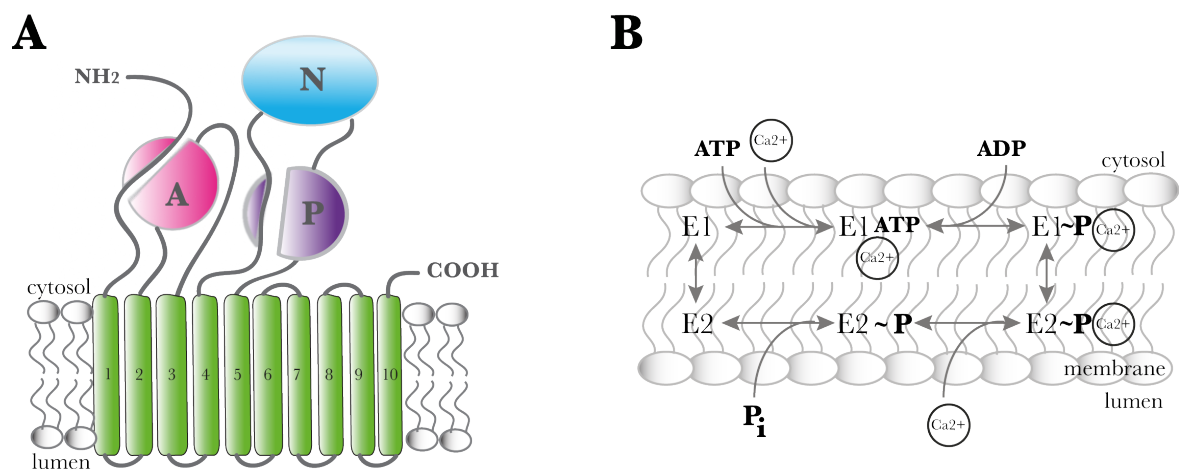


Figure 9: Structure and reaction scheme of calcium pump P-type ATPases using the example of SPCA1. (A) Cartoon of SPCA1 structure depicts domain structure of the Golgi-resident ATPase calcium pump. The cytosolic loops contain the actuator domain (A, pink), the nucleotide binding domain (N, blue) and the phosphorylation domain (P, purple), which assemble in the three-dimensional structure of the protein. The ten TM domains (green, Arabic numerals) bind the calcium ion for transport between domain 4 and 6. (B) Simplified reaction scheme of calcium transport across the membrane by P-type calcium pumps. In the high calcium affinity state E1 the pump binds calcium from the cytosolic side inside the membrane. ATP hydrolysis and attachment of phosphate to a highly conserved aspartic acid residue in the regulatory P-domain switches the pump to a low calcium affinity state E2. The whole process is accompanied by major structural changes in the protein. This drop in affinity leads to release of the calcium ion at the luminal side of the membrane. Part of the figure was adjusted from Brini et al., 2009¹⁹¹.

Several key architectural features are shared by the three proteins. They are all single subunit integral membrane proteins with ten TM domains and large cytosolic loops (Figure

9A). The cytosolic head groups contain a nucleotide binding (N) domain for ATP binding, a phosphorylation (P) domain, which becomes phosphorylated on a catalytic asparagine residue in an ATP-dependent manner, and an actuator (A) domain, which catalyzes dephosphorylation of the P domain after completed cation transport. The critical catalytic amino acid is part of the highly conserved **SDKTGTLT** sequence and mutations abolished calcium transport activity in yeast ¹⁸⁷.

The structural similarities pave the way to a common mode of action for calcium transport across the membranes, although some details of this process still remain to be elucidated ^{188,189} (Figure 9B). First, the pumps bind calcium ions at the cytosolic interface with high affinity (so called E1 state). Subsequently, the conserved asparagine residue is phosphorylated by hydrolysis of ATP (ADP sensitive state). This phosphoenzyme intermediate occludes the cations and undergoes a rate-limiting step towards the low-energy E2 state, which includes major conformational changes either of the cytosolic as well as six of ten transmembrane domains (ADP insensitive state). In this condition, calcium is released into the lumen or the ECM and the pumps are dephosphorylated by the actuator domains in the presence of water for regeneration of the enzymes (transition of E2 back to E1 state). Then a new cycle of transport can occur ¹⁹⁰.

This process enables SERCA to transport two calcium ions across the membrane, because it contains 2 calcium binding sites between TM domain M5 and M8 (site I) and between M4 and M6 (site II). However, due to point mutations SPCA and PMCA lack one of the crucial oxygen atoms, which disrupts calcium binding site I ¹⁹²⁻¹⁹⁴. Therefore, SPCA and PMCA transport calcium only with a stoichiometry of 1:1 instead of 2:1 observed for SERCA ^{188,189,194,195}. Nonetheless, SPCA exhibits the highest calcium affinity with a dissociation constant around 10 nM, probably necessary because SPCA transition from E1 to E2 is retarded. Another difference between the three pumps is the fact that SERCA and PMCA, but not SPCA, countertransport protons during calcium translocation. This is probably due to the poor conservation of necessary, protonable residues in SPCA1 and also the fact that some proteins inside the Golgi lumen are dependent on the presence of protons for proper activity ^{189,196,197}.

The ubiquitously expressed SPCA1 (encoded by up to four splice variants of ATP2C1) is highly conserved in *C.elegans*, *D.melanogaster*, *S.cerevisiae*, mammals and humans ¹⁹⁸⁻²⁰¹ and is therefore considered as house keeper variant of this protein. In contrast, the expression of SPCA2, is much more restricted and mainly found in mucus-producing cells like in the gastrointestinal tract, rectum, trachea, salivary gland, thyroid gland, keratinocytes, prostate tissue, mammary gland and brain testis ^{195,202,203}.

As already outlined above SPCA1 localizes to the Golgi compartment and regulates luminal calcium concentrations in synergy with SERCA (Figure 8). In epidermal keratinocytes SPCA1 is highly abundant and in this cell line up to 70 % of whole Golgi calcium is dependent on SPCA1 activity^{204,205}.

A unique feature of SPCA1 is the efficient transport of not only calcium, but also manganese into the Golgi lumen^{188,189}. Although manganese acts cytotoxic in high concentrations in the cytosol, several enzymes in the Golgi including mannosyl and fucosyl transferases and the Fam20C kinase^{152,206,207} need the cation for proper activity^{188,189,195,202,203,208-210}.

But what is the physiological relevance of SPCA1-dependent luminal calcium? A variety of mutations in one allele of ATP2C1 were connected to a disease called Familial benign chronic pemphigus (OMIM 16960) or Haily-Haily disease (HHD)^{211,212}. Reduced Golgi calcium content due to impaired SPCA1 activity caused acantholysis of epidermal cells, erosions and blistering of skin in human patients^{198,213}. These observations underline the importance of SPCA1-dependent calcium homeostasis at the Golgi.

3.4.4.2 Calcium release channels of the Golgi

Since the discovery of the SERCA calcium pump in the 1960s the question arose, how calcium is released from the secretory pathway compartments^{214,215}. In the past decades, several studies proved that calcium can be released from the ER upon extracellular stimuli by Inositol-1,4,5-triphosphate (IP₃)^{182,216} (Figure 8). Therefore, heterotrimeric G protein-coupled receptors are activated by ligand binding to their extracellular domains. This interaction activates the cytosolic G protein, which binds via its alpha domain to phospholipase C (PLC). PLC catalyzes the cleavage of phosphatidylinositol-4,5-bisphosphate (PIP₂) to diacylglycerol (DAG) and IP₃. Subsequently, IP₃ then opens the IP₃ receptor (IP₃R) channels in the membrane of the ER and calcium is released into the cytosol where it acts as secondary messenger²¹⁷⁻²²⁰.

However, the question of calcium release from the Golgi remained unanswered for several more years. Finally, in 1998 Pinton and colleagues presented data on the existence of the IP₃ release channels in the Golgi membranes by a calcium sensitive photoprotein¹⁸⁴. This finding was further supported by immunofluorescence analyses performed during studies on the calcium binding protein CALNUC (section 3.4.4.3) in the lab of Marilyn Farquhar¹⁸⁵. Lin and colleagues were able to show that IP₃Rs localize to the Golgi and the ER and that calcium can be released from these compartments in an IP₃-dependent manner. In

addition, the observations that ryanodine receptor (RyR) channels were absent from Golgi membranes as well as the lack of reports that other established release factors like cyclic adenosine diphosphate ribose (cADPR) or nicotinic acid adenine dinucleotide phosphate (NAADP) can trigger calcium release, strengthened the opinion that IP₃R channels are the only release mechanism^{186,221}. In contrast, a publication of 2001 proposed the Golgi as a RyR sensitive compartment and a putative role in intracellular calcium signaling in rat sympathetic neurons²²². Furthermore, caffeine stimulation of neonatal cardiac myocytes resulted in calcium release especially of the trans Golgi¹⁸¹.

In summary, the possibilities of calcium release from the Golgi compartment need further investigation. For example, questions concerning the correlation between SPCA/SERCA and RyR/ IP₃R channel expression, the proportional contributions of the mechanisms on overall calcium signaling or the influence of calcium waves on the enzymatic activity of Golgi resident proteins need to be addressed in the future²²³.

3.4.4.3 Calcium binding proteins in Golgi

The last critical component necessary to define the Golgi as a *bona fide* intracellular calcium store are luminal calcium binding proteins that bind the free cation and function as buffering system²²¹. In contrast to the multiple ER-resident calcium binding proteins, only the four proteins nucleobindin 1 (Nucb1), nucleobindin 2 (Nucb2), Calcium binding protein of 45 kDa (Cab45) and calumenin (CALU) were so far associated with the Golgi lumen²²⁴⁻²²⁷.

Nucb1 (also known as CALNUC) and Nucb2 (also known as p54/NEFA) are highly conserved and share 61 % sequence homology²²⁸. Both proteins contain two canonical EF hand motifs, a consensus pattern responsible for calcium binding, first identified in parvalbumin and named after the E and F loop of its crystal structure²²⁹⁻²³¹ (Figure 10). Structural analysis by Circular dichroism (CD) revealed that calcium binding induces conformational changes in the secondary structure of Nucbs to a more α -helical fold, while the EF hand remains unstructured in the absence of the cation²³⁰⁻²³². Furthermore, the same studies also showed that the two EF hand motifs bind calcium with different affinities in both Nucbs. An additional prove that Nucbs indeed contributes to in intra-Golgi calcium homeostasis is the observation by Lin and colleagues that HeLa cells overexpressing Nucb1 were able to store 2.5-fold more calcium inside the Golgi than comparable wild type cells¹⁸⁵.

Finally, in contrast to the soluble Cab45 and CALU (see below), Nucbs are not only tightly attached to the luminal leaflet of the Golgi, but can also be observed in the cytosol ²³³. Here Nucbs, by interaction of the acidic region between the EF hands with the GTP bound α -subunit of G-proteins, potentially modify intracellular signaling cascades ²³³⁻²³⁵.

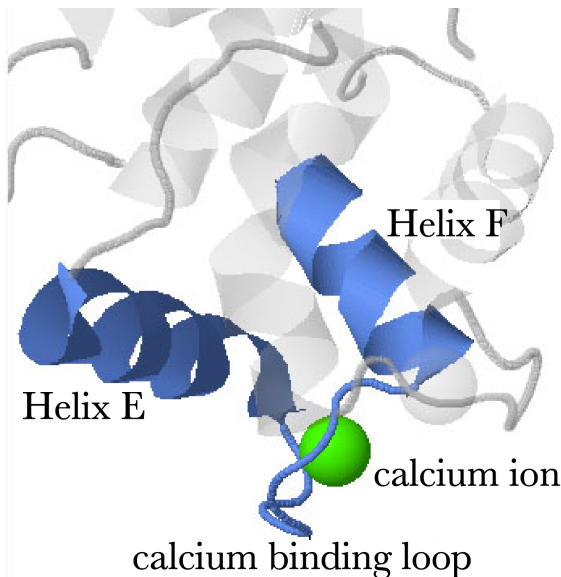


Figure 10: Structure of EF hand motif. Figure depicts ribbon diagram of highly conserved EF hand motif present in many calcium binding proteins. The two helices E (dark blue) and F (light blue) are connected by a loop, which coordinates the calcium ion (green). Figure was adjusted from www.protopedia.org/wiki/index.php/EF_hand d 17.05.2017 6 p.m.

Calumenin (CALU) is a member of the CREC protein family, a group of EF hand motif containing proteins localized throughout the secretory pathway ²³⁶. Other members and eponyms of this family are 45 kDa calcium binding protein (Cab45), reticulocalbin (RCN) and ER calcium binding protein of 55 kDa (ERC-55). Today also other non-mammalian proteins like *D.melanogaster* SCF or DCB45, or *C.elegans* CCB39 are included into this family ²³⁷⁻²⁴⁰. The ubiquitously expressed CALU has two splice isoforms of the same length, both containing a N-terminal SP and a C-terminal HDEF sequence ^{227,241}. Although the protein itself is soluble and also secreted it is attached to the membrane via its interactors ²²⁷. For example, CALU was shown to bind RyR and SERCA and negatively regulate both ²⁴²⁻²⁴⁴. This fact and the data that CALU binds calcium via 7 potential EF hand motifs with an affinity of $1.59 \times 10^3 \text{ M}^{-1}$ strengthens the assumption that CALU acts, similar to Nucbs as regulator for luminal calcium levels inside the secretory pathway ^{227,242,245,246}. Since the other CREC family member Cab45 is of major interest for this work structural and functional details will be discussed in a later section (section 3.5.3.4).

3.5 The TGN – the sorting hub

The last sections of the introduction summarized several characteristics crucial for efficient function of the Golgi and also central stages in protein maturation. However, all these steps are mainly a prerequisite for the actual function of the Golgi – the sorting of proteins and transport to different cellular destinations. The TGN functions herein as a sorting hub of the cell, a central station for protein identification, segregation and packaging for subsequent transport. To fulfil all necessary requirements the TGN needs to be highly dynamic in respect to volume and surface area and the morphology can be adjusted due to the required amount of protein transfer ^{247,248}.

Furthermore, not only the cargo proteins are diverse in terms of nature, topology and size, ranging from soluble (or large soluble aggregates) to 12 transmembrane domains (or even multimers of them) including uncountable posttranslational modifications, but there also exist a multitude of diverse cellular destinations: the apical and basolateral plasma membrane in polarized cells, early/sorting endosomes, late and recycling endosomes, the Golgi stack or the ER for retrograde transport and also some more specialized compartments in certain cell types ^{2,249}. Therefore, cells developed sophisticated sorting machineries to supervise and control these various exit routes. Complicated systems for protein identification, segregation and packaging evolved, which are in addition fine-tuned by environmental conditions like pH, salt concentrations and lipid composition of the TGN membranes. Unfortunately, only few of these sorting principles are well understood to date and observations that cargos for example destined for the same compartment use different sorting signals and different carriers still contribute to innumerable unresolved questions in the field. In the following, some well-studied sorting routes will be discussed in more detail.

3.5.1 Sorting by lipids

The special characteristic of the TGN compartment is a very distinct composition of membrane lipids in comparison to ER or cis Golgi. Therefore, not only cation and protein concentrations regulate biological functions at the TGN, but also the localization of different lipids is highly controlled within the cellular export routes. Thus, TGN membranes are especially enriched in cholesterol and sphingolipids like sphingomyelin ^{249,250}. The observations that depletion of both ²⁵¹⁻²⁵³ influences sorting processes in polarized MDCK cells gave rise to the lipid raft hypothesis ^{254,255}, which is based on the

assumption that biological membranes are heterogeneous in their lateral composition. Cholesterol can form short-lived microdomains in the TGN thereby changing the thickness and stiffness of the membrane in these areas ^{256,257}. Certain proteins preferentially associate to those microdomains (Figure 11). However, binding alone seems not to be sufficient for vesicle formation, but oligomerization of these proteins is required to cluster several lipid rafts into bigger domains ^{258,259}. Upon a certain size of these sorting platforms vesicle budding is induced and proteins can be transported in an adaptor and coat independent manner to their respective target membrane ²⁵⁶.

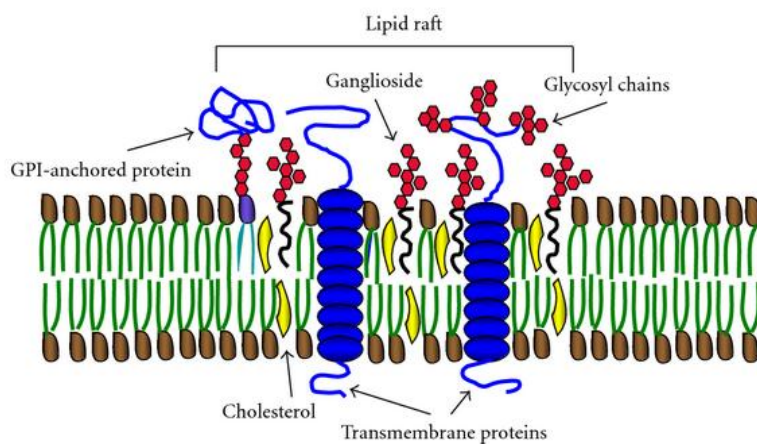


Figure 11: Schematic depiction of lipid raft model for sorting of proteins. Cholesterol-rich microdomains in the TGN membrane provide a special microenvironment and accumulate certain proteins like GPI-anchored proteins. Upon a certain size of the raft these domains bud from the TGN and are exported for transport to their subcellular destination. Figure originates from Malchiodi-Albedi et al., 2011 ²⁶⁰.

The best studied examples for this kind of lipid-dependent TGN export are glycosylphosphatidylinositol anchored proteins (GPI-APs). The GPI anchor is a lipid moiety with a glycan backbone, which is stepwise assembled at the luminal side of the ER. In a transamidation reaction the glycolipid is then transferred onto the C-terminus of soluble secretory cargo proteins, which attaches them to the luminal leaflet of the secretory pathway ^{261,262}. For TGN export the more saturated lipid environment supports first homodimerization of the GPI-APs and subsequently formation of bigger clusters. These lipid rafts are then sorted mainly to the apical membrane as shown in polarized cells ^{255,263}. However, the sorting by lipids rafts for proteins except the GPI-APs and secretory granules (section 3.5.3.1) is very poorly examined and still controversially discussed in literature.

3.5.2 Sorting of TM proteins

A better understood principle was described for the sorting of transmembrane proteins (TMPs). TMPs contain at least one cytosolic domain, which offers the possibility to interact directly with cytosolic proteins via short amino acid motifs ^{264,265}. These interactions enable

Introduction

at the same time recognition, accumulation and segregation of cargo proteins into certain TGN subdomains for export.

The best understood examples are tyrosine based (NPXY or YXX Φ) or dileucine based motifs ([DE]XXXL[LI]), which target the cargos to the endosomal or the basolateral membranes ²⁶⁵. The transport is mediated by clathrin-coated carriers. Clathrin forms triskelion shaped envelopes which are composed of three heavy and three light chains and induces membrane curvature similar to the COPII coat during vesicle formation ^{266,267}. However, also for this process TMPs need a cohort of accessory proteins like adaptors, GTPases and also lipids for efficient clathrin coat assembly ²⁶⁸, which will be discussed in the following.

The small GTPases of the manifold Arf family play a crucial role in sorting and vesicle formation at the TGN, because they initiate the recruitment of a wide variety of proteins ^{2,269}. Similar to Sar1, guanine nucleotide exchange factors (GEFs) activate Arfs by substituting GDP and GTP. This activation leads to a conformational change and the insertion of an amphipathic helix into the TGN membrane, bending the membrane and marking the point of vesicle formation ²⁷⁰⁻²⁷⁴. In addition, the change in conformation enables Arfs to recruit accessory proteins to the membrane including clathrin adaptor proteins (see below) and the Cdc42/N-WASP/Arp2/3 complex required for actin polymerization ^{270-273,275}. In collaboration with Arfs, the presence of the highly-enriched phosphatidylinositol-4-phosphate (PI4P) supports the recruitment of adaptors and BAR-domain containing proteins by direct interaction.

The actual physical connection between the TMPs and the clathrin coat form adaptor proteins. The four groups of adaptors known to date are so called adaptor protein complexes (APs), Golgi-localized, γ -ear-containing, Arf-binding proteins (GGAs), Epsin-related proteins (EpsinRs) and Exomer in yeast ^{2,276-279}.

Five different AP proteins (AP1 to AP5) are known to date and especially AP1, AP3 and AP4 were linked to TGN-endosome sorting and transport ^{2,280}. The heterotetrameric APs contain binding sites for tyrosine-based as well as for dileucine based motifs, which are often at the C-terminus of the cargo proteins, but can also be embedded inside the tertiary structure ²⁸¹⁻²⁸⁴. In addition, the selectivity of APs for their cargo proteins can be fine-tuned by expression of different isoforms and by the nature of amino acids surrounding the sorting motifs ^{285,286}.

Another adaptor family present in mammalian cells are the monomeric GGA proteins. GGAs bind acidic-cluster dileucine motifs (DXXLL) similar to APs by their N-terminal VHS (Vps27, Hrs, STAM) domain. If APs and GGAs interfere or collaborate due to the similarity in their recognition motifs or how they are spatiotemporally regulated in detail is an ongoing discussion in this research field.

The only mammalian protein of the epsin-related family acting at the TGN binds directly to various SNARE proteins and PI4P via its N-terminal ENTH domain. The unstructured C-terminal domains interact with the accessory binding domains of APs and GGAs^{287,288}. EpsinR was also shown to be required for retrograde transport of TGN46 or the mannose-6-phosphate receptor from early endosomes to the TGN²⁸⁹.

Finally, when the coat is stably attached to the TMPs, tubular vesicles are pulled out of the TGN via actin- and microtubule-based motors proteins^{290,291}. Presumably, after elongation of the tubules GTPases of the dynamin family constrict the membrane at the newly formed carrier pinches off upon GTP hydrolysis. Thereafter, vesicles are further transported along the cytoskeleton to their acceptor compartments for vesicle fusion, however, this mechanism requires further investigations.

3.5.3 Sorting of soluble proteins

The fact and obvious advantage that TMPs can interact with cytosolic components is simultaneously the biggest obstacle for sorting of soluble proteins. Evidently, the membrane bilayer prevents crosstalk and direct interaction between luminal cargo and the cytosolic coat machinery. Therefore, nature established different mechanisms to overcome this barrier.

Besides the sorting by lipid rafts (section 3.5.1) three principals were described in literature so far, namely sorting of soluble proteins into specific storage granules, receptor-mediated sorting and sorting by the Cofilin1/SPCA1/Cab45 machinery, which will be explained below in more detail (Figure 12).

3.5.3.1 Sorting into secretory storage granules

The sorting of soluble proteins into secretory storage granules (SSG) is a specialized storage and release mechanism observable in exocrine and endocrine cells (e.g. neuroendocrine cells). Thereby, usually enzymes and hormones like Chromogranin A and B, secretogranins, prohormone convertase or carboxypeptidase are packed at the TGN into

Introduction

vesicles of several hundred nanometers and released upon an external stimulus at the plasma membrane^{249,292-294}.

For this process two basic steps are necessary: (1) aggregation of cargo inside the TGN lumen and (2) maturation of the immature SSG and removal of mislocalized proteins.

Cargo proteins inside the SSG appear as dense cores in electron microscopy and they are highly condensed to enable a fast and concentrated release^{19,295,296}. This condensed state requires efficient aggregation of proteins already inside the TGN lumen, which also helps to segregate these proteins from other TGN luminal components.

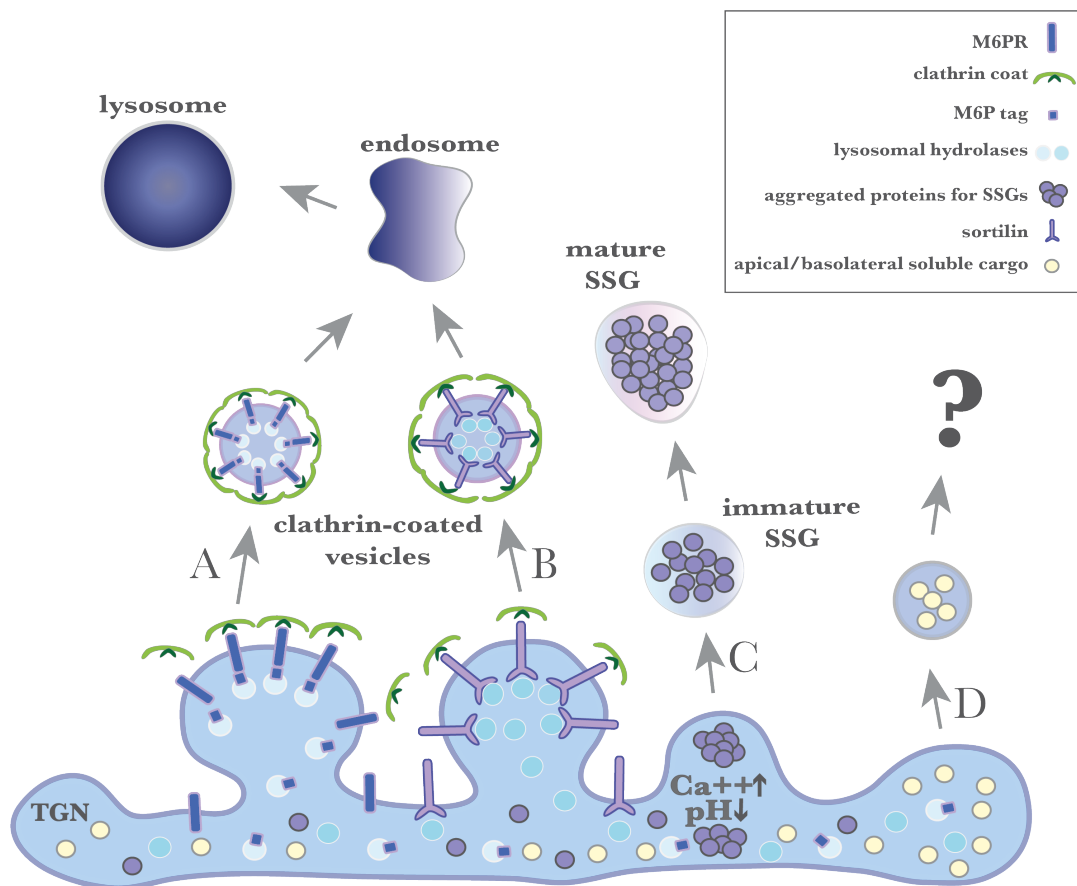


Figure 12: Different mechanisms for sorting of soluble cargo proteins in the TGN lumen. (A) and (B) Soluble proteins are sorted at the TGN by a variety of different mechanisms. They can either be modified by a M6P modification which can be recognized in the TGN by a TM receptor (dark blue) or they can directly bind to sortilin (purple). The TMPs in turn interact with adaptor proteins (dark green) and clathrin coat proteins (light green) and vesicles are transported to the endo-lysosomal system. (C) Proteins destined for secretory storage granules (SSG) accumulate in TGN subdomains with low pH and high calcium concentrations. These aggregates are then packed into vesicles which mature into SSGs and are stored inside the cell until an external stimulus releases them. (D) Many proteins that are not under the control of one of the other pathways also need to be sorted at the TGN, however, for a long time a suitable mechanism remained elusive. In recent years, it became evident that the receptor-independent sorting by CFL1/SPCA1/Cab45 is responsible for the sorting of a subset of soluble molecules at the TGN for transport to the plasma membrane. Nonetheless, other yet unknown mechanisms might be involved. Figure was adjusted from Kienzle and von Blume, 2014³⁰⁹.

The signal for oligomerization can either be due to intrinsic properties of the SSG proteins or be a receptor-mediated process ^{249,294,297}. However, in both cases certain environmental requirements like high calcium concentrations and an acidic compartment were necessary to induce aggregation ^{298,299}. Cargo conglomerates ready for export interact with cholesterol-rich membrane domains and subsequently formed vesicles pinch off in a GTP-consuming manner as immature SSGs ³⁰⁰⁻³⁰³. These carriers then shrink while condensing their content and removal of mislocalized proteins like furin or mannose-6-phosphate receptor by GGA-dependent export in clathrin-coated vesicles ^{294,304-306}. Mature SSGs are translocated upon external stimuli to the plasma membrane, where they secrete their cargos. In parallel, secretion triggers a positive feedback loop for mRNA stabilization and transcriptional activation to restore the SSG contingent ^{294,307,308}.

A similar sorting by selective aggregation mechanism was also observed for the apical transport of N- and O-linked glycan oligomers, which helps to isolate these proteins and transport them via lectin receptors to the plasma membrane ²⁹⁷.

3.5.3.2 Sorting by receptors

The second possibility is the sorting of soluble proteins by receptors that link them to the cytosolic clathrin coat machinery. To date mainly two of these receptors namely mannose-6-phosphate receptor (M6PR) and Vps10p-domain-containing receptors (VDCRs) for transport to the endosomal membranes are well documented.

In the cis Golgi soluble lysosomal proteins including hydrolyses, proteases, nucleases and lipases receive a mannose-6-phosphate (M6P) modification onto the subterminal mannose residues in the outer branches of their N-linked oligosaccharide by UDP-N-acetylglucosamine-1-phosphotransferase ^{310,311}. In a second enzymatic step the “uncovering enzyme” N-acetylglucosamine-1-phosphodiester α -N-acetylglucosaminidase removes the N-terminal GlcNAc to expose the M6P recognition signal for subsequent receptor interaction ^{312,313}. The two corresponding type I transmembrane receptors reside mainly in the TGN and differ in the size of the luminal domain, the number of M6P binding sites and their requirement for calcium ³¹⁴⁻³¹⁶. The observation that expression of one receptor cannot fully compensate for the loss of the other indicated complementary functions of both, although this aspect remains to be elucidated in more detail ^{314,315}. Acidic dileucine clusters in the cytosolic domain of the M6PRs recruit GGA and AP1 adaptor proteins (section 3.5.2) and subsequently the clathrin coatomers for vesicle transport to the early or late endosomes ³¹⁷⁻³¹⁹. The low pH of about 5.5 inside the endosomal system then

induces dissociation of the lysosomal enzymes from M6PRs. While the enzymes remain, the receptors are recycled to the TGN via the retromer complex in an Rab9/TIP47-dependent manner for a new cycle of sorting^{310,320-322}.

Misfunction of this system leads to secretion of lysosomal enzymes from cells and to lysosomal storage diseases in human patients³¹⁵. However, samples from patients suffering from I-cell disease (a lysosomal storage disorder with impaired function in M6P addition) indicate that also M6P-independent transport of lysosomal proteins exist^{323,324}.

One possibility for M6P-independent transport is the sorting of lysosomal proteins by sortilin and sortilin-related protein with A-type repeats (SorLA), both members of the mammalian Vps10p-domain-containing receptors (VDCRs) family³²⁵⁻³²⁷. The type I transmembrane proteins share several characteristics with M6PRs including typical consensus patterns in their cytosolic domains for adaptor protein interaction and are both involved in endosome-TGN transport^{325,328-330}. The N-terminal, luminal Vps10p domain of sortilin and SorLA contains a propeptide and conserved more C-terminal motif of 10 cysteines^{325,331}. The propeptide prevents premature ligand binding and is cleaved by furin in the TGN^{332,333}. The active protein forms a conical tunnel of a 10-bladed beta-propeller which houses binding sites for several ligands³³⁴. In addition, reports indicate that the conserved disulfide bridges formed by the 10 cysteine motif are essential for affinity for receptor-specific ligands³³⁵. In addition, SorLA contains low-density lipoprotein receptor class A repeats which are able to interact with several more cargos³³⁶. Due to their similarities it seems not surprising that sortilin and SorLA localize with M6PR in endosome-to-TGN carriers and seem to employ a common AP1-dependent retrograde transport mechanism via retromer^{326,337,338}.

Besides M6PR and VDCRs also lysosomal integral membrane protein type 2 (LIMP2) and Wntless were suggested as sorting receptors functioning via similar sorting motifs. However, poorly described cargo pools or mechanisms require more research on these sorting principles².

3.5.3.3 Sorting by the Cofilin1/SPCA1/Cab45 machinery

For decades, the idea of secretion of soluble cargo was dominated by the hypothesis that soluble proteins can just be constitutively and randomly transported to the cell surface by bulk flow³³⁹. Although receptor-dependent mechanisms for sorting to the endo-lysosomal compartments were described, a corresponding particular system seemed irrelevant. As a

result, the sorting of soluble proteins by the specific CFL1/SPCA1/Cab45 machinery was only recently discovered and the main focus of this thesis. Although the individual components of the system were known for several years, the connection was established only in 2006 by a genome wide screen in *D.melanogaster* S2 cells aimed to identify new components necessary for secretion of soluble secretory proteins³⁴⁰. This experiment revealed the drosophila homologue of mammalian Cofilin1 (CFL1)/actin depolymerizing factor (ADF), twinstar, as an essential regulator of secretion.

Mammalian cells express the three isoforms ADF, CFL1 and CFL2 from three different genes^{341,342}. All three are small proteins of about 18 kDa and share high sequence similarity up to 80 % and a highly conserved single folded ADF homology domain^{341,343}. Their common potential to regulate actin dynamics by binding filamentous and globular actin via a long α -helix³⁴⁴⁻³⁴⁶ renders them key regulators of many cellular processes including contractility, apoptosis and nuclear actin import, transcription and nuclear architecture³⁴⁷⁻³⁵⁰. Besides several levels of regulation like PIP₂ binding, competition with other actin binding proteins, cytosolic pH and mechanical forces on actin fibers^{345,351-357}, CFL1/ADF is inactivated by phosphorylation of Ser3 by LIM or TES kinases and reactivated by SSH phosphatases³⁵⁹⁻³⁶¹. Although it seemed surprising that a cytosolic protein, with a well-established function in actin dynamics, was responsible for secretory cargo sorting, subsequent analysis in HeLa and yeast cells proved, that siRNA knockdown of CFL1/ADF results in a missorting phenotype of soluble, but not the membrane-associated cargo proteins VSV-G or p75^{362,363}.

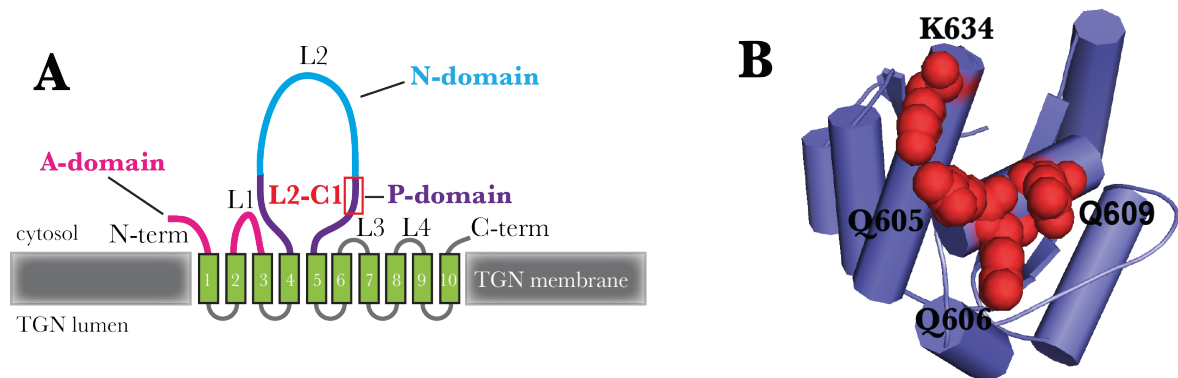


Figure 13: Schematic depiction of the SPCA1 domain structure and the CFL1 binding site. (A) Cartoon of SPCA1 structure depicts domain structure of the Golgi-resident ATPase calcium pump. The cytosolic loops (L1 to L4) contain the actuator domain (A, pink), the nucleotide binding domain (N, blue) and the phosphorylation domain (P, purple). In the C-terminal part of L2 (L2C1, red box) in the P-domain CFL1 binds to a patch of four amino acids and activates the calcium pump by parallel recruitment of F-actin. (B) Structural model of the CFL1 binding domain in the SPCA1-L2C1 domain (purple). The red spheres and numbers represent the four amino acid residues required for SPCA1- CFL1 interaction. Figure was adjusted from Kienzle et al., 2014³⁵⁸.

Later work revealed that only active, dephosphorylated CFL1 interacted directly with the C-terminal part of the cytosolic loop 2 of SPCA1 (SPCA1-L2C1) (Figure 13), as only KD of the SSH phosphatase, but not the LIM kinase resulted in impaired secretion of soluble proteins^{358,362,364}. Furthermore, the CLF1/SPCA1 interaction was crucial for actin recruitment to the Golgi, efficient calcium uptake and sorting. *In vitro* experiments proofed CLF-1-dependent actin recruitment onto beads covered with SPCA1-L2C1³⁵⁸. In addition, CLF1 localized to the TGN membranes only in the presence of polymerized actin in HeLa cells, because disruption of actin dynamics by drugs like latrunculin dispersed CLF1 into the cytosol³⁶⁴. Finally, overexpression of SPCA1-L2C1 inhibited cargo sorting and trafficking due to diminished CLF1 TGN recruitment³⁵⁸. In that line, a FRET-based calcium sensor targeted to the TGN lumen indicated less calcium influx upon overexpression of the SPCA1 loop2 or siRNA KD of CLF1 or SPCA1^{358,364}. As a consequence to the disturbances in actin recruitment and calcium uptake, soluble cargo proteins were inefficiently sorted and accumulated in the yeast and HeLa TGN lumen, which increased the volume as observed before upon temperature-dependent export block^{248,362,363}.

Taken together these studies underlined the importance of CFL1/actin recruitment to the TGN and the subsequent SPCA1-dependent calcium influx into the TGN lumen for efficient cargo sorting. However, the question how calcium levels subsequently regulate protein transport remained unanswered.

3.5.3.4 Cab45 – the missing link

The ‘missing link’ to this problem Cab45 was identified in 2012 by the research group of Vivek Malhotra as key regulator of secretory cargo sorting at the TGN³⁶⁵.

Initially, Cab45 was identified by Scherer and colleagues as the first soluble, Golgi apparatus resident protein in 1996 in mouse 3T3-L1 adipocytes, however, the function remained elusive at this time²²⁶. The protein is encoded by the SDF4 gene, which contains seven exons on chromosome 1.p36.33 and an ORF of 1086 bp^{236,366}. Some years later the splice isoforms cytosolic Cab45 (Cab45-C) and the secreted form (Cab45-S) were described in literature³⁶⁷⁻³⁶⁹.

The originally identified mouse protein was found to be highly conserved in mammalian tissues sharing 95 % with rat and 87 % with the human sequence. Especially the EF hand motifs show 100 % and 97 % homology to rat and human, respectively³⁷⁰. In addition,

Cab45 shares high homology to RCN1 and Erc-55 also outside the calcium binding domains ²²⁶.

The Cab45 protein contains 361 amino acids and is ubiquitously expressed, e.g. in lung, liver and brain, but also especially in adipose tissue ²²⁶ (Figure 14). The characteristic N-terminal SP for cotranslational import into the ER contains a charged arginine preceding a stretch of hydrophobic amino acids ^{29,226}. The proline residue located two amino acids downstream of the SP was suggested to act as crucial signal for ER export, since a mutation of the same residue in the calcium binding protein Nucb1 was shown to inhibit COPII mediated ER-Golgi transport ³⁷¹. As a member of the CREC family (section 3.4.4.3) six potential EF hand motifs enable Cab45 to bind calcium ions. Two of those EF hands fit perfectly the described EF hand motif of Szebenyi and Moffat, 3 EF hands have single point mutations and EF hand 3 shows 3 substitutions in the amino acid sequence ^{237,372}. At the very C-terminal end the four amino acids HEEF were suggested several times in literature as Golgi retention signal, analogous to the well-characterized KDEL retention motif of ER-resident proteins ^{225,227,370,373}.

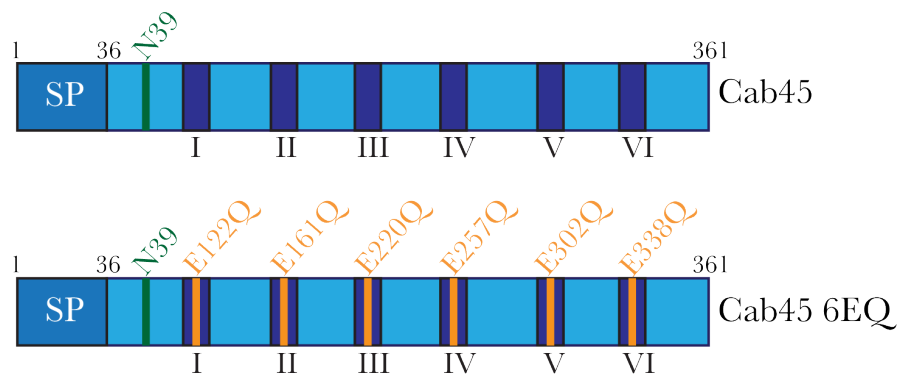


Figure 14: Schematic depiction of the Cab45 domain structure and the 6EQ mutant. The whole Cab45 wild type protein consists of 361 amino acids. It contains an N-terminal signal peptide (SP) for recognition by the SRP and ER import, a glycosylation site at asparagine 39 (green) and six EF hand motifs (dark blue boxes; Roman numerals) for calcium binding. In the 6EQ mutant all six calcium binding sites were disrupted by E to Q single point mutations (orange lines and numbers).

Already in the first description a N-glycosylation site of Cab45 was predicted for an asparagine residue on position 39 ²²⁶. This hypothesis was verified 10 years later by pulse chase experiments in pancreatic INS-1 cells, which indicated that Cab45 indeed gained a digest-resistant protein pool within 4 h after protein synthesis ³⁷⁴. Although the structure and function of this sugar modification was so far not analyzed in detail, Delcourt and colleagues ³⁷⁵ identified Cab45 in a mass spectrometric SILAC screen performed in zebrafish, which proves that Cab45 exhibits the typical sialic acid modification of Golgi-located proteins.

But how can the CFL1/SPCA1/Cab45 regulate secretion of soluble cargo proteins? Von Blume et al. showed in HeLa cells that Cab45 was released from the TGN if cellular calcium levels were depleted by addition of an ionophore to the cell medium ³⁶⁵. Furthermore, not only high calcium, but also the presence of SPCA1 at the Golgi was necessary to retain Cab45 inside the cells. In secretion assays, either the model cargo SP-HRP and physiological cargo molecules like the cartilage oligomeric matrix protein (COMP) or Lysozyme C (LyzC) were accumulated at the TGN upon SPCA1 or Cab45 siRNA KDs, while the sorting of the lysosomal hydrolase Cathepsin D (CathD) remained unaffected. These observations were in line with follow-up immunoprecipitation experiments. For these IPs, the 6EQ mutant of Cab45 was established, a calcium-binding deficient mutant with single point mutations in all six EF hand motifs (Figure 14). In contrast to the GST-fusion wild type protein purified from *E.coli* cells, the 6EQ mutant was not able to interact with COMP or LyzC.

Taken together, the results presented in this publication gave the first hints that calcium is an essential component for correct intracellular localization of Cab45 and also for Cab45-dependent cargo sorting. However, many crucial aspects of this sorting mechanism around the CFL1/SPCA1/Cab45 machinery remained unanswered and were hence central questions of this thesis.

4 Aims of this thesis

Efficient protein transport and secretion is a crucial requirement for a multitude of cellular aspects including cell homeostasis, cell-cell communication and tissue integrity. Therefore, malfunctioning of the system often leads to severe diseases. As a consequence, transport and sorting mechanisms are tightly regulated in cells, however, often only poorly understood so far. A more comprehensive knowledge about sorting of soluble proteins would deepen the insights into many vital cellular processes. Therefore, the specific aims of this thesis were:

1. Establishment of biochemical and cell biological tools to analyze the CLF1/SPCA1/Cab45 sorting machinery
2. Analysis of the role of calcium for the sorting mechanism
3. In detail study on the Cab45-cargo interaction
4. Analysis of Cab45 posttranslational modifications

5 Material and Methods

In the framework of this thesis, ImageJ (version 2.0.0-rc-43/1.51f), Prism software (Version 6.0h; GraphPad Software Inc., La Jolla, USA), Adobe illustrator CS6 (Version 16.0.0) and SnapGene (Version 2.4.3) were used for different applications (see below).

5.1 Molecular biological methods

For generation of expression vectors, the following general cloning protocols were applied. If not indicated differently, all enzymes were purchased from NEB (Ipswich, USA) and used according to the manufacturer's advice. For all PCR reactions, a Mastercycler Nexus Gradient (Eppendorf, Hamburg, Germany) PCR machine was used. GeneArt Strings DNA Fragment for MGP 3A insertion were purchased from Thermo Fisher Scientific (Waltham, USA).

5.1.1 Polymerase Chain Reaction (PCR) for standard cloning

For amplification of plasmid DNA 150 ng of template vector were incubated with 200 μ M dNTPs, 0.5 μ M forward and reverse primer (section 0) and 0.01 units of Phusion High-Fidelity DNA Polymerase (Thermo Fisher, Waltham, USA) in the corresponding 1x HF buffer in a total volume of 50 μ l.

To denature DNA strands samples were incubated for 5 min at 95 °C, before 35 cycles of denaturing (30 sec at 95 °C), annealing (30 sec dependent on the primer pair between 53 and 58 °C) and elongation (30 sec/500 bp at 72 °C) were performed. For final elongation, PCRs were kept for 10 min at 70 °C before storage cooling to 10 °C.

5.1.2 Annealing of sgRNAs and insertion into pX backbone vectors

For annealing of sgRNAs (sections 5.2.7 and 5.2.8) before insertion into backbone vectors, 100 μ M top and bottom oligo nucleotides were incubated in 1x T4 ligase buffer supplemented with 10 units polynucleotide kinase according to the following scheme: 37 °C for 30 min, 96 °C for 5 min, 95 °C for 1 min, 85 °C for 5 min, 80 °C for 1 min and then 0.1 °C/sec to 70 °C. Subsequently, annealed oligo nucleotides were stored at 10 °C.

Annealed oligo nucleotides were diluted 1:200 in water before standard ligation into o.n. BbsI digested, CIP-treated pX backbones (compare section 5.1.10).

5.1.3 Agarose gel analysis and DNA purification

Amplified DNA fragments of PCRs were analyzed by a 1 % agarose gel in TAE buffer stained by SYBR safe DNA gel stain (Thermo Fisher Scientific, Waltham, USA). Therefore, PCR samples were mixed with 10x DNA loading dye, applied on the agarose gel and run for 25 min at 100 V. For size standard, 8 µl of DNA ladder mix (Thermo Fisher Scientific, Waltham, USA) were analyzed along with the samples. Correct bands were extracted by mi-Gel Extraction Kit (Metabion, Martinsried, Germany) according to the manufacturer's protocol.

5.1.4 Restriction digest

Purified PCR products and corresponding vectors were digested o.n. at 37 °C with enzymes indicated in Table 2. 5' Phosphate of vectors was additionally removed by treatment with alkaline phosphatase for 1 h at 37 °C. After removal of enzymatic components by mi-PCR Purification Kit (Metabion, Martinsried, Germany), inserts were ligated into backbone vectors.

5.1.5 Ligation

Required amounts for ligation reactions were calculated by online tool provided by the university of Düsseldorf (www.insilico.uni-duesseldorf.de/Lig_input.html). For all reactions, a vector amount of 100 ng and a molar vector/insert ratio of 1/3 was used. Ligation reactions were performed for at least 1 h at RT with 10 units of T4 ligase in the corresponding buffer in a total volume of 20 – 30 µl.

5.1.6 Transformation of ligated DNA into *E.coli* cells

10 µl of the ligated DNA constructs were transformed into 50 µl chemically competent OmniMAX 2 T1 *E.coli* cells (section 5.1.9). Therefore, DNA and cells were incubated for 30 min on ice and then for 90 sec at 42 °C. After addition of 300 µl LB growth medium, cells recovered for at least 1 h at 37 °C while shaking constantly. For o.n. cultures, 20 µl of transformed cells were plated on ampicillin-containing LB agar plates (final concentration 100 µg/ml) and incubated at 37 °C.

5.1.7 Single clone isolation, DNA preparation and sequencing

Grown colonies were picked and cultured in 4 ml LB medium, supplemented with ampicillin (final concentration 100 µg/ml) o.n. at 37 °C while shaking. Plasmid DNA was isolated from colonies by NucleoSpin Plasmid EasyPure Kit (Macherey-Nagel, Düren, Germany) and DNA concentration was determined by Nanodrop 2000 spectrometer (Thermo Fisher Scientific, Waltham, USA). Correct DNA sequence was validated by sequencing. All sequencing reactions were performed with SmartSeq Kits from Eurofins Genomics (Ebersberg, Germany).

5.1.8 Mutagenesis for introduction of single point mutations

PCR reactions were carried out as described above (section 5.1.1), but with 400 µM dNTPs and 0.6 µM primers. Only 16 repeat cycles were performed for multiplication of the plasmids. After analysis of PCR product on agarose gel and purification (section 5.1.3), DNA was digested by DpnI for 1 h at 37 °C to destroy template DNA. 2.5 µl of treated DNA was subsequently transformed into 50 µl of competent OmniMAX 2 T1 *E.coli* cells and further treated as described previously (section 5.1.6 and 5.1.7).

5.1.9 Generation of chemically competent *E.coli* cells

100 ml LB growth medium were inoculated with 2 ml of o.n. *E.coli* OmniMax 2 T1 culture and grown until OD 0.5 at 37 °C in shaker. Then cells were cooled to 4 °C on ice and centrifuged for 15 min at 3000 rpm at 4 °C. SN was discarded and pellet was resuspended in 10 ml TSS buffer supplemented with 2.5 ml of 87 % glycerol. Aliquots were snap frozen and stored at -80 °C.

5.1.10 Plasmids

Backbone plasmid	Insert	Description/Function	Origin
pI-secSUMOstar	Cab45	Cab45 wt with N-terminal insect SP and His-SUMO tag for protein purification	This work
pI-secSUMOstar	Cab45 EFh1	Cab45 mutated at EF hand motif I (E122Q) and II (E161Q) with N-terminal insect SP and His-SUMO tag for protein purification	This work
pI-secSUMOstar	Cab45 EFh2	Cab45 mutated at EF hand motif III (E220Q) and IV (E257Q) with N-terminal insect SP and His-SUMO tag for protein purification	This work
pI-secSUMOstar	Cab45 EFh3	Cab45 mutated at EF hand motif V (E302Q) and VI (E338Q) with N-terminal insect SP and His-SUMO tag for protein purification	This work

pI-secSUMOstar	Cab45 Nfrag	N-terminal fragment of Cab45 (aa 1 to 206) with N-terminal insect SP and His-SUMO tag for protein purification	This work
pI-secSUMOstar	Cab45 Cfrag	C-terminal fragment of Cab45 (aa 207 to 361) with N-terminal insect SP and His-SUMO tag for protein purification	This work
pI-secSUMOstar	Cab45 MVKR	Cab45 with M104K and V105R mutations with N-terminal insect SP and His-SUMO tag for protein purification	This work
pIRESneo3	SP-SBP-EGFP-MGP	MGP wt fusion construct with N-terminal signal peptide-streptavidin binding protein-EGFP tag for RUSH assays	This work
pIRESneo3	SP-SBP-EGFP-MGP 3A	MGP with Y82A Y86A Y88A mutations fusion construct with N-terminal signal peptide-streptavidin binding protein-EGFP tag for RUSH assays	This work
pLPCX	Cab45 WT-HA	Cab45 wt with C-terminal HA tag for expression in HeLa cells	365
pLPCX	Cab45 6EQ-HA	Cab45 with E122Q E161Q E220Q E257Q E302Q E338Q mutations with C-terminal HA tag for expression in HeLa cells	365
pLPCX	Cab45 EFh1-HA	Cab45 mutated at EF hand motif I (E122Q) and II (E161Q) with C-terminal HA tag for expression in HeLa cells	This work
pLPCX	Cab45 EFh2-HA	Cab45 mutated at EF hand motif III (E220Q) and IV (E257Q) with C-terminal HA tag for expression in HeLa cells	This work
pLPCX	Cab45 EFh3-HA	Cab45 mutated at EF hand motif V (E302Q) and VI (E338Q) with C-terminal HA tag for expression in HeLa cells	This work
pLPCX	Cab45 MVKR-HA	Cab45 with M104K and V105R mutations with N-terminal insect SP and C-terminal HA tag for expression in HeLa cells	This work
pLPCX	SS-HA-Cab45	Cab45 with N-terminal HA tagged inserted after signal sequence of Cab45	This work
pLPCX	SS-eGFP-Cab45	Cab45 with N-terminal eGFP inserted after signal sequence of Cab45	This work (during supervision of Master student Judith Vlaar)
pLPCX	Fam20C-HA	Fam20C wt with C-terminal HA tag for expression in HeLa S3 cells for Golgi preparations	This work
pLPCX	Fam20C KD-HA	Fam20C with K478A mutation with C-terminal HA tag for expression in HeLa S3 cells for Golgi preparations	This work
pLPCX	LyzC-FLAG	LyzC wt with C-terminal triple FLAG tag for expression in HeLa cells	365
pX458	pSpCas9-hGEM-GFP-sgRNA3	CRISPR/Cas9 construct with sgRNA3, Cas9-GFP controlled by hGEM peptide for MIN-tag integration	This work (section 5.2.8)
pX459	pSpCas9-sgRNA1	CRISPR/Cas9 construct with sgRNA1 and Cas9 protein for KO targeting	This work (section 5.2.7)
pX459	pSpCas9-sgRNA2	CRISPR/Cas9 construct with sgRNA2 and Cas9 protein for KO targeting	This work (section 5.2.7)

Table 1: Overview of expression constructs used in this thesis.

5.1.11 Primers and restriction enzymes

Name	Sequences	Restriction enzymes
Cab45 fwd for pI-secSUMOstar	5' CAGCGTCTCAAGGTCGGCCTGCCAACCAC TCGTC 3'	BsmBI
Cab45 rev for pI-secSUMOstar	5' CAGTCTAGATTA AAACTCCTCGTGCACGCTGCG 3'	XbaI
Cab45 fwd Nfrag fwd for pI-secSUMOstar	5' GGGCGTCTCGAGGTCGGCCTGCCAACCAC 3'	BsmBI
Cab45 rev Nfrag rev for pI-secSUMOstar	5' GCTCTAGATTACTGGTACCAGCGGTCCTTC 3'	XbaI
Cab45 fwd Cfrag fwd for pI-secSUMOstar	5' GGGCGTCTCCAGGTCGGGACAGCCCCC 3'	BsmBI
Cab45 rev Cfrag rev for pI-secSUMOstar	5' GCTCTAGATTA AAACTCCTCGTGCACGC 3'	XbaI
Cab45 fwd for SP-HA-Cab45	5' GGG AGATCTATGGCTACAGGCTCCGGAC 3'	BglII
Cab45 rev for SP-HA-Cab45	5' GGCGGCCTTA AAACTCCTCGTGCACGC 3'	NotI
E122Q muta +	5' AGATCAGTGCCAAGCAGATGCAGCGCTGG 3'	Not required
E122Q muta -	5' CCAGCGCTGCATCTGCTTGGCACTGATCT 3'	Not required
E161Q muta +	5' GTCACGTGTCTTGGGACCAGTATAAGGTGA 3'	Not required
E161Q muta -	5' AAAC TTCACCTTATACTGGTCCCAAGACACGT 3'	Not required
E220Q muta +	5' TGCTGACGGAGGAGCAGTTCTGTGCTTC 3'	Not required
E220Q muta -	5' GAACGACAGGAACTGCTCCTCCGTCAGCA 3'	Not required
E257Q muta +	5' AGCTCTCTGTGCCCCAGTTCATCTCCCTG 3'	Not required
E257Q muta -	5' CAGGGAGATGAACTGGGGCACAGAGAGCT 3'	Not required
E302Q muta +	5' GTGACCGCCGAGCAGCTGGAGAGCT 3'	Not required
E302Q muta -	5' AGCTCTCCAGCTGCTCGGCGGTCAC 3'	Not required
E338Q muta +	5' CCTGGAGCCCCGAGCAGGTGCTCAAGTA 3'	Not required
E338Q muta -	5' TACTTGAGCACCTGCTCGGGCTCCAGG 3'	Not required
Fam20C muta K478D +	5' ATCATCCACTTAGCCAATGGAAGAGGGTTT 3'	Not required
Fam20C muta K478D -	5' AAACCCTCTTCCATTGGCTAAGTGGATGAT 3'	Not required
GFP fwd	5' CCGGAATTCCGGGGCGGCGGTCACGAACTC CAGCAG 3'	EcoRI
GFP rev	5' CCCAAGCTTGGGATGGTGAGCAAGGGCGAGGA GCTG 3'	HindIII
MGP 3A Gstring for pIRES	5' CCGGAATTCTGTGAATCACATGAAAGCATGGA ATCTTATGAACTTAATCCCTTCATTAACAGGAGA AATGCAAATACCTTCATATCCCCTCAGCAGAGAT GGAGAGCTAAAGTCCAAGAGAGGATCCGAGAAC GCTCTAAGCCTGTCCACGAGCTCAATAGGGAAG CCTGTGATGACTACAGACTTTGCGAACGCGCCG CCATGGTTGCTGGAGCCAATGCTGCCTATAATC GCTACTTCAGGAAGCGCCGAGGGACCAAATAAG CGGCCGCAAAGGAAAA	EcoRI/NotI
MGP fwd for pIRES	5' TGTACAAGGCCGGCCTCTCGAGTACCCATACGA CGTCCCAGAC 3'	BsrGI
MGP rev for pIRES	5' TTAATTAATTATTTGGTCCCTCGGCGC 3'	PacI
MVKR muta +	5' CCACCTTGAAAAGATGCGCTTCAGCTTCCTC CGGCTC 3'	Not required
MVKR muta -	5' GAGCCGGAGGAAGCTGAAGCGCATCTTTTCCA AGGTGG 3'	Not required
SeqPrim pLPCX fwd	5' AGCTGGTTTAGTGAACCGTCAGATC 3'	Not required
SeqPrim pLPCX rev	5' ACCTACAGGTGGGGTCTTTCATTCCTC 3'	Not required
SeqPrim pI	5' CAAGTAAAACCTCTACAAATGTG 3'	Not required

secSUMOstar fwd		
SeqPrim Cab45 fwd	5' AGCTACATGGACCCCATGAAC 3'	Not required
SeqPrim Cab45 rev	5' CCGGTCAGTGTTCACATCCAC 3'	Not required
SeqPrim pX plasmids	5' GAGGGCCTATTTCCCATGATTCC 3'	Not required

Table 2: Overview of primers for generation of cloned vectors used in this thesis and required restriction enzymes.

5.2 Cell culture methods

5.2.1 General culture conditions

HeLa cells were generally cultured in a standard incubator at 37 °C and 5 % CO₂ in Dulbecco's Modified Eagle Medium (DMEM), high glucose, GlutaMAX, supplemented with 10 % fetal bovine serum (FBS) and 1 % streptomycin/penicillin antibiotics. If not indicated otherwise all cell culture media, additives and other liquids including DPBS and DNA/RNase-free water were purchased from Thermo Fisher Scientific (Waltham, USA). All cell culture dishes were purchased from Corning Inc. (Corning Inc., Corning, USA)

For passaging adherent cells were washed once with sterile DPBS and incubated for 5 min in trypsinization solution at 37 °C. After centrifugation for 5 min at 1000 g and resuspension of cells in growth medium, cells were transferred to a new cell culture dish at the desired density and further supplemented with growth medium.

5.2.2 Freezing and thawing of cells

For long term storage, cells were detached as for passaging, centrifuged for 5 min at 500 g and resuspended in Freezing medium. After complete freezing at -80 °C of cells in cryo freezing containers cells were preserved in liquid nitrogen at -196 °C.

For quick thawing cells were incubated shortly in a 37 °C water bath. After addition of growth medium, cells were centrifuged for 5 min at 500 g. DMSO containing supernatant was discarded and cells resuspended in growth medium for transfer to cell culture dishes for further cultivation.

5.2.3 Plasmid transfection of cells

For plasmid transfection cells were cultured until approximately 50 % density under standard conditions. For transfection of a six-well dish by polyethylenimine (PEI) OptiMEM medium and 1.5 to 2.0 µg DNA were mixed and 7.5 µl PEI were added and vortexed for 5 min. After incubation for 15 min at RT PEI-DNA mixture was applied

Material and Methods

dropwise onto the cells. Cells were incubated at least o.n. or until further use under standard conditions. Amounts of reagents were adjusted according to size of cell culture dishes.

For transfection of cells by *TransIT* HeLaMONSTER reagent (Mirus Bio LLC, Madison, USA), cells were also cultured till 50 % density. Per 6-well dish, 4 μ l *TransIT* reagent were mixed with 2 μ g plasmid DNA in 100 μ l OptiMEM medium and vortexed. After incubation for 20 min at RT mixture was applied dropwise before addition of a 20 μ l of 1:10 dilution of HeLaMONSTER mix in water. Subsequently, cells were cultured at least o.n. or till further use.

5.2.4 Fluorescence activated cell sorting (FACS) of HeLa cells

HeLa cells were detached, pelleted and centrifuged as described above. Cell pellet was resuspended in FACS buffer and cells were filtered by cell strainer (Corning, Inc., Corning, USA) to avoid cell clumps. EGFP positive cells were isolated by a BD FACSAria II (BD Biosciences, San Jose, USA), pooled and seeded for single clone isolation.

5.2.5 Single clone isolation

For isolation of single clones, cells were detached as described above, counted by the Countess II system (Thermo Fisher Scientific, USA), and 100 cells were seeded in a 15 cm culture dish. When single cell clones were big enough, cells were manually scratched off the dish by pipette tip, transferred to a 96 well plate and cultured to the desired number.

5.2.6 Generation of stable cell line

Cells stably expressing Cab45 or its mutants were transfected by VSV-G pseudotyped retroviral particles produced by transiently transfected HEK293T cells as described before by Pfeifer and colleagues³⁷⁶. Viral particles were concentrated from cell culture supernatants and used for infection of HeLa cells. On the next day, HeLa cells were selected in 2 μ g/ml puromycin (Sigma-Aldrich, Munich, Germany) for 24 h and stored or used for experiments.

5.2.7 Generation of CRISPR/Cas9 KO cell lines

The CRISPR/Cas9 method, which gained more and more importance during recent years, was applied to generate first a KO and secondly a cell line containing a

multifunctional integrase (MIN) tag. Besides zinc finger nucleases (ZFN) and transcription activator-like effector nucleases (TALEN), CRISPR/Cas9 is the best studied system to edit the genome of mammalian cells³⁷⁷. Although first attempts of genome editing were already performed in the eighties^{378,379}, the first stable approach for modulating human cells was presented by Jinek and colleagues just recently³⁸⁰. They exploited a part of the bacterial and archaeal adaptive immune system which protects the aforementioned against phage-derived genomes or plasmids^{381,382}. In the simplest model derived from *S.pyrogenes* only three basic components, an endonuclease and two RNAs, are necessary to readily delete or insert regions of interest. The two guide sequences (Table 3) necessary for the targeting of exon 2 of SDF4 were designed using the CRISPR/Cas9 design tool at www.genome-engineering.org/crispr³⁸³. The guides were cloned into a mammalian expression vector (pX459) bearing the Cas9 coding sequence, the sequences encoding the RNA components and a puromycin selection cassette (Addgene plasmid 48139;³⁸⁴). The Cas9 endonuclease used here belongs to the serine subfamily and contains the two active centers, HNH and RuvC, which cleaves the complementary or non-complementary DNA strand, respectively, thereby inducing a double strand break^{380,385}. This double strand break can be repaired by non-homologous end joining (NHEJ) or by homology directed repair (HDR) (Figure 17). HeLa parental cells were transfected with TransIT HeLaMONSTER reagent as described above and selected in puromycin (2 µg/ml) for 48 h. Subsequently, single clones were isolated (see above), expanded and analyzed by western blotting, immunofluorescence microscopy and sequencing (see corresponding paragraphs). For sequencing, genomic DNA was isolated by GenElute Mammalian Genomic DNA Miniprep Kit according to manufacturer's protocol (Sigma-Aldrich, Munich, Germany). Screening primers were designed using the Primer-BLAST tool provided by the NCBI homepage (www.ncbi.nlm.nih.gov).

sgRNA 1 top oligo	5' TTG ATG AGG ACG CGG AGC CG 3'
sgRNA 1 bottom oligo	5' CGG CTC CGC GTC CTC ATC AA 3'
sgRNA 2 top oligo	5' TTC ACC CCG TTC AGG TGG TC 3'
sgRNA 2 bottom oligo	5' GAC CAC CTG AAC GGG GTG AA 3'
SDF4 screening primer fwd	5' CCG GAG AAA ACA AAT GCC ACG TGT GGT CCA GAG AAA AC 3'
SDF4 screening primer rev	5' CAC AGA GGC AGC AAG AGG GTC TCG GGA C 3'
sgRNA 1 off target screening primer fwd	5' TGC CCT ACC AGC ACC GGA TGG A 3'
sgRNA 1 off target screening primer rev	5' ACG CGG GCA CTG AGC CCA TTC 3'

Table 3. Overview of DNA primers for generation of SDF4 KO cell line including sgRNA oligo nucleotides and screening primers for sequence verification for on and off targets.

5.2.8 Generation of CRISPR/Cas9 MIN-tagged cell line

For integration of the MIN tag, a guide and a donor sequence were designed by the MIN-tag targeting guide (human.bio.lmu.de/_webtools/MINtool/MIN_guide.html). The guide sequence (Table 4) was cloned into the mammalian expression vector (pX459) encoding the guide mRNAs and the Cas9-eGFP fusion protein with an additional hGEM peptide to control protein expression during cell cycle ³⁸⁶. Cells were transfected by PEI reagent with 2 µg pX459 vector and 2 µg donor DNA. The 200 bp donor DNA was purchased as Ultramer DNA Oligonucleotides from Integrated DNA Technologies (IDT, USA). After FACS sorting of eGFP positive cells, cells were seeded for single clone isolation. Isolated colonies were screened by PCR as described in the protocol by Mulholland and colleagues ³⁸⁶.

sgRNA 3 top oligo	5' GTT GGC TAC TCT CTC TCG AG 3'
sgRNA 3 bottom oligo	5' CTC GAG AGA GAG TAG CCA AC 3'
MIN screening primer fwd	5' GGA TTG GAT TGG AGC CAG GA 3'
MIN screening primer rev	5' CAC ATG GCG GCA CCT ACT T 3'
MIN donor peptide	5' GTG GGG TCC CCT CAT TGG CCT GGC TCC GTG CTG CCT CTG GCT CCT GGG GGC AGT CCT TCT GAT GGA CGC GTC TGC AGG TTT GTC TGG TCA ACC ACC GCG GTC TCA GTG GTG TAC GGT ACA AAC CCG GCC TGC CAA CCA CTC GTC CAC TCG AGA GAG AGT AGC CAA CAG GGA GGA ATG AGA TCC TGC CCC CAG ACC ACC 3'

Table 4: Overview of DNA primers for generation of SDF4 MIN tag cell line including sgRNA oligo nucleotides, screening primers and donor construct.

5.3 Biochemical methods

5.3.1 Sample preparation for SDS Page analysis and western blotting

For cell lysate preparation cells were washed three times in DPBS, incubated for 20 min in 1 % TritonX-100 in DPBS on ice and finally scratched off the cell culture dish with cell scrapers (Sarstedt, Newton, USA). To remove cell debris lysates were centrifuged 20 min at 13200 rpm at 4 °C and transferred to a new tube. Required protein amounts were normalized by relative Bradford assay using Quick Start Bradford 1x Dye Reagent (Bio-Rad, Germany) and a Sunrise™ absorbance reader (Tecan, Männedorf, Switzerland). Samples of supernatants and lysates were finally incubated with 1 x loading dye for 5 min at 95 °C before application on SDS Page.

5.3.2 Western blot analysis

For western blot analysis samples were applied on either 12 % self-made SDS Pages for 90 min at 130 V or on 1 mm NuPAGE® Novex 4-12 % Bis-Tris protein gels (Invitrogen, Waltham, USA) for 45 min at 200 V. Therefore, SDS running buffer or NuPage® MES SDS Running Buffer (Invitrogen, Waltham, USA) were used, respectively. Gels were subsequently blotted either by Mini-PROTEAN Tetra cell electrophoresis chamber with Transfer buffer for 70 min at 100 V onto membrane or by iBlot® Dry Blotting system with corresponding iBlot® Gel Transfer stacks for 8 min in program P0 (Invitrogen, Waltham, USA). After analysis of membranes by Ponceau S (AppliChem, Darmstadt, Germany) solution and blocking of membrane in 5 % BSA in TBS for at least 1 h, first antibodies diluted in 5 % BSA in TBS were incubated for 1 h at RT or o.n. at 4 °C (dilutions for primary antibodies are listed in Table 5). After washing in TBS buffer supplemented with 0.1 % Tween-20 several times, secondary HRP-coupled antibodies (Santa Cruz Biotechnology, Dallas, USA) diluted 1:10000 in 5 % BSA in TBS were incubated for 1-2 h at RT. For detection Immobilon Western HRP Substrate (Merck Millipore, Darmstadt, Germany) and a ChemiDoc™ Touch Western Blot Imaging System (Biorad, Hercules, USA) was used.

Antibody	Dilution	Company	Product ID
α -actin	1:2000	Sigma-Aldrich	A5441
α -Cab45	1:2000	Self-made	Crevenna et al., 2016 ³⁸⁷
α -COMP	1:1000	Abcam	Ab74524
α -Flag	1:500	Sigma-Aldrich	F3165
α -HA	1:1000	Roche	11867423001
α -TGN46	1:1000	AbD Serotec	AHP500G
α -mouse-HRP	1:10000	Santa Cruz	Sc-2314
α -sheep-HRP	1:10000	Santa Cruz	Sc-2473
α -rabbit-HRP	1:10000	Santa Cruz	Sc-2004
α -rat-HRP	1:10000	Santa Cruz	Sc-2303

Table 5: Overview of antibodies used for western blotting with the corresponding dilutions.

5.3.3 Protein expression and purification

Recombinant His-SUMO-tagged Cab45 proteins were expressed in SF9 insect cells by a pI-secSUMOstar based plasmid system by the MPIB Biochemical Service Facility. Proteins were then purified from cell supernatants using nickel-affinity chromatography with cComplete His-tag Purification Resin (Roche, Penzberg, Germany) and His Binding Buffer. After washing of column in the same buffer, protein was eluted in His Elution buffer and

proteins were dialyzed in GeBAflex tubes 3.5 kDa (Scienova, Jena, Germany) against Cab45 buffer for storage at -80 °C. For visual analysis of the purification steps, samples were analyzed on SDS Page as described for western blotting (section 5.3.2). Subsequently, SDS Pages were stained in Coomassie solution for 30 min and destained in Destain Solution until proper visualization was possible.

5.3.4 Protein fluorescence labeling

Recombinant Cab45 was labeled with NHS-ATTO488 (Sigma Aldrich, Munich, Germany) or NHS-Cy5 dye (GE Healthcare, Little Chalfont, UK) according to the protocol of the manufacturer. The protein was first concentrated in Amicon Ultra Centrifugal Filters (MWCO 10000; Millipore, USA) to a concentration of 2 mg/ml and rebuffered in Zeba Spin Desalting Columns (Thermo Fisher Scientific, USA) to Solution C. Subsequently, the protein was incubated with a 3 x excess of NHS-dye ester for 25 min at RT in the dark while shaking gently. Unbound dye was then removed by gel filtration of the protein in DextraSEC PRO2 columns (AppliChem, Darmstadt, Germany) with Solution A. Using again Amicon Ultra Centrifugal Filters (MWCO 10000; Millipore, USA), residual unbound dye was removed and Cab45 was rebuffered and concentrated to Solution A. After determination of labeling efficiency proteins were snap frozen and stored at - 80 °C. NHS-Cy5 labeling for Cathepsin D (Creative Biomart, Shirley, USA) was conducted accordingly.

Recombinant COMP was labeled with maleimide Alexa Fluor 647 dye (Thermo Fisher Scientific, USA). COMP was first concentrated in Amicon Ultra Centrifugal Filters (MWCO 10000; Millipore, USA) to a concentration of 1.5 mg/ml. After addition of 10 x DTT and 2 x Alexa Fluor 647 protein was stirred o.n. at 4 °C. On the next day, unbound dye was removed by DextraSEC PRO2 columns (AppliChem, Darmstadt, Germany) and Illustra AutoSeq G50 Dye Terminator Removal Kit (GE Healthcare, Little Chalfont, UK) using Solution A. After determination of labeling efficiency proteins were snap frozen and stored at - 80 °C.

5.3.5 NativePage analysis

Golgi membranes extracted from HeLa cells (detailed protocol see section 5.5.1) were diluted in Breaking buffer (BB) and pelleted by centrifugation at 100,000 x g for 1 h. The pellet was resuspended in 50 µl BB and incubated with DMSO or BAPTA-AM (25 µM) for

15 min at 37 °C. Membranes were subsequently lysed in NativePAGE sample buffer (ThermoFisher Scientific, Waltham, USA) supplemented with 1 % DDM for 15 min and centrifuged at 20,000 g for 30 min at 4 °C. The same protocol was followed for membranes extracted from the cell lines Cab45 KO, Cab45 KO rescued with Cab45 and Cab45 KO rescued with 6EQ. Supernatants were aliquoted into microcentrifuge tubes and stored at -80 °C. Recombinant His-Sumo-tagged Cab45 was either left untreated or incubated with 1 mM calcium or 1 mM calcium/1 mM EGTA for 15 minutes on ice prior to electrophoresis.

Golgi membranes or recombinant Cab45 were supplemented with 5 % G-250 sample additive (ThermoFisher Scientific, Waltham, USA) and loaded on a NativePAGE™ Novex Bis-Tris Gel (3 – 12 %) (ThermoFisher Scientific, Waltham, USA). Gels were then either stained by Coomassie brilliant blue (section 5.3.3), or transferred onto PDVF membranes. After transfer of the proteins onto a PDVF membrane for 90 min, the membrane was immersed in 6 % acetic acid for 15 min, then air-dried and washed with 100 % methanol. Finally, membranes were blocked with 4 % BSA in TBS for 30 min and subsequently treated as for western blotting as described above (section 5.3.2).

5.3.6 *In vitro* IPs with recombinant full-length proteins

Recombinant His-SUMO-tagged Cab45 was incubated with Protino NiNTA beads (Macherey-Nagel; Düren, Germany) in PIPES Buffer and 1 mM calcium o.n. at 4 °C. After washing beads three times with PBS by centrifugation, purified LyzC (NANOCS, New York, USA), COMP or CathD (both Creative Biomart, Shirley, USA) was added and incubated for 1 h at 4 °C on turning wheel. After again washing three times with PBS, soluble fraction was removed and beads were boiled in 1 x loading dye and applied on SDS Page, as described above for western blotting (section 5.3.2). Subsequently, SDS Pages were stained in Coomassie solution for 30 min and destained in Destain Solution until proper visualization was possible.

5.3.7 *In vitro* IPs with peptides

Biotin-labeled, freeze-dried peptides (produced by MPIB Biochemical Service facility; Table 6) were weight and dissolved in PIPES Buffer to a final concentration of 1 mM and solubilized o.n. at 4 °C in rotating wheel.

On the next day, Dynabeads MyOne Steptavidin C1 beads (20 µl per condition; Thermo Fisher Scientific, Waltham, USA) were added and incubated for 6 h as before. After

Material and Methods

washing of beads three times in PIPES Buffer by a DynaMag Spin (Thermo Fisher Scientific, Waltham, USA), 350 μ l cell lysate per condition (equates a 90 % confluent 10 cm culture dish; lysates were prepared as described in section 5.3.1) of HeLa cells stably overexpressing Cab45 wt was added and incubated o.n. at 4 °C in turning wheel.

Name	Sequence	MW (in Da; incl. biotin label and GS linker)
MGP1	ERYAMVYGYN	1633.702
COMP1	DDYAGFIFGYQ	1663.698
RCN1	DDYAGFVFGYQ	1649.682
scr MGP1	AYMRVNGYYE	1633.702
scr COMP1	GAYIQFFGDYD	1663.698
scr RCN1	FFDVAYGYDGO	1649.682
MGP1-1	ERAAMVAGAN	1357.621
MGP1-2	AAAAMVYGYN	1398.604
MGP1-3	ERYAMVAGAA	1406.642
MGP1-4	ERYAAAAGAN	1361.613
MGP1-5	ERYAMVAGAN	1305.594
MGP1-6	ERYAMVFGFN	1457.657
MGP1-7	ERYAMVEGEN	1421.605
MGP1-8	ERYAMVYGAN	1397.620
MGP1-9	ERYAMVAGYN	1397.620
MGP1-10	ERpYAMVYGYN	1713.666
MGP1-11	ERYAMVpYGYN	1713.666
MGP1-12	ERYAMVYGpYN	1713.666
MGP1-13	ERpYAMVpYGpYN	1873.599
Neg. ctrl.	GSGSGSGSGSG	1107.424

Table 6: Overview of peptides used for *in vitro* peptide IPs to study the interaction of cargo proteins with Cab45. Peptides were produced by the MPIB Biochemical service facility. All peptides contained a GS-linker at the N-terminus, a biotin modification and were protected at the C-terminus. Molecular weights were determined by mass spectrometry. Mutated aa residues were highlighted in red.

Before boiling of beads in 70 μ l 1 x loading dye for 5 min at 95 °C, beads were again washed three times with PIPES Buffer. Subsequently, samples were applied on SDS Page and analyzed by western blotting with α -HA antibody as described in section 5.3.2.

5.4 Cell biological method

5.4.1 Sample preparation for analysis of overexpressed Cab45 in HeLa cells

To analyze secretion of cells, cells were seeded and cultured until 80-90 % confluence. Then cells were washed in PBS or DMEM medium five times and incubated in 500 μ l (6 well culture dish) or 5 ml (10 cm culture dish) for 4 h under normal culture conditions. Supernatants were subsequently collected and if necessary concentrated in Amicon Ultra Centrifugal Filters (MWC0 10000; Millipore, USA) to required amounts. Lysates were

prepared as described in section 5.3.1. Supernatants and lysates were adjusted by Bradford assay and analyzed by western blotting.

5.4.2 Cargo secretion assays

HeLa control cells and Cab45 knock-out cells or cells stably expressing Cab45 wild type or Cab45 6EQ, respectively, were transfected with Flag-LyzC. Cells were washed five times with serum-free medium and then grown in serum-free medium for 4 h. Cells were then counted and lysed in PBS supplemented with 1 % CHAPS. Media from each cell line were collected, clarified by passage through a 0.45 μm filter (Millipore, Darmstadt, Germany) and centrifuged at $5,000 \times g$ for 15 min. Samples were then concentrated using Amicon Ultra Centrifugal Filters (MWCO 3000; Millipore, Darmstadt, Germany). Cell lysates and concentrated media were subsequently analyzed by western blotting using anti-COMP antibody or anti-Flag antibody (to detect LyzC) as described above (section 5.3.2).

5.4.3 Proliferation assays

For comparative analysis of cell growth cell lines of interest were seeded (20 000 cells / 12 well) in triplets and cell numbers were counted by Countess II (Thermo Fisher Scientific, Waltham, USA) on four consecutive days. For technical replicates, Countess II chambers were measured three times each. Experiment was performed three times. Data was visualized by Prism software and illustrated as interleaved scatter blot of mean with SEM.

5.5 Physical methods and bioinformatics methods

5.5.1 Isolation of Golgi membranes for NativePage analysis and mass spectrometry

HeLa cells stably expressing Cab45 wild type or Cab45 6EQ mutant (for NativePage analysis; 5 15 cm dishes per condition) and or HeLa S3 cells stably expressing Fam20C or Fam20C-KD (for mass spec analysis; 4 l roller culture per condition) were harvested and pelleted. Pellets were then washed once in Breaking Buffer (BB), diluted 1:5 in BB supplemented with cComplete Tablets Mini EDTA-free (Roche, Basel, Switzerland) and homogenized with an EMBL cell cracker (ball size 8.002 mm; 9 μm gap). After addition of

1 mM EDTA, the sucrose concentration of the homogenate was adjusted to 37 % (w/v) and overlaid with 35 % and 29 % sucrose in 10 mM Tris (pH 7.4). Cellular components were separated by ultracentrifugation for 3 h at 133,000 g. The Golgi membrane fraction was extracted, adjusted to BB conditions and snap-frozen in liquid nitrogen for storage at -80 °C.

5.5.2 Mass spectrometry for phosphoproteomic analysis

Golgi fractions of HeLa S3 suspension cells stably overexpressing Fam20C or the kinase-dead mutant Fam20C-KD were isolated as described in section 5.5.1. All samples were lysed in MS lysis buffer, boiled and sonicated, and precipitated o.n. using ice-cold acetone (v/v = 80 %). After centrifugation (4000 g) the pellet was washed at least twice with 80 % ice-cold acetone before air drying and resuspension (sonication) in TFE buffer. Proteins were digested using LyzC and trypsin (1:100), over-night at 37 °C and phosphopeptides enriched as described previously³⁸⁸. Samples were prepared in triplets.

For LC-MS/MS sample preparation peptides were purified using in-house prepared stage tips³⁸⁹ Empore™ SPE disks SDB-RPS (Sigma-Aldrich, St. Louis, USA) before LC-MS/MS analysis as described previously³⁹⁰. Briefly, stage tips were prepared by inserting two layers of SDB-RPS matrix into a 200 µl pipette tip using an in-house prepared syringe device. Stage-tips were first activated with 100 µl MS buffer C and then washed with 100 µl MS buffer D before loading of the acidified peptides (1 % trifluoroacetic acid v/v). After centrifugation, the stage-tips were washed three times (200 µl each) with MS buffer D. Elution was performed using 60 µl MS buffer E. Eluates were collected in 200 µl PCR tubes and dried using a Concentrator plus SpeedVac centrifuge (Eppendorf, Hamburg, Germany) at 60 °C. Peptides were resuspended in MS buffer F and briefly sonicated (Branson Ultrasonics, Danbury, USA) before LC/MS-MS analysis.

For LC-MS/MS measurements peptides were loaded on a 20 or 50 cm reversed phase column (75 µm inner diameter, packed in-house with ReproSil-Pur C18-AQ 1.9 µm resin (Dr. Maisch, Ammerbruch, Germany). Column temperature was maintained at 55 °C using a homemade column oven. An EASY-nLC 1200 system (Thermo Fisher Scientific, Waltham, USA) was directly coupled online with the mass spectrometer (Q Exactive) via a nano-electrospray source, and peptides were separated with a binary buffer system of MS buffer A and MS buffer G, at a flow rate of 250 or 350 nl/min. Peptides were eluted with a nonlinear 270-minute gradient of 5–60 % MS buffer G. After each gradient, the column was washed with 95 % MS buffer G for 5 min. The mass spectrometer was programmed to

acquire in a data-dependent mode (Top10) using a fixed ion injection time strategy. Full scans were acquired in the Orbitrap mass analyzer with resolution 60,000 at 200 m/z (3E6 ions were accumulated with a maximum injection time of 25 ms). The top intense ions (N for TopN) with charge states ≥ 2 were sequentially isolated to a target value of 1E5 (maximum injection time of 120 ms, 20% underfill), fragmented by HCD (NCE 25, Q Exactive) and detected in the Orbitrap (Q Exactive, R= 15,000 at m/z 200).

Raw mass spectrometry data were processed using MaxQuant version 1.5.3.15³⁹¹ with an FDR < 0.01 at the level of proteins, peptides and modifications. Searches were performed against the Mouse or Human UniProt FASTA database (September 2015). Enzyme specificity was set to trypsin. The search included cysteine carbamidomethylation as a fixed modification and N-acetylation of protein, oxidation of methionine, and/or phosphorylation of Ser, Thr, Tyr residue (PhosphoSTY) as variable modifications. Up to two missed cleavages were allowed for protease digestion. 'Match between runs' was enabled, with a matching time window of 0.5-0.7 min. Bioinformatic analyses were performed with Perseus (www.perseus-framework.org) and Microsoft Excel and data visualized using Graph Prism (GraphPad Software Inc., La Jolla, USA) or Perseus³⁹². Significance was assessed using one sample t-test, two-sample student's t-test and ANOVA analysis, for which replicates were grouped, and statistical tests performed with permutation-based FDR correction for multiple hypothesis testing. Were indicated, missing data points were replaced by data imputation after filtering for valid values (all valid values in at least one experimental group). Error bars are mean \pm SEM or mean \pm SD.

5.5.3 Mass spectrometric screen for comparison of secretomes

For sample preparation 9 15 cm dishes of HeLa wt cells or Cab45 CRISPR/Cas9 KO cells were seeded and cultured until 90 % density. Cells were washed five times in DMEM without serum and incubated for 4 h in 7.5 ml of the same medium under normal culture conditions. Subsequently, SN was collected and concentrated in Amicon Pro Ultra Centrifugal Filters (MWCO 3500; Millipore, USA) to a final volume of 200 μ l. The samples were then washed three times on the filter with 500 μ l Urea buffer by centrifuging at 10000 g at RT. The samples were incubated with 500 μ l Urea buffer containing 50 mM chloroacetamide at RT for 60 minutes. Following reduction and alkylation of proteins the sample was further treated three times with 50 mM ammonium bicarbonate solution. To this sample 1 μ g of trypsin (Promega V5111, Madison, USA) was added and digested o.n. at 37 °C. Peptides after o.n. digestion were collected from the filter by inverting the filter

with additional rinse of the filter with 200 μ l of ammonium bicarbonate solution in order to recover the maximum peptides possible from the filter surface. The collected peptides were then purified via C18 StageTips³⁹³. Triplets of samples were prepared and analyzed in the following setup.

Peptides were loaded on to a C18 column (15 cm long inner diameter of 75 μ m packed with 1.9 μ m Reprosil beads from Dr Maisch, Ammerbruch, Germany) via the autosampler of the LC system (Thermo Easy nLC 1200, Thermo Scientific, Waltham, USA). Peptides were eluted over a 120 min gradient using MS buffer A and B and directly sprayed into bench top Orbitrap mass spectrometer (Q Exactive HF, Thermo Scientific, Waltham, USA). The column was maintained at a constant temperature of 50 °C for reproducible retention times and better resolution of separation. The mass spectrometer was operated in data dependent mode with survey scans acquired at 60,000 resolution after accumulating up to 3E6 charges in the C-trap. Up to 15 peptides like features were selected for fragmentation by HCD and fragmentation scans were acquired at 15,000 resolution (at $m/z = 200$). In order to minimize futile repeat sequencing dynamic exclusion was enabled and precursors selected for fragmentation were excluded for 30s³⁹⁴.

The raw data were processed using MaxQuant computational platform version 1.5.2.2³⁹¹. Peak lists generated were searched using Andromeda search engine against human Uniprot reference proteome sequence³⁹⁵. Initial precursor and fragment tolerance were set to 4.5 and 20 ppm, respectively. Carbamidomethylation of cysteine was set as fixed modification together with methionine oxidation and N-terminal protein acetylation as variable modification. Match between the runs feature in MaxQuant was enabled and protein quantification was performed using the MaxLFQ algorithm inbuilt in the software³⁹⁶. Initial bioinformatics and statistical analysis were performed using Perseus software³⁹².

5.5.4 Peptide identification

Proteins with at least 50 % change in secretion extracted by mass spectrometric screen of the proteome comparing HeLa wt cells and Cab45 KO cells were given to the group of Bianca Habermann (former MPI of Biochemistry Munich, now IBDM Marseille) for analysis. Based on this protein list, a putative Cab45 interaction model was extracted by a Hidden Markov Model comparison published in Prytuliak et al., 2017³⁹⁷.

5.5.5 Structural model of Cab45

The structural model of Cab45 was assembled by the collaborating group of Bianca Habermann (former MPI of Biochemistry Munich, now IBDM Marseille). The methods applied in this case were published in Crevenna et al., 2016 ³⁸⁷.

5.5.6 Circular dichroism spectroscopy (CD)

CD measurements were performed in a 1-mm (path length) cuvette at 10 °C on a JASCO J-715 spectrometer. Protein samples (0.2 mg/ml) were dissolved in CD buffer, and the indicated amounts of calcium were added before spectra were recorded. An average of 10 (\pm calcium analysis) or 4 (titration assay) independent spectra (from 195 to 250 nm with 0.1 nm spacing) were documented. Data was normalized to molecular ellipticity of protein and FFT filter was applied. CONTIN analysis was done using CDPro. CONTIN decomposes the CD signal into 6 secondary structure elements: regular alpha-helical, distorted alpha-helical, regular beta sheet, distorted beta sheet, turn and unordered. Reported values for the alpha-helical and beta sheet content were the sum of regular and distorted fractions for each secondary element.

5.6 Microscopy methods

5.6.1 Immunofluorescence (IF) analysis

For immunofluorescence stainings, cells were cultured on 1.5 mm Menzel glass slides (12 mm diameter; Thermo Fisher Scientific, Waltham, USA), fixed for 10 min at RT in 4 % paraformaldehyde in PBS, washed with PBS and subsequently permeabilized for 5 min in permeabilization solution. After washing again in PBS and blocking of slides for at least 1 h in 4 % BSA in PBS, cells were incubated with primary antibodies for at least 1 h at RT or o.n. at 4 °C. After washing several times in PBS the secondary antibody (all diluted 1:500 Invitrogen, Waltham, USA) was subsequently incubated for 1 h at RT, before washing and mounting the glass slides with Prolong Gold Antifade reagent onto SuperFrost Microscope slides (90 °C ground edges; 1 mm) (both Thermo Fisher Scientific, Waltham, USA). DAPI (Sigma-Aldrich, Munich, Germany) was always used 1:6000 and incubated together with the secondary antibody. Dried samples were imaged on a ZEISS confocal laser-scanning LSM 780 microscope equipped with 40x (NA 1.4 oil) or 100x

Material and Methods

(NA 1.46 oil) Plan-Apochromat objectives (ZEISS, Oberkochen, Germany). Pictures were acquired using ZEN 2010 software and processed in ImageJ.

Antibody	Dilution	Company	Product ID
α -Cab45	1:300	Self-made	Crevenna et al., 2016 ³⁸⁷
α -Calnexin	1:300	BD BioSciences	610523
α -GM130	1:300	BD BioSciences	610822
α -HA	1:250	Roche	11867423001
α -p230	1:300	BD BioSciences	611281

Table 7: Overview of antibodies used for immunofluorescence stainings with the corresponding dilutions. All secondary fluorescently labeled antibodies were diluted 1:500 and purchased from Invitrogen (Waltham, USA).

For improved visualization images were processed in ImageJ, background of all pictures was subtracted and contrast enhanced. If necessary, contrast was manually adjusted by enhance contrast function.

5.6.2 Quantifications of vesicular structures in calcium-binding deficient mutants

For quantification, images of HeLa Cab45 KO cells stably expressing Cab45 wt, Cab45 6EQ, Cab45 EFh1, Cab45 EFh2 or Cab45 EFh3 were acquired with 40x oil objective as described above (section 5.6.1).

For data analysis in ImageJ, the background was automatically subtracted and the contrast enhanced. Median filter was applied and the picture transformed into an 8-bit image. Suitable cells were manually selected by drawing a region of interest. Threshold was set automatically, and binary image (generated by thresholding) was analyzed by “analyze particle function” for chosen regions of interest. Thereby, only particles of the size of 4 to 20 pixels were included in the analysis. Data was visualized by Prism Software.

5.6.3 Retention using selective hooks (RUSH)

For tracking of MGP wt or its 3A mutant along the secretory pathway, HeLa wt or HeLa CRISPR/Cas9 Cab45 KO cells were seeded on glass slides. Cells were transfected by PEI reagent as described above with pIRES constructs (section 5.2.3 and Table 1) and cultured for 24 h. On the next day, cells were washed twice with DPBS and incubated for indicated periods (0 min, 20 min or 40 min) in 100 μ M biotin in growth medium. Subsequently, cells were immediately washed twice, fixed, permeablized and stained with α -p230 antibody as described above. Z-stacks were acquired with LSM780 as indicated previously (section 5.6.1) with a constant distance of 0.35 μ m between layers.

For data analysis in ImageJ, the background was automatically subtracted and the contrast enhanced. After maximum intensity projection of the Z-stacks, Median Filter was applied and the picture transformed into an 8-bit image. Suitable cells were manually selected by drawing a region of interest. For thresholding, the algorithms yen or otsu were used and controlled, and if necessary adjusted, by hand. The binary image (generated by thresholding) was analyzed by “analyze particle function” for chosen regions of interest. Thereby, only particles of the size of 4 to 20 pixels were included in the analysis.

For statistical evaluation, the two highest and two lowest values were eliminated for each cell line and time point and a non-parametrical test (Kolmogorov-Smirnov-Test) was performed by Prism software.

5.6.4 Oligomerization assays

For oligomerization assays all proteins were thawed on ice and centrifuged 15 min at 13200 rpm at 4 °C to remove aggregates. Protein concentrations were adjusted to 2.5 µM in PBS pH 7.4. For measurements proteins were diluted 1:100 in a total volume of 100 µl in PBS pH 7.4 and analyzed in Lab-Tek 8 Chamber #1.0 borosilicate coverglass system (Nunc, Rochester, USA) with a LSM780 confocal microscope as described above (section 5.6.1) under the indicated conditions. Proteins used in this assay were either selfmade (section 5.3.3) or purchased (compare section 5.3.6). LyzC-Cy5 protein was purchased from Nanocs (New York, USA) and Cathepsin D (Creative Biomart, Shirley, USA).

5.6.5 Fluorescence recovery after photobleaching (FRAP)

Fluorescence recovery after photobleaching (FRAP) experiments of recombinant fluorescently labeled proteins were conducted on a spinning-disk confocal microscope system (Revolution system; Andor Technology, Belfast, UK) consisting of a Nikon base (TE2000E; Nikon, Tokyo, Japan) and a spinning-disk unit (CSU10; Yokogawa) with a Nikon 100× oil immersion objective (NA 1.49) at 20 °C. The detection path was equipped with an Optosplit II (Cairn Research Ltd., Faversham, UK) for dual-color detection, a filter set for enhanced green fluorescent protein (eGFP) and Cy5 (BS562, HC525/50, and ET605/70; AHF Analysentechnik AG), and a DU-897 Ixon EMCCD camera (Andor Technology). In addition, a triple-band dichroic beam splitter was used to separate laser excitation from fluorescence emission (Di01-T405/488/568/647; Semrock, Rochester, NY). The excitation was controlled with a tunable acousto-optic filter (Gooch & Housego, Ilminster, UK). FRAP experiment were done by first acquiring 5 frames, then applying a

bleaching pulse for 5 s and finally acquiring 300 frames. The chosen time interval between consecutive frames was 2 s. Proteins used for this experiment were unlabeled Cab45 wild type (5.3.3), Alexa647 labeled COMP (5.3.4) and LyzC-Cy5 purchased from Nanocs (New York, USA).

5.6.6 Three-dimensional structured illumination (3D-SIM) microscopy

For Super-resolution imaging, cells were seeded and treated as described above in section 5.6.1. Three-dimensional structured illumination microscopy was performed with a DeltaVision OMX v3 (GE, Fairfield, USA) equipped with a 100x/1.40 NA PlanApo oil immersion objective (Olympus, Center Valley, USA), Cascade II:512 EMCCD cameras (Photometrics, Tucson, USA) and 405, 488 and 593 nm diode lasers. Samples were illuminated with coherent scrambled laser light directed through a movable optical grating. Image stacks with 15 images per plane (5 phases, 3 angles) and a z-distance of 125 nm were acquired and subjected to a computational reconstruction (softWoRX, Applied Precision, Bratislava, Slovakia).

3D SIM raw data were first reconstructed with the GE software softWoRx 6.0 Beta 19 (unreleased) and corrected for color shifts. A custom-made macro in Fiji was used to establish composite TIFF stacks that are subsequently loaded as RGB into the Volocity calculation software (Volocity 6.1.2 (Perkin Elmer, Waltham, USA). Structures were obtained, segmented and measured in all channels by using the threshold commands “threshold using intensity” and “exclude objects by size”. Reconstruction artifacts and background were also removed. Colocalizing structures were recognized by the “intersect and compartmentalize” command, and quantified according to volume and number. Several small volumes belonging to one compartment were combined. Cab45 was set as 100 %. Overlapping volumes were used to calculate the degree of overlap in %. Finally, a histogram was calculated using 10 % bins.

5.7 Buffers

Breaking Buffer (BB)	10 mM Tris pH 7.4, 250 mM sucrose
Cab45 buffer	20 mM PIPES, pH 6.8, 500 mM NaCl, 10 % glycerol vol/vol
CD buffer	1.3 mM PIPES pH 6.8, 33 mM NaCl and 0.7 % glycerol
Coomassie solution	40 % v/v methanol, 10 % v/v acetic acid, 0.1 % w/v Coomassie Brilliant Blue R
Destain solution	40 % v/v methanol, 10 % v/v acetic acid
DNA loading dye	3 % glycerol, 0.15 % OrangeG
FACS buffer	3 % BSA in PBS
Freezing medium	90 % FBS, 10 % DMSO
LB growth medium	1 % w/v Trypsin-Peptone, 1 % w/v NaCl, 0.5 % w/v yeast extract
Loading dye for SDS Pages	200 μ M Tris pH 6.8, 4 μ M EDTA, 84.5 % glycerol, 8 % SDS, 4 % β -mercaptoethanol, 0.05 % bromophenol blue
His Binding Buffer	50 mM NaP, pH 8.0, 500 mM NaCl.
His Elution Buffer	50 mM NaP, pH 8.0, 500 mM NaCl, 250 mM imidazole
MS buffer A	0.1 % formic acid
MS buffer B	0.1% formic acid and 80% acetonitrile
MS buffer C	30 % methanol, 1 % trifluoroacetic acid
MS buffer D	2 % acetonitrile, 0.2 % trifluoroacetic acid
MS buffer E	60 % acetonitrile, 1.25 % ammonium hydroxide
MS buffer F	2 % acetonitrile, 0.1 % trifluoroacetic acid
MS buffer G	80 % acetonitrile, 0.1 % formic acid
MS lysis buffer	10 mM Tris pH 7.5, 4 % SDS, 10 mM DTT
PBS	10 mM Na ₂ HPO ₄ , 1.7 mM NH ₂ PO ₄ pH 7.4; 2.6 mM KCl, 137 mM NaCl
PEI solution	1.25 mg/ml PEI in sterile water; pH 7.4
Permeabilization solution	0.2 % TritonX-100 and 0.5 % SDS in 4 % BSA in PBS
PIPES buffer	20 mM PIPES, pH 6.8, 500 mM NaCl
Running buffer	25 mM Tris pH 7.4, 190 mM glycine, 0.1 % SDS
Separating gel (12 %)	375 mM Tris pH 8.8, 12 % v/v acrylamide, 0.1 % w/v SDS, 0.01 % v/v APS, 0.0015 % v/v TEMED
Stacking gel (5 %)	125 mM Tris pH 6.8, 5 % v/v acrylamide, 0.1 % SDS, 0.01 % v/v APS, 0.001 % v/v TEMED
Solution A	PBS, pH 7.4
Solution C	PBS pH 7.4, 10 mM sodium bicarbonate
TAE buffer	40 mM Tris, 1 mM EDTA, pH 8.3
Transfer buffer	25 mM Tris pH 7.4, 192 mM glycine, 20 % v/v methanol
TBS buffer	25 mM Tris pH 7.4, 150 mM NaCl
TFE buffer	10% 2-2-2-trifluoroethanol, 100 mM ammonium bicarbonate (ABC)
Trypsinization solution	10 % Trypsin-EDTA in PBS
TSS buffer	1 % tryptone-peptone, 0.5 % yeast extract, 100 mM NaCl, 10 % PEG (MW3000/3500), 5 % DMSO, 50 mM MgCl ₂ , pH 6.5
Urea buffer	4 M Urea, 25 mM Tris pH 8.0, 10 mM DTT

Table 8: Summary of buffers used in this thesis. All buffers listed were prepared with Millipore water.

6 Results

The first aim of this thesis was to generate and optimize certain cell biological and biochemical tools for analysis of the CFL1/SPCA1/Cab45 machinery in living cells and *in vitro*. Firstly, the purification process needed to be optimized, because the protein yields obtained by purification from *E.coli* cultures via GST-tag, as described before by von Blume and colleagues, did not provide suitable protein amounts for extensive *in vitro* studies³⁶⁵. Secondly, the transient overexpression of Cab45 in HeLa cells results in massive secretion far beyond the physiological levels, which might influence the natural functionality inside the Golgi lumen. Therefore, mutants controlled by the endogenous promoter system should be established by the clustered regularly interspaced short palindromic repeat (CRISPR/Cas9) technique to maintain adequate protein levels also of potential mutants.

6.1 Cab45 was purified from SF9 cells in high amounts

In order to obtain higher protein yields of Cab45 for *in vitro* analyses, several characteristics of the purification process were changed. First of all, expression was switched from a prokaryotic to the eukaryotic SF9 insect cell system, which provides more suitable environmental conditions concerning e.g. pH, salts and lipid composition, for the human Golgi protein. Furthermore, Cab45 was expressed as fusion protein with a cleavable His-SUMO tag to enhance solubility and to facilitate the subsequent purification steps. In addition, the fact that overexpression causes secretion of Cab45 was exploited for purification, because less unwanted impurities are found in the supernatants and the protein can be isolated more easily during less purification steps than from cell lysates.

Figure 15A illustrates the progress of one exemplary purification of wild type Cab45 from one liter SF9 supernatant. The purification of all mutants mentioned throughout this thesis was conducted accordingly. The faint band around 65 kDa in the input lane of the Coomassie brilliant blue stained SDS page shows that Cab45 was highly expressed in the insect cells and that it was the predominant protein in the supernatant.

The flow through (FT) and the wash lane on the gel prove that the whole amount of protein was bound to the Ni-NTA column during the first purification step and, in

concordance with the western blot (Figure 15B), only a small amount of protein was lost during washing of the column.

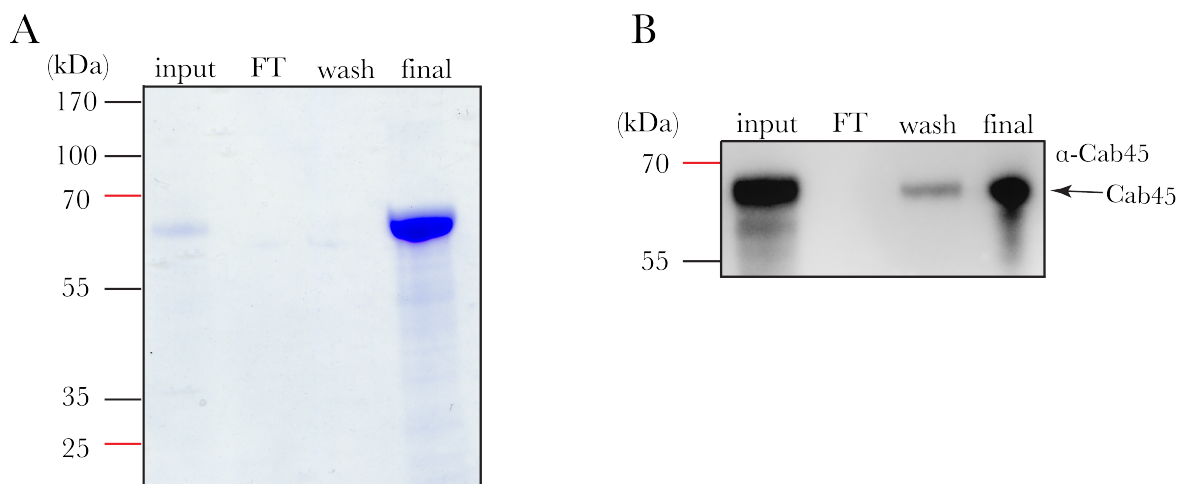


Figure 15: Successful optimization of Cab45 protein purification from SF9 cell supernatants. (A) Coomassie brilliant blue stained SDS page of sequential steps of the Cab45 purification process. The input lane indicates that Cab45 was highly enriched in the supernatants of SF9 cells. The absence of the Cab45 band during column application (flow through; FT) and washing (wash) shows that all protein was bound to the Ni-NTA column and no protein was lost during the washing steps. The final lane depicts the highly-concentrated protein after purification. (B) Western blot analysis of the samples described in (A) proves that the Coomassie signal is specific and that indeed Cab45 was purified in high amounts from insect cells.

The eluted protein was subsequently concentrated and stored or used for *in vitro* analysis after buffer exchange (see lane “final”). The strong band in the final lane of the SDS page indicates that the protein was efficiently isolated and the western blot, detected by an anti-Cab45 antibody, proves that the signal observed in the Coomassie brilliant blue stain is specific for Cab45. These results imply that Cab45 could be successfully isolated from SF9 cells and yields between 2 to 3 mg per liter supernatant were sufficient for further *in vitro* studies.

6.2 Successful generation of two CRISPR/Cas9 cell lines

The major problem during in-cell analysis of Cab45, was the high amount of aberrant secretion after transient expression of the protein in HeLa cells (Figure 16). As a consequence of high expression levels, the protein is no longer retained inside the Golgi, which might affect its natural function. Therefore, one aim of this thesis was to establish a genome editing technique to generate mutants under the control of the endogenous SDF4 promoter. This would also pave the way to identify new cargos and other interactors by reducing overexpression-induced, unspecific interactions. Furthermore, a KO cell line

Results

would shed light on Cab45 dependent cargo sorting and secretion, and would abolish the need of time-consuming siRNA experiments.

Consequently, the CRISPR/Cas9 method was applied to generate first a KO and secondly a cell line containing a multifunctional integrase (MIN) tag (Figure 17). Therefore, the Cas9 protein together with single guide RNAs (sgRNAs) was transfected into HeLa cells^{384,398}.

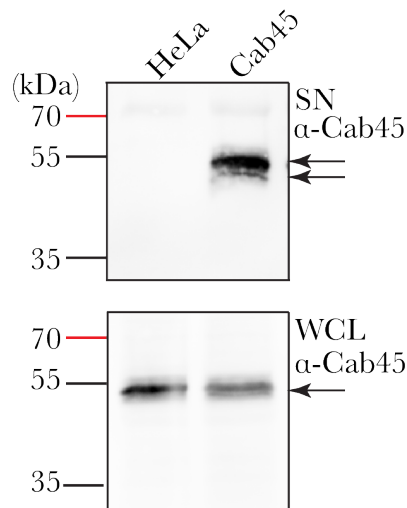


Figure 16: Transient overexpression of Cab45 results in secretion of the Golgi resident protein from HeLa cells. Western blot analysis with α -Cab45 antibody of supernatants (SN) and cell lysates (WCL) indicate secretion of Cab45 in cells overexpressing the protein in contrast to HeLa wild type cells. WCL blot indicates similar cellular amounts of both samples. Characteristic double band (black arrows) of secreted Cab45 in the SN is due to differential glycosylation patterns as observed before by Lara-Lemus and colleagues³⁷⁴.

The combination of the endonuclease with sgRNA induces a specific double strand break inside the genomic region of interest, which can be repaired by healthy cells either by non-homologous end joining (NHEJ) or by homology directed repair (HDR)^{380,385}. During NHEJ, cells just re-ligate blunt ends without regard to homologies, which often results in deletion or insertion of a few nucleotides potentially leading to a frame shift mutation and a premature stop codon (Figure 17)³⁹⁹. In contrast, the cell mediates HDR by employment of an undamaged sister chromatid or a homologous region as template^{400,401}. This pathway enables integration of a sequence of interest into the genomic locus.

In the framework of this thesis two CRISPR/Cas9 modified HeLa cell lines were generated. In a first approach, we applied the NHEJ method to produce a Cab45 KO cell line in order to study cellular dynamics and morphology according to the protocol of Ann Ran and colleagues³⁸⁴. Furthermore, we integrated a MIN-tag by HDR after the endogenous signal sequence of Cab45 to establish a genetic platform for the integration of Cab45 mutants for analysis of those under the control of the endogenous promoter³⁸⁶.

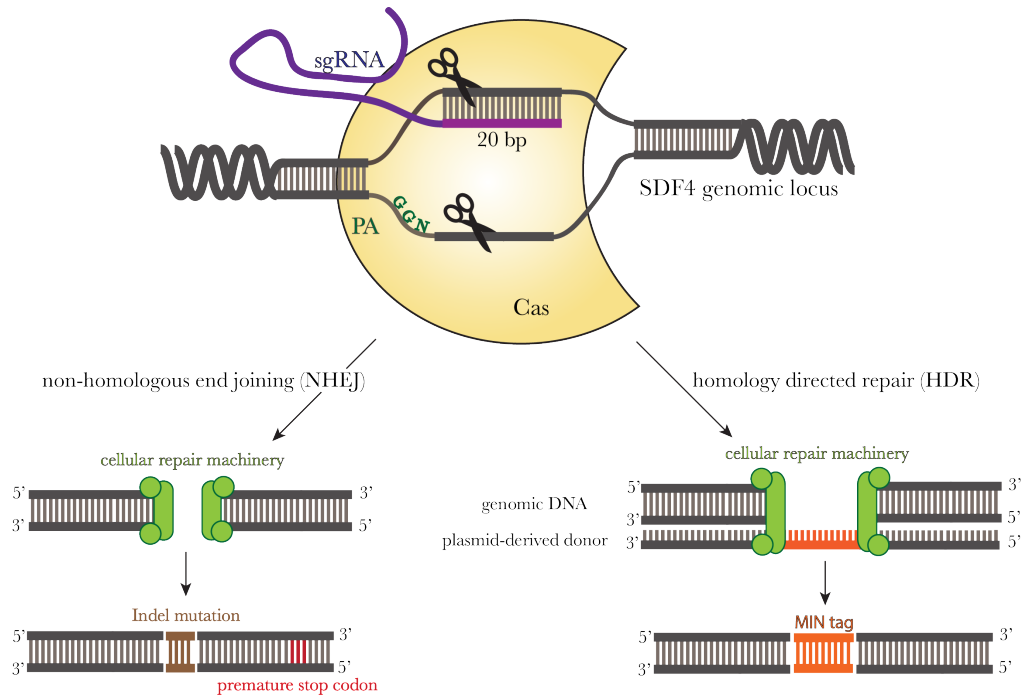


Figure 17: Schematic depiction of CRISPR/Cas9 system. The endonuclease Cas9 (yellow) is guided to the SDF4 genomic locus by the sgRNA, a fusion construct of complementary crRNA (pink) and the tractRNA (purple). There, a double strand break is mediated 3 bp upstream of the PAM recognition sequence NGG (dark green). This DNA damage is subsequently repaired by the cell's innate machinery (light green) by either non-homologous end joining (NHEJ; left pathway) or by homology directed repair (HDR; right pathway). During NHEJ the cells re-ligate the blunt ends of the DNA often causing insertions or deletions (brown) in this area which both can result in a frame shift mutation and a premature stop codon (red). In HDR a 200 bp fragment transfected together with the CRISPR/Cas9 machinery serves as homologous sequence or repair template. This enables insertion of the MIN tag (orange) into the SDF4 genomic locus during DNA repair processes. Figures were adjusted from Ran et al., 2013³⁸⁴ and Crevenna et al., 2016³⁸⁷.

6.2.1 CRISPR/Cas9 KO targeting by two different sgRNAs was highly efficient

Because the efficiency of different sgRNAs can differ due to accessibility of the target and Cas9 expression levels, we targeted the second exon of SDF4 by two different sgRNAs in parallel^{383,402}.

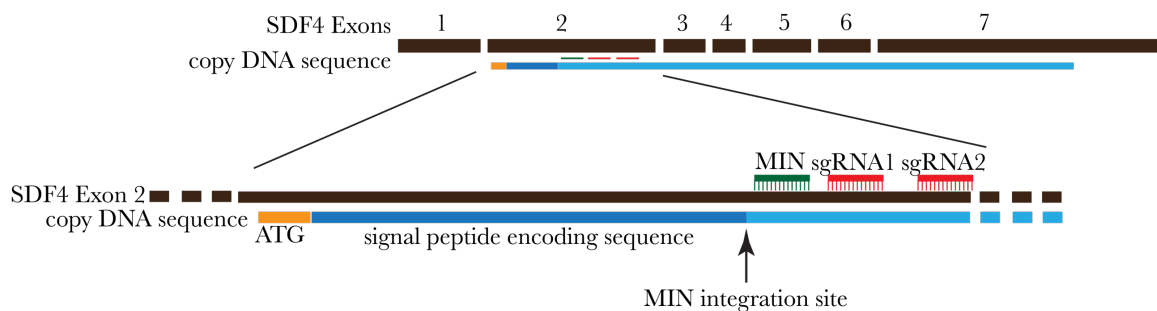


Figure 18: Schematic depiction of CRISPR/Cas9 targeting approaches. For the generation of Cab45 KO HeLa cell lines the second exon of the SDF4 genomic locus (black lines, Arabic numerals) were targeted by two different sgRNAs (red) after the initial ATG codon (orange) and the signal peptide encoding sequence (dark blue). In the same region, the sgRNA for the MIN tag integration (dark green) hybridized with the genomic DNA for insertion of the MIN tag just behind the signal peptide (black arrow).

Results

After antibiotic selection and expansion of single cell colonies the clones were initially screened by western blot (Figure 19) and then verified by immunofluorescence microscopy (Figure 20) and sequencing (Figure 21).

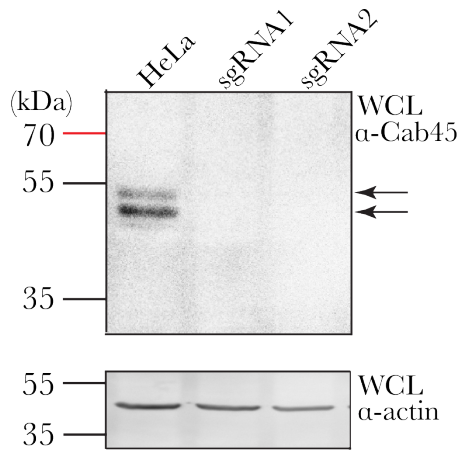


Figure 19: Western blot analysis of CRISPR/Cas9 Cab45 KO clones. Western blot analysis of cellular lysates of HeLa wild type cells and CRISPR/Cas9 Cab45 KO cell lines indicates specific Cab45 bands at the expected size for the control. In contrast, the cells treated with sgRNA1 or sgRNA2 lack the protein specific band, which indicates the successful KO of Cab45. Detection of actin levels prove comparable loading amounts.

For western blot analysis Cab45 expression of the KO clones was compared to HeLa wild type cells (Figure 19). The CRISPR/Cas9 KO clones show no Cab45 band at the expected size of around 55 kDa, while the HeLa wild type fraction indicates a double band, i.e. normal expression of the protein. The actin loading control confirms equal loaded amounts of lysate.

6.2.2 CRISPR/Cas9 KO cell lines show no change in Golgi morphology

To further verify the Cab45 KO, the protein and the Golgi marker GM130 were stained by antibodies for analysis by immunofluorescence microscopy (Figure 20). In the wild type control Cab45 is localized in the Golgi region. The signal nicely colocalizes with GM130, while the DAPI stain indicates the correct localization of both proteins in the perinuclear region. In contrast, images of both KO cell lines confirm the absence of Cab45. However, the staining by the marker protein and DAPI indicates intact Golgi and nuclear signal also in the absence of Cab45.

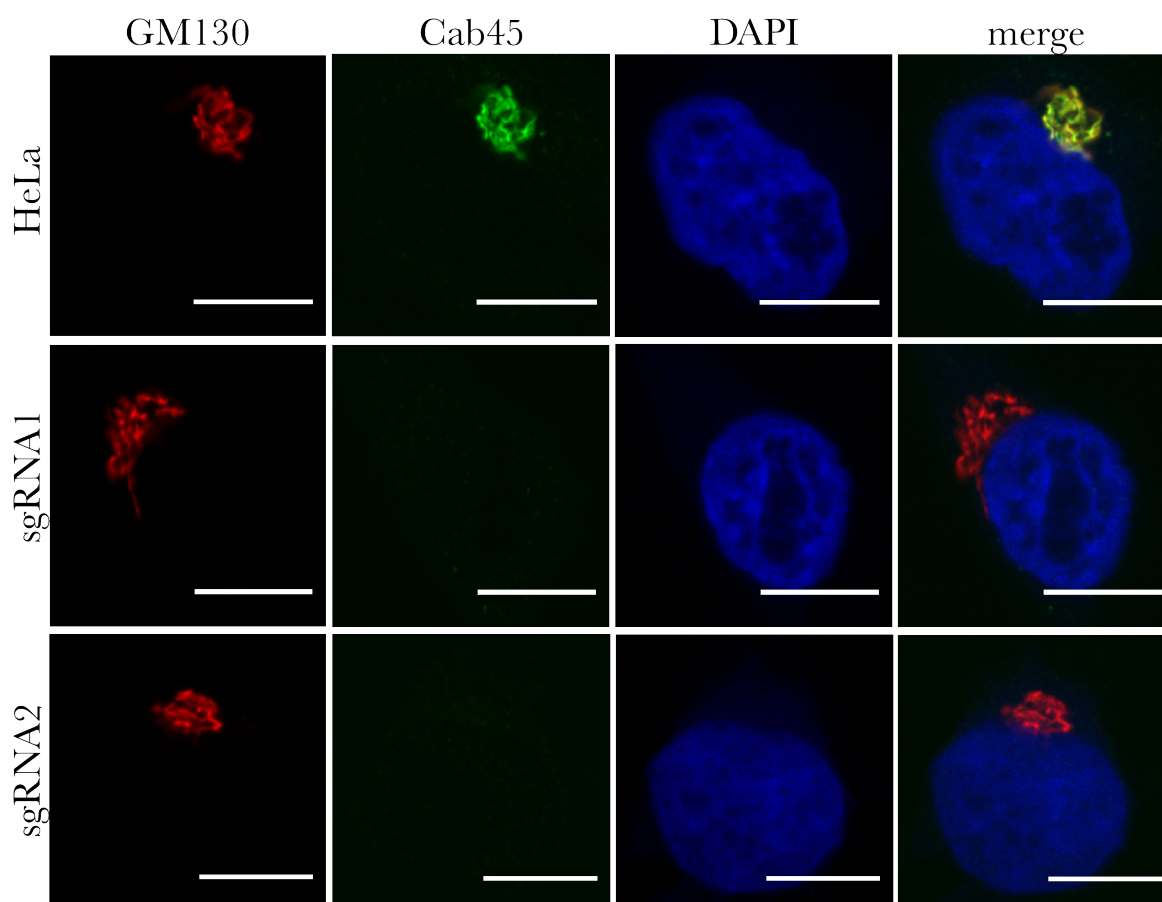


Figure 20: Immunofluorescence analysis of Cab45 KO cell lines. Cab45 KO cell lines were analyzed with respect to overall cell morphology by immunofluorescence microscopy. HeLa wild type cells exhibit characteristic, tube-like staining pattern of the Golgi in the perinuclear region by marker protein GM130 (red channel). In these cells, Cab45 localizes to the same area (green channel) and merged picture indicates high levels of co-localization of both proteins (yellow). In KO cells, GM130 distribution seems comparable to wild type cells, but Cab45 is no longer present at the Golgi (green channel). However, DAPI and Golgi marker underline normal Golgi and nuclear morphology. Scale bars represent 10 μm .

6.2.3 CRISPR/Cas9 KO could also be verified on genomic level

Finally, the introduced changes on DNA levels were analyzed by sequencing. To this end, genomic DNA of the KO clones was isolated and the region of interest amplified by PCR. The resulting PCR product was subjected to sequencing.

As an example, the sequencing results of the KO clone of sgRNA1 are shown, as this clone was subsequently used throughout the whole thesis.

Figure 21A indicates, that 8 base pairs of the original HeLa sequence were excised in the sgRNA1 clone due to incorrect cellular repair mechanisms after double strand break by Cas9. This deletion led to a frameshift, which resulted in a stop codon after 15 subsequent base pairs. In addition, the location of the deletion corresponds nicely to the described Cas9 cutting site three bp upstream of the PAM ^{384,398}. This finding and also the

Results

experiments mentioned above, support the success of the KO of Cab45 in the HeLa cell line.

The majorly discussed drawback of the CRISPR/Cas9 system is the generation of so-called off-target effects ^{403,404}. Off-target effects can occur by annealing and cleavage of the sgRNA/Cas9 complex to unintended target sites.



Figure 21: Sequencing analysis of SDF4 KO clone. (A) Extract of sequencing result of SDF4 KO clone was compared to HeLa wild type genome. While points indicate accordance of the two sequences the eight horizontal lines signal missing bases in the SDF4 KO sequence. The observed deletion in this area matches either the sgRNA binding site (blue) and the predicted cutting site of Cas9 three bp upstream of the PAM sequence (green). This mutation leads to a frameshift and an early stop codon, which supports the findings of the absence of Cab45 in these KO cells described above. (B) Sequencing result of off-target region. The first off-target region calculated by the online tool was sequenced and compared to HeLa wild type genome. The black dots indicate complete homology of both sequences in the region of the unintended sgRNA binding (blue). Also, close to the PAM recognition sequence (green) no changes are detectable. This finding indicates that the Cab45 genomic locus was efficiently targeted by the used sgRNA and that changes in protein secretion are probably not caused by other reasons than Cab45 KO.

This can happen because the short sequence of 20 bp might appear similarly more often in the whole genome and because certain mismatches might only decrease, but not abolish binding. The potential off-target sites for our guides were determined by the online tool of the Zhang lab available at crispr.mit.edu and evaluated by a score value which reports the reliability of the guide. The calculated Score of 77 was based on potential 124 off-target sites, whereof 43 of these sites were located in an exonic area (first three are shown in Table 9). To study the actual impact of sgRNA1 off-targets, the first exonic target was analyzed by sequencing (Figure 21B).

	Sequence of off-target site	Score	Number of mismatches	Gene name
1.	TGGCCGAGGC CGCGGAGCCG CAG	1.3	4	NM_053277
2.	ACGATGAGGA CGTGGAGCCG CAG	1.2	3	NM_174911
3.	CTGAGGCCGA CGCGGAGCCG GGG	0.9	4	NM_020764

Table 9: Overview of first three sgRNA1 off-targets sites. Mismatches to original guide sequence were highlighted in red, seed sequence of sgRNA1 in yellow and PAM in green. Scores and gene names were obtained by CRISPR design tool available at crispr.mit.edu.

All three off-target sites share at least one mismatch in the PAM sequence (highlighted in green), but most of the mismatches were located outside the seed region (highlighted in yellow), the 10-12 bp adjacent to the PAM sequence, which is especially important for proper annealing^{401,405}.

This resulted in a comparably high score and high probability of a double strand break induced by Cas9 on unintended target regions. Nonetheless, the sequencing result demonstrated a correct DNA sequence (Figure 21B). The sequence is identical with the HeLa wild type genome and the site seems not to have been modified during the CRISPR/Cas9 KO targeting. This finding supports the idea, which subsequent changes in cargo sorting and secretion are not due to unwanted effects, but caused by Cab45 absence.

6.2.4 Modified cell lines proliferate normally

To further analyze the phenotype the CRISPR/Cas9 cells, I performed a proliferation assay of control versus Cab45 KO or MIN-tagged cells. Therefore, cell numbers were counted on four consecutive days (Figure 22). The figure demonstrates that the three cell lines proliferate in a comparable manner. The Cab45 KO cell line (orange) and the Cab45 MIN-tagged line (black) exhibit a similar proliferation rate as HeLa wild type cells (blue). Therefore, a KO of Cab45 does not seem to have an effect on cell division.

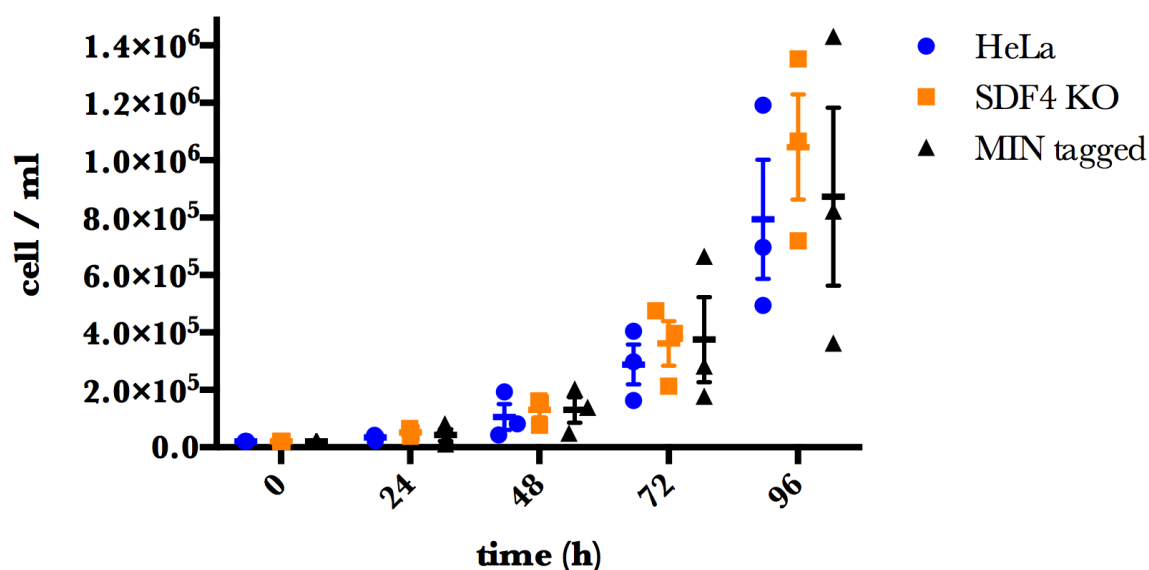


Figure 22: Growth assay of SDF4 CRISPR/Cas9 cell lines shows no significant difference in cell proliferation. HeLa control cells (blue), SDF4 CRISPR/Cas9 KO (orange) and MIN-tagged cells (black) were counted each 24 h and growth curves were depicted in the units cells/ml. All three cell lines proliferate to comparable levels, also in the absence of Cab45. Depicted is the mean of data points with SEM. Assays was conducted three times in triplets.

6.2.5 CRISPR/Cas9 KO cell lines mimic siRNA KD phenotype in secretion assays

Finally, the KO clones were compared functionally in secretion assays. Experiments performed previously with siRNA KD of Cab45 and SPCA1 in HeLa cells showed a missorting phenotype of Cab45-dependent cargo proteins including COMP and LyzC ³⁶⁵. In both cases absence of Cab45 resulted in accumulation of the secreted proteins inside the cell, while TGN sorting, export and secretion was inhibited. This phenotype could also be observed for both Cab45 KO cell lines (Figure 23).

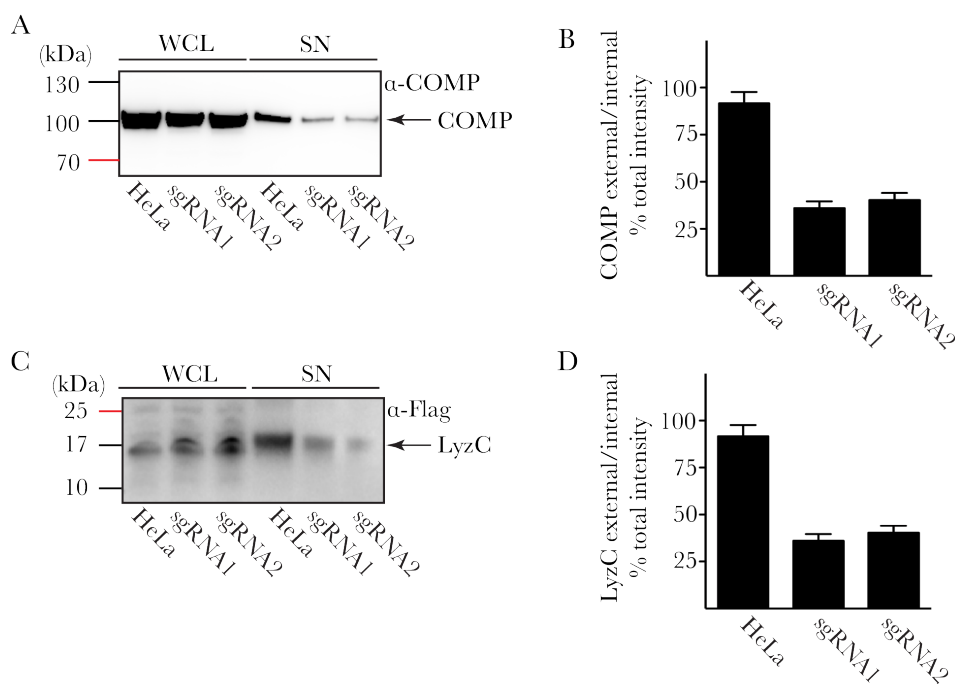


Figure 23: Secretion assays with Cab45 KO cell lines. Functionality of Cab45 KO cell lines was tested in secretion assays as described before by Vivek Malhotra's group ³⁶⁵. The secretion of two known cargo proteins, COMP (A and B) and LyzC (C and D) in HeLa and Cab45 KO cells was analyzed by western blot. Both proteins are present either in the cellular fractions (WCL) and in the supernatants (SN) of control cells. However, upon Cab45 KO especially LyzC accumulates inside the cells and secretion is strongly diminished. This phenotype is in line with results obtained from Cab45 and SPCA1 siRNA KD experiments published in ³⁶⁵.

Especially LyzC fractions increased in the lysate in comparison to wild type HeLa cells, while only faint bands remained detectable in the supernatants, which indicated that protein secretion was impaired (Figure 23A and C). The quantifications of the western blots underline that protein secretion was significantly reduced for COMP and LyzC with both sgRNAs to around 40 % of wild type levels (Figure 23B and D).

This experiment demonstrated that KD and KO of Cab45 caused the same defects in protein sorting and secretion at the TGN and the generated KO cells are suitable on a

genomic and functional basis for further analysis of the CFL1/SPCA1/Cab45 sorting machinery.

6.2.6 MIN-tag was successfully integrated into SDF4 locus

For the integration of the so-called MIN-tag by HDR, to generate a genetic platform for easy modification of the Cab45 genomic locus, only one sgRNA was used³⁸⁶(Figure 18). In addition, a 200 bp donor fragment containing homology arms and an attB site was transfected together with Cas9-GFP and a specific MIN sgRNA. After FACS sorting and single clone expansion, clones were lysed for genomic DNA isolation. DNA was used as template for amplification of the genomic region of interest by PCR. The PCR product was then subject to restriction enzyme digest. Positive clones could be identified on agarose gel by a shift, as an additional HincII cutting site was integrated along with the attB cassette.

One of 250 screened clones contained the correct insertion of the MIN tag. For this clone, the complete PCR product obtained from the genomic region of interest (around 450 bp) was digested by HincII to around 220 bp, as no band is longer visible at the size of the wild type control (Figure 24A). This proves that the clone received a homozygous insertion of the MIN tag, as a heterozygous clone would exhibit a double band.

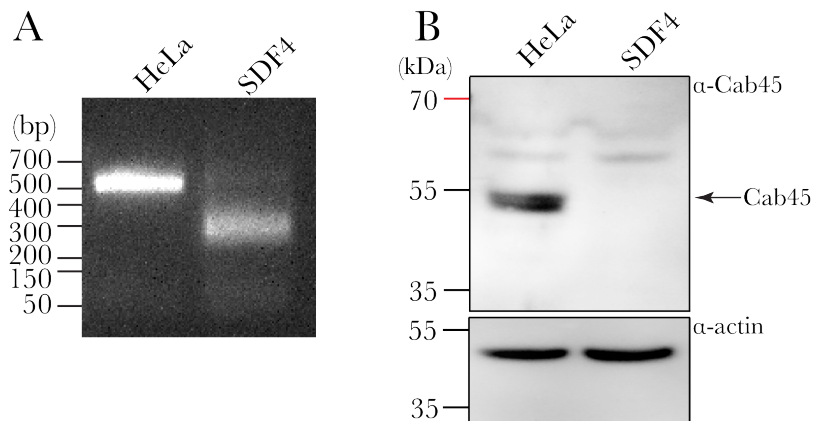


Figure 24: Characterization of MIN-tag SDF4 HeLa cell line. (A) Agarose gel analysis after HincII restriction digest of the PCR fragment of the SDF4 integration site in comparison to HeLa wild type control. The shift in the SDF4 MIN from 450 bp to around 220 bp hints to correct integration of the MIN-tag after the endogenous signal sequence. The absence of a band at the wild type level proves homozygous integration of the MIN-tag in this clone. (B) Western blot of WCLs of HeLa wild type and SDF4 MIN cell line suggests that Cab45 protein expression was abolished due to MIN-tag integration. Actin control attests similar amounts of loaded protein.

Results

Surprisingly, the specific Cab45 band on the western blot, comparing WCLs of HeLa wild type and the MIN-tagged clone, remained absent (Figure 24B). This indicated that protein expression was abolished in the clone, although the MIN tag was correctly inserted.

This finding was also supported by the microscopy analysis as no Cab45 signal was detectable by immunofluorescence. Again, the GM130 marker indicated no morphological changes of the Golgi as observed before for the intended KO clones (Figure 20). Finally, also the proliferation of this clone was comparable to the behavior of the KO cell line (Figure 22).

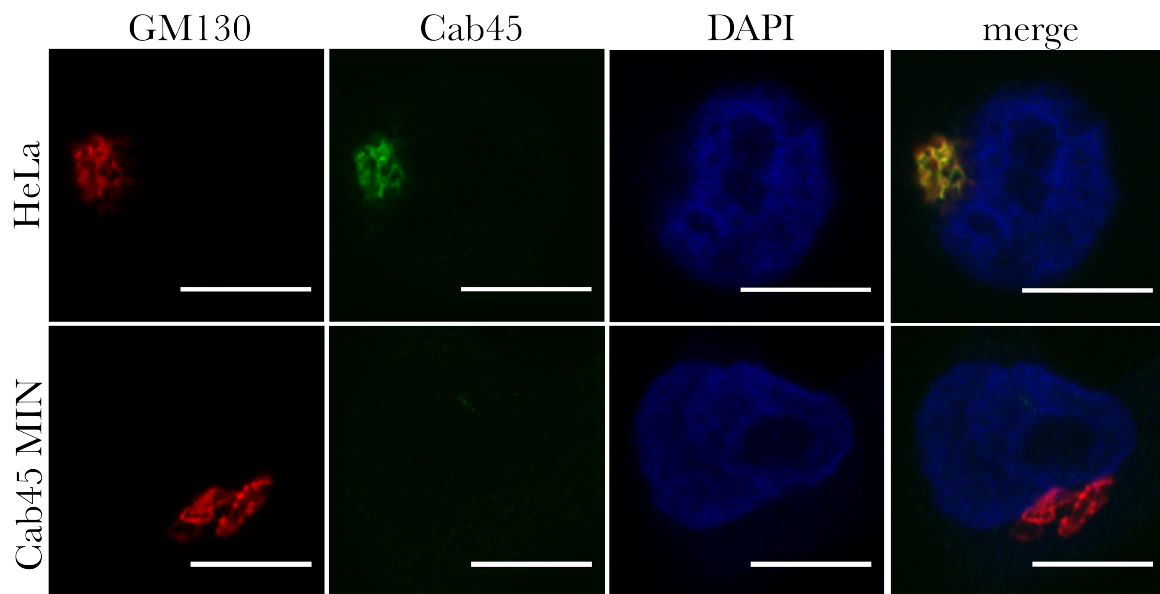


Figure 25: Immunofluorescence analysis of MIN-tag SDF4 cell line. Microscopy analysis of MIN-tagged SDF4 clone verifies absence of Cab45 protein from Cab45 MIN cells in comparison to HeLa wild type control (green channel). The GM130 Golgi marker (red channel) and the nuclear DAPI staining (blue channel) reveal the typical cellular structures and therefore no morphological changes, comparable to the KO cell lines described above (Figure 20). Scale bars represent 10 μm .

6.3 Cab45 oligomerizes in a calcium-dependent manner

Already in the first description in 1996, six stretches that match the consensus motif of EF hands were described in Cab45²²⁶. Consequently, Cab45 was considered as calcium binding protein, although the influence and function of this interaction have never been studied in detail. Therefore, the second aim of this thesis was to analyze the effect of calcium binding on Cab45 function.

The first indications that Cab45 is mainly dependent on its calcium binding sites were found in 2012, as treatment of HeLa cells with an ionophore led to secretion of Cab45 from HeLa cells⁽³⁶⁵⁾; section 3.5.3.4). Furthermore, disruption of the calcium binding

motifs by point mutations resulted in deficient cargo binding in IP experiments, but the direct impact of calcium on Cab45 remained obscure at this point.

6.3.1 Cab45 exhibits high molecular weight fraction in NativePAGE analysis

The key finding that calcium might be responsible for the oligomeric state of the protein was revealed by a Blue NativePAGE analysis of recombinant Cab45. Purified Cab45 was either left untreated or incubated with a high calcium concentration in the absence or presence of EGTA (Figure 26A). After separation by gel electrophoresis the calcium sample without EGTA showed two main fractions of Cab45, one lower band, matching the size of the western blot on a denaturing SDS PAGE (below), and one high molecular weight fraction of about 1000 to 1500 kDa.

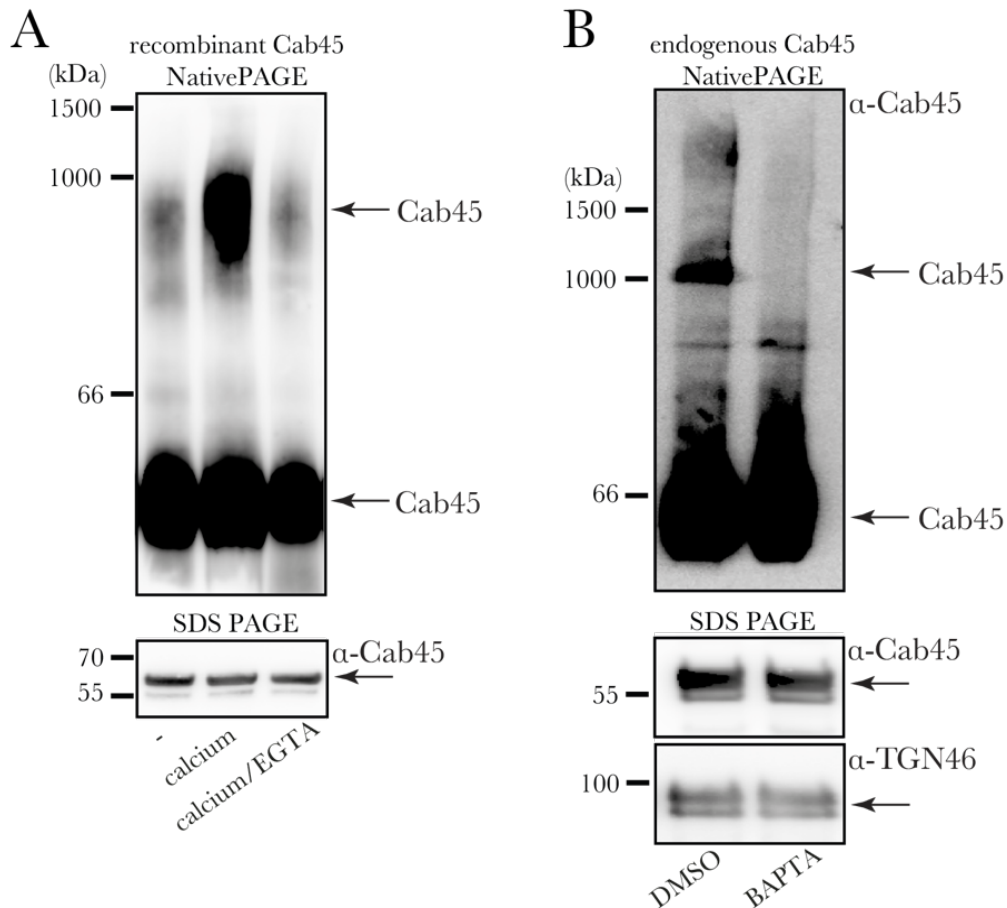


Figure 26: Blue NativePAGE analysis of recombinant and endogenous Cab45 reveal high molecular mass fraction in the presence of calcium. (A) Blue NativePAGE comparison of purified recombinant Cab45, which was either untreated or in the presence of high calcium or incubated with calcium and EGTA. While the calcium only sample reveals a high molecular weight fraction in addition to monomeric Cab45, this oligomer is absent in the untreated sample or the presence of EGTA. (B) Isolated Golgi membranes were incubated under control (DMSO) or calcium depleted conditions (BAPTA-AM) and analyzed by Blue NativePAGE and western blot. Similar to the recombinant protein, endogenous Cab45 exhibited a high molecular weight fraction in the presence of calcium.

Results

This upper band was less prominent in the presence of EGTA or the untreated sample. This indicated that Cab45 might appear in more than one molecular state, probably with a high molecular weight fraction.

To gain further insights into the change of the oligomerization state of Cab45 by calcium in living cells a similar assay was performed with endogenous protein. Therefore, purified Golgi membranes were incubated under control or calcium depleted conditions (in the presence of the calcium chelator BAPTA-AM) and subjected to Blue NativePAGE analysis and western blotting (Figure 26B). As observed for recombinant proteins, the cells treated by BAPTA-AM lacked the band of high molecular mass, which was detected in the control sample. These two experiments indicate the presence of an oligomeric form of Cab45 exists in living cells, which might be crucial for its physiological function.

6.3.2 Recombinant Cab45 forms oligomers *in vitro*

Based on those findings above, the oligomerization process of ATTO488 fluorescently labeled protein was visualized by confocal microscopy (Figure 27).

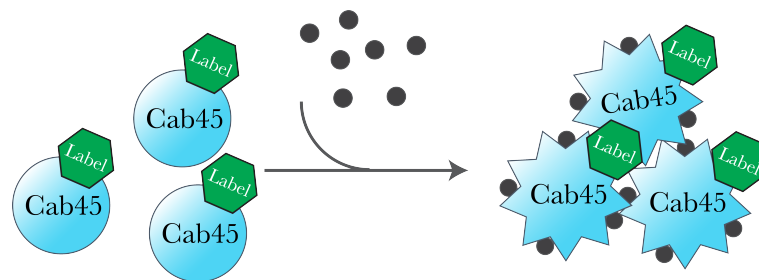


Figure 27: Principle of microscopy based oligomerization assay. Fluorescently labeled Cab45 (blue circles) can form oligomers (accumulation of blue stars) in the presence of high calcium concentrations (black dots). Sufficiently big oligomers can subsequently be visualized by confocal microscopy.

In buffer conditions, no fluorescent signal was detectable, i.e. no oligomers could be observed at this stage. However, addition of 1 mM calcium induced formation of multiple fluorescent dots, which represented the Cab45 oligomers, observed before during the Blue NativePAGE analysis. The subsequent addition of an equimolar amount of EGTA reversed the effect and dispersed the oligomers almost completely (Figure 28A).

To examine the calcium specificity for this reaction, a control assay was conducted with magnesium, another two-valent cation (Figure 28B). While 1 mM magnesium induced no oligomer formation, 10 mM of magnesium revealed a very low number of oligomers (white arrows). However, the effect was not comparable to calcium-induced oligomerization. Hence, the process seems to be calcium specific.

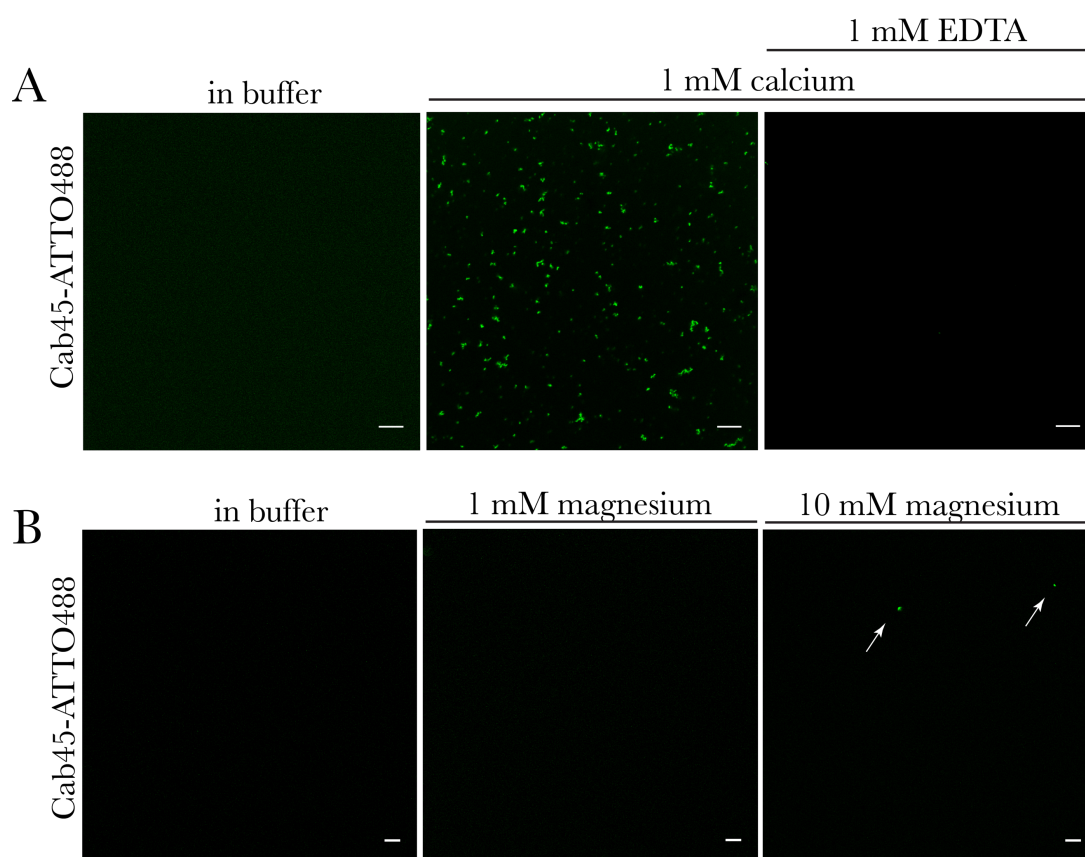


Figure 28: Confocal microscopy of fluorescently labeled recombinant Cab45 for visualization of oligomerization process. (A) ATTO488-labeled recombinant Cab45 was monitored by confocal microscopy. In the absence of calcium, no oligomers were detectable. Excess of calcium formation of fluorescent dots, which represent Cab45 high oligomeric weight fraction. Addition of EDTA reversed the calcium effect and dispersed the oligomers. (B) In the control experiment the same assay as described in A was conducted in the presence of the two-valent cation magnesium. Magnesium did not induce oligomerization at a concentration of 1 mM, and only very slightly at 10 mM (white arrows). However, amounts of oligomers were not comparable to calcium experiment. Scale bars represent 10 μm.

6.3.3 Calcium binding induces conformational change of Cab45

In many cases like calmodulin or the LDL receptor, calcium binding was attended by a conformational change of the protein ⁴⁰⁶. Therefore, Cab45 was tested by circular dichroism (CD) spectroscopy for changes in its secondary structure in the presence of calcium (Figure 29).

In the initial experiment Cab45 was first measured in buffer conditions (blue line). Here, the graph constantly decreases between 250 and 215 nm. Then a steeper drop with a minimum around 205 nm follows, before the values increase constantly until 190 nm. However, the ellipticity here remains on a low level. In contrast, a significant conformational shift is detectable in the presence of an excess of calcium (green line). The cation induces a faster decrease at the beginning of the measurement and causes two

Results

minima around 222 nm and 208 nm. In addition, ellipticity strongly increases after the second minimum. Based on model substrates, this curve progression indicates that Cab45 adopts a more alpha-helical fold in the presence of calcium ⁴⁰⁷.

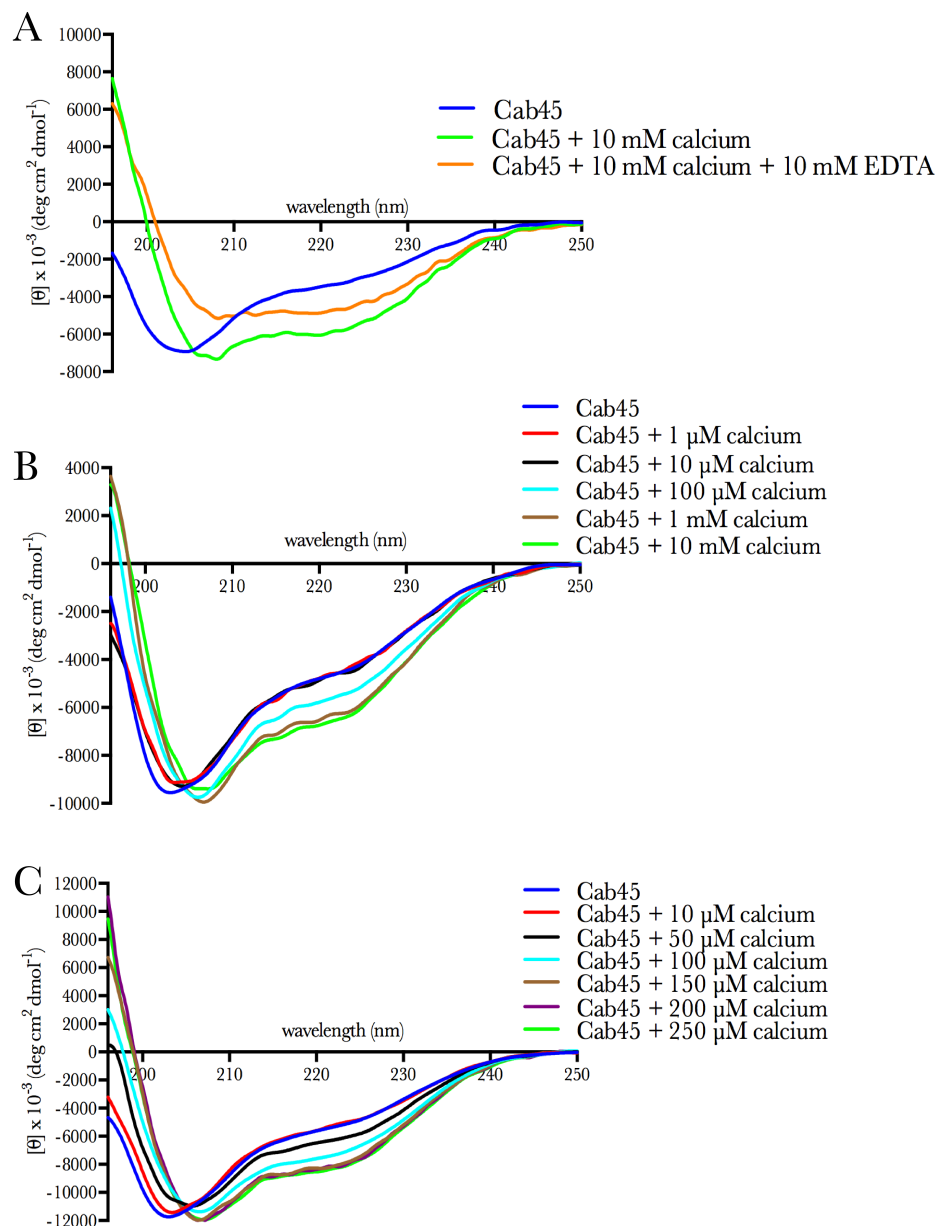


Figure 29: CD spectra of Cab45 wild type in presence and absence of calcium and calcium titrations. (A) Recombinant Cab45 was analyzed in the presence and absence of an excess of calcium by circular dichroism (CD) spectroscopy. In comparison to buffer conditions (blue line) the spectra of Cab45 in the presence of 10 mM calcium (green line) exhibit two minima around 222 and 208 nm, which indicate a shift to a more α -helical fold. This conformational change can be partly reversed by addition of EGTA (orange line). (B) and (C) Titration experiments reveal that the shift is induced around 50 to 100 μM calcium (black line in C and light blue line in B and C) and that the reaction is finished at concentrations above 150 μM (brown, green and purple lines).

Results of the secondary structure analysis by the CONTIN software supported the conformational shift from β -sheet (average decrease from 0.32 to 0.25) to increased α -helicity (average increased from 0.14 to 0.22) without significant alterations in random coil

content (Supplementary Table 1). Finally, equimolar addition of EDTA reversed the effect calcium, however, only partly (orange line). The presence of the chelator could not re-establish completely the fold of untreated Cab45. Instead, both curves represent some kind of folding intermediate between untreated and calcium bound Cab45.

In a second approach calcium was titrated stepwise to Cab45 to investigate the calcium sensitivity. Therefore, two independent experiments were conducted with different calcium ranges. In the first measurement (Figure 29B), the curves representing calcium concentrations between 0 and 10 μM (blue, red and black line) exhibit similar progressions as observed before for untreated Cab45 (Figure 29A). However, 100 μM calcium induced a conformational change to a more α -helical fold (light blue line). This shift was further intensified by 1 mM calcium (brown line). As no differences can be observed between 1 mM (brown line) and 10 mM (green line) calcium, the reaction was obviously already saturated at this point.

The second set of CD spectra (Figure 29C) focused on the area between 0 and 250 μM calcium, as this represents the range of the physiological calcium concentrations assumed for the trans regions of the Golgi apparatus^{178,408}. The results of this measurement are in line with the previous one, as no change in conformation was detectable with 10 μM calcium or below (blue and red line). However, the first switch was noticeable at 50 μM (black line), which intensified at 100 μM (light blue line). At 150 μM or above (brown, purple and green line) Cab45 has achieved its final shape.

Taken together the CD spectra proof that Cab45 undergoes indeed a conformational shift during calcium binding. Furthermore, calcium titration experiments reveal that around 150 μM calcium are necessary to induce this change. Given that the physiological calcium levels range around 130 μM in the TGN (Figure 8), the oligomers we observed during NativePage analysis (Figure 26) and microscopy experiments (Figure 28) likely represent the form of Cab45 found in the Golgi of living cells.

6.3.4 Only four of six EF hand motifs are required for calcium binding and oligomerization

To further assess the calcium binding properties of Cab45 a set of four mutants, containing point mutations of critical amino acids of the EF hand motifs, should be purified and analyzed in the assays described above (Figure 30).

The Cab45 6EQ mutant contains six E to Q amino acid exchanges, one in each EF hand motif. Based on the publication of Lam and colleagues³⁶⁷ these modifications disrupt the

Results

calcium binding sites and also cargo interaction as shown before by von Blume and colleagues in IP experiments³⁶⁵.

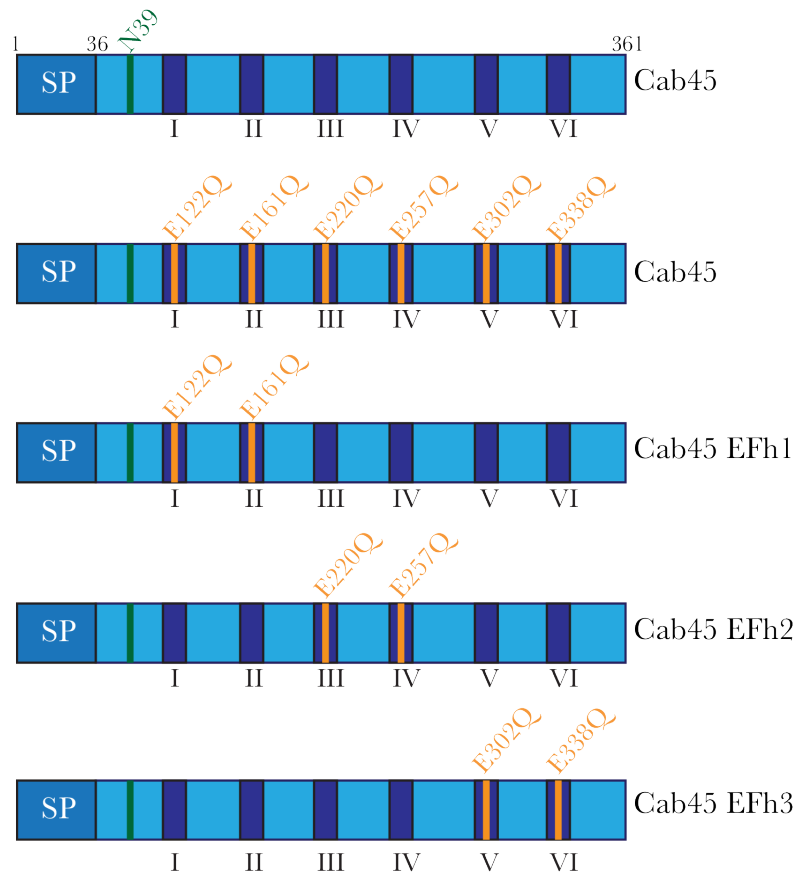


Figure 30: Schematic depiction of Cab45 and its calcium-binding deficient mutants. Cab45 (light blue box) contains a signal peptide (marked with SP) from amino acid 1 to 36 and a putative glycosylation site at N39 (green line)²²⁶. The six EF hands (dark blue boxes; marked by Roman numerals) are located between amino acid 39 and 361. In the 6EQ mutant six point mutations in the EF hand motifs (indicated by orange lines) were introduced to disrupt calcium binding sites. EFh1, EFh2 and EFh3 contain only two point mutations in adjacent EF hand motifs.

The other Cab45 mutants (EFh1, EFh2 and EFh3) comprise point mutations in two adjacent EF hand motifs, respectively (Figure 30). These alterations were based on a predicted 3D model by Bianca Habermann's Group (former MPI of Biochemistry, now IBDM Marseille) (Figure 31). The model give rise to the assumption that two neighboring EF hand motifs reside in close spatial proximity and coordinate calcium ions in a manner dependent upon each other.

To get a first idea about the importance of the calcium binding sites for Cab45 function the 6EQ mutant was analyzed in comparison to Cab45 wild type in biochemical and cell biological assays.

The first striking observation was that more of the 6EQ mutant is secreted, when overexpressed on Cab45 KO background (Figure 32A, SN blot). Furthermore, the faint band in the lysate of 6EQ (WCL blot) indicates that also less of the calcium-binding deficient mutant can be retained inside the Golgi.

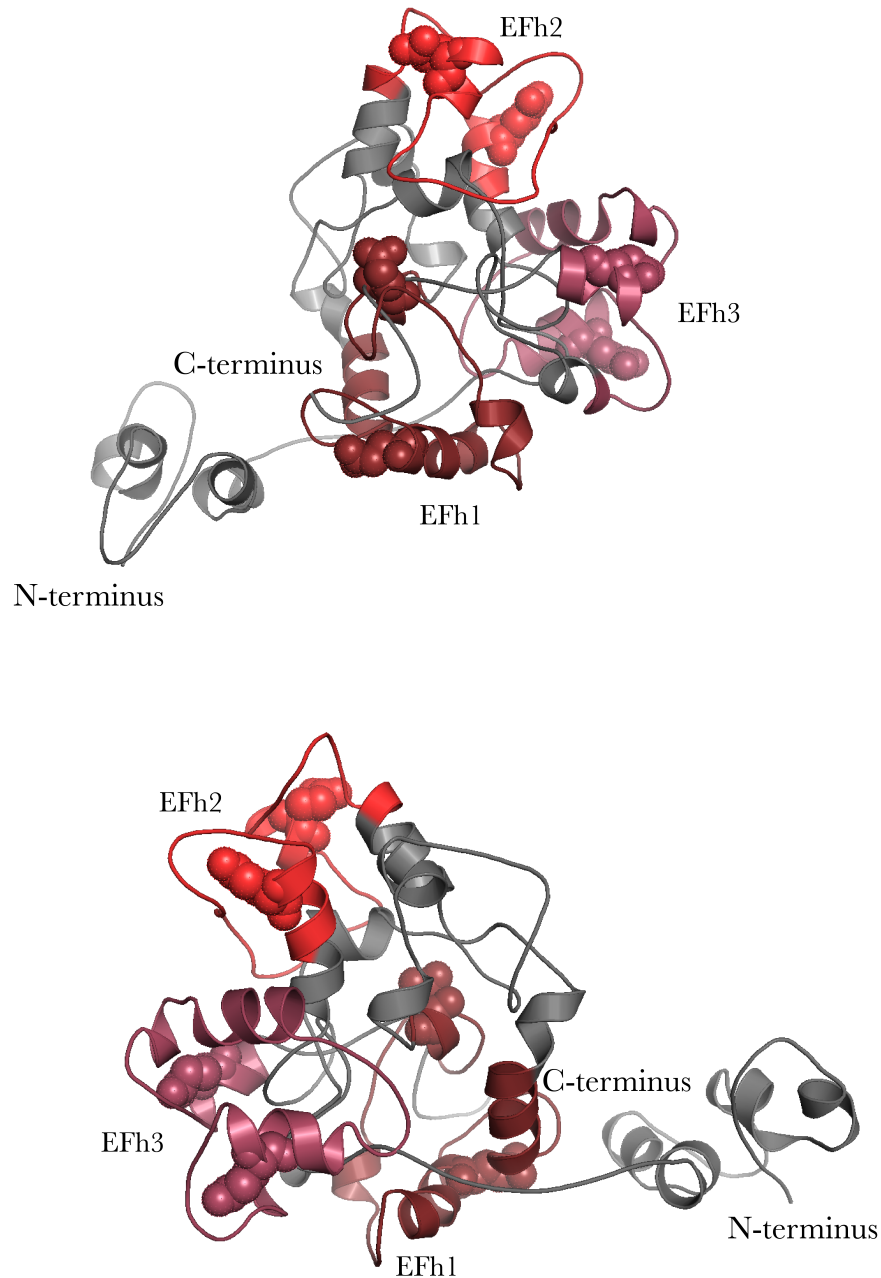


Figure 31: Predicted structural model of human Cab45 indicates paired EF hand motifs. 3D Model of Cab45 designed with MacPyMOL software (as described in Crevenna et al., 2016 ³⁸⁷. The model depicts front and rear views of the Cab45 protein coordinating calcium ions (spherical structures) by EF hands 1 and 2 (dark red), EF hands 3 and 4 (bright red) and EF-hands 5 and 6 (magenta). EF hand motifs exhibit the typical helix-loop-helix structure found in parvalbumin by Kretsinger and Nockolds ²²⁹ and pairwise assembly of EF hands in the 3D model. The N-terminus of protein is rather globular, while the C-terminus is mainly unstructured. Figure published in ⁴⁰⁹.

Results

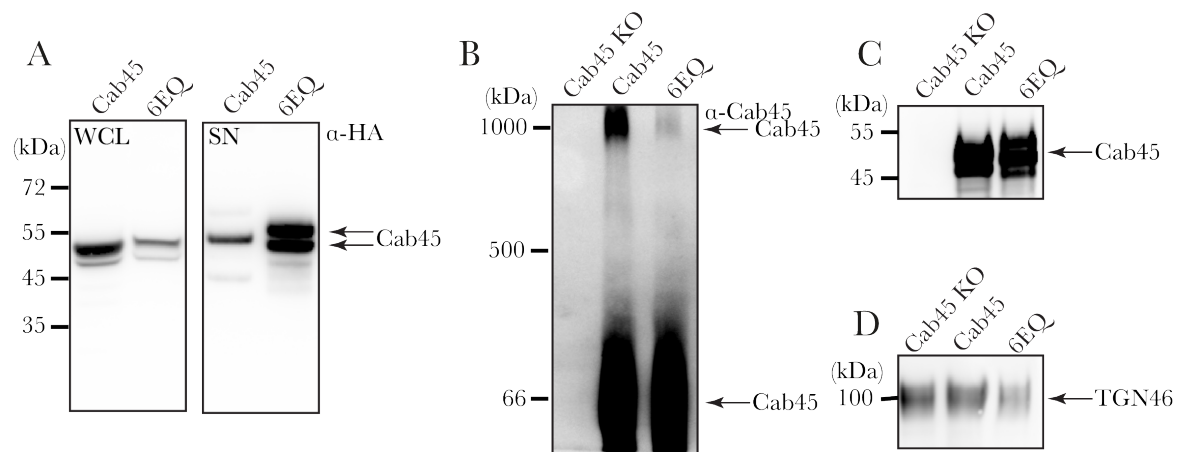


Figure 32: The Cab45 6EQ mutant is secreted in high amounts and forms no high oligomeric weight fractions. (A) HeLa Cab45 KO cells overexpressing either wild type Cab45 or the 6EQ mutant secreted more 6EQ into the supernatant (SN). The western blot of the cell lysates (WCL) also indicates that less of the mutant is retained inside the cells. (B) Western blot analysis of Blue NativePage presents isolated Golgi fractions of Cab45 KO cells or KO cells overexpressing wild type Cab45 or 6EQ. The bands demonstrate that only Cab45, but not the mutant can form high oligomeric weight fractions under physiological conditions. (C) and (D) Western blots of SDS Pages show that same amounts of Cab45 proteins or the TGN marker TGN46 were loaded for the analysis.

Secondly, isolated Golgi fractions from Cab45 KO cells, or Cab45 KO cells overexpression either wild type Cab45 or the 6EQ mutant were subjected to Blue NativePage analysis (Figure 32B). The western blot of the NativePage demonstrates that only Cab45, but not the calcium-binding deficient mutant can form high molecular weight fractions under physiological conditions. Furthermore, the Western Blots of the denaturing SDS pages depicted in Figure 32C and D prove that similar protein amounts were loaded for the experiment.

Finally, the 6EQ mutant was tested concerning its ability to sort cargo proteins properly by secretion assays (Figure 33).

Therefore, Cab45 wild type or the 6EQ mutant were stably expressed on Cab45 KO background (Figure 33A) and the secretion of COMP (Figure 33B) and LyzC (Figure 33C) were analyzed by Western Blotting. Both, COMP and LyzC, were less secreted upon Cab45 KO as observed before (compare Figure 23). However, overexpression of wild type, but not 6EQ, was able to rescue the secretion, as only weak bands are detectable in the 6EQ sample.

Based on these insights, the impact of the single calcium binding sites should be addressed by analysis of the pairwise EF hand mutants EFh1, EFh2 and EFh3 *in vitro* (Figure 30).

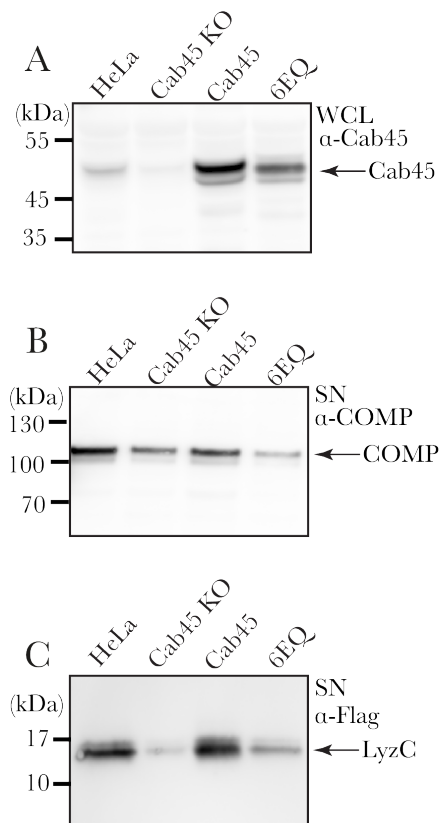


Figure 33: The Cab45 6EQ mutant cannot rescue the Cab45 KO phenotype in secretion assays. (A) Cab45 wild type or the calcium-binding deficient mutant were overexpressed on top of the Cab45 KO background. As observed before, less 6EQ is retained in the cell. (B) and (C) Secretion assays with COMP or LyzC demonstrate that secretion is reduced upon Cab45 KO in comparison to HeLa cells. Overexpression of Cab45 wild type, but not the 6EQ mutant, can rescue the phenotype for both cargo proteins.

Therefore, the set of mutants was purified by the established insect cell system as described in section 6.1 and labeled with a fluorescent dye. Subsequently, the EFh mutants were first tested with respect to their ability to form oligomers in the presence of calcium.

The results arranged in Figure 34 demonstrate that the ATTO488 labeled Cab45 oligomerized in the presence of 1 mM calcium as observed before (Figure 28). In contrast, EFh1 showed only very little green dots and therefore basically no polymerization (white arrow). EFh2 indicated many green clusters and oligomerization capacity seems comparable to wild type behavior. Finally, EFh3 exhibited some, but not many green spots in the microscopy experiment, which indicates some residual oligomerization, however, explicitly below wild type levels (white arrows). In summary, only one mutant, namely EFh2, is able to properly polymerize in the presence of calcium, while for EFh1 and EFh3 only residual oligomerization is observable.

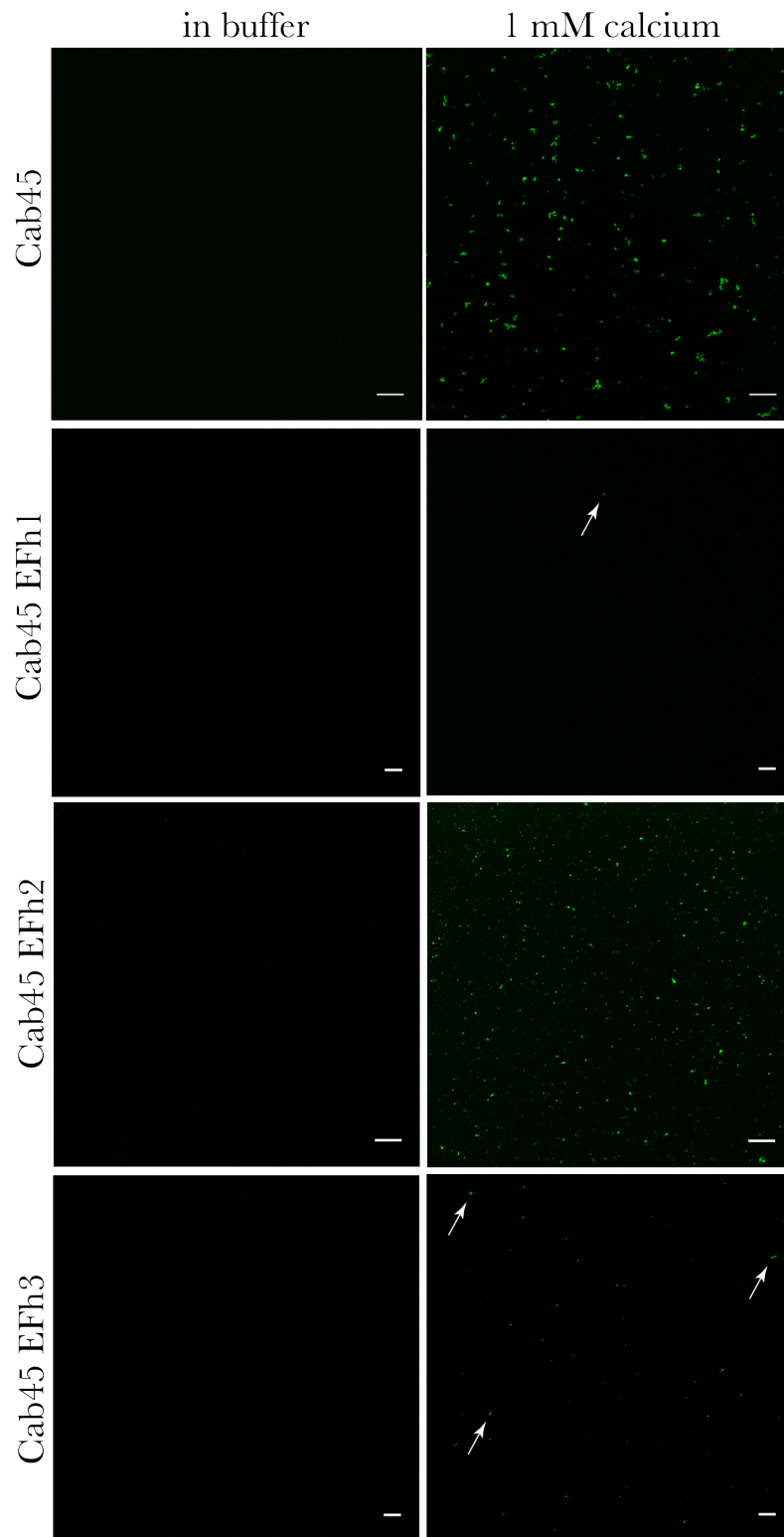


Figure 34: Oligomerization assay of Cab45 calcium-binding deficient mutants. In confocal microscopy Cab45 wild type labeled with ATTO488 dye exhibited oligomerization in the presence of 1 mM calcium (green dots), but not in its absence, as observed before (Figure 28). In contrast, the EFh1 and EFh3 mutant only showed some green dots (highlighted by white arrows) in the presence of the cation. EFh2 showed proper polymerization behavior comparable to wild type levels. Scale bars represent 10 μm .

6.3.5 Only EFh2 undergoes conformational change in the presence of calcium

To see if the results of the EFh mutants is in concordance with their presumptive change in secondary structure, the three proteins were subject to CD spectroscopy. While the control experiment with wild type Cab45 (Figure 35A) presents the same curve progression as found earlier for 1 mM and even 250 μ M calcium (Figure 29), the graphs of EFh1 and EFh3 show no change in secondary structure after addition of the cation (Figure 35B and D). However, the curve of EFh2 (Figure 35C) demonstrates that this mutant indeed gains a more alpha helical fold in the presence of 250 μ M calcium. Interestingly, while addition of more calcium has no effect on the wild type protein (Figure 35A), addition of higher calcium concentrations (1 mM) leads to a stronger structural change of EFh2. In line with this observation the titration of the EFh2 mutant in the range between 0 and 250 μ M also exhibited a slight delay during the transition to the calcium bound state (Supplementary Figure 1).

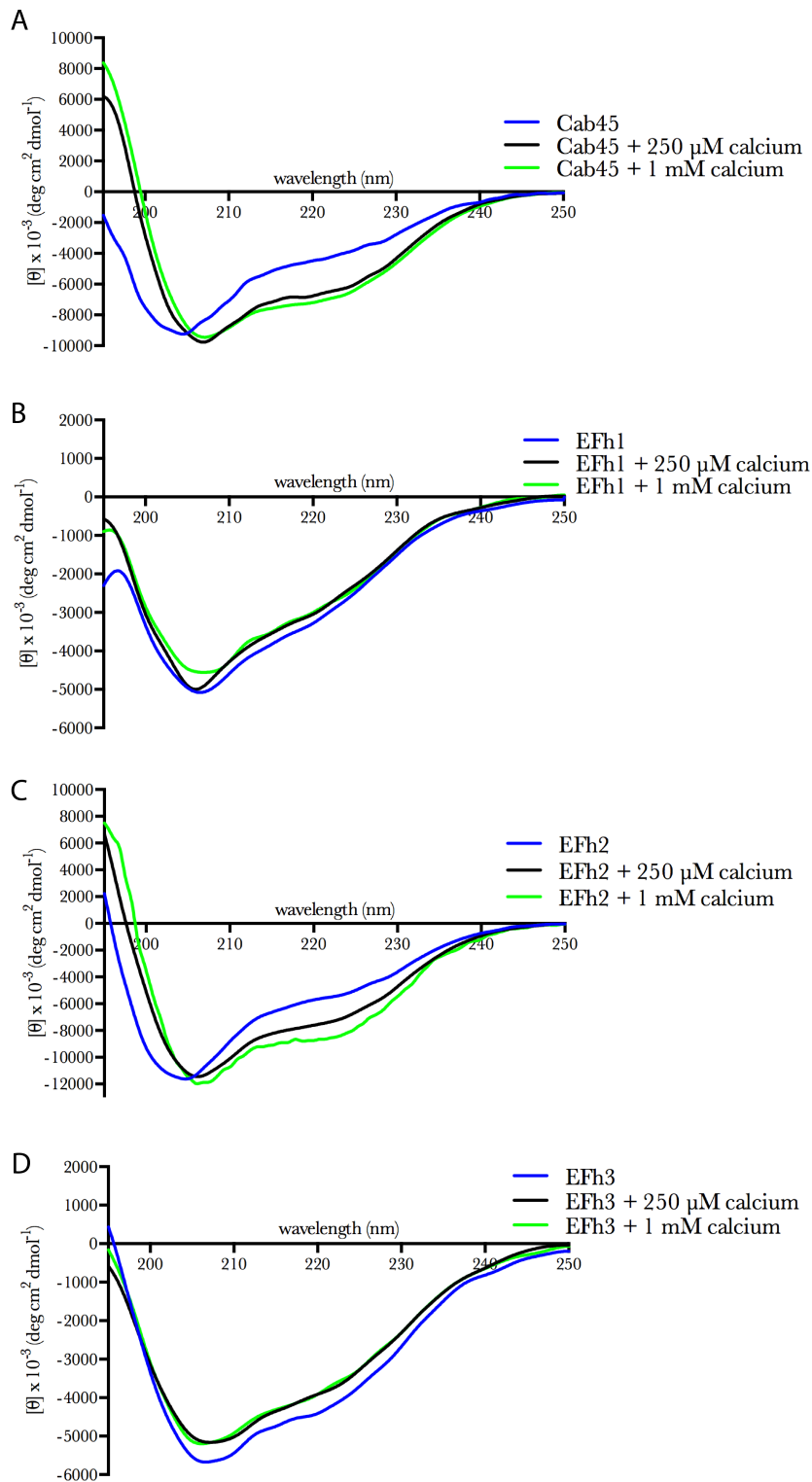


Figure 35: CD spectra of calcium-binding deficient mutants in the presence and absence of calcium. (A) Control experiment with wild type Cab45 in the presence and absence of calcium by circular dichroism (CD) spectroscopy. In comparison to buffer conditions (blue line) the spectra of Cab45 in the presence of 250 mM calcium (black line) exhibit two minima around 222 and 208 nm, which indicate a shift to a more α -helical fold. Addition of more calcium (1mM; green line) did not change the spectrum further. (B to D) CD spectra of calcium-binding deficient mutants EFh1, EFh2 and EFh3. The results show that EFh1 and EFh3 are not able to change their secondary structure in the presence of neither 250 μ M (black lines) nor 1 mM calcium (green lines). In contrast, EFh2 shows comparable behavior as wild type control 250 μ M calcium (black line), although alpha helical fold intensified upon 1 mM cation concentration (green line).

6.3.6 All EFh mutants mimic the phenotype of the 6EQ mutants in cells

The next step was to address the function of this multimerization process inside living cells. Thus, the calcium-binding deficient mutants were stably expressed in HeLa cells and the localization of the proteins was visualized by immunofluorescence (Figure 36).

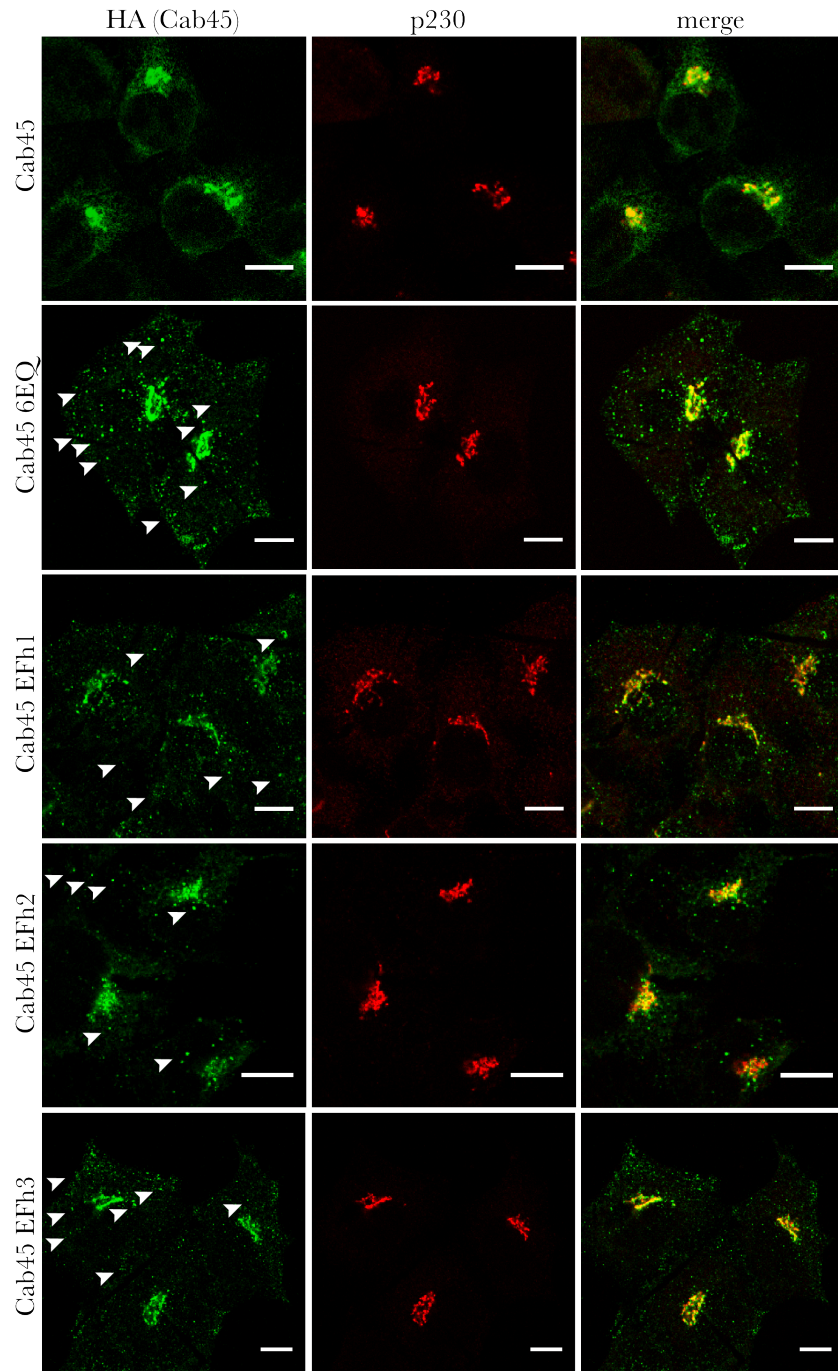


Figure 36: Immunofluorescence analysis of calcium-binding deficient Cab45 mutants in HeLa cells. Cab45 wild type or mutants were stably overexpressed in HeLa cells and detected by an anti-HA antibody (green channel). As Golgi marker, p230 was co-stained (red channel). In contrast to wild type control all mutants exhibit vesicular dotted structures (white arrowheads) in addition to the normal strong Golgi-located signal. Golgi signal colocalizes with marker protein as expected (merge). Number of vesicles are quantified in Figure 37). Scale bars represent 10 μm.

Results

Cab45 and its mutants were therefore detected by a C-terminally α -HA antibody and an α -p230 antibody was used as Golgi marker protein in this experiment. Cab45 reveals a strong signal in Golgi area where it colocalizes with p230. Surprisingly, all EF hand mutants including 6EQ exhibit a multitude of dotted structure around the Golgi apparatus, which have an appearance distinct of the wild type ER staining (white arrowheads). However, the number of these putative vesicular structures differ between the mutants. While in the 6EQ and EFh3 samples numerous of them are detectable, less are visible in the EFh1 and EFh2 probes. The corresponding quantification of vesicle numbers supports this finding (Figure 36). All mutants, although to a different extent, demonstrate significant increase in vesicular structures containing Cab45 in correlation to the wild type control.

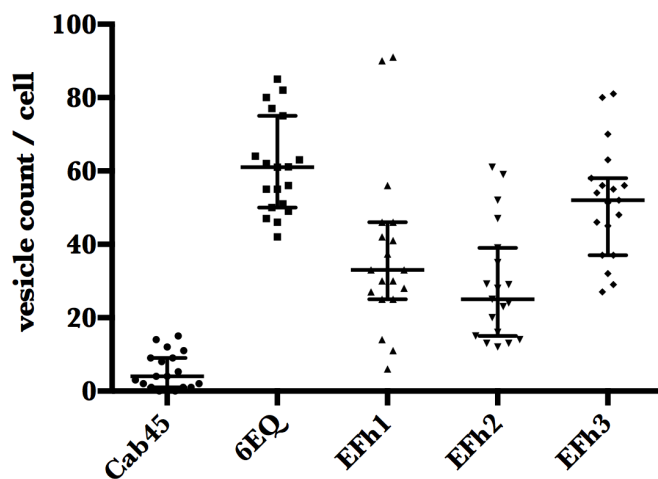


Figure 37: Quantification of vesicles in HeLa cells overexpressing Cab45 wild type or calcium-binding deficient mutants. The quantification of IF pictures in Figure 36 demonstrates that all mutants show significantly elevated levels of vesicular structures in HeLa cells ($n = 18$ for all cell lines). In concordance with the microscopy analysis, 6EQ reveals highest levels of vesicles, while mutants range between wild type and 6EQ. The scatter blot depicts medians of values with interquartile range.

In summary, the observations above indicate that especially EFh1 and EFh3 are crucial for calcium binding and the oligomerization process, because both mutants show neither a conformational shift in CD spectroscopy nor oligomerization in microscopy experiments. The EFh2 mutants behaves mainly like wild type Cab45 as it is still able to acquire a more α -helical fold in CD in the presence of high calcium, although maybe with little less affinity than the control, and it is still capable of multimerization.

6.3.7 Predicted oligomerization-prone mutant can still oligomerize

Subsequently, two different approaches were applied to identify a putative oligomerization domain. Firstly, an online tool was used to identify aggregation prone areas in the amino acid sequence of Cab45. Secondly, Cab45 was divided into an N- and a C-terminal fragment (Figure 39), purified and subjected to microscopy analysis (Figure 40).

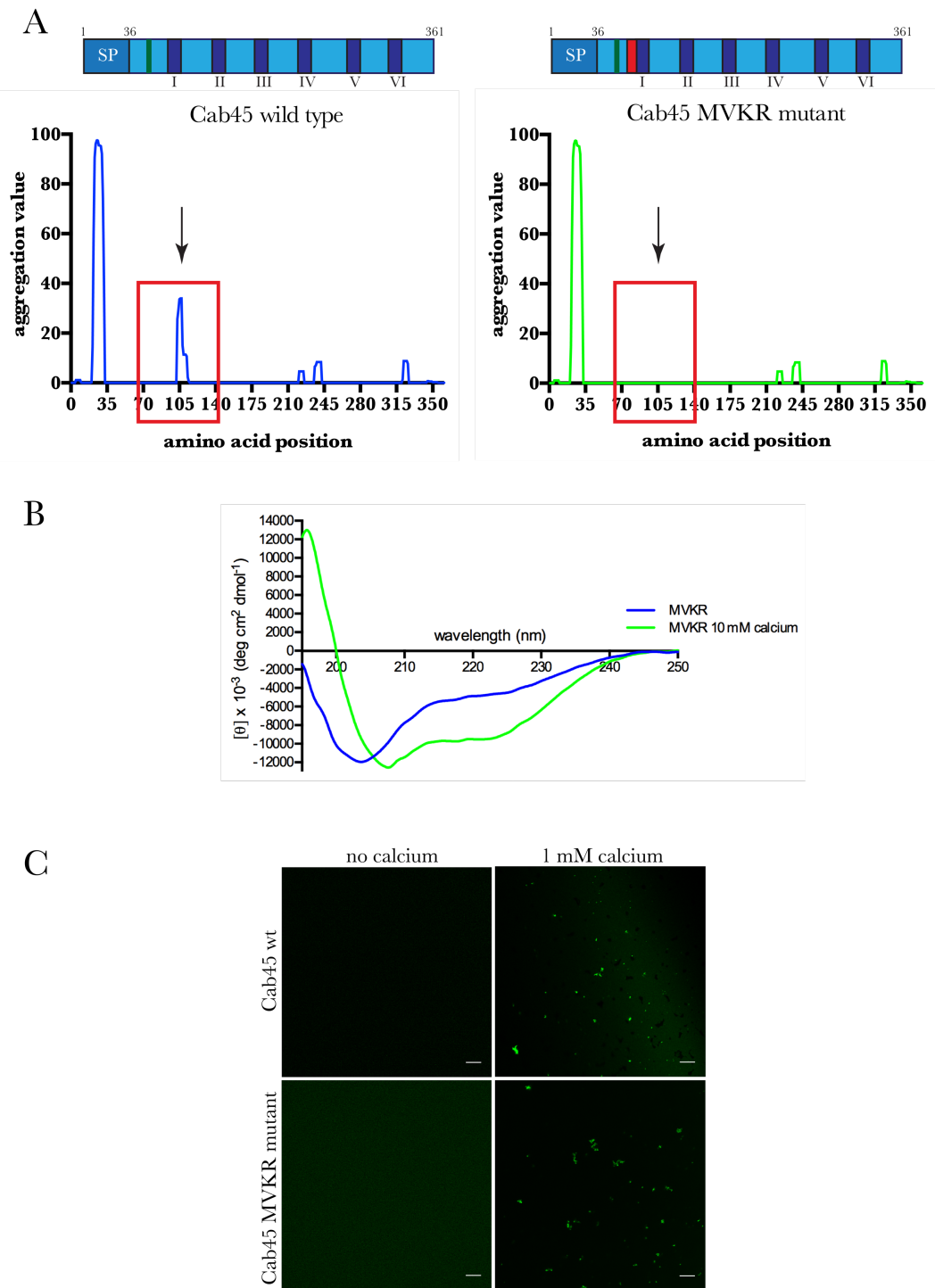


Figure 38: Characterization of putative aggregation-inhibited Cab45 MVKR mutant. (A) Result of TANGO algorithm analysis of wild type Cab45 (left graph) and MVKR mutant (right graph). The curve progression indicates two main peaks, i.e. aggregation prone areas, in the sequence of wild type Cab45 (blue). As the first hotspot is located in the SP of the protein and therefore no part of the mature protein this area was neglected during subsequent analyses. Mutations of two adjacent amino acids abolished the aggregation propensity in this area around amino acids 105 (red box in graph and cartoon) completely. (B) CD spectroscopy of MVKR mutant exhibits similar curve progression as the wild type protein. In the presence of calcium also the mutant performs a conformational change to a more helical fold (green line). (C) *In vitro* oligomerization assay with ATTO488 labeled Cab45 wild type and MVKR mutant. Both proteins show comparable oligomerization potential in the presence of 1 mM calcium.

Results

The first approach was based on the TANGO online tool, a prediction tool of aggregating regions in unfolded polypeptide chains (<http://tango.crg.es>). This algorithm tries to identify hydrophobic areas within the protein sequence, which might favor multimerization. The result of the analysis indicated two main hotspots inside the protein, which fulfill the necessary requirements. The first hotspot is located inside the SP of Cab45, an area that should be cleaved off during co-translational ER import and therefore not be part of the mature protein (compare also section 3.2.2). Thus, this area was neglected during the subsequent analysis. However, the second hotspot was a small region of 6 amino acids directly before the first EF hand motif (Figure 38A). This area was mutated at two amino acids, which abolished the oligomerization potential according to the TANGO algorithm. The protein was purified, labeled and analyzed by microscopy (Figure 38C). However, the mutant still exhibited polymerization potential comparable to wild type levels. Therefore, Cab45 was alternatively divided into a N- and a C-terminal part to limit the area of a potential oligomerization domain.

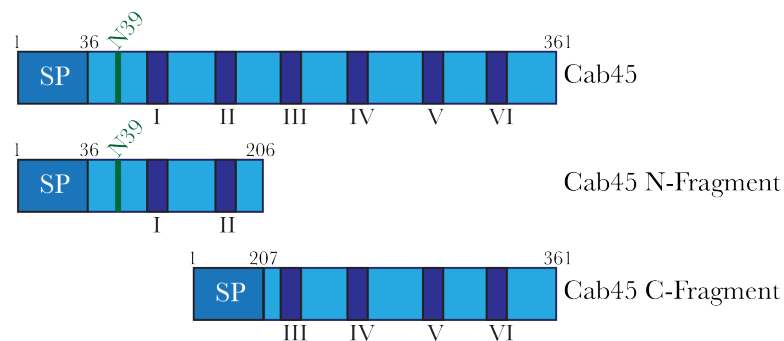


Figure 39: Schematic depiction of Cab45 N- and C-terminal fragments for identification of oligomerization domain. Cab45 wild type was divided into a N- and a C-terminal fragment in the area between EF hand motif II and III (dark blue boxes; Roman numerals). The C-terminal fragment starts from amino acid 207, whereby a signal peptide (SS) was added at its N-terminus. Cab45 C-Fragment comprises the complete EFh2 and EFh3. Green line marks putative glycosylation site at amino acid N39.

6.3.8 N- and C-terminal fragments of Cab45 oligomerize independently

To generate two fragments of Cab45 with similar length and without disrupting the EF hand structures, the N-Fragment was cut off in the loop after EF hand motif II at amino acid 206 (Figure 39). For proper localization, a SP was added to the C-Fragment, which contains the complete EFh2 and EFh3 region. Both proteins were labeled and analyzed by the oligomerization assay (Figure 40). In the control experiment Cab45 wild type labeled with either ATTO488 or Cy5 were incubated together in the presence of 1 mM calcium. The overlap in the merge picture proves that both proteins form oligomers together.

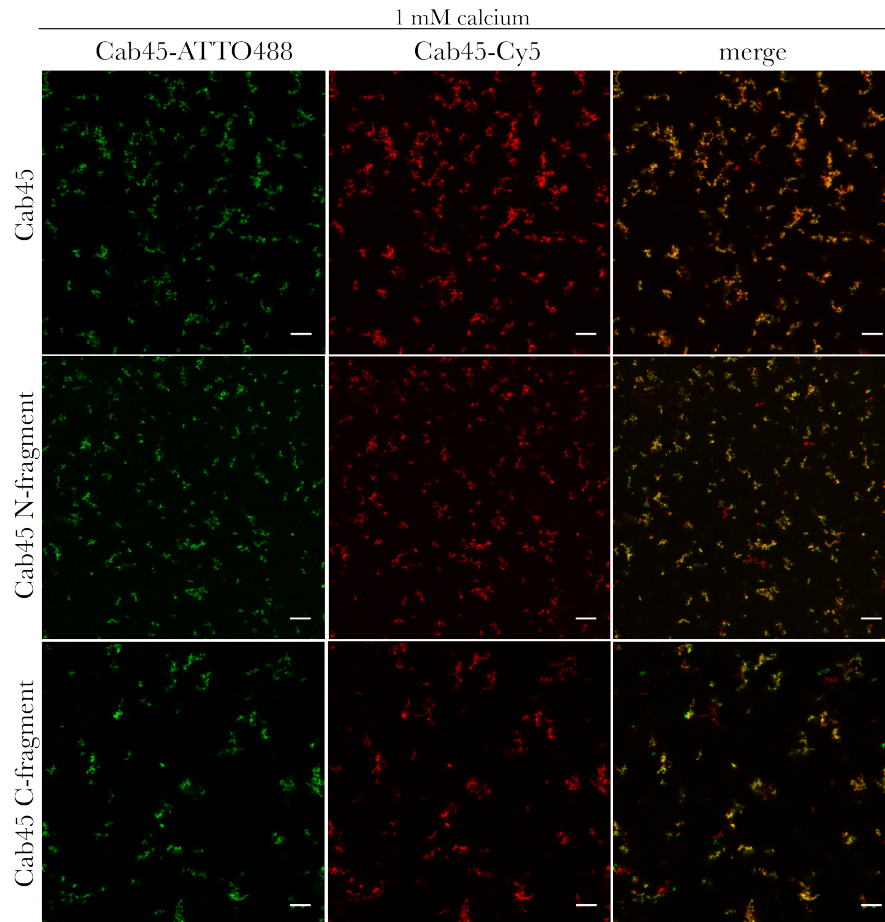


Figure 40: Oligomerization assay of N- and C-terminal fragment of Cab45. In the wild type control experiment Cab45 was labeled either with ATTO488 or Cy5 dye and incubated together in the presence of 1 mM calcium. Either the green and the red channel indicate oligomerization of the wild type protein as expected. The merge of both channels proves that both proteins are present in the same structure, i.e. that they polymerize together. The same is true for the N- and the C-fragment, as both proteins are able to form oligomeric structures together with wild type Cab45. Scale bars represent 10 μm .

As the same results are observable for the ATTO488-labeled N- and C-Fragment, the experiment indicates that both, the N-terminal as well as the C-terminal part of Cab45 are able to directly interact with wild type Cab45. This suggests, that both fragments contain domain capable of binding the wild type protein, e.g. a potential oligomerization domain. Therefore, currently smaller fragments are generated to determine the minimal requirements for oligomerization.

6.4 Oligomeric Cab45 directly interacts with cargo via tyrosine residues

The third aim of this thesis focused on the Cab45 cargo interaction. Although it was already published earlier that Cab45 interacts with certain secreted proteins in

Results

immunoprecipitation experiments from HeLa cell lysates ³⁶⁵, the interaction was so far not characterized in detail.

6.4.1 The Cab45-cargo interaction is direct

For this reason, first the direct interaction of purified protein in *in vitro* pull down experiments should abolish the possibility that Cab45 interacts with its cargo via adaptor or other proteins. For this approach, recombinant purified Cab45 was attached to beads and incubated either with buffer as control condition or with the previously demonstrated recombinant cargo proteins LyzC or COMP. Cathepsin D (CathD) was used as negative control here, as the lysosomal hydrolase should be transported via a Cab45 independent pathway to early endosomes.

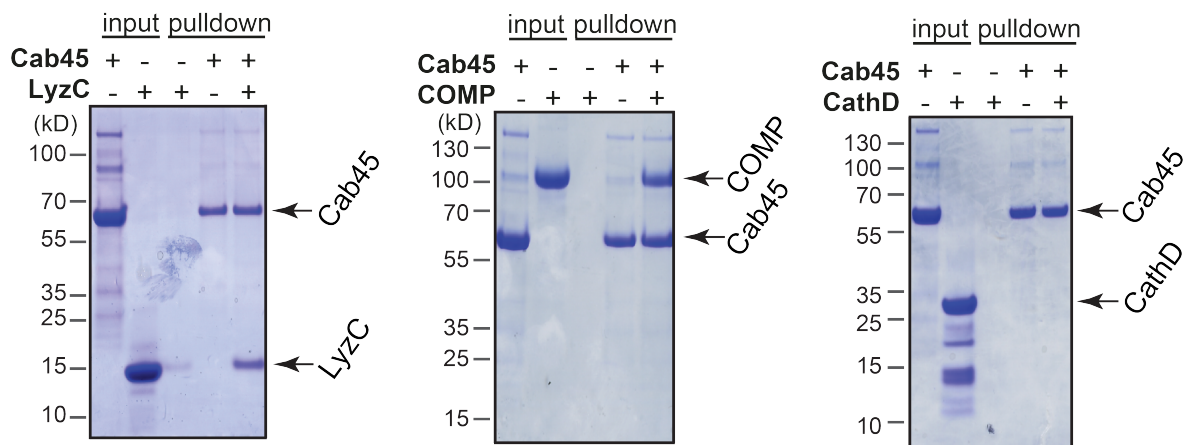


Figure 41: *In vitro* immunoprecipitation assays with recombinant, purified Cab45 and cargo proteins. To demonstrate direct interaction between Cab45 and cargo proteins recombinant Cab45 was attached to beads and incubated either with a buffer control or the previously published cargo molecules LyzC and COMP. The Coomassie stained SDS Pages of both experiments indicate that Cab45 can pull down both LyzC and COMP from the sample, as the last pull down lane clearly shows the expected bands at around 15 kDa or around 100 kDa, respectively. The first input lane proves that there was no unspecific interaction of the cargo with the beads. As expected, the band in the gel of the negative control CathD remained absent and proves that no interaction between Cab45 and CathD occurred in this assay.

The Coomassie stain of the SDS pages reveal that Cab45 can indeed directly interact with LyzC and COMP (Figure 41). On both gels, the bands at the expected sizes (around 15 kDa for LyzC and around 100 kDa for COMP) appear in the last pull down lane, when both proteins are present. The control (first pulldown lane) proves that the interaction is real and only detectable if Cab45 is present and not due to unspecific binding of the cargos to the beads. In contrast, CathD exhibits no interaction with Cab45, as the CathD band in the last pulldown lane is absent, although clearly visible in the input. This result proves for

the first time, that Cab45 interacts directly with cargo molecules, independently of other proteins.

6.4.2 Cab45 oligomerizes together with cargo

Subsequently, the question arose, if Cab45 is capable of oligomerization and cargo binding in parallel. To address this, oligomerization assays were performed with recombinant, fluorescently labeled Cab45 and cargo (Figure 42).

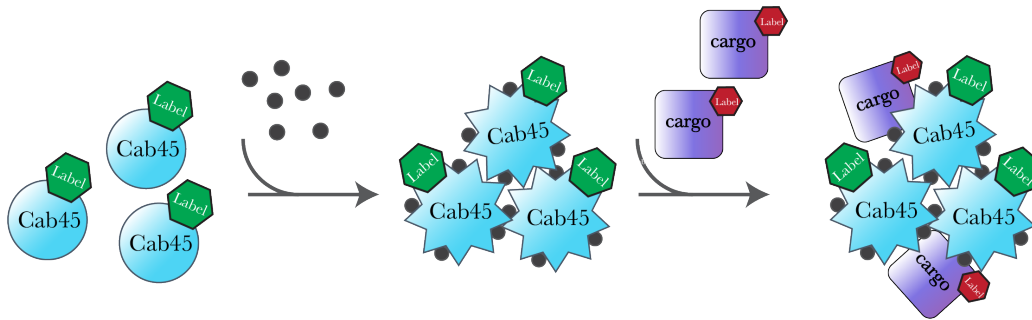


Figure 42: Schematic depiction of oligomerization process of Cab45 in the presence of cargo molecules. Fluorescently labeled Cab45 forms oligomers in the presence of calcium. Cab45 oligomers subsequently bind differently labeled cargo molecules and form hetero-oligomeric structures, which can be visualized by confocal microscopy.

In theory, Cab45 should oligomerizes together with the cargo and both proteins should be detectable in the same structures under the microscope. According to the immunoprecipitation experiments LyzC-Cy5 and COMP-Alexa647 were used as model cargos and CathD-Cy5 as negative control.

The microscopy results of the oligomerization assay indeed prove that Cab45 and the cargo oligomerize together in the presence of 1 mM calcium. Furthermore, the merge of both channels underlines that both proteins are part of the same hetero-oligomeric structures. In addition, the multimers dissolve completely upon addition of EGTA. In contrast, CathD does not colocalize with Cab45 wild type, which is in concordance with the idea that CathD is sorted independently of Cab45 inside the secretory pathway. Control experiments with LyzC and COMP prove that clustering was not induced by fluorescent dyes (Supplementary Figure 2).

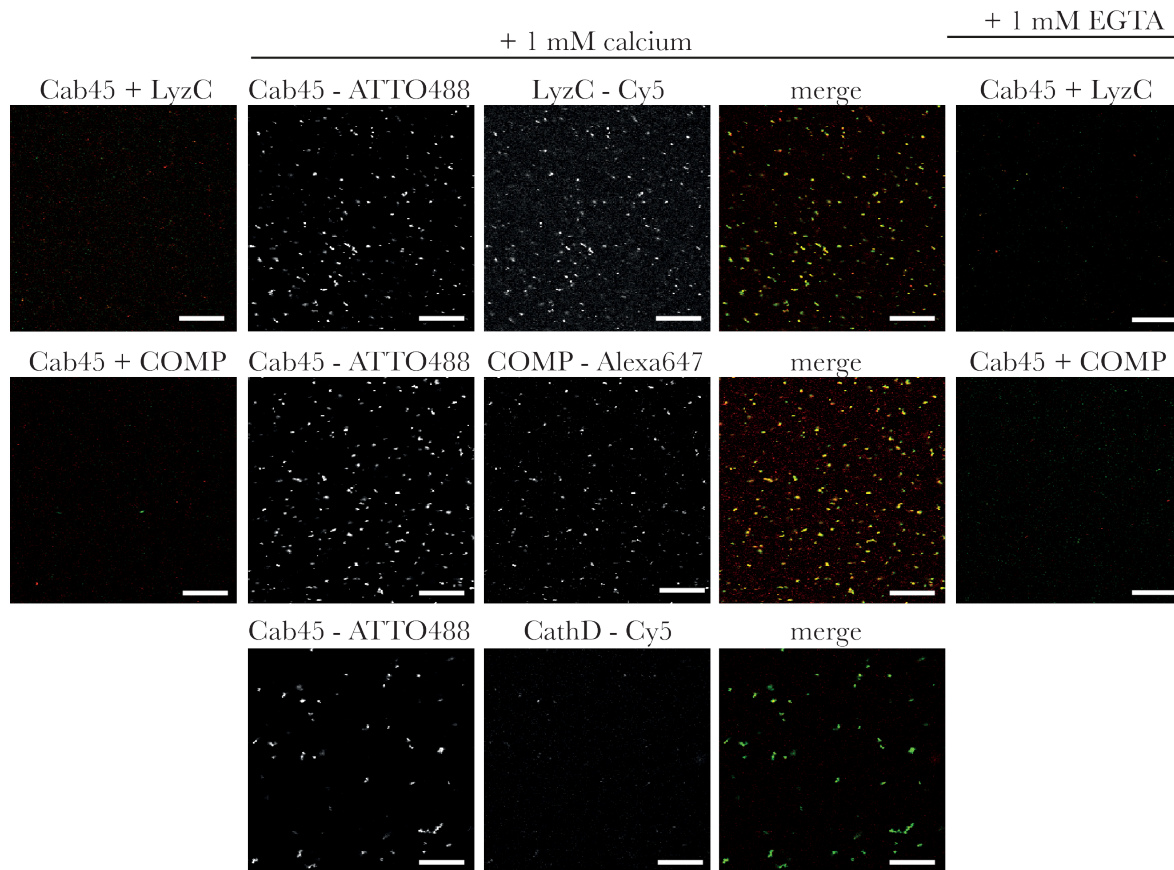


Figure 43: Oligomerization assay of Cab45 in the presence of cargo molecules. Recombinant ATTO488 labeled Cab45 was incubated either with Cy5 labeled LyzC or Alexa647 labeled COMP in the presence of 1 mM calcium. Either the Cab45 channel and the LyzC/COMP channel indicate that the proteins form cation-induced multimers. The merge proves that the proteins are part of the same structures. The negative control CathD does hardly colocalizes with Cab45 and therefore does not interact with the protein. Scale bar represents 20 μm .

6.4.3 Formed Cab45-cargo oligomers are highly stable *in vitro*

Because the hetero-oligomers of Cab45 and cargo proteins appeared to form comparably stable structures during the *in vitro* characterization, a Fluorescence Recovery After Photobleaching (FRAP) experiment was conducted to analyze the dynamics of the complexes. Therefore, unlabeled Cab45 and labeled cargo were incubated together and fluorescence of formed oligomers were bleached out by laser pulse and fluorescence recovery was subsequently tracked for 10 min.

The diagrams of LyzC and COMP show that fluorescence intensity does not recover within the monitored time frame as the intensity value remains on a constant low level. In addition, the pictures of the inset support the finding that no exchange of proteins took place during this measurement, because no fluorescent signal is observable after 590 s.

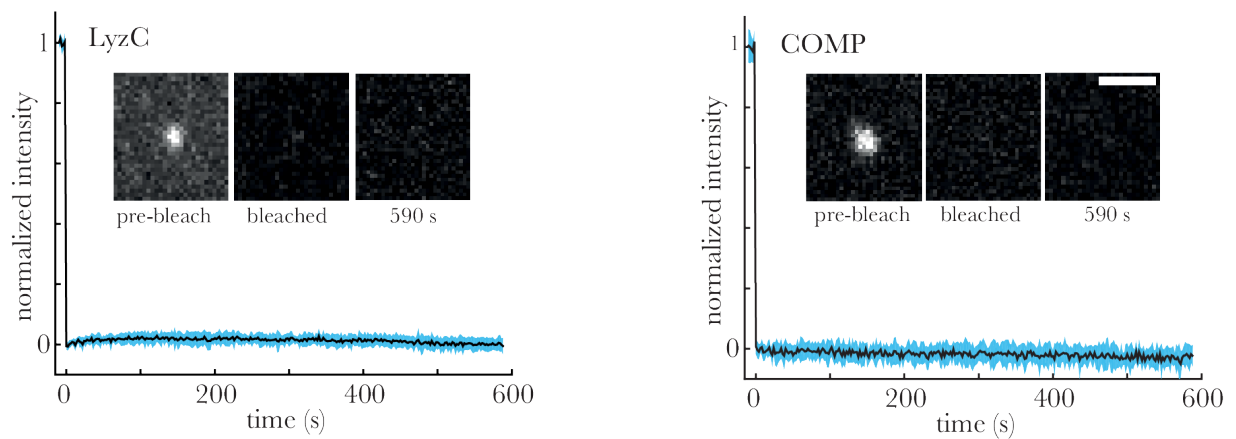


Figure 44: FRAP experiment for analysis of Cab45-cargo oligomer dynamics. FRAP analysis of LyzC-Cy5 and COMP-Alexa647 were incubated with unlabeled Cab45 in the presence of calcium. The diagrams represent the normalized fluorescence intensities during a monitored time of 10 min. The black line is the mean signal, whereas the light blue trace represents one SD on either side ($n = 13$ for LyzC and 15 for COMP). The insets show examples of a Cab45-cargo oligomer before (prebleach) and immediately after (bleach) bleaching and after around 10 min (590s). Scale bar represents $2 \mu\text{m}$.

This result indicates that the Cab45-cargo complexes are not dynamic and further unknown modifications or other factors are required to modulate or dissolve the multimers in a physiological context.

6.4.4 Cab45 colocalizes with SPCA1 and LyzC but not p230 in super-resolution microscopy

To visualize the Cab45 cargo interaction in living cells, HeLa cells were subjected to 3D-SIM super-resolution microscopy (Figure 45). First, the localization of Cab45 with respect to SPCA1-HA was analyzed (Figure 45A). SPCA1-HA (blue channel) overlaps nicely with the signal of endogenous Cab45 (red channel). Both proteins show a characteristic staining of the elongated Golgi cisternae. In addition, Cab45 also colocalizes strikingly with the LyzC signal (blue channel; Figure 45B). In contrast, the trans Golgi marker p230 (red channel; Figure 45C) shows no overlap with the calcium binding protein, although both proteins seem to reside in close vicinity. The probability (e.g. normalized frequencies) of Cab45 colocalization with SPCA1, LyzC or p230 are depicted in Figure 45D.

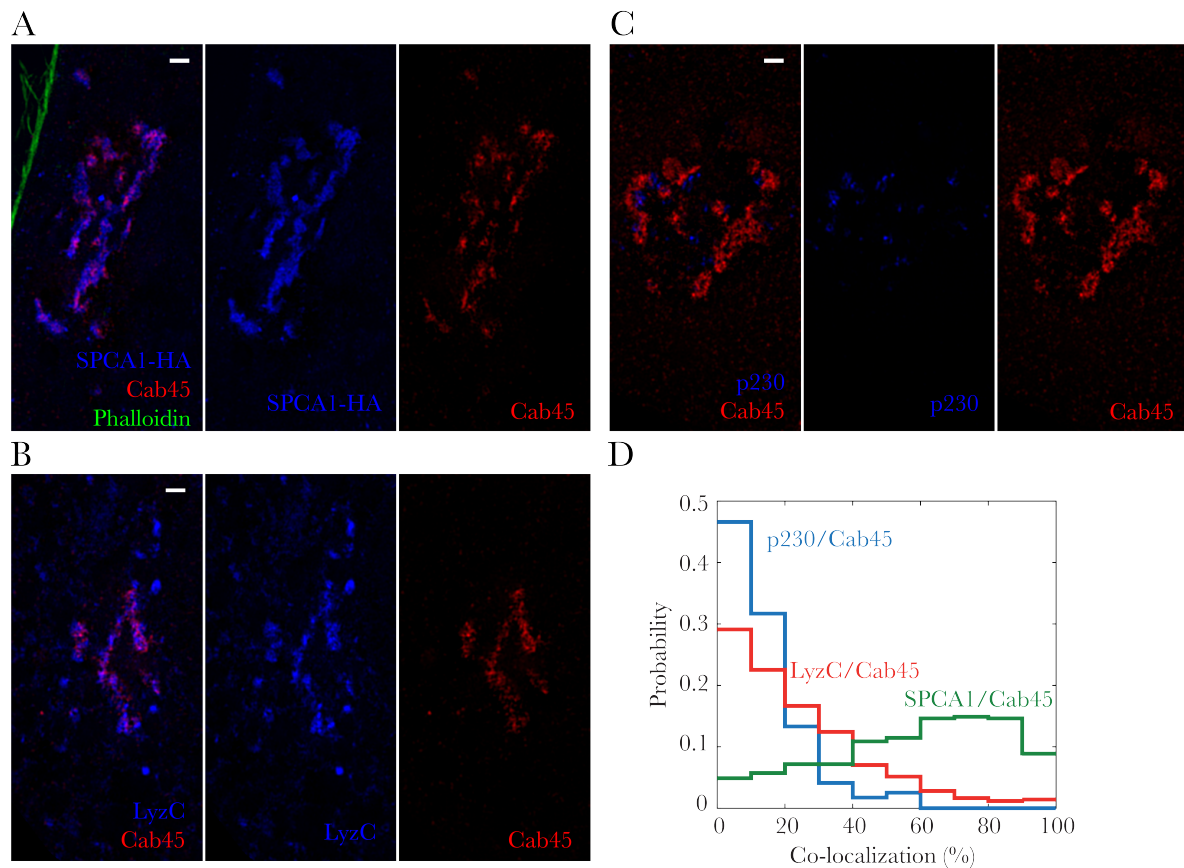


Figure 45: Analysis of Cab45, SPCA1 and LyzC localization in HeLa cells using the 3D-SIM super-resolution microscopy technique. (A) HeLa cells overexpressing HA-tagged SPCA1 were stained for actin (phalloidin, green) and endogenous Cab45 (red channel). Overlapping regions (pink color) indicates significant SPCA1 and Cab45 colocalization. (B) HeLa cells overexpressing LyzC (blue channel) depict significant colocalization of Cab45 and LyzC. (C) Staining of endogenous p230 (blue channel) and endogenous Cab45 (red channel) in HeLa cells reveals that proteins do not show colocalization, but both proteins locate to characteristic Golgi structures in close vicinity. (D) Graphical evaluation of probability (e.g. normalized frequencies) of colocalization for indicated protein combination. Scale bars represent 5 μ m.

6.4.5 Tyrosine residues are crucial for the Cab45-cargo interaction

One further important question that remained elusive in previous publications was a potential Cab45 cargo recognition motif. The initial SILAC-based screen in HeLa cells revealed around 20 secreted proteins differentially sorted by the SPCA1/CFL1/Cab45 machinery³⁴⁰. Five of these, LyzC, COMP, TIMP1, MGP and RCN3, were confirmed to interact with Cab45 in immunoprecipitation experiments³⁶⁵; partly unpublished). To expand the set of potential Cab45 cargos, the secretomes of HeLa wild type cells and Cab45 CRISPR/Cas9 KO cells were compared in a mass spectroscopy based screen.

In this setup, several proteins were identified as differentially secreted upon Cab45 depletion. These protein sequences were bioinformatically analyzed by the Group of Bianca Habermann (former MPI of Biochemistry, now IBDM Marseille) and the following recognition motif was extracted:

[DE]-X-Y-A-X-(X)-[VI]-[FY]-G-Y-[NQ]

Due to the fact that the motif was short (10 amino acids), I established a pulldown assay to test the putative interaction of the motif or variations of that with Cab45. Therefore, the in-house biochemical service facility synthesized the peptides and added a biotin modification. These peptides were subsequently immobilized on magnetic streptavidin-covered beads, which were in turn incubated with lysates obtained from HeLa cells stably overexpressing Cab45 wild type. The interaction of the peptides was then evaluated by Cab45 detection via western blot.

In the first assay three peptides corresponding to the original sequences of the known Cab45 interactors MGP, COMP and RCN (for subsequent experiments named MGP1, COMP1 and RCN1) were analyzed by this setup (Figure 46A). As negative control scrambled peptides were used, as well as a bead control without peptide. The result of the western blot demonstrates that the three peptides of MGP, COMP and RCN indeed bind Cab45 wild type. The bead control revealed only mild binding of Cab45 to the bead surface. Surprisingly, also the scramble controls show strong interaction with our protein of interest. As this unspecific interaction might be due to charges within the sequence, four mutants of MGP1 (MGP1-1 to MGP1-4) containing different alanine substitutions (marked with red letters) were designed and synthesized (Figure 46B). Firstly, western blot analysis revealed that the result of the MGP1 and the scramble peptide was reproducible. In addition, a poly GS peptide as negative control showed no Cab45 interaction, which strengthened the finding of the first experiment. Secondly, the four mutated peptides indeed exhibited differential binding properties. While MGP1-2 bound to Cab45 in a manner comparable to the wild type sequence, MGP1-3, and especially MGP1-1 and MGP1-4 showed drastically reduced binding levels. Considering the alanine substitutions in these mutants, all three of them lack two nearly adjacent tyrosine residues. Therefore, these sites were systematically analyzed in the next pulldown assay (Figure 46C). The tyrosines were substituted alone against alanine (MGP1-5), against phenylalanine (MGP1-6) to evaluate the importance of the aromatic ring structure, against negatively charged glutamic acids (MGP1-7), or individually substituted against alanine (MGP1-8 and MGP1-9). Cab45 bound to the MGP1 reference as observed previously, while repeatedly no interaction was observable for MGP1-1. However, Cab45 was able to interact with MGP1-5, which suggests that also the first and not only the last two tyrosine residues are crucial

Results

for the interaction. While the aromatic ring structures of phenylalanine seems not to influence this behavior the introduction of negative charges actually completely abolishes Cab45 binding capacity of MGP1-7. In line with MGP1-5, the individual substitutions do not affect binding of Cab45. Based on the finding that the additional negative charges of MGP1-7 had such a strong effect on Cab45 cargo interaction, one may reasonable expect that a modification like phosphorylation might also have an impact on binding. Therefore, in the next screen three phosphorylations were introduced at the tyrosine residues (MGP1-10 to MGP1-13).

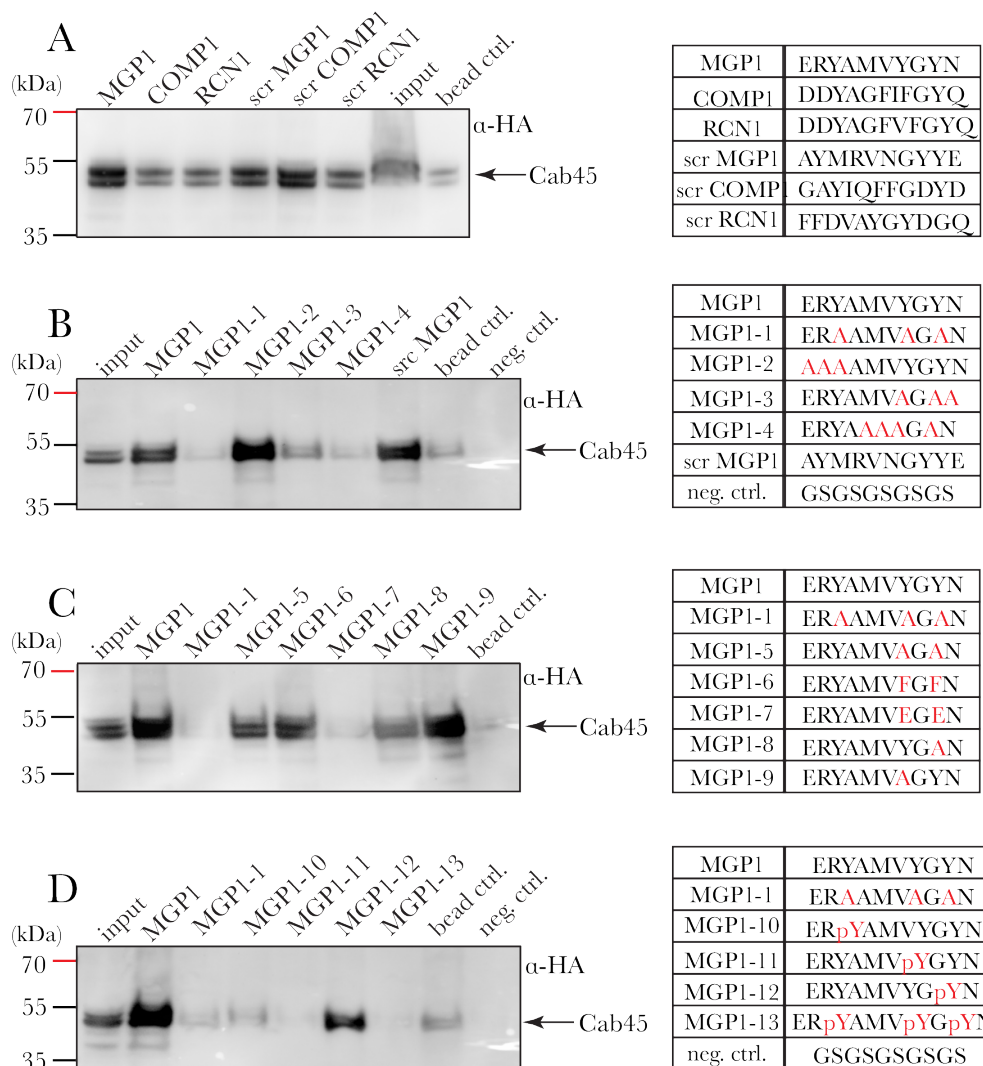


Figure 46: Immunoprecipitation experiments of Cab45 peptide interaction studies. Synthesized peptides were immobilized by biotin modification on streptavidin-covered beads. Interaction of peptides with Cab45 was studied by incubation of beads with cell lysate from HeLa cells, overexpressing Cab45 wild type. (A) Peptides or scramble controls of the three known Cab45 targets MGP (MGP1), COMP (COMP1) and RCN (RCN1) were tested and interaction was analyzed by western blotting. All peptides including the scramble controls were able to interact with Cab45. (B) Four different variants of the MGP1 peptide revealed binding deficiencies of the mutant peptides lacking tyrosine residues. (C) In detail analysis of tyrosine residues demonstrated further the importance of the first tyrosine residue and that introduction of negative charges additionally regulates interactions negatively. (D) Phosphorylation of two of three tyrosine residues abolished peptide-Cab45 interaction.

Modification of the first (MGP1-10) and the second tyrosine (MGP1-11) and as a consequence also the triple mutant (MGP1-13) actually abolished Cab45 binding.

However, MGP1-12 still exhibited proper interaction with Cab45, which proves that not the negative charge itself, but also the location inside the protein is important.

In summary, these pulldown assays indicate that Cab45 interacts with the extracted protein sequence *in vitro* and that phosphorylation of two certain tyrosine residues can abolish cargo binding. They further support the idea that phosphorylation might function as signal for cargo release and vesicle packaging also in a physiological context.

6.4.6 Mutation of cargo binding site and KO of Cab45 show same delay in export dynamics

In order to prove that the found tyrosine modifications also influence Cab45 dependent sorting in cells, MGP constructs for the Retention Using Selective Hooks (RUSH) system were cloned (Figure 47). The principle of the RUSH system is based on a hook protein containing a streptavidin and the KDEL sequence, which retains the hook inside the ER. In addition, the protein of interest is fused to an EGFP and a streptavidin-binding protein (SBP), which bind the streptavidin of the hook. Upon addition of an excess of biotin to the cell culture medium the SBP is displaced from its binding site and the protein of interest is transported along the secretory pathway to the Golgi and further to the plasma membrane for secretion. This secretion process and its kinetics can be easily tracked and visualized by confocal microscopy.

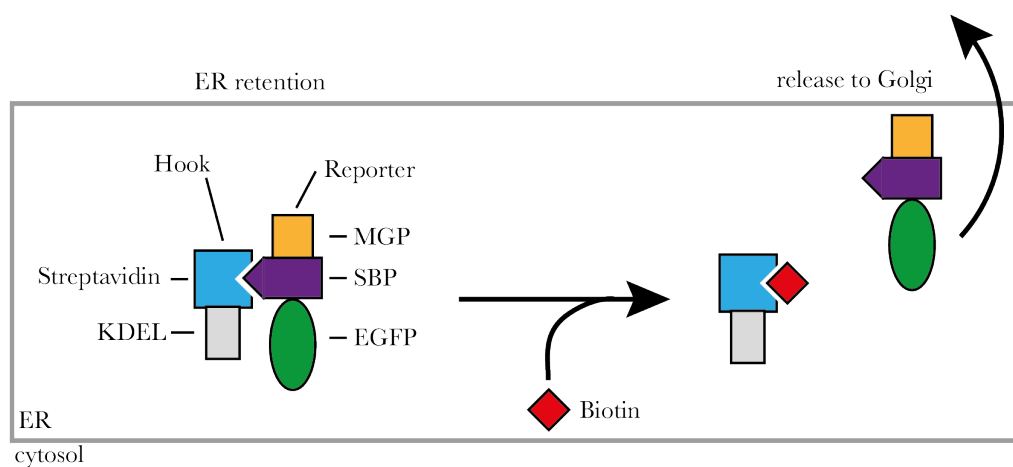


Figure 47: RUSH principle. The retention using selective hooks (RUSH) method uses a hook consisting of streptavidin protein (blue) fused to the KDEL retention motif (grey), which interacts with a streptavidin binding protein (SBP, purple). SBP in turn is fused to a EGFP (green) and the protein of interest – here MGP (orange). Upon biotin (red) addition SBP is displaced from streptavidin due to the high biotin-streptavidin affinity. The transport of the released MGP fusion protein from the ER to the Golgi and later to the PM can be tracked by confocal microscopy via the EGFP tag. Figure was adjusted from Boncompain et al., 2012⁴¹⁰.

Results

The immunofluorescence stainings of the time points 0, 20 and 40 min after biotin addition show that the MGP wild type is already in vesicles after 20 min (Figure 48). While the MGP 3A mutant also shows some, however less, vesicular structures, the MGP wild type on the Cab45 KO background exhibits hardly any Golgi export. In line with this, after 40 min biotin incubation the MGP wild type protein is still released from the Golgi of the HeLa wild type cells, either for MGP and MGP 3A. However, still only very few vesicles are detectable even after 40 min in the Cab45 KO cells.

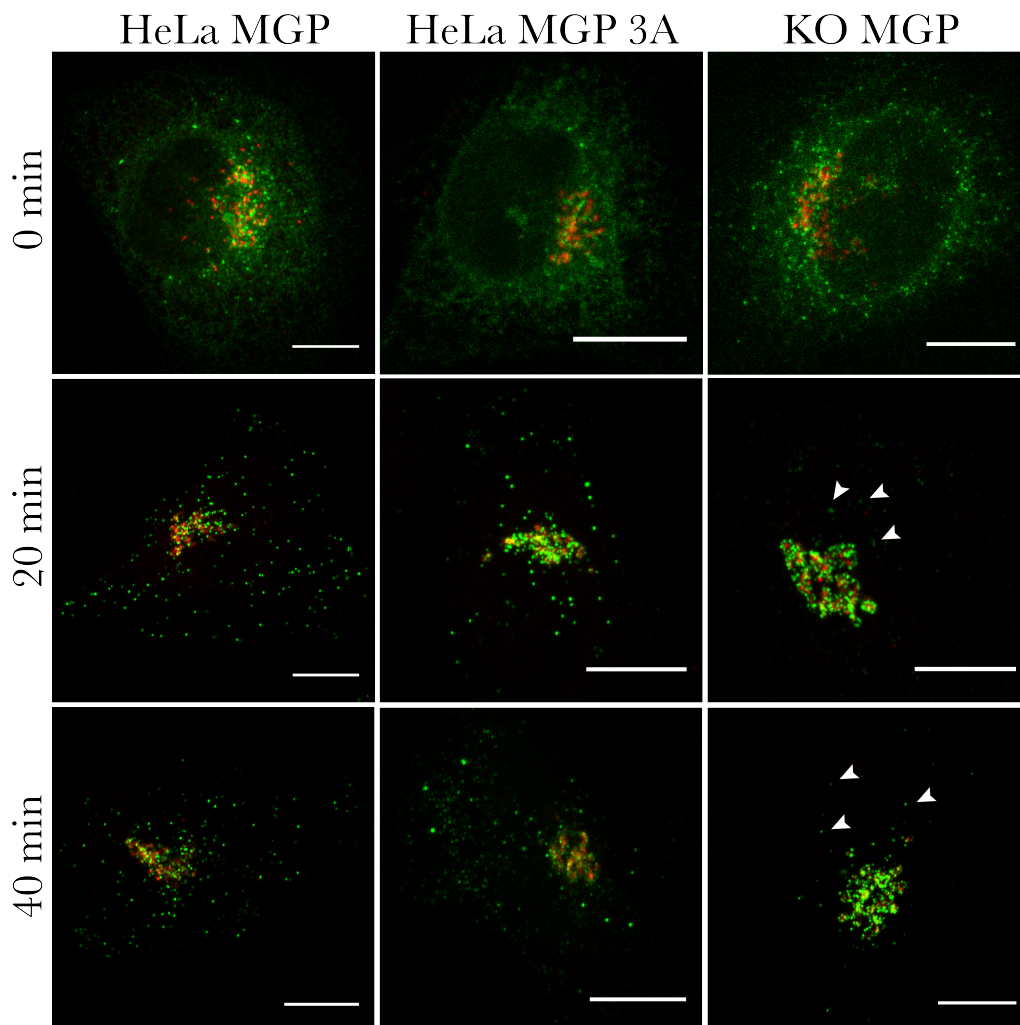


Figure 48: Microscopy analysis of the RUSH construct of MGP in HeLa and Cab45 KO cells and the 3A mutant. For visualization of the RUSH kinetics of MGP cells were incubated for 0, 20 or 40 min with biotin and fixed and stained afterwards. MGP exhibits many vesicles after 20 min (first column), while less are observable for the 3A mutant (second column) in the HeLa background. Hardly any vesicles formed at this time point in the Cab45 KO cell line (third column). After 40 min biotin incubation, this delay in Golgi export is still striking in the Cab45 KO background. The MGP/MGP 3A GPF fusion constructs are depicted in green, the p230 Golgi comarker is depicted in red. Scale bars represents 10 μ m.

For quantification, the number of vesicles was counted after 20 min and 40 min of biotin addition of all three cell lines (Figure 49). The data of the scatter blot proves that both the MGP 3A mutant and the MGP wild type on KO background show a delay of Golgi vesicle

export, especially after 40 min. This and also the observation that all cell lines show strong Golgi staining after 20 min, might hint to the fact that especially Golgi export, but not ER to Golgi transport, is delayed.

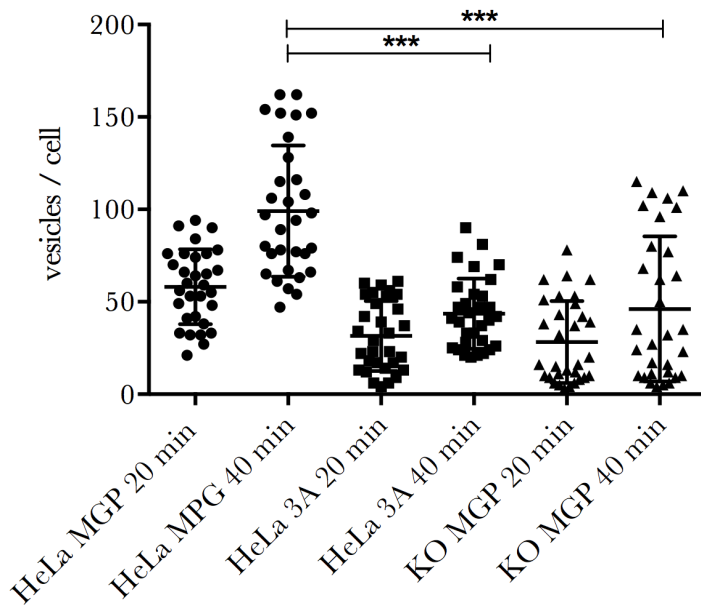


Figure 49: Quantification of vesicles of RUSH assay. For quantification, the number of vesicles per cell was counted for the three different cell lines HeLa MGP (circles), HeLa MGP 3A (boxes) and Cab45 KO MGP (triangles). The data shows that the delay in vesicle export from the Golgi is significant for either HeLa MGP 3A and Cab45 KO MGP in comparison to HeLa MGP ($n=35$; $P<0.05$). Both cell lines show less vesicular structures after 20 and after 40 min. Scatter blots depicts mean values with SD.

In summary, the RUSH system supported the *in vitro* data above, as indeed the 3A mutation of MGP exhibits the same delay in sorting as observed for the Cab45 KO cell line.

6.5 Cab45 is phosphorylated by Fam20C

Phosphorylation is generally known as a widespread and fast posttranslational modification of proteins throughout the cell and key mediator of cell signaling. However, although the existence of phosphorylated secretory pathway proteins was evident from early on, the issue is only poorly understood so far, mainly also due to the lack of suitable kinases.

Recently, the identification of the serine/threonine kinase Fam20C massively promoted the interest in this research field ¹⁵². Therefore, many new insights were gained on the secretory pathway phosphoproteome in the last years. The question, which proteins are modified inside the Golgi and if secretory cargo sorting is influenced by this modification, was addressed by a mass spectrometric approach, which should identify potential phosphorylated sites from isolated Golgi fractions. In this screen, more than 8200 phosphorylation sites were identified, whereby nearly 86 % of them were modified serine residues (Figure 50A). Few threonine residues were phosphorylated (13.7 %) and only very

Results

few (0.8 %) tyrosine residues, which can be considered as not significant. The phosphorylation pattern, which can be extracted from the found hits were S-X-E and T-X-E (Figure 50B). The former matches exactly the published Fam20C phosphorylation site ¹⁵². The threonine modifications in this context seem not surprising as many kinases have affinities for both amino acids, although often to a different extend ⁴¹¹.

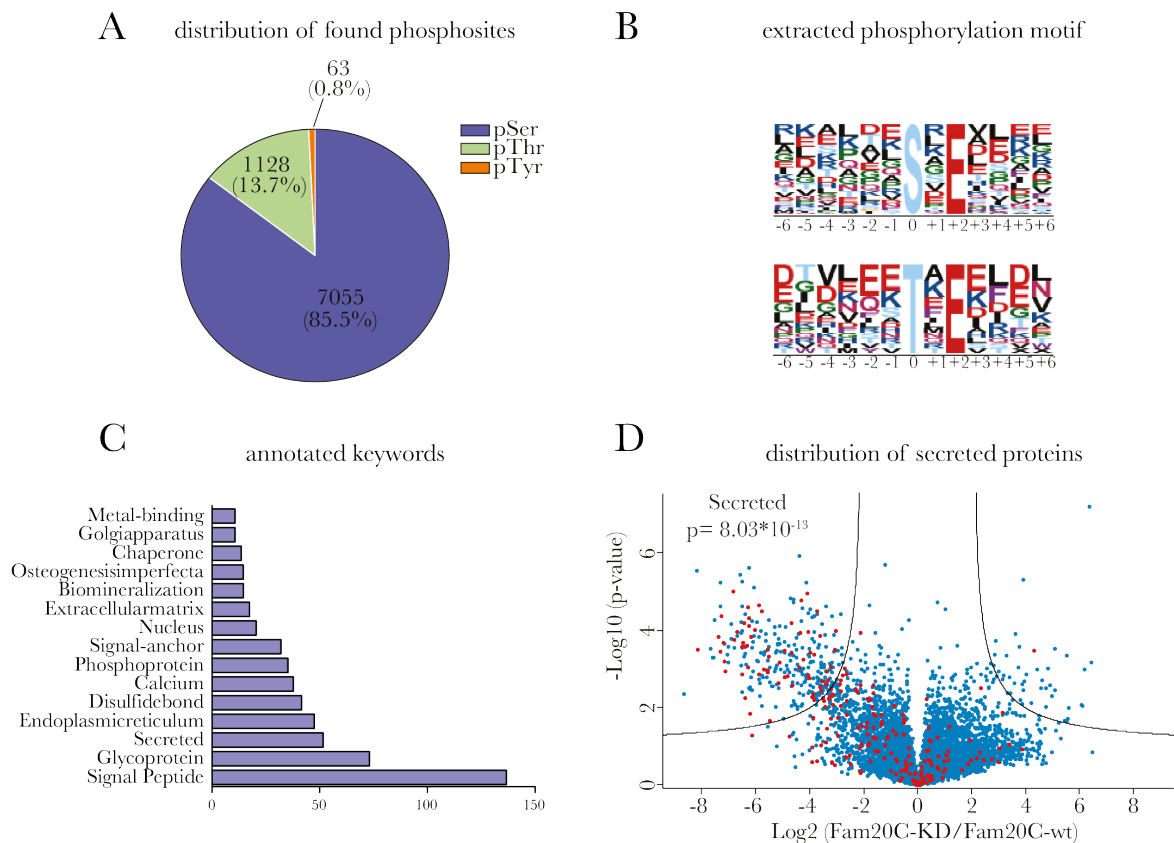


Figure 50: Results of mass spectrometric analysis of the phosphoproteome in Fam20C or Fam20C-KD overexpressing cells. (A) The pie chart depicts the amount and relative percentage of phosphopeptides identified in the mass spectrometric screen. Most of the modified residues were serines (purple), a few threonines (green) and only around 0.8 % tyrosine residues (orange). (B) The recognition motif of the Fam20C kinase which could be extracted from the hits was S/T-X-E. The short motif was described before as pattern for Fam20C-dependent phosphorylation ¹⁵⁰. (C) The bar chart correlates the identified phosphoproteins with annotated keywords. (D) The volcano blot depicts the phosphoproteins identified in the mass spectrometric screen. Proteins annotated as secreted, which are enriched in the Fam20C overexpressing fraction, are highlighted in red.

Figure 50C depicts the amount of proteins, which were annotated to different characteristics of secretory pathway proteins like signal peptide, glycoproteins or secreted. The amount of those proteins found in this screen underlines that indeed many proteins of the secretory pathway and the Golgi were found to be modified by phosphorylation, which might have an effect on their respective conformation and proper function.

In addition, the volcano blot of secreted proteins (indicated by red dots) shows that many of the phosphorylated proteins are enriched when the wild type kinase, but not its dominant

negative mutant is overexpressed (Figure 50D). This also proves that Fam20C affects a multitude of proteins not only inside the cell, but also in the extracellular space.

Position	Amino acid	Sequence window
99	S	GKDLGGFDEDAEPRISRRKLMVIFSKVDVNT
131	T	RKISAKEMQRWIMEKTAEHFQEAMEESKTHF
142	S	IMEKTAEHFQEAMEESKTHFRAVDPDGDGHV
193	T	ADAIRLNEELKVDEITQEVLENLKDRWYQAD
349	S	LEPEEVLKYSEFFT SKLVDYARSVHEEF

Table 10: Overview of Fam20C-dependent Cab45 phosphorylation sites identified by mass spectrometry. Analysis of phosphorylated peptide was performed in Golgi fractions isolated from S3 cell overexpressing either Fam20C wild type or the dominant negative mutant. Five phosphosites on either serine or threonine were identified (phosphorylated residues are highlighted in red in sequence windows).

Finally, the screen revealed also five Cab45 phosphorylation sites (Table 10). As depicted in the volcano blot (Figure 51A), these phosphosites are highly enriched in the Golgi apparatus of cells overexpressing Fam20C wild type. Among these hits, three serine and two threonine residues were identified. Four of these modified sites reside in the area around EF hand motif 1, 2 and 3, i.e. more in the N-terminal region of Cab45 (highlighted in cartoon in Figure 51B).

In summary, the mass spectrometric screen revealed that Fam20C indeed phosphorylates a multitude of proteins inside the secretory pathway and of the extracellular matrix as proposed before ¹⁵⁰. However, this screen also revealed so far unknown Cab45 phosphorylation sites, which are highly abundant in Fam20C overexpressing cells.

Unfortunately, the role of this serine/threonine modification and its effect on Cab45-mediated sorting of secretory cargo proteins under physiological conditions remains elusive at this point and requires further *in vitro* and *in vivo* verifications and investigations, which are currently ongoing in the von Blume lab.

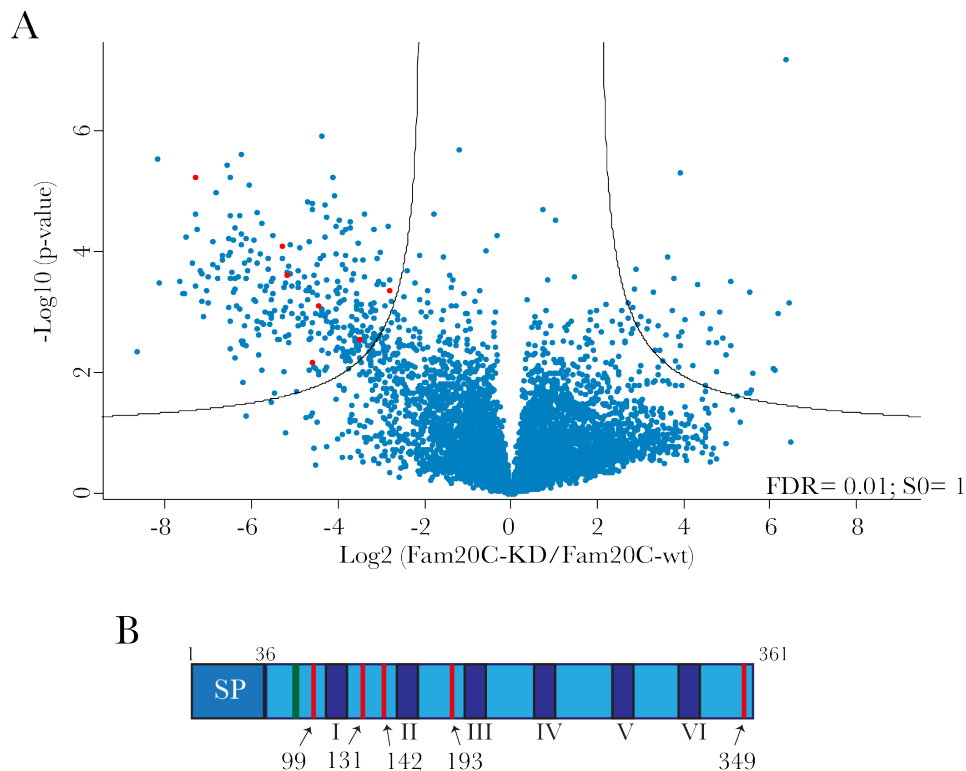


Figure 51: Vulcano blot of mass spectrometric screen highlights five Fam20C-dependent Cab45 phosphorylation sites. (A) Vulcano blot of mass spectrometric screen depicts enrichment of phosphopeptides in the presence of high Fam20C expression (blue dots of left branch). Cab45 specific phosphosites are highlighted in red. Two of the found peptide had a multiplicity of 2, therefore 7 dots are highlighted. (B) Cartoon of Cab45 visualizes the positions of the identified phosphosites (red lines) within the protein structure. Four of the five phosphopeptides accumulate in the region of EF hand motif 1, 2 and 3 (dark blue boxes; Roman numerals).

7 Discussion

Tissue integrity and cell-cell communication are two indispensable features to guarantee viability and proper function of a cellular system. To achieve these goals, cells interact by secretion of different factors such as hormones, cytokines or extracellular matrix components. As the malfunction of this protein secretion processes leads to severe diseases like diabetes, autoimmune disorders, skeletal dysplasia or cancer, the secretion machinery is under constant and tight surveillance and regulation ⁴¹²⁻⁴¹⁶.

One pivotal checkpoint is the sorting of proteins at the TGN. Proteins arrive at the TGN after their co-translational insertion into the ER and transport through the Golgi stack. Over the past decades, the mechanisms for sorting of transmembrane proteins have been described extensively ⁴¹⁷, however, the molecular mechanism for sorting and packing of soluble proteins destined for secretion have remained largely unknown.

Although the idea that soluble proteins are secreted by unselective bulk flow or by receptor-dependent mechanisms prevailed for a long time in the research field, in recent years it became evident that nature established regulated processes like the sorting by the CFL1/SPCA1/Cab45 machinery for this purpose ^{358,362-365}

Unfortunately, the details of this unique system are only at the beginning of their complete comprehension. Therefore, this thesis was focused on the in-detail characterization of the central component Cab45. In this study, state-of-the-art techniques were applied to analyze the intrinsic oligomerization potential of this protein and the implications for cellular retention. Additionally, Cab45-cargo interaction studies revealed, how intra-Golgi calcium levels can substantially influence the sorting process inside the Golgi lumen.

7.1 The CRISPR/Cas9 system - Boon and Bane

The CRISPR/Cas9 system was praised as extremely easy and highly efficient tool for genome editing of mammalian cells. Indeed, the flexible design of the sgRNAs, as well as the high efficiency for KO approaches make this system superior to comparable approaches like TALEN or Zink finger nucleases, even in HeLa cells with a difficult genomic environment. Furthermore, also knock-in approaches seem to work with reasonable efficiency. However, in addition to the widely-discussed drawbacks of the system like off-target effects, CRISPR/Cas9 bears in some cases additional risks ⁴¹⁸. For example, highly dynamic systems with overlapping fields of activity like kinase networks might circumvent KOs of single components easily. Therefore, short transient KD approaches might show different phenotypes than a constant KO of a gene as observed e.g. with morpholinos against *egfl7* in zebrafish or for the *DOCK6* gene in HeLa cells ^{419,420}. Also, single cells in culture start to compensate the KO, which can result in a strong spread of data in microscopy experiments until they lose the phenotype completely. For example, the data points of the RUSH experiments depicted in Figure 49 in the KO cell line indicate that, although all cells derive from a single cell clone, the cell line is not homogenous, i.e. that some cells start to compensate the KO effect, while others show still strongly impaired transport characteristics.

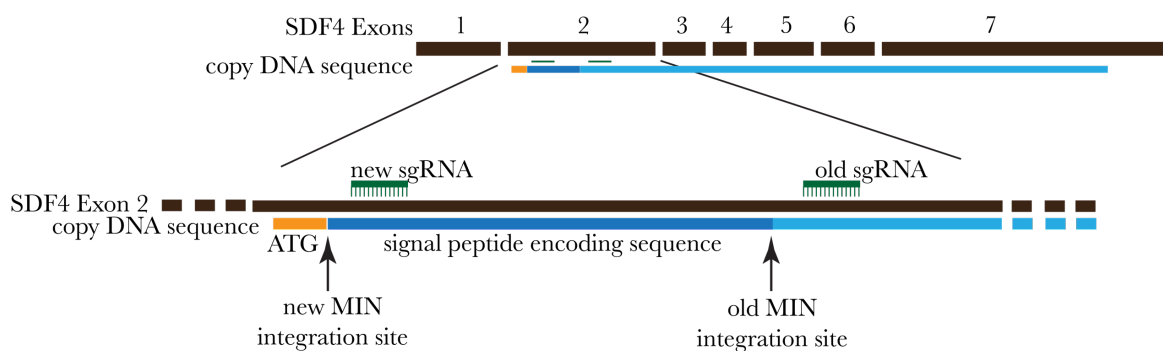


Figure 52: Schematic depiction of MIN tag integration sites. For the integration of the MIN tag the second exon of the SDF4 genomic locus (black lines, Arabic numerals) was first targeted by the sgRNA (dark green) in the area behind the signal peptide encoding sequence (dark blue). As this approach resulted surprisingly in a KO of Cab45, a second trial will target the area after the initial ATG codon (orange) to establish a functional platform for knock-in of Cab45 mutants behind the endogenous promoter.

The MIN-tag integration into the SDF4 locus presented above (section 6.2.6) resulted in an unexpected KO phenotype of Cab45. This finding was surprising as the integration of either an HA-tag of comparable length or a GFP tag in the same position in a construct for transient HeLa cell expression exhibited normal expression levels (Supplementary Figure

3). This might be due to the fact that processes like mammalian transcription initiation or termination, splice processes or genomic regulation are only insufficiently understood so far^{421,422}. This adds additional obstacles to efficient genome targeting, because knock-in of tags or fluorescent labels can prevent proper gene processing and expression.

Based on these results, it seems not possible to generate a functional MIN-tagged cell line behind the endogenous signal sequence of SDF4. Therefore, the generation of a new MIN-tag SDF4 cell line directly after the initial ATG start codon is currently in progress (Figure 52), because to date no alternative method provides such a multitude of applications to edit the mammalian genome within a few weeks and study proteins on endogenous levels.

7.2 Cab45 oligomerizes in a calcium-dependent manner under physiological conditions

The few studies on Cab45 published at the beginning of this thesis were performed in cells or in organisms. However, no publication, except one, presented data on recombinant, purified protein³⁶⁵. Therefore, successful purification of wild type Cab45 and its three EF hand mutants as a His-SUMO fusion protein in high amounts was one major accomplishment and paved the way for detailed *in vitro* analysis (Figure 15). Unfortunately, the 6EQ mutant did not express properly, probably due to misfolding or insolubility and could therefore not be purified by this approach or neither by an alternative test in HEK293 cells⁴²³.

NativePage analysis (Figure 26) and oligomerization studies with fluorescently labeled protein by confocal microscopy (Figure 28) proved that Cab45 is able to form oligomers in the presence of calcium. For this task, especially EF1 and EFh3 seems to be required, as these mutants lose the wild type feature (Figure 34 and Figure 35).

This behavior was observed several times before for other calcium binding proteins^{424,425}. For example, based on data of the crystal structure and small-angle X-ray experiments, calsequestrin can acquire different oligomeric states from dimer to long branched polymers dependent on calcium concentrations⁴²⁶.

Also proteins of the PEF protein family like peflin, ALG-2 or sorcin are known to form homo- or heterodimers via their unpaired last EF hand motif in a calcium-dependent manner, which seems essential for their overall stabilization^{424,427,428}. Now, the experiments presented above indicated for the first time that also Cab45 has a higher oligomeric state.

Furthermore, experiments with magnesium excluded the possibility of unspecific protein aggregation with a two-valent cation (Figure 28). In line with these observations, CD spectroscopy visualized the conformational change within the secondary structure of the protein upon calcium binding (Figure 29). This shift in secondary structure might expose hydrophobic regions, which can serve as trigger for oligomerization or for other interactions, e.g. with lipids. This characteristic was observed before for proteins like calmodulin and casein⁴²⁹⁻⁴³¹.

Besides, Cab45 might change its conformation upon calcium binding in a way that some calcium ions become covered inside the core of the protein. Those might be harder to release even in the presence of the calcium chelator EGTA (Figure 29).

7.2.1 But is this oligomeric phenotype of Cab45 physiological relevant?

The first hint that these multimers have indeed physiological relevance were given by experiments with isolated Golgi fractions, which indicated oligomers of the endogenous Cab45 of similar size as the recombinant protein on NativePage analyses (Figure 26). Furthermore, tests with STORM super-resolution microscopy in HeLa cells, which were performed in collaborations in the framework of this thesis, showed that oligomeric structures existed also inside the cells, but only when calcium was maintained at normal levels, and not after treatment with ionomycin ³⁸⁷.

Of course, the calcium concentrations used in some of the assays were high in comparison to published levels in the secretory pathway ¹⁷⁸. However, a face blot analysis, which correlates the protein and calcium concentrations necessary for polymerization demonstrated that high concentrations of Cab45, which might exist inside the TGN due to limited volume, reduce the amount of needed calcium immensely ³⁸⁷. Furthermore, calcium titrations in CD spectroscopy supported the idea that changes in secondary structure of Cab45 occur already between 50 and 150 μM , which ranges in the published area (Figure 29; ¹⁷⁸).

Similar arguments hold true for the size of the oligomers observed during *in vitro* assays. Limitations of space and protein inside the TGN lumen will restrict the size of the oligomers. In addition, STORM images indicate that the oligomers inside the cell might be significantly smaller than observed in confocal microscopy (Figure 28). This fact was also described before for the ER resident chaperone BiP, which forms huge agglomerations *in vitro*, but only smaller oligomers in cells (personal communication with David Ron, CIMR, Cambridge, UK).

Finally, Cab45 oligomerization might be influenced by several additional factors in a physiological context. For example, the impact of differential glycosylation of the human Cab45 might play a critical role for the endogenous Cab45, as observed for the von Willebrand factor ⁴³². Besides sugar modifications, the multimerization process might be strongly pH dependent, which would at the same time prevent the premature reaction inside the ER lumen. Also, high local calcium concentrations in the direct vicinity of the SPCA1 calcium pump, the area of localization of Cab45 found in Crevenna et al., 2016, may act as trigger point for Cab45 dependent sorting of soluble cargo proteins. In summary, deeper insights into current research topics like the overall regulation of calcium homeostasis at the TGN are necessary to reach a final conclusion on these profound questions.

7.2.2 The remaining problem of the Cab45 oligomerization domain

Naturally, the amount of data on Cab45 oligomerization evokes the requirement for a potential oligomerization domain. Unfortunately, so far, no defined domain inside the protein structure could be identified. The aggregation prone area detected by the TANGO algorithm and the thereof resulting MVKR mutant did not exhibit impaired oligomeric potential (Figure 38). Also, the stepwise approach to analyze fragments of Cab45 did not result in the identification of a potential hotspot (Figure 40). However, this might be due to the fact that Cab45 might oligomerize via one of its EF hands, as observed before for other EF hand proteins like Alg2⁴³³. This would also give a potential explanation for the problem that Cab45, considering the size of the polymers, needs more than one oligomerization domain. Based on these considerations, more research on this topic is necessary to answer the open question satisfyingly.

7.2.3 Oligomerization might be a potential retention mechanism for Cab45

Another critical topic was the Golgi retention of Cab45. As Cab45 contains no hydrophobic stretch long enough to span the membrane²²⁶ and no transmembrane interactor is known to date as for the other secretory pathway calcium binding protein Calnuc, which interacts with COX1 and COX2^{434,435} the mechanism how Cab45 remains in the Golgi lumen while cargos are packed into vesicles remained subject of discussions.

At the very C-terminal end of Cab45 the four amino acids HEEF were suggested several times in literature as Golgi retention signal^{225,227,370} analogous to the well-studied KDEL retention peptide of the ER³⁷³. But although Lara-Lemus and colleagues³⁷⁴ showed a C-terminal truncation mutant (Cab45_{308 Myc}) to be unphysiologically secreted from COS cells, this study unfortunately lacked a wild type control. As a consequence, the possibility that secretion of this mutant was due to overexpression, but not lack of the HEEF signal, as it was observed by⁴³⁶ in HeLa cells, cannot be excluded. Furthermore, the C-terminal HDEF motif of CALU also seems to be insufficient as retention signal, as CALU is found throughout the secretory pathway and also secreted under natural conditions^{227,245,437}. However, exactly this HDEF motif was suggested by another publication as a sufficient retention signal for the endoplasmic reticulum⁴³⁸. In addition, the ER located UGGP enzyme, contains a HEEL sequence, which triggers ER localization⁵². In contrast, multimerization itself was suggested as a general mechanism for protein retention inside organelles^{439,440}. This is based on the observation, that for example calsequestrin forms a matrix-like or gel-like structure inside the transverse tubuli of the sarcoplasmic reticulum in

a calcium-dependent manner and that also ER located calcium binding proteins are released from cells upon calcium depletion by ionophores ⁴⁴¹. The Cab45 oligomers might reflect a preform of this gel-like matrix, which forms under physiological conditions inside the Golgi and retains it, while cargo is secreted.

Nonetheless, the matrix-forming potential of Cab45 needs further investigation, but also the HEEF-based retention needs to be analyzed with endogenous proteins levels. In addition, a potential Golgi receptor, the counterpart of the ER KDEL receptor, would be necessary to convincingly support this theory.

7.3 Cab45 releases cargo upon phosphorylation

Immunoprecipitation experiments with GST-tagged Cab45 indicated already in 2012 that Cab45 can interact with cargo proteins like COMP or LyzC in cell lysates ³⁶⁵. In this thesis, we could finally show that this interaction is indeed direct and no additional adaptor proteins are needed (Figure 41). Furthermore, fluorescence correlation spectroscopy (FCS) measurements of one of our collaborators indicate that only calcium bound Cab45 is able to interact with cargo proteins ³⁸⁷. However, the *in vitro* complexes formed by Cab45 and cargo are very stable in FRAP experiments (Figure 44). Hence, cellular environments obviously provide additional mechanisms for subsequent cargo release.

One putative signal for cargo release might be tyrosine phosphorylation. IP experiments with synthetic peptides proved that phosphorylation of two different tyrosine residues of the MGP cargo protein abolishes Cab45 interaction completely (Figure 46). In addition, phosphorylation of a third tyrosine in direct vicinity had no effect. This finding was also supported by RUSH assays. Here, a significant delay in cargo transport across the secretory pathway was detectable after 40 min when tyrosine residues were mutated in MGP (Figure 48). This phenotype was also mimicked by the KO of Cab45 in HeLa cells.

However, which is the kinase responsible for this mechanism? One potential candidate, is TPK-PKDCC or VLK. TPK-PKDCC was described as sensitive not only for magnesium, but also for calcium ¹⁶⁹. Furthermore, overexpression of VLK caused delay in Golgi export of a transmembrane protein, which might be due to enhanced sorting and packaging of Cab45-dependent, soluble cargos ¹⁶⁶. Finally, a phosphosite database (phosphosite.org) contains the entry, that MGP was found several times in human cells to be phosphorylated at tyrosine residue Y82, one of the identified phosphosites of the peptide pull-downs ⁴⁴²⁻⁴⁴⁴. Unfortunately, no consensus pattern for TPK-PKDCC phosphorylation is known to date.

Indeed, all this data supports the idea, that phosphorylation plays a crucial role in Cab45-dependent cargo sorting. However, although we know already from the mass spectrometric screen of Golgi fractions (Figure 51) that not only the cargo, but also Cab45 is phosphorylated, the specific role of this modification is unclear. The accumulation of phosphorylation site in the N-terminal region of the protein might either hint to the fact, that Cab45 is more accessible in this area for the kinase, or less accessible for the corresponding unknown phosphatase due to protein conformation. However, spatial-temporal synergy of all those modification events remains to be elucidated in detail.

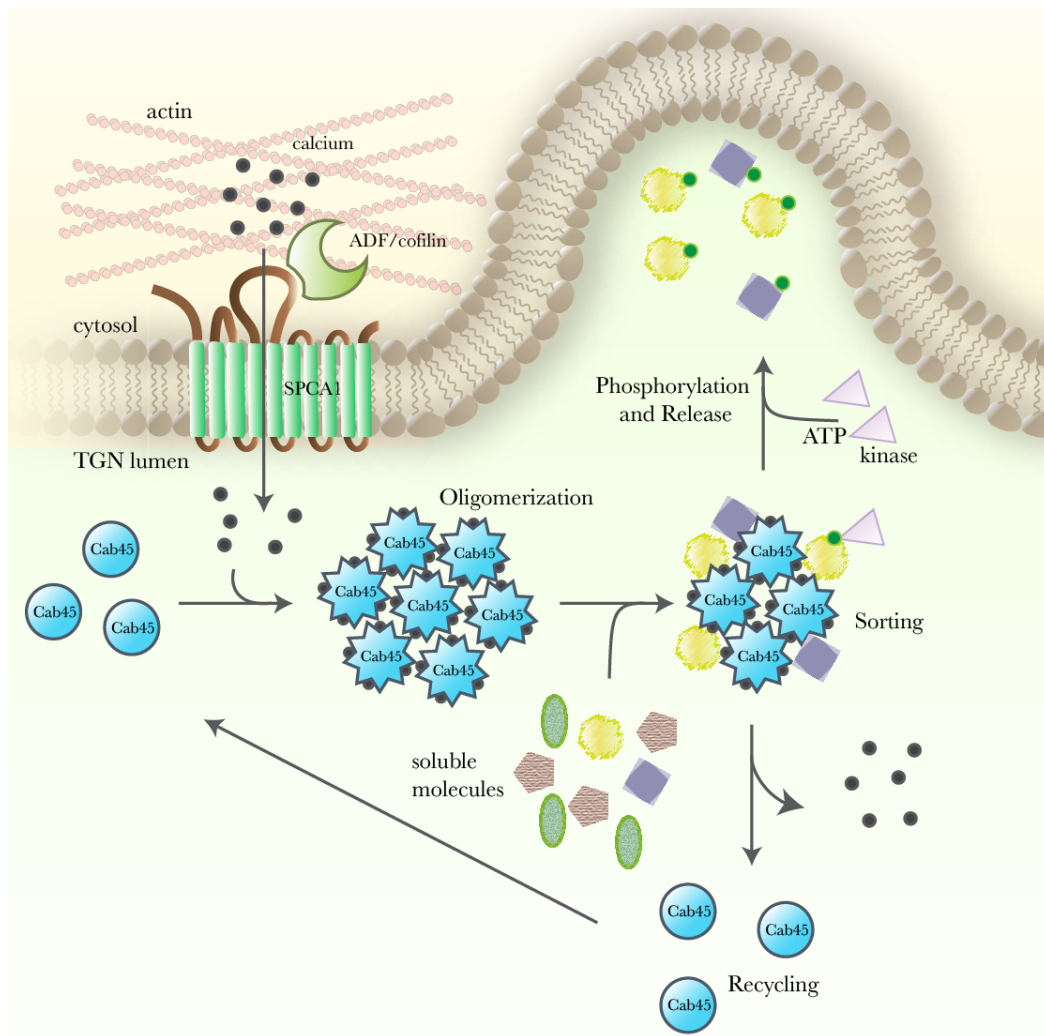


Figure 53: Sorting mechanism by CLF1/SPCA1/Cab45 machinery. Active CFL1 (light green crescent) binds via a patch formed by four amino acids to the second cytosolic loop of SPCA1 (green/brown). As a consequence, SPCA1 pumps calcium (grey circles) in an ATP-consuming manner into the TGN lumen. Calcium is then bound by Cab45 (blue circles/stars) which forms oligomers. In this state, Cab45 binds cargo molecules and accumulates then in a certain subdomain of the TGN and, through this, separates them from other soluble proteins. Phosphorylation of cargo (green circles) by TPK-PKDCC kinase (rose triangles) trigger release of the cargo and packaging into vesicles for transport to the PM. Cab45 is retained in the Golgi due to the size of the oligomers, Cab45 can be reused for a new round of soluble cargo sorting.

Besides, phosphorylation of the cargo, instead of Cab45 itself as a release signal, would offer a possibility to maintain phosphorylations necessary for functions in the extracellular matrix of cargo proteins. Furthermore, dephosphorylation of Cab45 would not be necessary before a new cycle of cargo sorting at the TGN can begin.

Finally, the Cab45 oligomers decorated with cargo proteins might not be accessible enough for the kinase. Therefore, the role of Cab45 phosphorylation by Fam20C remains a mystery to date.

In summary, the results of this thesis contributed to gain a better understanding of the mechanism underlying Cab45-dependent cargo sorting at the TGN. Based on the data presented above and previous publication by the von Blume group, we propose the following model for the sorting of soluble proteins by CFL1/SPCA1/Cab45 sorting machinery (Figure 53):

Active CFL1 interacts with the second cytosolic loop of SPCA1 via a patch of four amino acids and recruits actin to the TGN membrane. This CFL1-SPCA1 interaction activates the calcium pump, which transports calcium in a ATP-consuming manner across the Golgi membrane. On the luminal side Cab45 binds the newly imported calcium ions, which triggers a conformational switch of the protein and oligomerization. In parallel, cargo is bound by Cab45 oligomers and accumulated in the Golgi for subsequent vesicle packaging and export. This process probably occurs in a subdomain of the TGN, which is devoid of other Golgi resident proteins, as suggested by the results of the superresolution microscopy (Figure 45). Upon cargo phosphorylation, the cargo is released from the hetero-oligomer and while secretory proteins are transported to the PM, Cab45 is retained by its oligomeric form inside the lumen. After calcium release, Cab45 monomers are available of a new round of cargo sorting.

8 Outlook and open questions

In this thesis, several to date unknown aspects of secretory cargo sorting were elucidated. However, some aspects require additional research to consolidate the data presented above. In future studies, newly established tools, like the CRISPR/Cas9 KO HeLa cell line and also the recombinant protein will help to address profound questions around this sorting mechanism. For example, no data exists how calcium homeostasis by SPCA1 is regulated in living cells, i.e. if the CFL1-SPCA1 dependent pumping mechanisms is constitutive, or initiated by an extra- or intracellular signal. This would also give a hint, under which conditions cargo molecules are exported from the TGN, or if for example high amount of cargo proteins can signal “inside-out” to activate the SPCA1 machinery.

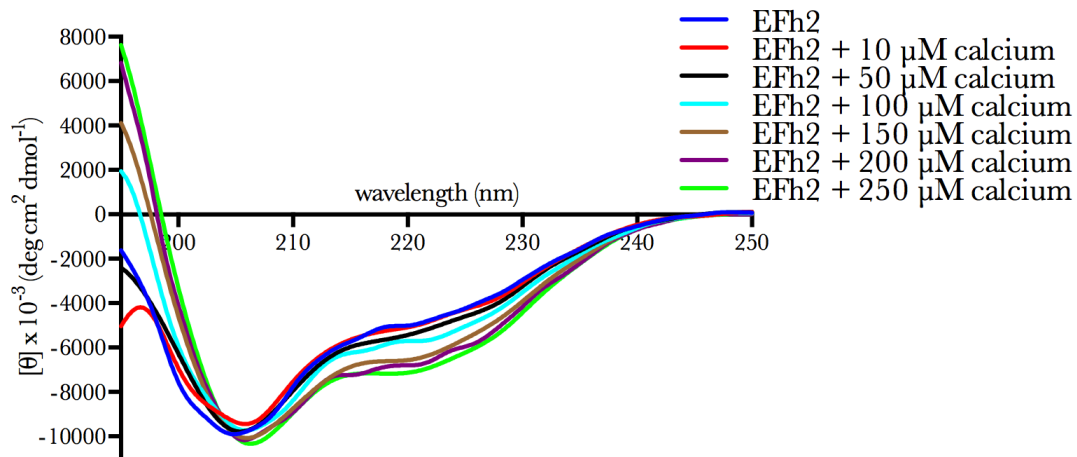
In this line, the Cab45-calcium interactions requires further examinations. Although it is now evident that calcium binding is required for the conformation of Cab45, detailed dissociation constants of the different EF hand motifs would further support our overall understanding. Also, the cooperativity of the calcium binding by the determination of the Hill coefficient. Finally, the release of the bound calcium is a critical step and under current investigation.

Another aspect of interest is how many proteins are under influence of the CLF1/SPCA1/Cab45 machinery. Although this thesis augmented the number of potential cargos from around 20 of the initial screen to around 140 candidates, further mass spectrometric screens might further increase the number. Besides, the sequence pattern around the tyrosine residues found in MGP might serve as template for a bioinformatics search to identify new unknown interactors. As a follow up, the RUSH method will provide a powerful tool to study the dynamics of cargo export of already known and new cargo proteins.

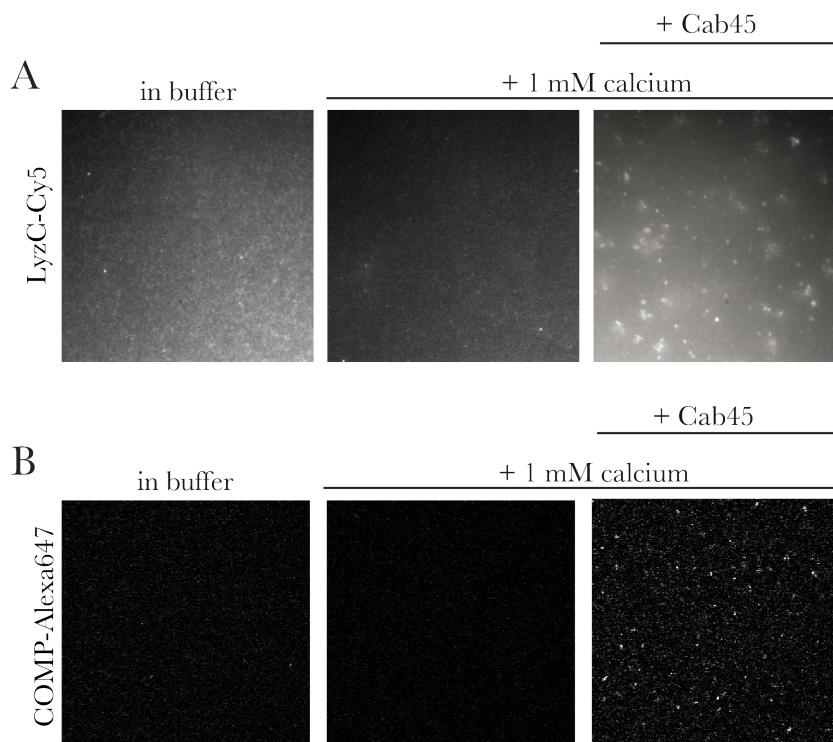
Additionally, many biochemical aspects including the influences of Cab45 phosphorylation by Fam20C, pH dependency and the effect of differential glycosylation need to be examined further. Finally, the identity of vesicle, which transport the cargo proteins to the plasma membrane, will help to understand this complex mechanism of basic research. Immunofluorescence studies will also elucidate the difference between transport carriers and the vesicles containing the calcium-binding deficient mutants of Cab45.

Taken together, the answers to all these questions will help to understand the mechanisms of sorting of secretory cargo sorting, and as a consequence, will also deepen our insights in the fundamental role of the Golgi apparatus in cellular homeostasis and integrity.

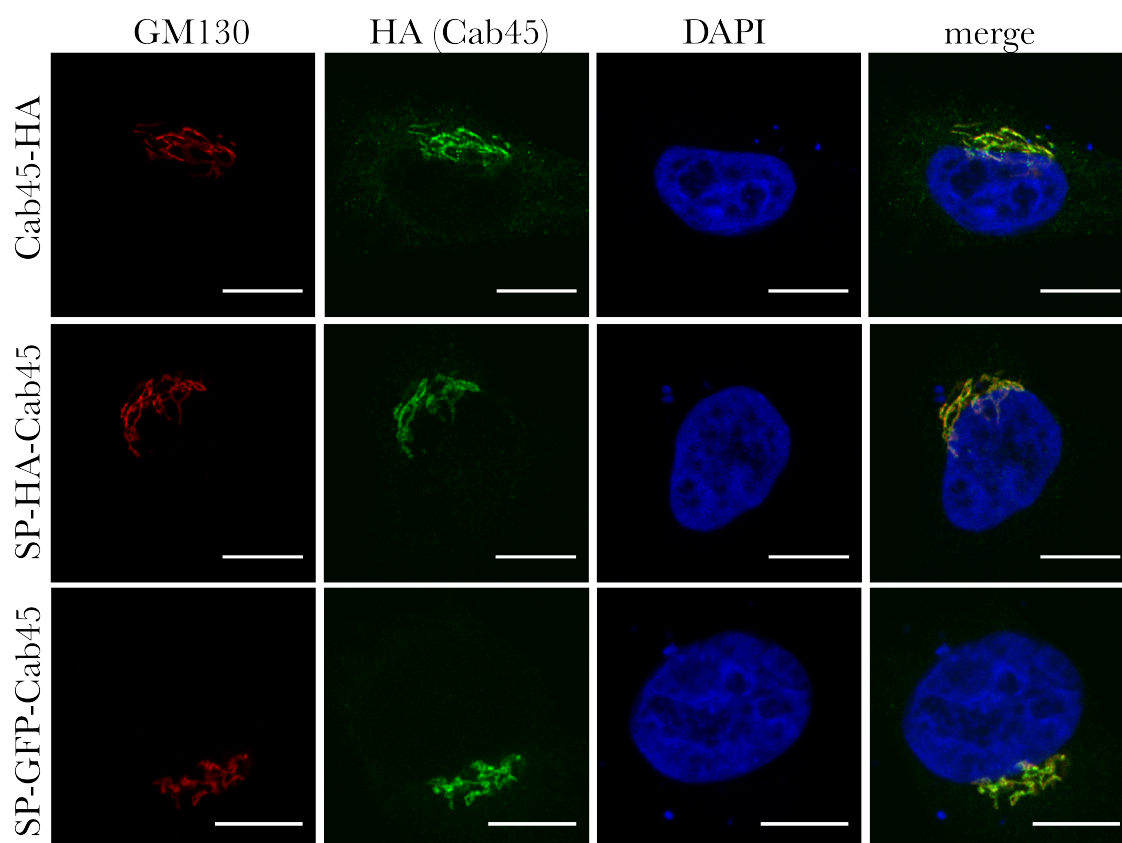
9 Supplementary Figure and Tables



Supplementary Figure 1: CD spectroscopy of titration experiment with EFh2 mutant. EFh2 mutant was analyzed with different calcium concentrations between 0 and 250 μM by CD spectroscopy. The change in secondary structure begins at around 50 μM (black line). Similar to the wild type protein EFh2 is in a transitional state at 100 μM (turquoise line). However, EFh2 has not completely finished its conformational shift at 150 μM (brown line), but is still sensitive to calcium changes up to 250 μM (green line).



Supplementary Figure 2: LyzC and COMP only oligomerize in the presence of Cab45. (A) and (B) Control experiments with LyzC-Cy5 and COMP-Alexa647 for oligomerization assays in the absence of Cab45. Both proteins were incubated in buffer in the presence and absence of 1 mM calcium. Under these conditions, neither COMP nor LyzC depict any oligomers. After addition of Cab45 both proteins form clusters as observed before.



Supplementary Figure 3: Analysis of HeLa cells overexpressing wild type Cab45 with C-terminal HA tag, Cab45 with N-terminal HA tag or an N-terminal GFP tag. The microscopy analysis of all cells overexpressing differently tagged constructs of Cab45 show strong expression of the proteins regardless of the position of the HA or the GFP tag (green channel). In all cell lines Cab45 resides in the vicinity of the GM130 Golgi marker (red channel and merge) and exhibit normal nuclear morphology (blue channel). Therefore, integration of the MIN tag in the position of the N-terminal HA or GFP tag, which resulted in a KO of Cab45, was not to be expected. Scale bars represent 10 μ m.

α -helical content (w/o calcium)	α -helical content (with calcium)	β -sheet content (w/o calcium)	β -sheet content (with calcium)	Random coil content (w/o calcium)	Random coil content (with calcium)
0.096	0.201	0.346	0.271	0.558	0.518
0.170	0.213	0.301	0.248	0.530	0.539
0.150	0.256	0.307	0.241	0.541	0.503
0.139	0.223	0.318	0.253	0.543	0.520

Supplementary Table 1: Summary of secondary structure prediction by CONTIN software of three replicates of Cab45 conformational change in presence of 1 mM calcium. Reported values for the alpha-helical and beta sheet content were the sum of regular and distorted fractions for each secondary element.

10 References

1. Blázquez, M. & Shennan, K. I. Protein Secretory Pathways. 349, (John Wiley & Sons, Ltd, 2001).
2. Guo, Y., Sirkis, D. W. & Schekman, R. Protein sorting at the trans-Golgi network. *Annual Review of Cell and Developmental Biology* 30, 169–206 (2014).
3. Zimmermann, R., Eyrich, S., Ahmad, M. & Helms, V. Protein translocation across the ER membrane. *Biochimica et Biophysica Acta (BBA) - Biomembranes* 1808, 912–924 (2011).
4. Christodoulou, A., Santarella-Mellwig, R., Santama, N. & Mattaj, I. W. Transmembrane protein TMEM170A is a newly discovered regulator of ER and nuclear envelope morphogenesis in human cells. *J. Cell. Sci.* 129, 1552–1565 (2016).
5. English, A. R. & Voeltz, G. K. Endoplasmic Reticulum Structure and Interconnections with Other Organelles. *Cold Spring Harb Perspect Biol* 5, a013227–a013227 (2013).
6. Phillips, M. J. & Voeltz, G. K. Structure and function of ER membrane contact sites with other organelles. *Nat. Rev. Mol. Cell Biol.* 17, 69–82 (2016).
7. Shibata, Y., Voeltz, G. K. & Rapoport, T. A. Rough Sheets and Smooth Tubules. *Cell* 126, 435–439 (2006).
8. Terasaki, M. et al. Stacked endoplasmic reticulum sheets are connected by helicoidal membrane motifs. *Cell* 154, 285–296 (2013).
9. Lee, C. & Chen, L. B. Dynamic behavior of endoplasmic reticulum in living cells. *Cell* 54, 37–46 (1988).
10. Dreier, L. & Rapoport, T. A. In vitro formation of the endoplasmic reticulum occurs independently of microtubules by a controlled fusion reaction. *J. Cell Biol.* 148, 883–898 (2000).
11. Terasaki, M., Chen, L. B. & Fujiwara, K. Microtubules and the endoplasmic reticulum are highly interdependent structures. *J. Cell Biol.* 103, 1557–1568 (1986).
12. Waterman-Storer, C. M. & Salmon, E. D. Endoplasmic reticulum membrane tubules are distributed by microtubules in living cells using three distinct mechanisms. *Curr. Biol.* 8, 798–806 (1998).

13. Friedman, J. R., Webster, B. M., Mastronarde, D. N., Verhey, K. J. & Voeltz, G. K. ER sliding dynamics and ER-mitochondrial contacts occur on acetylated microtubules. *J. Cell Biol.* 190, 363–375 (2010).
14. Clapham, D. E. Calcium signaling. *Cell* 131, 1047–1058 (2007).
15. Fagone, P. & Jackowski, S. Membrane phospholipid synthesis and endoplasmic reticulum function. *J. Lipid Res.* 50 Suppl, S311–6 (2009).
16. Braakman, I. & Hebert, D. N. Protein folding in the endoplasmic reticulum. *Cold Spring Harb Perspect Biol* 5, a013201–a013201 (2013).
17. Koenig, P.-A. & Ploegh, H. L. Protein quality control in the endoplasmic reticulum. *F1000Prime Rep* 6, 49 (2014).
18. Schwarz, D. S. & Blower, M. D. The endoplasmic reticulum: structure, function and response to cellular signaling. *Cell. Mol. Life Sci.* 73, 79–94 (2016).
19. Palade, G. Intracellular aspects of the process of protein synthesis. *Science* 189, 867–867 (1975).
20. Palade, G. Intracellular aspects of the process of protein synthesis. *Science* 189, 347–358 (1975).
21. Voeltz, G. K., Rolls, M. M. & Rapoport, T. A. Structural organization of the endoplasmic reticulum. *EMBO Rep.* 3, 944–950 (2002).
22. Orci, L. et al. Mammalian Sec23p homologue is restricted to the endoplasmic reticulum transitional cytoplasm. *Proc. Natl. Acad. Sci. U.S.A.* 88, 8611–8615 (1991).
23. Shibata, Y. et al. Mechanisms Determining the Morphology of the Peripheral ER. *Cell* 143, 774–788 (2010).
24. Orci, L. Some aspects of the morphology of insulin-secreting cells. *Acta Histochem.* 55, 147–158 (1976).
25. Wassermann, D. Multiple rough endoplasmic cisternae in the endocrine pancreas of the adult rat. *Cell Tissue Res.* 160, 539–549 (1975).
26. Nyathi, Y., Wilkinson, B. M. & Pool, M. R. Co-translational targeting and translocation of proteins to the endoplasmic reticulum. *Biochimica et Biophysica Acta (BBA) - Molecular Cell Research* 1833, 2392–2402 (2013).
27. Johnson, N., Powis, K. & High, S. Post-translational translocation into the endoplasmic reticulum. *Biochim. Biophys. Acta* 1833, 2403–2409 (2013).
28. Walter, P. & Blobel, G. Translocation of proteins across the endoplasmic reticulum III. Signal recognition protein (SRP) causes signal sequence-dependent and site-

References

- specific arrest of chain elongation that is released by microsomal membranes. *J. Cell Biol.* 91, 557–561 (1981).
29. Heijne, G. On the Hydrophobic Nature of Signal Sequences. *European Journal of Biochemistry* 116, 419–422 (1981).
 30. Mitra, K., Frank, J. & Driessen, A. Co- and post-translational translocation through the protein-conducting channel: analogous mechanisms at work? *Nat. Struct. Mol. Biol.* 13, 957–964 (2006).
 31. Ott, C. M. & Lingappa, V. R. Integral membrane protein biosynthesis: why topology is hard to predict. *J. Cell. Sci.* 115, 2003–2009 (2002).
 32. Janda, C. Y. et al. Recognition of a signal peptide by the signal recognition particle. *Nature* 465, 507–510 (2010).
 33. Lütcke, H., High, S., Römisch, K., Ashford, A. J. & Dobberstein, B. The methionine-rich domain of the 54 kDa subunit of signal recognition particle is sufficient for the interaction with signal sequences. *EMBO J.* 11, 1543–1551 (1992).
 34. Meyer, D. I., Krause, E. & Dobberstein, B. Secretory protein translocation across membranes—the role of the "docking protein". *Nature* 297, 647–650 (1982).
 35. Gilmore, R., Walter, P. & Blobel, G. Protein translocation across the endoplasmic reticulum. II. Isolation and characterization of the signal recognition particle receptor. *J. Cell Biol.* 95, 470–477 (1982).
 36. Halic, M. & Beckmann, R. The signal recognition particle and its interactions during protein targeting. *Curr. Opin. Struct. Biol.* 15, 116–125 (2005).
 37. Pfeffer, S. et al. Structure of the native Sec61 protein-conducting channel. *Nat Commun* 6, 8403 (2015).
 38. Van den Berg, B. et al. X-ray structure of a protein-conducting channel. *Nature* 427, 36–44 (2004).
 39. Connolly, T., Rapiejko, P. J. & Gilmore, R. Requirement of GTP hydrolysis for dissociation of the signal recognition particle from its receptor. *Science* 252, 1171–1173 (1991).
 40. Borgese, N. & Fasana, E. Targeting pathways of C-tail-anchored proteins. *Biochim. Biophys. Acta* 1808, 937–946 (2011).
 41. Stefanovic, S. & Hegde, R. S. Identification of a targeting factor for posttranslational membrane protein insertion into the ER. *Cell* 128, 1147–1159 (2007).
 42. Aviram, N. et al. The SND proteins constitute an alternative targeting route to the endoplasmic reticulum. *Nature* 540, 134–138 (2016).

43. Weihofen, A., Binns, K., Lemberg, M. K., Ashman, K. & Martoglio, B. Identification of signal peptide peptidase, a presenilin-type aspartic protease. *Science* 296, 2215–2218 (2002).
44. Voss, M., Schröder, B. & Flührer, R. Mechanism, specificity, and physiology of signal peptide peptidase (SPP) and SPP-like proteases. *Biochim. Biophys. Acta* 1828, 2828–2839 (2013).
45. Xu, C. & Ng, D. T. W. Glycosylation-directed quality control of protein folding. *Nat. Rev. Mol. Cell Biol.* 16, 742–752 (2015).
46. Bieberich, E. Synthesis, Processing, and Function of N-glycans in N-glycoproteins. *Adv Neurobiol* 9, 47–70 (2014).
47. Hammond, C., Braakman, I. & Helenius, A. Role of N-linked oligosaccharide recognition, glucose trimming, and calnexin in glycoprotein folding and quality control. *Proc. Natl. Acad. Sci. U.S.A.* 91, 913–917 (1994).
48. Helenius, A. How N-linked oligosaccharides affect glycoprotein folding in the endoplasmic reticulum. *Mol. Biol. Cell* 5, 253–265 (1994).
49. Williams, D. B. Beyond lectins: the calnexin/calreticulin chaperone system of the endoplasmic reticulum. *J. Cell. Sci.* 119, 615–623 (2006).
50. Pollock, S. et al. Specific interaction of ERp57 and calnexin determined by NMR spectroscopy and an ER two-hybrid system. *EMBO J.* 23, 1020–1029 (2004).
51. Kozlov, G. et al. Structural basis of cyclophilin B binding by the calnexin/calreticulin P-domain. *J. Biol. Chem.* 285, 35551–35557 (2010).
52. Tessier, D. C. et al. Cloning and characterization of mammalian UDP-glucose glycoprotein: glucosyltransferase and the development of a specific substrate for this enzyme. *Glycobiology* 10, 403–412 (2000).
53. Trombetta, E. S., Simons, J. F. & Helenius, A. Endoplasmic reticulum glucosidase II is composed of a catalytic subunit, conserved from yeast to mammals, and a tightly bound noncatalytic HDEL-containing subunit. *J. Biol. Chem.* 271, 27509–27516 (1996).
54. D'Alessio, C., Caramelo, J. J. & Parodi, A. J. UDP-Glc:glycoprotein glucosyltransferase-glucosidase II, the ying-yang of the ER quality control. *Semin. Cell Dev. Biol.* 21, 491–499 (2010).
55. McCaffrey, K. & Braakman, I. Protein quality control at the endoplasmic reticulum. *Essays Biochem.* 60, 227–235 (2016).
56. Hetz, C. The unfolded protein response: controlling cell fate decisions under ER stress and beyond. *Nat. Rev. Mol. Cell Biol.* 13, 89–102 (2012).

References

57. Ron, D. & Walter, P. Signal integration in the endoplasmic reticulum unfolded protein response. *Nat. Rev. Mol. Cell Biol.* 8, 519–529 (2007).
58. Doroudgar, S. et al. Hrd1 and ER-Associated Protein Degradation, ERAD, are Critical Elements of the Adaptive ER Stress Response in Cardiac Myocytes. *Circ. Res.* 117, 536–546 (2015).
59. Baldrige, R. D. & Rapoport, T. A. Autoubiquitination of the Hrd1 Ligase Triggers Protein Retrotranslocation in ERAD. *Cell* 166, 394–407 (2016).
60. Ruggiano, A., Foresti, O. & Carvalho, P. Quality control: ER-associated degradation: protein quality control and beyond. *J. Cell Biol.* 204, 869–879 (2014).
61. Bannykh, S. I., Rowe, T. & Balch, W. E. The organization of endoplasmic reticulum export complexes. *J. Cell Biol.* 135, 19–35 (1996).
62. Hammond, A. T. & Glick, B. S. Dynamics of transitional endoplasmic reticulum sites in vertebrate cells. *Mol. Biol. Cell* 11, 3013–3030 (2000).
63. Stephens, D. J. De novo formation, fusion and fission of mammalian COPII-coated endoplasmic reticulum exit sites. *EMBO Rep.* 4, 210–217 (2003).
64. Bielli, A. et al. Regulation of Sar1 NH2 terminus by GTP binding and hydrolysis promotes membrane deformation to control COPII vesicle fission. *J. Cell Biol.* 171, 919–924 (2005).
65. Barlowe, C. & Schekman, R. SEC12 encodes a guanine-nucleotide-exchange factor essential for transport vesicle budding from the ER. *Nature* 365, 347–349 (1993).
66. Weissman, J. T., Plutner, H. & Balch, W. E. The mammalian guanine nucleotide exchange factor mSec12 is essential for activation of the Sar1 GTPase directing endoplasmic reticulum export. *Traffic* 2, 465–475 (2001).
67. Lee, M. C. S. et al. Sar1p N-terminal helix initiates membrane curvature and completes the fission of a COPII vesicle. *Cell* 122, 605–617 (2005).
68. Miller, E. A. et al. Multiple cargo binding sites on the COPII subunit Sec24p ensure capture of diverse membrane proteins into transport vesicles. *Cell* 114, 497–509 (2003).
69. Gomez-Navarro, N. & Miller, E. A. COP-coated vesicles. *Curr. Biol.* 26, R54–7 (2016).
70. Gomez-Navarro, N. & Miller, E. Protein sorting at the ER-Golgi interface. *J. Cell Biol.* 215, 769–778 (2016).
71. D'Arcangelo, J. G., Stahmer, K. R. & Miller, E. A. Vesicle-mediated export from the ER: COPII coat function and regulation. *Biochim. Biophys. Acta* 1833, 2464–2472 (2013).

72. Dancourt, J. & Barlowe, C. Protein sorting receptors in the early secretory pathway. *Annual Review of Biochemistry* 79, 777–802 (2010).
73. Appenzeller-Herzog, C., Roche, A.-C., Nufer, O. & Hauri, H.-P. pH-induced conversion of the transport lectin ERGIC-53 triggers glycoprotein release. *J. Biol. Chem.* 279, 12943–12950 (2004).
74. Velloso, L. M., Svensson, K., Schneider, G., Pettersson, R. F. & Lindqvist, Y. Crystal structure of the carbohydrate recognition domain of p58/ERGIC-53, a protein involved in glycoprotein export from the endoplasmic reticulum. *J. Biol. Chem.* 277, 15979–15984 (2002).
75. Dancourt, J. & Barlowe, C. Erv26p-dependent export of alkaline phosphatase from the ER requires lumenal domain recognition. *Traffic* 10, 1006–1018 (2009).
76. Sato, K. & Nakano, A. Dissection of COPII subunit-cargo assembly and disassembly kinetics during Sar1p-GTP hydrolysis. *Nat. Struct. Mol. Biol.* 12, 167–174 (2005).
77. Chen, Y. A. & Scheller, R. H. SNARE-mediated membrane fusion. *Nat. Rev. Mol. Cell Biol.* 2, 98–106 (2001).
78. Muppirala, M., Gupta, V. & Swarup, G. Syntaxin 17 cycles between the ER and ERGIC and is required to maintain the architecture of ERGIC and Golgi. *Biol. Cell* 103, 333–350 (2011).
79. Gillon, A. D., Latham, C. F. & Miller, E. A. Vesicle-mediated ER export of proteins and lipids. *Biochim. Biophys. Acta* 1821, 1040–1049 (2012).
80. Sesso, A., de Faria, F. P., Iwamura, E. S. & Corrêa, H. A three-dimensional reconstruction study of the rough ER-Golgi interface in serial thin sections of the pancreatic acinar cell of the rat. *J. Cell. Sci.* 107 (Pt 3), 517–528 (1994).
81. Sesso, A., Azimovas, S. R. & Ferreira, M. A. Freeze-fracture and thin section study of the rough ER-Golgi interface in the pancreatic acinar cell. Resemblance between the intramembranal architecture of the outermost Golgi cisterna and the post-rough ER vesicular and tubular elements. *Biol. Cell* 81, 165–176 (1994).
82. Klumperman, J. et al. The recycling pathway of protein ERGIC-53 and dynamics of the ER-Golgi intermediate compartment. *J. Cell. Sci.* 111 (Pt 22), 3411–3425 (1998).
83. Hauri, H. P., Kappeler, F., Andersson, H. & Appenzeller, C. ERGIC-53 and traffic in the secretory pathway. *J. Cell. Sci.* 113 (Pt 4), 587–596 (2000).
84. Lewis, M. J. & Pelham, H. R. A human homologue of the yeast HDEL receptor. *Nature* 348, 162–163 (1990).
85. Letourneur, F. et al. Coatamer is essential for retrieval of dilysine-tagged proteins to the endoplasmic reticulum. *Cell* 79, 1199–1207 (1994).

References

86. Itin, C., Roche, A. C., Monsigny, M. & Hauri, H. P. ERGIC-53 is a functional mannose-selective and calcium-dependent human homologue of leguminous lectins. *Mol. Biol. Cell* 7, 483–493 (1996).
87. Dogic, D., Dubois, A., de Chassey, B., Lefkir, Y. & Letourneur, F. ERGIC-53 KKAA signal mediates endoplasmic reticulum retrieval in yeast. *Eur. J. Cell Biol.* 80, 151–155 (2001).
88. Lewis, M. J. & Pelham, H. R. Ligand-induced redistribution of a human KDEL receptor from the Golgi complex to the endoplasmic reticulum. *Cell* 68, 353–364 (1992).
89. Mironov, A. A., Sesorova, I. V. & Beznoussenko, G. V. Golgi's way: a long path toward the new paradigm of the intra-Golgi transport. *Histochem. Cell Biol.* 140, 383–393 (2013).
90. Klumperman, J. Architecture of the mammalian Golgi. *Cold Spring Harb Perspect Biol* 3, a005181–a005181 (2011).
91. Rabouille, C., Misteli, T., Watson, R. & Warren, G. Reassembly of Golgi stacks from mitotic Golgi fragments in a cell-free system. *J. Cell Biol.* 129, 605–618 (1995).
92. Pelletier, L. et al. Golgi biogenesis in *Toxoplasma gondii*. *Nature* 418, 548–552 (2002).
93. Golgi, C. On the structure of nerve cells. 1898. *Journal of microscopy* 155, 3–7 (1989).
94. Golgi, C. On the structure of the nerve cells of the spinal ganglia. 1898. *Journal of microscopy* 155, 9–14 (1989).
95. Farquhar, M. G. & Rinehart, J. F. Electron microscopic studies of the anterior pituitary gland of castrate rats. *Endocrinology* 54, 516–541 (1954).
96. Dalton, A. J. & Felix, M. D. A comparative study of the Golgi complex. *J Biophys Biochem Cytol* 2, 79–84 (1956).
97. Novikoff, A. B., Goldfischer, S. & Essner, E. The importance of fixation in a cytochemical method for the Golgi apparatus. *J. Histochem. Cytochem.* 9, 459–460 (1961).
98. Rambourg, A., Clermont, Y. & Marraud, A. Three-dimensional structure of the osmium-impregnated Golgi apparatus as seen in the high voltage electron microscope. *Am. J. Anat.* 140, 27–45 (1974).
99. Rambourg, A. & Clermont, Y. Three-dimensional electron microscopy: structure of the Golgi apparatus. *Eur. J. Cell Biol.* 51, 189–200 (1990).

100. Ladinsky, M. S., Mastronarde, D. N., McIntosh, J. R., Howell, K. E. & Staehelin, L. A. Golgi structure in three dimensions: functional insights from the normal rat kidney cell. *J. Cell Biol.* 144, 1135–1149 (1999).
101. Koga, D., Ushiki, T. & Watanabe, T. Novel scanning electron microscopy methods for analyzing the 3D structure of the Golgi apparatus. *Anat Sci Int* 92, 37–49 (2017).
102. Rambourg, A. & Clermont, Y. in *The Golgi Apparatus* 37–61 (Birkhäuser Basel, 1997). doi:10.1007/978-3-0348-8876-9_2
103. Mellman, I. & Simons, K. The Golgi complex: in vitro veritas? *Cell* 68, 829–840 (1992).
104. Weidman, P. J. Anterograde transport through the Golgi complex: do Golgi tubules hold the key? *Trends Cell Biol.* 5, 302–305 (1995).
105. Colanzi, A. et al. Role of NAD⁺ and ADP-ribosylation in the maintenance of the Golgi structure. *J. Cell Biol.* 139, 1109–1118 (1997).
106. Mironov, A. A., Weidman, P. & Luini, A. Variations on the intracellular transport theme: maturing cisternae and trafficking tubules. *J. Cell Biol.* 138, 481–484 (1997).
107. Marsh, B. J., Volkmann, N., McIntosh, J. R. & Howell, K. E. Direct continuities between cisternae at different levels of the Golgi complex in glucose-stimulated mouse islet beta cells. *Proc. Natl. Acad. Sci. U.S.A.* 101, 5565–5570 (2004).
108. Trucco, A. et al. Secretory traffic triggers the formation of tubular continuities across Golgi sub-compartments. *Nat. Cell Biol.* 6, 1071–1081 (2004).
109. Rambourg, A., Clermont, Y. & Hermo, L. Three-dimensional architecture of the golgi apparatus in Sertoli cells of the rat. *Am. J. Anat.* 154, 455–476 (1979).
110. Farquhar, M. Progress in Unraveling Pathways of Golgi Traffic. *Annual Review of Cell and Developmental Biology* 1, 447–488 (1985).
111. Dunphy, W. G. & Rothman, J. E. Compartmental organization of the Golgi stack. *Cell* 42, 13–21 (1985).
112. Day, K. J., Staehelin, L. A. & Glick, B. S. A three-stage model of Golgi structure and function. *Histochem. Cell Biol.* 140, 239–249 (2013).
113. Martínez-Alonso, E., Tomás, M. & Martínez-Menárguez, J. A. Morpho-functional architecture of the Golgi complex of neuroendocrine cells. *Front Endocrinol (Lausanne)* 4, 41 (2013).
114. Munro, S. The golgin coiled-coil proteins of the Golgi apparatus. *Cold Spring Harb Perspect Biol* 3, a005256–a005256 (2011).
115. Xiang, Y. & Wang, Y. New components of the Golgi matrix. *Cell Tissue Res.* 344, 365–379 (2011).

References

116. Witkos, T. M. & Lowe, M. The Golgin Family of Coiled-Coil Tethering Proteins. *Front Cell Dev Biol* 3, 86 (2015).
117. Rivero, S., Cardenas, J., Bornens, M. & Rios, R. M. Microtubule nucleation at the cis-side of the Golgi apparatus requires AKAP450 and GM130. *EMBO J.* 28, 1016–1028 (2009).
118. Efimov, A. et al. Asymmetric CLASP-dependent nucleation of noncentrosomal microtubules at the trans-Golgi network. *Dev. Cell* 12, 917–930 (2007).
119. Kodani, A. & Sütterlin, C. A new function for an old organelle: microtubule nucleation at the Golgi apparatus. *EMBO J.* 28, 995–996 (2009).
120. Baschieri, F. et al. Spatial control of Cdc42 signalling by a GM130-RasGRF complex regulates polarity and tumorigenesis. *Nat Commun* 5, 4839 (2014).
121. Barr, F. A., Puype, M., Vandekerckhove, J. & Warren, G. GRASP65, a protein involved in the stacking of Golgi cisternae. *Cell* 91, 253–262 (1997).
122. Shorter, J. et al. GRASP55, a second mammalian GRASP protein involved in the stacking of Golgi cisternae in a cell-free system. *EMBO J.* 18, 4949–4960 (1999).
123. Yoshimura, S. I. et al. Direct targeting of cis-Golgi matrix proteins to the Golgi apparatus. *J. Cell. Sci.* 114, 4105–4115 (2001).
124. Zhang, X. & Wang, Y. GRASPs in Golgi Structure and Function. *Front Cell Dev Biol* 3, 84 (2015).
125. Preisinger, C. et al. Plk1 docking to GRASP65 phosphorylated by Cdk1 suggests a mechanism for Golgi checkpoint signalling. *EMBO J.* 24, 753–765 (2005).
126. Wang, Y., Seemann, J., Pypaert, M., Shorter, J. & Warren, G. A direct role for GRASP65 as a mitotically regulated Golgi stacking factor. *EMBO J.* 22, 3279–3290 (2003).
127. Rabouille, C. et al. Mapping the distribution of Golgi enzymes involved in the construction of complex oligosaccharides. *J. Cell. Sci.* 108 (Pt 4), 1617–1627 (1995).
128. Grasse, P. P. Ultrastructure, polarity and reproduction of Golgi apparatus. *C. R. Hebd. Seances Acad. Sci.* 245, 1278–1281 (1957).
129. Morré, D. J. & Ovtracht, L. Dynamics of the Golgi apparatus: membrane differentiation and membrane flow. *Int Rev Cytol Suppl* 61–188 (1977).
130. Glick, B. S. & Luini, A. Models for Golgi traffic: a critical assessment. *Cold Spring Harb Perspect Biol* 3, a005215–a005215 (2011).
131. Emr, S. et al. Journeys through the Golgi--taking stock in a new era. *The Journal of cell biology* 187, 449–453 (2009).

132. Potelle, S., Klein, A. & Foulquier, F. Golgi post-translational modifications and associated diseases. *J. Inherit. Metab. Dis.* 38, 741–751 (2015).
133. Klein, A. & Roussel, P. O-acetylation of sialic acids. *Biochimie* 80, 49–57 (1998).
134. Mandal, C., Mandal, C., Chandra, S., Schauer, R. & Mandal, C. Regulation of O-acetylation of sialic acids by sialate-O-acetyltransferase and sialate-O-acetyltransferase activities in childhood acute lymphoblastic leukemia. *Glycobiology* 22, 70–83 (2012).
135. Kehoe, J. W. & Bertozzi, C. R. Tyrosine sulfation: a modulator of extracellular protein-protein interactions. *Chem. Biol.* 7, R57–61 (2000).
136. Yang, Y.-S. et al. Tyrosine sulfation as a protein post-translational modification. *Molecules* 20, 2138–2164 (2015).
137. Wu, C. C. et al. Organellar proteomics reveals Golgi arginine dimethylation. *Mol. Biol. Cell* 15, 2907–2919 (2004).
138. Salaun, C., Greaves, J. & Chamberlain, L. H. The intracellular dynamic of protein palmitoylation. *J. Cell Biol.* 191, 1229–1238 (2010).
139. Vey, M., Schäfer, W., Berghöfer, S., Klenk, H. D. & Garten, W. Maturation of the trans-Golgi network protease furin: compartmentalization of propeptide removal, substrate cleavage, and COOH-terminal truncation. *J. Cell Biol.* 127, 1829–1842 (1994).
140. Caffaro, C. E., Hirschberg, C. B. & Berninsone, P. M. Independent and simultaneous translocation of two substrates by a nucleotide sugar transporter. *Proc. Natl. Acad. Sci. U.S.A.* 103, 16176–16181 (2006).
141. Gawlitzek, M., Ryll, T., Lofgren, J. & Sliwkowski, M. B. Ammonium alters N-glycan structures of recombinant TNFR-IgG: degradative versus biosynthetic mechanisms. *Biotechnol. Bioeng.* 68, 637–646 (2000).
142. Humphrey, S. J., James, D. E. & Mann, M. Protein Phosphorylation: A Major Switch Mechanism for Metabolic Regulation. *Trends Endocrinol. Metab.* 26, 676–687 (2015).
143. Whitmarsh, A. J. & Davis, R. J. Regulation of transcription factor function by phosphorylation. *Cell. Mol. Life Sci.* 57, 1172–1183 (2000).
144. Suryadinata, R., Sadowski, M. & Sarcevic, B. Control of cell cycle progression by phosphorylation of cyclin-dependent kinase (CDK) substrates. *Biosci. Rep.* 30, 243–255 (2010).
145. Arber, S. et al. Regulation of actin dynamics through phosphorylation of cofilin by LIM-kinase. *Nature* 393, 805–809 (1998).

References

146. Tamura, Y., Simizu, S. & Osada, H. The phosphorylation status and anti-apoptotic activity of Bcl-2 are regulated by ERK and protein phosphatase 2A on the mitochondria. *FEBS Lett.* 569, 249–255 (2004).
147. Manning, G., Whyte, D. B., Martinez, R., Hunter, T. & Sudarsanam, S. The protein kinase complement of the human genome. *Science* 298, 1912–1934 (2002).
148. Hammarsten, O. Zur Frage, ob das Casein ein einheitlicher Stoff sei. *Zeitschrift für Physiologische Chemie* (1883).
149. Ishikawa, H. O., Takeuchi, H., Haltiwanger, R. S. & Irvine, K. D. Four-jointed Is a Golgi Kinase That Phosphorylates a Subset of Cadherin Domains. *Science* 321, 401–404 (2008).
150. Tagliabracci, V. S. et al. A Single Kinase Generates the Majority of the Secreted Phosphoproteome. *Cell* 161, 1619–1632 (2015).
151. Sreelatha, A., Kinch, L. N. & Tagliabracci, V. S. The secretory pathway kinases. *Biochimica et Biophysica Acta (BBA) - Proteins and Proteomics* 1854, 1687–1693 (2015).
152. Tagliabracci, V. S. et al. Secreted Kinase Phosphorylates Extracellular Proteins That Regulate Biomineralization. *Science* 336, 1150–1153 (2012).
153. Wang, X. et al. Expression of FAM20C in the osteogenesis and odontogenesis of mouse. *J. Histochem. Cytochem.* 58, 957–967 (2010).
154. Hao, J., Narayanan, K., Muni, T., Ramachandran, A. & George, A. Dentin matrix protein 4, a novel secretory calcium-binding protein that modulates odontoblast differentiation. *J. Biol. Chem.* 282, 15357–15365 (2007).
155. Brunati, A. M., Marin, O., Bisinella, A., Salviati, A. & Pinna, L. A. Novel consensus sequence for the Golgi apparatus casein kinase, revealed using proline-rich protein-1 (PRP1)-derived peptide substrates. *Biochemical Journal* 351 Pt 3, 765–768 (2000).
156. Salvi, M., Cesaro, L., Tibaldi, E. & Pinna, L. A. Motif analysis of phosphosites discloses a potential prominent role of the Golgi casein kinase (GCK) in the generation of human plasma phospho-proteome. *J. Proteome Res.* 9, 3335–3338 (2010).
157. Bahl, J. M. C., Jensen, S. S., Larsen, M. R. & Heegaard, N. H. H. Characterization of the human cerebrospinal fluid phosphoproteome by titanium dioxide affinity chromatography and mass spectrometry. *Anal. Chem.* 80, 6308–6316 (2008).
158. Zhou, W. et al. An initial characterization of the serum phosphoproteome. *J. Proteome Res.* 8, 5523–5531 (2009).

159. Tagliabracci, V. S. et al. Dynamic regulation of FGF23 by Fam20C phosphorylation, GalNAc-T3 glycosylation, and furin proteolysis. *Proc. Natl. Acad. Sci. U.S.A.* 111, 5520–5525 (2014).
160. Lasa, M., Chang, P. L., Prince, C. W. & Pinna, L. A. Phosphorylation of osteopontin by Golgi apparatus casein kinase. *Biochem. Biophys. Res. Commun.* 240, 602–605 (1997).
161. Raine, J., Winter, R. M., Davey, A. & Tucker, S. M. Unknown syndrome: microcephaly, hypoplastic nose, exophthalmos, gum hyperplasia, cleft palate, low set ears, and osteosclerosis. *J. Med. Genet.* 26, 786–788 (1989).
162. Xiao, J., Tagliabracci, V. S., Wen, J., Kim, S.-A. & Dixon, J. E. Crystal structure of the Golgi casein kinase. *Proc. Natl. Acad. Sci. U.S.A.* 110, 10574–10579 (2013).
163. Ohyama, Y. et al. FAM20A binds to and regulates FAM20C localization. *Scientific Reports* 6, 27784 (2016).
164. O'Sullivan, J. et al. Whole-Exome sequencing identifies FAM20A mutations as a cause of amelogenesis imperfecta and gingival hyperplasia syndrome. *Am. J. Hum. Genet.* 88, 616–620 (2011).
165. Cui, J. et al. A secretory kinase complex regulates extracellular protein phosphorylation. *Elife* 4, e06120 (2015).
166. Kinoshita, M., Era, T., Jakt, L. M. & Nishikawa, S.-I. The novel protein kinase Vlk is essential for stromal function of mesenchymal cells. *Development* 136, 2069–2079 (2009).
167. Gonçalves, L. et al. Identification and functional analysis of novel genes expressed in the Anterior Visceral Endoderm. *Int. J. Dev. Biol.* 55, 281–295 (2011).
168. Dudkiewicz, M., Lenart, A. & Pawłowski, K. A novel predicted calcium-regulated kinase family implicated in neurological disorders. *PLoS ONE* 8, e66427 (2013).
169. Bordoli, M. R. et al. A secreted tyrosine kinase acts in the extracellular environment. *Cell* 158, 1033–1044 (2014).
170. Maddala, R., Skiba, N. P. & Rao, P. V. Vertebrate Lonesome Kinase Regulated Extracellular Matrix Protein Phosphorylation, Cell Shape and Adhesion in Trabecular Meshwork Cells. *J. Cell. Physiol.* (2016). doi:10.1002/jcp.25582
171. Imuta, Y., Nishioka, N., Kiyonari, H. & Sasaki, H. Short limbs, cleft palate, and delayed formation of flat proliferative chondrocytes in mice with targeted disruption of a putative protein kinase gene, *Pkdcc* (AW548124). *Developmental Dynamics* 238, spcone–spcone (2009).

References

172. Probst, S., Zeller, R. & Zuniga, A. The hedgehog target Vlk genetically interacts with Gli3 to regulate chondrocyte differentiation during mouse long bone development. *Differentiation* 85, 121–130 (2013).
173. Meldolesi, J. & Pozzan, T. The endoplasmic reticulum Ca²⁺ store: a view from the lumen. *Trends in Biochemical Sciences* 23, 10–14 (1998).
174. Bronner, F. Extracellular and intracellular regulation of calcium homeostasis. *ScientificWorldJournal* 1, 919–925 (2001).
175. Felbel, J., Trockur, B., Ecker, T., Landgraf, W. & Hofmann, F. Regulation of cytosolic calcium by cAMP and cGMP in freshly isolated smooth muscle cells from bovine trachea. *J. Biol. Chem.* 263, 16764–16771 (1988).
176. Raychaudhury, B., Gupta, S., Banerjee, S. & Datta, S. C. Peroxisome is a reservoir of intracellular calcium. *Biochim. Biophys. Acta* 1760, 989–992 (2006).
177. Pizzo, P., Lissandron, V. & Pozzan, T. The trans-golgi compartment: A new distinct intracellular Ca store. *Commun Integr Biol* 3, 462–464 (2010).
178. Pizzo, P., Lissandron, V., Capitanio, P. & Pozzan, T. Ca²⁺ signalling in the Golgi apparatus. *Cell Calcium* 50, 184–192 (2011).
179. Montero, M. et al. Monitoring dynamic changes in free Ca²⁺ concentration in the endoplasmic reticulum of intact cells. *EMBO J.* 14, 5467–5475 (1995).
180. Montero, M. et al. Ca²⁺ homeostasis in the endoplasmic reticulum: coexistence of high and low [Ca²⁺] subcompartments in intact HeLa cells. *J. Cell Biol.* 139, 601–611 (1997).
181. Lissandron, V., Podini, P., Pizzo, P. & Pozzan, T. Unique characteristics of Ca²⁺ homeostasis of the trans-Golgi compartment. *Proc. Natl. Acad. Sci. U.S.A.* 107, 9198–9203 (2010).
182. Mitchell, K. J. et al. Dense core secretory vesicles revealed as a dynamic Ca²⁺ store in neuroendocrine cells with a vesicle-associated membrane protein aequorin chimera. *J. Cell Biol.* 155, 41–51 (2001).
183. Chandra, S., Kable, E. P., Morrison, G. H. & Webb, W. W. Calcium sequestration in the Golgi apparatus of cultured mammalian cells revealed by laser scanning confocal microscopy and ion microscopy. *J. Cell. Sci.* 100 (Pt 4), 747–752 (1991).
184. Pinton, P., Pozzan, T. & Rizzuto, R. The Golgi apparatus is an inositol 1,4,5-trisphosphate-sensitive Ca²⁺ store, with functional properties distinct from those of the endoplasmic reticulum. *EMBO J.* 17, 5298–5308 (1998).

185. Lin, P., Yao, Y., Hofmeister, R., Tsien, R. Y. & Farquhar, M. G. Overexpression of CALNUC (nucleobindin) increases agonist and thapsigargin releasable Ca²⁺ storage in the Golgi. *J. Cell Biol.* 145, 279–289 (1999).
186. Surroca, A. & Wolff, D. Inositol 1,4,5-trisphosphate but not ryanodine-receptor agonists induces calcium release from rat liver Golgi apparatus membrane vesicles. *J. Membr. Biol.* 177, 243–249 (2000).
187. Sorin, A., Rosas, G. & Rao, R. PMR1, a Ca²⁺-ATPase in yeast Golgi, has properties distinct from sarco/endoplasmic reticulum and plasma membrane calcium pumps. *J. Biol. Chem.* 272, 9895–9901 (1997).
188. Dode, L. et al. Functional comparison between secretory pathway Ca²⁺/Mn²⁺-ATPase (SPCA) 1 and sarcoplasmic reticulum Ca²⁺-ATPase (SERCA) 1 isoforms by steady-state and transient kinetic analyses. *J. Biol. Chem.* 280, 39124–39134 (2005).
189. Dode, L. et al. Dissection of the Functional Differences between Human Secretory Pathway Ca²⁺/Mn²⁺-ATPase (SPCA) 1 and 2 Isoenzymes by Steady-state and Transient Kinetic Analyses. *J. Biol. Chem.* 281, 3182–3189 (2006).
190. Brini, M., Cali, T., Ottolini, D. & Carafoli, E. Calcium pumps: why so many? *Compr Physiol* 2, 1045–1060 (2012).
191. Brini, M. & Carafoli, E. Calcium pumps in health and disease. *Physiol. Rev.* 89, 1341–1378 (2009).
192. Toyoshima, C., Nakasako, M., Nomura, H. & Ogawa, H. Crystal structure of the calcium pump of sarcoplasmic reticulum at 2.6 Å resolution. *Nature* 405, 647–655 (2000).
193. Clarke, D. M., Loo, T. W., Inesi, G. & MacLennan, D. H. Location of high affinity Ca²⁺-binding sites within the predicted transmembrane domain of the sarcoplasmic reticulum Ca²⁺-ATPase. *Nature* 339, 476–478 (1989).
194. Andersen, J. P. & Vilsen, B. Structure-function relationships of cation translocation by Ca(2+)- and Na⁺, K(+)-ATPases studied by site-directed mutagenesis. *FEBS Lett.* 359, 101–106 (1995).
195. Vanoevelen, J. et al. The secretory pathway Ca²⁺/Mn²⁺-ATPase 2 is a Golgi-localized pump with high affinity for Ca²⁺ ions. *J. Biol. Chem.* 280, 22800–22808 (2005).
196. Caplan, M. J. et al. Dependence on pH of polarized sorting of secreted proteins. *Nature* 329, 632–635 (1987).
197. Mellman, I., Fuchs, R. & Helenius, A. Acidification of the Endocytic and Exocytic Pathways. *Annual Review of Biochemistry* 55, 663–700 (1986).

References

198. Sudbrak, R. et al. Hailey-Hailey disease is caused by mutations in ATP2C1 encoding a novel Ca(2+) pump. *Hum. Mol. Genet.* 9, 1131–1140 (2000).
199. Antebi, A. & Fink, G. R. The yeast Ca(2+)-ATPase homologue, PMR1, is required for normal Golgi function and localizes in a novel Golgi-like distribution. *Mol. Biol. Cell* 3, 633–654 (1992).
200. Van Baelen, K., Vanoevelen, J., Missiaen, L., Raeymaekers, L. & Wuytack, F. The Golgi PMR1 P-type ATPase of *Caenorhabditis elegans*. Identification of the gene and demonstration of calcium and manganese transport. *J. Biol. Chem.* 276, 10683–10691 (2001).
201. Southall, T. D. et al. Novel subcellular locations and functions for secretory pathway Ca²⁺/Mn²⁺-ATPases. *Physiol. Genomics* 26, 35–45 (2006).
202. Xiang, M., Mohamalawari, D. & Rao, R. A novel isoform of the secretory pathway Ca²⁺,Mn(2+)-ATPase, hSPCA2, has unusual properties and is expressed in the brain. *J. Biol. Chem.* 280, 11608–11614 (2005).
203. Dmitriev, R. I. et al. [Tissue specificity of alternative splicing products of mouse mRNA encoding new protein hampin homologous to the *Drosophila* MSL-1 protein]. *Bioorg. Khim.* 31, 363–371 (2005).
204. Hu, Z. et al. Mutations in ATP2C1, encoding a calcium pump, cause Hailey-Hailey disease. *Nat. Genet.* 24, 61–65 (2000).
205. Callewaert, G. et al. Similar Ca²⁺-signaling properties in keratinocytes and in COS-1 cells overexpressing the secretory-pathway Ca²⁺-ATPase SPCA1. *Cell Calcium* 34, 157–162 (2003).
206. Palma, A. S., Morais, V. A., Coelho, A. V. & Costa, J. Effect of the manganese ion on human alpha3/4 fucosyltransferase III activity. *Biometals* 17, 35–43 (2004).
207. Kaushal, G. P. & Elbein, A. D. Purification and properties of beta-mannosyltransferase that synthesizes Man-beta-GlcNAc-GlcNAc-pyrophosphoryldolichol. *Arch. Biochem. Biophys.* 250, 38–47 (1986).
208. Fairclough, R. J. et al. Effect of Hailey-Hailey Disease mutations on the function of a new variant of human secretory pathway Ca²⁺/Mn²⁺-ATPase (hSPCA1). *J. Biol. Chem.* 278, 24721–24730 (2003).
209. Kaufman, R. J., Swaroop, M. & Murtha-Riel, P. Depletion of manganese within the secretory pathway inhibits O-linked glycosylation in mammalian cells. *Biochemistry* 33, 9813–9819 (1994).

210. Dürr, G. et al. The medial-Golgi ion pump Pmr1 supplies the yeast secretory pathway with Ca²⁺ and Mn²⁺ required for glycosylation, sorting, and endoplasmic reticulum-associated protein degradation. *Mol. Biol. Cell* 9, 1149–1162 (1998).
211. Hailey, H. Familial benign chronic pemphigus. *Archives of Dermatology* 39, 679 (1939).
212. Hailey, H. Familial benign chronic pemphigus; report thirteen years after first observation of a new entity. *South. Med. J.* 46, 763–765 (1953).
213. Burge, S. M. Hailey-Hailey disease: the clinical features, response to treatment and prognosis. *Br. J. Dermatol.* 126, 275–282 (1992).
214. Ebashi, F. & Ebashi, S. Removal of calcium and relaxation in actomyosin systems. *Nature* 194, 378–379 (1962).
215. Makinose, M. & Hasselbach, W. Die Bedingungen der Calciumaufnahme durch die Erschlaffungsgrana des Muskels. *Pflügers Archiv für die Gesamte Physiologie des Menschen und der Tiere* 274, 9–9 (1961).
216. Putney, J. W., Jr., DeWitt, L. M., Hoyle, P. C. & McKinney, J. S. Calcium, prostaglandins and the phosphatidylinositol effect in exocrine gland cells. *Cell Calcium* 2, 561–571 (1981).
217. Berridge, M. J. & Fain, J. N. Inhibition of phosphatidylinositol synthesis and the inactivation of calcium entry after prolonged exposure of the blowfly salivary gland to 5-hydroxytryptamine. *Biochemical Journal* 178, 59–69 (1979).
218. Berridge, M. J. & Irvine, R. F. Inositol trisphosphate, a novel second messenger in cellular signal transduction. *Nature* 312, 315–321 (1984).
219. Foskett, J. K., White, C., Cheung, K.-H. & Mak, D.-O. D. Inositol trisphosphate receptor Ca²⁺ release channels. *Physiol. Rev.* 87, 593–658 (2007).
220. Taylor, C. W. & Tovey, S. C. IP(3) receptors: toward understanding their activation. *Cold Spring Harb Perspect Biol* 2, a004010–a004010 (2010).
221. Dolman, N. J. & Tepikin, A. V. Calcium gradients and the Golgi. *Cell Calcium* 40, 505–512 (2006).
222. Cifuentes, F. et al. A ryanodine fluorescent derivative reveals the presence of high-affinity ryanodine binding sites in the Golgi complex of rat sympathetic neurons, with possible functional roles in intracellular Ca²⁺ signaling. *Cellular Signalling* 13, 353–362 (2001).
223. Aulestia, F. J., Alonso, M. T. & García-Sancho, J. Differential calcium handling by the cis and trans regions of the Golgi apparatus. *Biochem. J.* 466, 455–465 (2015).

References

224. Weiss, T. S. et al. α 5 binding to calnuc on Golgi membranes in living cells monitored by fluorescence resonance energy transfer of green fluorescent protein fusion proteins. *Proc. Natl. Acad. Sci. U.S.A.* 98, 14961–14966 (2001).
225. Nesselhut, J. et al. Golgi retention of human protein NEFA is mediated by its N-terminal Leu/Ile-rich region. *FEBS Lett.* 509, 469–475 (2001).
226. Scherer, P. E. et al. Cab45, a novel (Ca^{2+}) -binding protein localized to the Golgi lumen. *J. Cell Biol.* 133, 257–268 (1996).
227. Vorum, H., Hager, H., Christensen, B. M., Nielsen, S. & Honoré, B. Human Calumenin Localizes to the Secretory Pathway and Is Secreted to the Medium. *Experimental Cell Research* 248, 473–481 (1999).
228. Karabinos, A. et al. The divergent domains of the NEFA and nucleobindin proteins are derived from an EF-hand ancestor. *Mol. Biol. Evol.* 13, 990–998 (1996).
229. Kretsinger, R. H. & Nockolds, C. E. Carp muscle calcium-binding protein. II. Structure determination and general description. *J. Biol. Chem.* 248, 3313–3326 (1973).
230. de Alba, E. & Tjandra, N. Structural studies on the Ca^{2+} -binding domain of human nucleobindin (calnuc). *Biochemistry* 43, 10039–10049 (2004).
231. Miura, K., Kurosawa, Y. & Kanai, Y. Calcium-binding activity of nucleobindin mediated by an EF hand moiety. *Biochem. Biophys. Res. Commun.* 199, 1388–1393 (1994).
232. Kroll, K. A. et al. Heterologous overexpression of human NEFA and studies on the two EF-hand calcium-binding sites. *Biochem. Biophys. Res. Commun.* 260, 1–8 (1999).
233. Lin, P. et al. The mammalian calcium-binding protein, nucleobindin (CALNUC), is a Golgi resident protein. *J. Cell Biol.* 141, 1515–1527 (1998).
234. Lin, P., Fischer, T., Weiss, T. & Farquhar, M. G. Calnuc, an EF-hand Ca^{2+} binding protein, specifically interacts with the C-terminal α 5-helix of G(α)i3. *Proc. Natl. Acad. Sci. U.S.A.* 97, 674–679 (2000).
235. Kanuru, M., Samuel, J. J., Balivada, L. M. & Aradhyam, G. K. Ion-binding properties of Calnuc, Ca^{2+} versus Mg^{2+} --Calnuc adopts additional and unusual Ca^{2+} -binding sites upon interaction with G-protein. *FEBS J.* 276, 2529–2546 (2009).
236. Honoré, B. The rapidly expanding CREC protein family: members, localization, function, and role in disease. *Bioessays* 31, 262–277 (2009).

237. Honoré, B. & Vorum, H. The CREC family, a novel family of multiple EF-hand, low-affinity Ca(2+)-binding proteins localised to the secretory pathway of mammalian cells. *FEBS Lett.* 466, 11–18 (2000).
238. Kobayashi, M. et al. DNA supercoiling factor localizes to puffs on polytene chromosomes in *Drosophila melanogaster*. *Mol. Cell. Biol.* 18, 6737–6744 (1998).
239. Kobayashi, M. & Hirose, S. Functional dissection of DNA supercoiling factor: EF-hand domains and C-terminal HDEF motif are essential for its activity. *Genes Cells* 4, 33–40 (1999).
240. La Greca, N., Hibbs, A. R., Riffkin, C., Foley, M. & Tilley, L. Identification of an endoplasmic reticulum-resident calcium-binding protein with multiple EF-hand motifs in asexual stages of *Plasmodium falciparum*. *Mol. Biochem. Parasitol.* 89, 283–293 (1997).
241. Jung, D. H. & Kim, D. H. Characterization of isoforms and genomic organization of mouse calumenin. *Gene* 327, 185–194 (2004).
242. Jung, D. H., Mo, S. H. & Kim, D. H. Calumenin, a multiple EF-hands Ca²⁺-binding protein, interacts with ryanodine receptor-1 in rabbit skeletal sarcoplasmic reticulum. *Biochem. Biophys. Res. Commun.* 343, 34–42 (2006).
243. Philippe, R. et al. Calumenin contributes to ER-Ca(2+) homeostasis in bronchial epithelial cells expressing WT and F508del mutated CFTR and to F508del-CFTR retention. *Cell Calcium* 62, 47–59 (2017).
244. Sahoo, S. K. et al. Characterization of calumenin-SERCA2 interaction in mouse cardiac sarcoplasmic reticulum. *J. Biol. Chem.* 284, 31109–31121 (2009).
245. Yabe, D., Nakamura, T., Kanazawa, N., Tashiro, K. & Honjo, T. Calumenin, a Ca²⁺-binding protein retained in the endoplasmic reticulum with a novel carboxyl-terminal sequence, HDEF. *J. Biol. Chem.* 272, 18232–18239 (1997).
246. Sahoo, S. K. & Kim, D. H. Calumenin interacts with SERCA2 in rat cardiac sarcoplasmic reticulum. *Mol. Cells* 26, 265–269 (2008).
247. Griffiths, G. et al. The dynamic nature of the Golgi complex. *J. Cell Biol.* 108, 277–297 (1989).
248. Ladinsky, M. S., Wu, C. C., McIntosh, S., McIntosh, J. R. & Howell, K. E. Structure of the Golgi and distribution of reporter molecules at 20 degrees C reveals the complexity of the exit compartments. *Mol. Biol. Cell* 13, 2810–2825 (2002).
249. De Matteis, M. A. & Luini, A. Exiting the Golgi complex. *Nat. Rev. Mol. Cell Biol.* 9, 273–284 (2008).

References

250. Surma, M. A., Klose, C. & Simons, K. Lipid-dependent protein sorting at the trans-Golgi network. *Biochim. Biophys. Acta* 1821, 1059–1067 (2012).
251. Lipardi, C., Nitsch, L. & Zurzolo, C. Detergent-insoluble GPI-anchored proteins are apically sorted in fischer rat thyroid cells, but interference with cholesterol or sphingolipids differentially affects detergent insolubility and apical sorting. *Mol. Biol. Cell* 11, 531–542 (2000).
252. Hansen, G. H., Niels-Christiansen, L. L., Thorsen, E., Immerdal, L. & Danielsen, E. M. Cholesterol depletion of enterocytes. Effect on the Golgi complex and apical membrane trafficking. *J. Biol. Chem.* 275, 5136–5142 (2000).
253. Keller, P. & Simons, K. Post-Golgi biosynthetic trafficking. *J. Cell. Sci.* 110 (Pt 24), 3001–3009 (1997).
254. van Meer, G. & Simons, K. Lipid polarity and sorting in epithelial cells. *Journal of Cellular Biochemistry* 36, 51–58 (1988).
255. Simons, K. & Ikonen, E. Functional rafts in cell membranes. *Nature* 387, 569–572 (1997).
256. Simons, K. & Sampaio, J. L. Membrane organization and lipid rafts. *Cold Spring Harb Perspect Biol* 3, a004697–a004697 (2011).
257. Lundbæk, J. A., Andersen, O. S., Werge, T. & Nielsen, C. Cholesterol-Induced Protein Sorting: An Analysis of Energetic Feasibility. *Biophysical Journal* 84, 2080–2089 (2003).
258. Paladino, S. et al. Protein oligomerization modulates raft partitioning and apical sorting of GPI-anchored proteins. *J. Cell Biol.* 167, 699–709 (2004).
259. Lisanti, M. P., Caras, I. W., Davitz, M. A. & Rodriguez-Boulant, E. A glycosphospholipid membrane anchor acts as an apical targeting signal in polarized epithelial cells. *J. Cell Biol.* 109, 2145–2156 (1989).
260. Malchiodi-Albedi, F., Paradisi, S., Matteucci, A., Frank, C. & Diociaiuti, M. Amyloid oligomer neurotoxicity, calcium dysregulation, and lipid rafts. *Int J Alzheimers Dis* 2011, 906964–17 (2011).
261. Muniz, M. & Zurzolo, C. Sorting of GPI-anchored proteins from yeast to mammals - common pathways at different sites? *J. Cell. Sci.* 127, 2793–2801 (2014).
262. Paladino, S., Lebreton, S. & Zurzolo, C. Trafficking and Membrane Organization of GPI-Anchored Proteins in Health and Diseases. *Curr Top Membr* 75, 269–303 (2015).

263. Brown, D. A. & Rose, J. K. Sorting of GPI-anchored proteins to glycolipid-enriched membrane subdomains during transport to the apical cell surface. *Cell* 68, 533–544 (1992).
264. Wickner, W. T. & Lodish, H. F. Multiple mechanisms of protein insertion into and across membranes. *Science* 230, 400–407 (1985).
265. Rodriguez-Boulan, E., Kreitzer, G. & Müsch, A. Organization of vesicular trafficking in epithelia. *Nat. Rev. Mol. Cell Biol.* 6, 233–247 (2005).
266. Fotin, A. et al. Molecular model for a complete clathrin lattice from electron cryomicroscopy. *Nature* 432, 573–579 (2004).
267. Musacchio, A. et al. Functional organization of clathrin in coats: combining electron cryomicroscopy and X-ray crystallography. *Mol. Cell* 3, 761–770 (1999).
268. Anitei, M. & Hoflack, B. Exit from the trans-Golgi network: from molecules to mechanisms. *Curr. Opin. Cell Biol.* 23, 443–451 (2011).
269. D'Souza-Schorey, C. & Chavrier, P. ARF proteins: roles in membrane traffic and beyond. *Nat. Rev. Mol. Cell Biol.* 7, 347–358 (2006).
270. Luna, A. et al. Regulation of protein transport from the Golgi complex to the endoplasmic reticulum by CDC42 and N-WASP. *Mol. Biol. Cell* 13, 866–879 (2002).
271. Stamnes, M. A. & Rothman, J. E. The binding of AP-1 clathrin adaptor particles to Golgi membranes requires ADP-ribosylation factor, a small GTP-binding protein. *Cell* 73, 999–1005 (1993).
272. Bonifacino, J. S. The GGA proteins: adaptors on the move. *Nat. Rev. Mol. Cell Biol.* 5, 23–32 (2004).
273. Traub, L. M., Ostrom, J. A. & Kornfeld, S. Biochemical dissection of AP-1 recruitment onto Golgi membranes. *J. Cell Biol.* 123, 561–573 (1993).
274. Donaldson, J. G. & Jackson, C. L. ARF family G proteins and their regulators: roles in membrane transport, development and disease. *Nat. Rev. Mol. Cell Biol.* 12, 362–375 (2011).
275. Fucini, R. V. et al. Activated ADP-ribosylation factor assembles distinct pools of actin on golgi membranes. *J. Biol. Chem.* 275, 18824–18829 (2000).
276. Hoya, M. et al. Traffic Through the Trans-Golgi Network and the Endosomal System Requires Collaboration Between Exomer and Clathrin Adaptors in Fission Yeast. *Genetics* 205, 673–690 (2017).
277. Nakayama, K. & Wakatsuki, S. The structure and function of GGAs, the traffic controllers at the TGN sorting crossroads. *Cell Struct. Funct.* 28, 431–442 (2003).

References

278. Legendre-Guillemain, V., Wasiak, S., Hussain, N. K., Angers, A. & McPherson, P. S. ENTH/ANTH proteins and clathrin-mediated membrane budding. *J. Cell. Sci.* 117, 9–18 (2004).
279. Feliziani, C. et al. The giardial ENTH protein participates in lysosomal protein trafficking and endocytosis. *Biochim. Biophys. Acta* 1853, 646–659 (2015).
280. Newell-Litwa, K., Seong, E., Burmeister, M. & Faundez, V. Neuronal and non-neuronal functions of the AP-3 sorting machinery. *J. Cell. Sci.* 120, 531–541 (2007).
281. Doray, B., Lee, I., Knisely, J., Bu, G. & Kornfeld, S. The gamma/sigma1 and alpha/sigma2 hemicomplexes of clathrin adaptors AP-1 and AP-2 harbor the dileucine recognition site. *Mol. Biol. Cell* 18, 1887–1896 (2007).
282. Janvier, K. et al. Recognition of dileucine-based sorting signals from HIV-1 Nef and LIMP-II by the AP-1 gamma-sigma1 and AP-3 delta-sigma3 hemicomplexes. *J. Cell Biol.* 163, 1281–1290 (2003).
283. Mattera, R., Boehm, M., Chaudhuri, R., Prabhu, Y. & Bonifacino, J. S. Conservation and diversification of dileucine signal recognition by adaptor protein (AP) complex variants. *J. Biol. Chem.* 286, 2022–2030 (2011).
284. Ma, D. et al. Golgi export of the Kir2.1 channel is driven by a trafficking signal located within its tertiary structure. *Cell* 145, 1102–1115 (2011).
285. Ohno, H. et al. The medium subunits of adaptor complexes recognize distinct but overlapping sets of tyrosine-based sorting signals. *J. Biol. Chem.* 273, 25915–25921 (1998).
286. Rous, B. A. et al. Role of adaptor complex AP-3 in targeting wild-type and mutated CD63 to lysosomes. *Mol. Biol. Cell* 13, 1071–1082 (2002).
287. Ford, M. G. J. et al. Curvature of clathrin-coated pits driven by epsin. *Nature* 419, 361–366 (2002).
288. Owen, D. J., Collins, B. M. & Evans, P. R. Adaptors for clathrin coats: structure and function. *Annual Review of Cell and Developmental Biology* 20, 153–191 (2004).
289. Saint-Pol, A. et al. Clathrin adaptor epsinR is required for retrograde sorting on early endosomal membranes. *Dev. Cell* 6, 525–538 (2004).
290. Almeida, C. G. et al. Myosin 1b promotes the formation of post-Golgi carriers by regulating actin assembly and membrane remodelling at the trans-Golgi network. *Nat. Cell Biol.* 13, 779–789 (2011).
291. Delevoye, C. et al. AP-1 and KIF13A coordinate endosomal sorting and positioning during melanosome biogenesis. *J. Cell Biol.* 187, 247–264 (2009).

292. Taupenot, L., Harper, K. L. & O'Connor, D. T. The chromogranin-secretogranin family. *N. Engl. J. Med.* 348, 1134–1149 (2003).
293. Steiner, D. F. The proprotein convertases. *Curr Opin Chem Biol* 2, 31–39 (1998).
294. Borgonovo, B., Ouwendijk, J. & Solimena, M. Biogenesis of secretory granules. *Curr. Opin. Cell Biol.* 18, 365–370 (2006).
295. Rambourg, A., Clermont, Y. & Hermo, L. Formation of secretion granules in the Golgi apparatus of pancreatic acinar cells of the rat. *Am. J. Anat.* 183, 187–199 (1988).
296. Bendayan, M. Ultrastructural localization of insulin and C-peptide antigenic sites in rat pancreatic B cell obtained by applying the quantitative high-resolution protein A-gold approach. *Am. J. Anat.* 185, 205–216 (1989).
297. Delacour, D. et al. Apical sorting by galectin-3-dependent glycoprotein clustering. *Traffic* 8, 379–388 (2007).
298. Jamieson, J. D. & Palade, G. E. Synthesis, intracellular transport, and discharge of secretory proteins in stimulated pancreatic exocrine cells. *J. Cell Biol.* 50, 135–158 (1971).
299. Greene, L. J., Hirs, C. H. & Palade, G. E. On the protein composition of bovine pancreatic zymogen granules. *J. Biol. Chem.* 238, 2054–2070 (1963).
300. Tooze, S. A., Martens, G. J. & Huttner, W. B. Secretory granule biogenesis: rafting to the SNARE. *Trends Cell Biol.* 11, 116–122 (2001).
301. Kim, T., Gondré-Lewis, M. C., Arnaoutova, I. & Loh, Y. P. Dense-core secretory granule biogenesis. *Physiology (Bethesda)* 21, 124–133 (2006).
302. Tooze, S. A., Weiss, U. & Huttner, W. B. Requirement for GTP hydrolysis in the formation of secretory vesicles. *Nature* 347, 207–208 (1990).
303. Glombik, M. M. & Gerdes, H. H. Signal-mediated sorting of neuropeptides and prohormones: secretory granule biogenesis revisited. *Biochimie* 82, 315–326 (2000).
304. Kakhlon, O., Sakya, P., Larijani, B., Watson, R. & Tooze, S. A. GGA function is required for maturation of neuroendocrine secretory granules. *EMBO J.* 25, 1590–1602 (2006).
305. Kuliawat, R., Klumperman, J., Ludwig, T. & Arvan, P. Differential sorting of lysosomal enzymes out of the regulated secretory pathway in pancreatic beta-cells. *J. Cell Biol.* 137, 595–608 (1997).
306. Dittié, A. S., Thomas, L., Thomas, G. & Tooze, S. A. Interaction of furin in immature secretory granules from neuroendocrine cells with the AP-1 adaptor

References

- complex is modulated by casein kinase II phosphorylation. *EMBO J.* 16, 4859–4870 (1997).
307. Trajkovski, M. et al. Nuclear translocation of an ICA512 cytosolic fragment couples granule exocytosis and insulin expression in β -cells. *J. Cell Biol.* 167, 1063–1074 (2004).
308. Mziaut, H. et al. Synergy of glucose and growth hormone signalling in islet cells through ICA512 and STAT5. *Nat. Cell Biol.* 8, 435–445 (2006).
309. Kienzle, C. & Blume, von, J. Secretory cargo sorting at the trans-Golgi network. *Trends Cell Biol.* 24, 584–593 (2014).
310. Braulke, T. & Bonifacio, J. S. Sorting of lysosomal proteins. *Biochim. Biophys. Acta* 1793, 605–614 (2009).
311. Coutinho, M. F., Prata, M. J. & Alves, S. Mannose-6-phosphate pathway: a review on its role in lysosomal function and dysfunction. *Molecular Genetics and Metabolism* 105, 542–550 (2012).
312. Varki, A. & Kornfeld, S. Purification and characterization of rat liver alpha-N-acetylglucosaminyl phosphodiesterase. *J. Biol. Chem.* 256, 9937–9943 (1981).
313. Lee, W.-S., Rohrer, J., Kornfeld, R. & Kornfeld, S. Multiple signals regulate trafficking of the mannose 6-phosphate-uncovering enzyme. *J. Biol. Chem.* 277, 3544–3551 (2002).
314. Ludwig, T. et al. Differential sorting of lysosomal enzymes in mannose 6-phosphate receptor-deficient fibroblasts. *EMBO J.* 13, 3430–3437 (1994).
315. Munier-Lehmann, H., Mauxion, F., Bauer, U., Lobel, P. & Hoflack, B. Re-expression of the mannose 6-phosphate receptors in receptor-deficient fibroblasts. Complementary function of the two mannose 6-phosphate receptors in lysosomal enzyme targeting. *J. Biol. Chem.* 271, 15166–15174 (1996).
316. Kornfeld, S. & Mellman, I. The biogenesis of lysosomes. *Annu. Rev. Cell Biol.* 5, 483–525 (1989).
317. Kucera, A. et al. Spatiotemporal Resolution of Rab9 and CI-MPR Dynamics in the Endocytic Pathway. *Traffic* 17, 211–229 (2016).
318. Pols, M. S. et al. hVps41 and VAMP7 function in direct TGN to late endosome transport of lysosomal membrane proteins. *Nat Commun* 4, 1361 (2013).
319. Hirst, J. et al. Spatial and functional relationship of GGAs and AP-1 in *Drosophila* and HeLa cells. *Traffic* 10, 1696–1710 (2009).

320. Arighi, C. N., Hartnell, L. M., Aguilar, R. C., Haft, C. R. & Bonifacino, J. S. Role of the mammalian retromer in sorting of the cation-independent mannose 6-phosphate receptor. *J. Cell Biol.* 165, 123–133 (2004).
321. Seaman, M. N. J. Cargo-selective endosomal sorting for retrieval to the Golgi requires retromer. *J. Cell Biol.* 165, 111–122 (2004).
322. Ghosh, P., Griffith, J., Geuze, H. J. & Kornfeld, S. Mammalian GGAs act together to sort mannose 6-phosphate receptors. *J. Cell Biol.* 163, 755–766 (2003).
323. Tiede, S. et al. Mucopolidiosis II is caused by mutations in GNPTA encoding the alpha/beta GlcNAc-1-phosphotransferase. *Nat. Med.* 11, 1109–1112 (2005).
324. Kollmann, K. et al. Mannose phosphorylation in health and disease. *Eur. J. Cell Biol.* 89, 117–123 (2010).
325. Hermeijer, G. The Vps10p-domain receptor family. *Cell. Mol. Life Sci.* 66, 2677–2689 (2009).
326. Canuel, M., Korkidakis, A., Konnyu, K. & Morales, C. R. Sortilin mediates the lysosomal targeting of cathepsins D and H. *Biochem. Biophys. Res. Commun.* 373, 292–297 (2008).
327. Progida, C. & Bakke, O. Bidirectional traffic between the Golgi and the endosomes - machineries and regulation. *J. Cell. Sci.* 129, 3971–3982 (2016).
328. Westergaard, U. B. et al. Functional organization of the sortilin Vps10p domain. *J. Biol. Chem.* 279, 50221–50229 (2004).
329. Nielsen, M. S. et al. The sortilin cytoplasmic tail conveys Golgi-endosome transport and binds the VHS domain of the GGA2 sorting protein. *EMBO J.* 20, 2180–2190 (2001).
330. Nielsen, M. S. et al. Sorting by the cytoplasmic domain of the amyloid precursor protein binding receptor SorLA. *Mol. Cell. Biol.* 27, 6842–6851 (2007).
331. Seidah, N. G. & Chrétien, M. Eukaryotic protein processing: endoproteolysis of precursor proteins. *Curr. Opin. Biotechnol.* 8, 602–607 (1997).
332. Jacobsen, L. et al. Activation and functional characterization of the mosaic receptor SorLA/LR11. *J. Biol. Chem.* 276, 22788–22796 (2001).
333. Petersen, C. M. et al. Propeptide cleavage conditions sortilin/neurotensin receptor-3 for ligand binding. *EMBO J.* 18, 595–604 (1999).
334. Quistgaard, E. M. et al. Ligands bind to Sortilin in the tunnel of a ten-bladed beta-propeller domain. *Nat. Struct. Mol. Biol.* 16, 96–98 (2009).
335. Westergaard, U. B. et al. SorCS3 does not require propeptide cleavage to bind nerve growth factor. *FEBS Lett.* 579, 1172–1176 (2005).

References

336. Gliemann, J. et al. The mosaic receptor sorLA/LR11 binds components of the plasminogen-activating system and platelet-derived growth factor-BB similarly to LRP1 (low-density lipoprotein receptor-related protein), but mediates slow internalization of bound ligand. *Biochem. J.* 381, 203–212 (2004).
337. Seaman, M. N. J. Identification of a novel conserved sorting motif required for retromer-mediated endosome-to-TGN retrieval. *J. Cell. Sci.* 120, 2378–2389 (2007).
338. Mari, M. et al. SNX1 defines an early endosomal recycling exit for sortilin and mannose 6-phosphate receptors. *Traffic* 9, 380–393 (2008).
339. Pfeffer, S. R. & Rothman, J. E. Biosynthetic protein transport and sorting by the endoplasmic reticulum and Golgi. *Annual Review of Biochemistry* 56, 829–852 (1987).
340. Bard, F. et al. Functional genomics reveals genes involved in protein secretion and Golgi organization. *Nature* 439, 604–607 (2006).
341. Maciver, S. K. & Hussey, P. J. The ADF/cofilin family: actin-remodeling proteins. *Genome Biol.* 3, reviews3007 (2002).
342. Bamburg, J. R., Harris, H. E. & Weeds, A. G. Partial purification and characterization of an actin depolymerizing factor from brain. *FEBS Lett.* 121, 178–182 (1980).
343. Kanellos, G. & Frame, M. C. Cellular functions of the ADF/cofilin family at a glance. *J. Cell. Sci.* 129, 3211–3218 (2016).
344. Vartiainen, M. K. et al. The three mouse actin-depolymerizing factor/cofilins evolved to fulfill cell-type-specific requirements for actin dynamics. *Mol. Biol. Cell* 13, 183–194 (2002).
345. Yeoh, S., Pope, B., Mannherz, H. G. & Weeds, A. Determining the differences in actin binding by human ADF and cofilin. *J. Mol. Biol.* 315, 911–925 (2002).
346. Chen, J. et al. Cofilin/ADF is required for cell motility during *Drosophila* ovary development and oogenesis. *Nat. Cell Biol.* 3, 204–209 (2001).
347. Wiggan, O., Shaw, A. E., DeLuca, J. G. & Bamburg, J. R. ADF/cofilin regulates actomyosin assembly through competitive inhibition of myosin II binding to F-actin. *Dev. Cell* 22, 530–543 (2012).
348. Chua, B. T. et al. Mitochondrial translocation of cofilin is an early step in apoptosis induction. *Nat. Cell Biol.* 5, 1083–1089 (2003).
349. Kanellos, G. et al. ADF and Cofilin1 Control Actin Stress Fibers, Nuclear Integrity, and Cell Survival. *Cell Rep* 13, 1949–1964 (2015).

350. Dopic, J., Skarp, K.-P., Rajakylä, E. K., Tanhuanpää, K. & Vartiainen, M. K. Active maintenance of nuclear actin by importin 9 supports transcription. *Proc. Natl. Acad. Sci. U.S.A.* 109, E544–52 (2012).
351. Hawkins, M., Pope, B., Maciver, S. K. & Weeds, A. G. Human actin depolymerizing factor mediates a pH-sensitive destruction of actin filaments. *Biochemistry* 32, 9985–9993 (1993).
352. Bernstein, B. W. & Bamburg, J. R. Tropomyosin binding to F-actin protects the F-actin from disassembly by brain actin-depolymerizing factor (ADF). *Cell Motil.* 2, 1–8 (1982).
353. Hayakawa, K., Tatsumi, H. & Sokabe, M. Actin filaments function as a tension sensor by tension-dependent binding of cofilin to the filament. *J. Cell Biol.* 195, 721–727 (2011).
354. Tojkander, S., Gateva, G., Husain, A., Krishnan, R. & Lappalainen, P. Generation of contractile actomyosin bundles depends on mechanosensitive actin filament assembly and disassembly. *Elife* 4, e06126 (2015).
355. Zhao, H., Hakala, M. & Lappalainen, P. ADF/cofilin binds phosphoinositides in a multivalent manner to act as a PIP(2)-density sensor. *Biophysical Journal* 98, 2327–2336 (2010).
356. Yonezawa, N., Homma, Y., Yahara, I., Sakai, H. & Nishida, E. A short sequence responsible for both phosphoinositide binding and actin binding activities of cofilin. *J. Biol. Chem.* 266, 17218–17221 (1991).
357. Yonezawa, N., Nishida, E., Iida, K., Yahara, I. & Sakai, H. Inhibition of the interactions of cofilin, destrin, and deoxyribonuclease I with actin by phosphoinositides. *J. Biol. Chem.* 265, 8382–8386 (1990).
358. Kienzle, C. et al. Cofilin recruits F-actin to SPCA1 and promotes Ca²⁺-mediated secretory cargo sorting. *J. Cell Biol.* 206, 635–654 (2014).
359. Toshima, J. et al. Cofilin phosphorylation by protein kinase testicular protein kinase 1 and its role in integrin-mediated actin reorganization and focal adhesion formation. *Mol. Biol. Cell* 12, 1131–1145 (2001).
360. Ohashi, K., Hosoya, T., Takahashi, K., Hing, H. & Mizuno, K. A *Drosophila* homolog of LIM-kinase phosphorylates cofilin and induces actin cytoskeletal reorganization. *Biochem. Biophys. Res. Commun.* 276, 1178–1185 (2000).
361. Niwa, R., Nagata-Ohashi, K., Takeichi, M., Mizuno, K. & Uemura, T. Control of actin reorganization by Slingshot, a family of phosphatases that dephosphorylate ADF/cofilin. *Cell* 108, 233–246 (2002).

References

362. Blume, von, J. et al. Actin remodeling by ADF/cofilin is required for cargo sorting at the trans-Golgi network. *J. Cell Biol.* 187, 1055–1069 (2009).
363. Curwin, A. J., Blume, von, J. & Malhotra, V. Cofilin-mediated sorting and export of specific cargo from the Golgi apparatus in yeast. *Mol. Biol. Cell* 23, 2327–2338 (2012).
364. Blume, von, J. et al. ADF/cofilin regulates secretory cargo sorting at the TGN via the Ca²⁺ ATPase SPCA1. *Dev. Cell* 20, 652–662 (2011).
365. Blume, von, J. et al. Cab45 is required for Ca(2+)-dependent secretory cargo sorting at the trans-Golgi network. *J. Cell Biol.* 199, 1057–1066 (2012).
366. Koivu, T., Laitinen, S., Riento, K. & Olkkonen, V. M. Sequence of a human cDNA encoding Cab45, a Ca²⁺-binding protein with six EF-hand motifs. *DNA Seq.* 7, 217–220 (1997).
367. Lam, P. P. L. et al. A cytosolic splice variant of Cab45 interacts with Munc18b and impacts on amylase secretion by pancreatic acini. *Mol. Biol. Cell* 18, 2473–2480 (2007).
368. Chen, L. et al. Cab45S inhibits the ER stress-induced IRE1-JNK pathway and apoptosis via GRP78/BiP. *Cell Death Dis* 5, e1219 (2014).
369. Chen, L. et al. Cab45S promotes cell proliferation through SERCA2b inhibition and Ca²⁺ signaling. *Oncogene* 35, 35–46 (2016).
370. Zhu, Y., Wang, Q., Xu, W. & Li, S. The ethanol response gene Cab45 can modulate the impairment elicited by ethanol and ultraviolet in PC12 cells. *J Genet Genomics* 35, 153–161 (2008).
371. Tsukumo, Y., Tsukahara, S., Saito, S., Tsuruo, T. & Tomida, A. A Novel Endoplasmic Reticulum Export Signal. *J. Biol. Chem.* 284, 27500–27510 (2009).
372. Szebenyi, D. M. E. & Moffat, K. The refined structure of vitamin D-dependent calcium-binding protein from bovine intestine. Molecular details, ion binding, and implications for the structure of other calcium-binding proteins.. (1986). doi:10.2210/pdb3icb/pdb
373. Munro, S. & Pelham, H. R. A C-terminal signal prevents secretion of luminal ER proteins. *Cell* 48, 899–907 (1987).
374. Lara-Lemus, R. et al. Luminal protein sorting to the constitutive secretory pathway of a regulated secretory cell. *J. Cell. Sci.* 119, 1833–1842 (2006).
375. Delcourt, N. et al. Targeted identification of sialoglycoproteins in hypoxic endothelial cells and validation in zebrafish reveal roles for proteins in angiogenesis. *J. Biol. Chem.* 290, 3405–3417 (2015).

376. Pfeiffer, J. K., Georgiadis, M. M. & Telesnitsky, A. Structure-based moloney murine leukemia virus reverse transcriptase mutants with altered intracellular direct-repeat deletion frequencies. *J. Virol.* 74, 9629–9636 (2000).
377. Carroll, D. Genome engineering with targetable nucleases. *Annual Review of Biochemistry* 83, 409–439 (2014).
378. Smithies, O., Gregg, R. G., Boggs, S. S., Koralewski, M. A. & Kucherlapati, R. S. Insertion of DNA sequences into the human chromosomal beta-globin locus by homologous recombination. *Nature* 317, 230–234 (1985).
379. Thomas, K. High frequency targeting of genes to specific sites in the mammalian genome. *Cell* 44, 419–428 (1986).
380. Jinek, M. et al. A programmable dual-RNA-guided DNA endonuclease in adaptive bacterial immunity. *Science* 337, 816–821 (2012).
381. Marraffini, L. A. & Sontheimer, E. J. CRISPR interference: RNA-directed adaptive immunity in bacteria and archaea. *Nat. Rev. Genet.* 11, 181–190 (2010).
382. Sorek, R., Kunin, V. & Hugenholtz, P. CRISPR--a widespread system that provides acquired resistance against phages in bacteria and archaea. *Nat. Rev. Microbiol.* 6, 181–186 (2008).
383. Hsu, P. D. et al. DNA targeting specificity of RNA-guided Cas9 nucleases. *Nat. Biotechnol.* 31, 827–832 (2013).
384. Ran, F. A. et al. Genome engineering using the CRISPR-Cas9 system. *Nat Protoc* 8, 2281–2308 (2013).
385. Gasiunas, G., Barrangou, R., Horvath, P. & Siksnys, V. Cas9-crRNA ribonucleoprotein complex mediates specific DNA cleavage for adaptive immunity in bacteria. *Proc. Natl. Acad. Sci. U.S.A.* 109, E2579–86 (2012).
386. Mulholland, C. B. et al. A modular open platform for systematic functional studies under physiological conditions. *Nucleic Acids Res.* 43, e112–e112 (2015).
387. Crevenna, A. H. et al. Secretory cargo sorting by Ca²⁺-dependent Cab45 oligomerization at the trans-Golgi network. *J. Cell Biol.* 213, 305–314 (2016).
388. Humphrey, S. J., Azimifar, S. B. & Mann, M. High-throughput phosphoproteomics reveals in vivo insulin signaling dynamics. *Nat. Biotechnol.* 33, 990–995 (2015).
389. Rappsilber, J., Ishihama, Y. & Mann, M. Stop and go extraction tips for matrix-assisted laser desorption/ionization, nanoelectrospray, and LC/MS sample pretreatment in proteomics. *Anal. Chem.* 75, 663–670 (2003).

References

390. Kulak, N. A., Pichler, G., Paron, I., Nagaraj, N. & Mann, M. Minimal, encapsulated proteomic-sample processing applied to copy-number estimation in eukaryotic cells. *Nat. Methods* 11, 319–324 (2014).
391. Cox, J. & Mann, M. MaxQuant enables high peptide identification rates, individualized p.p.b.-range mass accuracies and proteome-wide protein quantification. *Nat. Biotechnol.* 26, 1367–1372 (2008).
392. Tyanova, S. et al. The Perseus computational platform for comprehensive analysis of (prote)omics data. *Nat. Methods* 13, 731–740 (2016).
393. Rappsilber, J., Mann, M. & Ishihama, Y. Protocol for micro-purification, enrichment, pre-fractionation and storage of peptides for proteomics using StageTips. *Nat Protoc* 2, 1896–1906 (2007).
394. Nagaraj, N. et al. System-wide perturbation analysis with nearly complete coverage of the yeast proteome by single-shot ultra HPLC runs on a bench top Orbitrap. *Mol. Cell Proteomics* 11, M111.013722 (2012).
395. Cox, J. et al. Andromeda: a peptide search engine integrated into the MaxQuant environment. *J. Proteome Res.* 10, 1794–1805 (2011).
396. Cox, J. et al. Accurate proteome-wide label-free quantification by delayed normalization and maximal peptide ratio extraction, termed MaxLFQ. *Mol. Cell Proteomics* 13, 2513–2526 (2014).
397. Prytuliak, R., Volkmer, M., Meier, M. & Habermann, B. H. HH-MOTiF: de novo detection of short linear motifs in proteins by Hidden Markov Model comparisons. *Nucleic Acids Res.* (2017). doi:10.1093/nar/gkx341
398. Ran, F. A. et al. In vivo genome editing using *Staphylococcus aureus* Cas9. *Nature* 520, 186–191 (2015).
399. Lieber, M. R. The mechanism of double-strand DNA break repair by the nonhomologous DNA end-joining pathway. *Annual Review of Biochemistry* 79, 181–211 (2010).
400. Liang, F., Han, M., Romanienko, P. J. & Jasin, M. Homology-directed repair is a major double-strand break repair pathway in mammalian cells. *Proc. Natl. Acad. Sci. U.S.A.* 95, 5172–5177 (1998).
401. Cong, L. et al. Multiplex genome engineering using CRISPR/Cas systems. *Science* 339, 819–823 (2013).
402. Pattanayak, V. et al. High-throughput profiling of off-target DNA cleavage reveals RNA-programmed Cas9 nuclease specificity. *Nat. Biotechnol.* 31, 839–843 (2013).

403. Cho, S. W. et al. Analysis of off-target effects of CRISPR/Cas-derived RNA-guided endonucleases and nickases. *Genome Res.* 24, 132–141 (2014).
404. Zhang, X.-H., Tee, L. Y., Wang, X.-G., Huang, Q.-S. & Yang, S.-H. Off-target Effects in CRISPR/Cas9-mediated Genome Engineering. *Molecular Therapy - Nucleic Acids* 4, e264 (2015).
405. Wu, X., Kriz, A. J. & Sharp, P. A. Target specificity of the CRISPR-Cas9 system. *Quant Biol* 2, 59–70 (2014).
406. Dirlam-Schatz, K. A. & Attie, A. D. Calcium induces a conformational change in the ligand binding domain of the low density lipoprotein receptor. *J. Lipid Res.* 39, 402–411 (1998).
407. Greenfield, N. J. Using circular dichroism spectra to estimate protein secondary structure. *Nat Protoc* 1, 2876–2890 (2006).
408. Missiaen, L. et al. SPCA1 pumps and Hailey-Hailey disease. *Biochem. Biophys. Res. Commun.* 322, 1204–1213 (2004).
409. Blank, B. & Blume, von, J. Cab45-Unraveling key features of a novel secretory cargo sorter at the trans-Golgi network. *Eur. J. Cell Biol.* (2017). doi:10.1016/j.ejcb.2017.03.001
410. Boncompain, G. et al. Synchronization of secretory protein traffic in populations of cells. *Nat. Methods* 9, 493–498 (2012).
411. Chen, C. et al. Identification of a major determinant for serine-threonine kinase phosphoacceptor specificity. *Mol. Cell* 53, 140–147 (2014).
412. Antonelli, A. et al. Circulating chemokine (CXC motif) ligand (CXCL)9 is increased in aggressive chronic autoimmune thyroiditis, in association with CXCL10. *Cytokine* 55, 288–293 (2011).
413. Brosseau, C., Pirianov, G. & Colston, K. W. Role of insulin-like growth factor binding protein-3 in 1, 25-dihydroxyvitamin-d₃-induced breast cancer cell apoptosis. *Int J Cell Biol* 2013, 960378–9 (2013).
414. Chen, C. D. et al. Furin initiates gelsolin familial amyloidosis in the Golgi through a defect in Ca²⁺ stabilization. *EMBO J.* 20, 6277–6287 (2001).
415. Harding, H. P. et al. Diabetes mellitus and exocrine pancreatic dysfunction in *perk*^{-/-} mice reveals a role for translational control in secretory cell survival. *Mol. Cell* 7, 1153–1163 (2001).
416. Maddox, B. K., Garofalo, S., Smith, C., Keene, D. R. & Horton, W. A. Skeletal development in transgenic mice expressing a mutation at Gly574Ser of type II collagen. *Dev. Dyn.* 208, 170–177 (1997).

References

417. Pelham, H. R. & Munro, S. Sorting of membrane proteins in the secretory pathway. *Cell* 75, 603–605 (1993).
418. Schaefer, K. A. et al. Unexpected mutations after CRISPR-Cas9 editing in vivo. *Nat. Methods* 14, 547–548 (2017).
419. Rossi, A. et al. Genetic compensation induced by deleterious mutations but not gene knockdowns. *Nature* 524, 230–233 (2015).
420. Cerikan, B. et al. Cell-Intrinsic Adaptation Arising from Chronic Ablation of a Key Rho GTPase Regulator. *Dev. Cell* 39, 28–43 (2016).
421. Makino, S., Fukumura, R. & Gondo, Y. Illegitimate translation causes unexpected gene expression from on-target out-of-frame alleles created by CRISPR-Cas9. *Scientific Reports* 6, 39608 (2016).
422. Mou, H. et al. CRISPR/Cas9-mediated genome editing induces exon skipping by alternative splicing or exon deletion. *Genome Biol.* 18, 108 (2017).
423. Wingfield, P. T. Overview of the purification of recombinant proteins. *Curr Protoc Protein Sci* 80, 6.1.1–35 (2015).
424. Kitaura, Y., Satoh, H., Takahashi, H., Shibata, H. & Maki, M. Both ALG-2 and peflin, penta-EF-hand (PEF) proteins, are stabilized by dimerization through their fifth EF-hand regions. *Arch. Biochem. Biophys.* 399, 12–18 (2002).
425. Lowe, R., Pountney, D. L., Jensen, P. H., Gai, W. P. & Voelcker, N. H. Calcium(II) selectively induces alpha-synuclein annular oligomers via interaction with the C-terminal domain. *Protein Sci.* 13, 3245–3252 (2004).
426. Sanchez, E. J., Lewis, K. M., Danna, B. R. & Kang, C. High-capacity Ca²⁺ binding of human skeletal calsequestrin. *J. Biol. Chem.* 287, 11592–11601 (2012).
427. Hamada, H., Okochi, E., Oh-hara, T. & Tsuruo, T. Purification of the Mr 22,000 calcium-binding protein (sorcini) associated with multidrug resistance and its detection with monoclonal antibodies. *Cancer Res.* 48, 3173–3178 (1988).
428. Kitaura, Y., Matsumoto, S., Satoh, H., Hitomi, K. & Maki, M. Peflin and ALG-2, members of the penta-EF-hand protein family, form a heterodimer that dissociates in a Ca²⁺-dependent manner. *J. Biol. Chem.* 276, 14053–14058 (2001).
429. Curley, D. M., Kumosinski, T. F., Unruh, J. J. & Farrell, H. M. Changes in the secondary structure of bovine casein by Fourier transform infrared spectroscopy: effects of calcium and temperature. *J. Dairy Sci.* 81, 3154–3162 (1998).
430. Finn, B. E. et al. Calcium-induced structural changes and domain autonomy in calmodulin. *Nat. Struct. Biol.* 2, 777–783 (1995).

431. Reid, R. E., Clare, D. M. & Hodges, R. S. Synthetic analog of a high affinity calcium binding site in rabbit skeletal troponin C. *J. Biol. Chem.* 255, 3642–3646 (1980).
432. Wagner, D. D., Mayadas, T. & Marder, V. J. Initial glycosylation and acidic pH in the Golgi apparatus are required for multimerization of von Willebrand factor. *J. Cell Biol.* 102, 1320–1324 (1986).
433. Maki, M., Suzuki, H. & Shibata, H. Structure and function of ALG-2, a penta-EF-hand calcium-dependent adaptor protein. *Sci China Life Sci* 54, 770–779 (2011).
434. Ballif, B. A., Mincek, N. V., Barratt, J. T., Wilson, M. L. & Simmons, D. L. Interaction of cyclooxygenases with an apoptosis- and autoimmunity-associated protein. *Proc. Natl. Acad. Sci. U.S.A.* 93, 5544–5549 (1996).
435. Aradhyam, G. K., Balivada, L. M., Kanuru, M., Vadivel, P. & Vidhya, B. S. Calnuc: Emerging roles in calcium signaling and human diseases. *IUBMB Life* 62, 436–446 (2010).
436. Luo, J. et al. A Novel Role of Cab45-G in Mediating Cell Migration in Cancer Cells. *Int. J. Biol. Sci.* 12, 677–687 (2016).
437. Vorum, H., Liu, X., Madsen, P., Rasmussen, H. H. & Honoré, B. Molecular cloning of a cDNA encoding human calumenin, expression in *Escherichia coli* and analysis of its Ca²⁺-binding activity. *Biochim. Biophys. Acta* 1386, 121–131 (1998).
438. Kaletta, K., Kunze, I., Kunze, G. & Köck, M. The peptide HDEF as a new retention signal is necessary and sufficient to direct proteins to the endoplasmic reticulum. *FEBS Lett.* 434, 377–381 (1998).
439. Booth, C. & Koch, G. L. Perturbation of cellular calcium induces secretion of luminal ER proteins. *Cell* 59, 729–737 (1989).
440. Sambrook, J. F. The involvement of calcium in transport of secretory proteins from the endoplasmic reticulum. *Cell* 61, 197–199 (1990).
441. Meissner, G. Isolation and characterization of two types of sarcoplasmic reticulum vesicles. *Biochim. Biophys. Acta* 389, 51–68 (1975).
442. Mertins, P. et al. Proteogenomics connects somatic mutations to signalling in breast cancer. *Nature* 534, 55–62 (2016).
443. Yoshida, T. et al. Tyrosine phosphoproteomics identifies both codrivers and cotargeting strategies for T790M-related EGFR-TKI resistance in non-small cell lung cancer. *Clin. Cancer Res.* 20, 4059–4074 (2014).
444. Tzouros, M. et al. Development of a 5-plex SILAC method tuned for the quantitation of tyrosine phosphorylation dynamics. *Mol. Cell Proteomics* 12, 3339–3349 (2013).

Acknowledgements

At the end of this work I want to thank many people without whom this thesis could not be accomplished in this way.

First of all, I want to thank my group leader Dr. Julia von Blume for the years of supervision and guidance. Thank you for accepting me as part of your lab and for the fruitful collaborations on my project. I especially appreciate your generous support also on tasks beyond lab work which will be highly valuable for my future.

Of course, my thanks go also to my doctor father and head of the department of molecular medicine Prof. Dr. Reinhard Fässler, who accompanied my work with helpful discussions and suggestions, also in the framework of my Thesis Advisory Committee.

My wholehearted thank goes to all alumni and current members of the von Blume lab. Dr. Christine “Nicky/Dr.U” Kienzle for teaching me innumerable useful techniques upon my arrival in lab and for her unfailing helpfulness and indescribable humor. Gisela Beck for bravely accompanying my whole thesis on the bench next to me, for tolerating all my bad moods, for her always helpful hands in lab and for keeping things down to earth. Thanks, Mehrshad for establishing a bunch of new methods in lab, including great macros and the RUSH system, and together with Natalia Pacheco-Fernandez for helpful discussions and novel ideas. Renate Gautsch for all the cell culture work, which saved me days, especially during the end of my thesis, and all the other members and lab students, especially my former Bachelor students Tobias Hecht and Mai Ly Tran for the always positive, collaborative and motivating atmosphere in our lab.

The acquisition of data presented in this thesis would not have been possible without support of our collaborators. In this context, I want to thank Dr. Alvaro Crevenna, who was always helpful to setup crucial experiments for our joint publication and for new ideas and inputs. Furthermore, the profound bioinformatical skills of Dr. Bianca Habermann’s group and her PhD student Roman Prytuliak enabled us to identify the cargo binding motif of Cab45. The corresponding mass spectrometry experiment, besides other analyses, was performed by Dr. Martin Steger, who promoted the Fam20C project majorly. I want

to thank Andreas Maiser, who invested a lot of time and effort in the 3D-SIM experiments. And last but not least the CRISPR/Cas9 MIN tag project was supported in word and deed by Dr. Sebastian Bultmann's group, including Christopher Mulholland and Michael Bartoschek.

Throughout my thesis, I worked together with many members of the MPI Core Facilities. Dr. Sabine Suppmann, Judith Scholz and Melanie Ried contributed majorly to the success of this thesis by supporting out lab with protein expression and purifications. Dr. Nagarjuna Nagaraj demonstrated infinite help and patience with mass spectrometry data acquisition and analysis, while Dr. Stephan Uebel supported many kinds of different biophysical trials and synthesis of the biotinylated peptides together with Stefan Pettera. Furthermore, I want to thank Hildegard "Mischa" Reiter for the generation of all stable cell lines used throughout this work and Dr. Maik Veelders for help with CD measurements. Thanks also to all members of the department of molecular medicine for good collaborations and daily support with all the little annoying problems of lab life.

Thanks to Dr. Mark Hipp and Dr. Biertümpel for their helpful suggestions and discussions during my TAC meetings.

My explicit thanks go also to Dr. Carsten Grashoff and his whole group for critical questions and input during all talks, pre-talks and test-talks in Monday seminars and hilarious lunch-time discussions.

Finally, of course I want to thank my whole family for their perpetual support throughout my whole academic career and their honest interest and everlasting efforts to understand the topic of my thesis.

And my special thanks go to Daniel Feldmeier, for his unshakable patience and his unbroken understanding, for his realistic views and for the invaluable way of keeping me happy.